THE UNIVERSITY
of EDINBURGH

Rhenium Polyhydride Complexes of Boron–Hydride Ligands and their Application in Catalysis

Liam J. Donnelly

A thesis submitted for the degree of

Doctor of Philosophy

EaStCHEM School of Chemistry

The University of Edinburgh

April 2021

Declaration

The work described in this thesis is entirely my own, except where I have either acknowledged help from a named person or given reference to a published source. Text taken from another source will be enclosed in quotation marks and a reference given. This thesis has not been submitted, in whole or in part, for any other degree.

Signature: Date: 16/04/2021

Abstract

The synthesis of transition metal complexes containing metal-boron bonds is of particular interest due to the relevance of these complexes as intermediates in catalytic C–X (X = H or halogen) borylation to prepare synthetically valuable organoboronate esters. The most widely used catalysts are Ir complexes typically of the form $[Ir(Bpin)_3(L)_2]$, where L is a neutral monodentate or bidentate ligand, and invoke an Ir(III)/Ir(V) redox couple. In the past 30 years metal-oxos have been studied in the activation of X–H (X = B, Si, P) bonds for applications in catalytic hydrofunctionalisation reactions. The mechanism of these reactions can proceed by functionalisation and/or cleavage of the M=O bond to produce compounds that are inaccessible by conventional methods. However, this reactivity has not been significantly explored for anionic metal-oxo complexes (e.g. ReO_4^-, RuO_4^- and WO_4^{2-}). This thesis presents the synthesis of a number of rhenium polyhydride complexes of boron-hydride ligands from perrhenate (ReO_4^-), the structural characterisation of these complexes, their application in C–H borylation catalysis and hydroboration, and the exploration of the mechanisms of these reactions.

Chapter One introduces C–H functionalisation catalysis and the relevance of transition metal polyhydride and transition metal dihydroborate/σ-borane/boryl complexes as catalysts, and catalytically-relevant intermediates, in this chemistry. Previously reported methods for X–H (X = B or Si) activation by high oxidation transition metal-oxo complexes are also discussed.

Chapter Two details the synthesis and characterisation of the reactive rhenium boron-polyhydride anion $[K(DME)(18\text{-c-}6][ReH_7(Bpin)_3]$ by exhaustive deoxygenation of the commercially available ReO_4^- anion with pinacol borane (HBpin). This complex is shown to be a reagent for the stoichiometric C–H borylation of carboarenes with high *meta* regioselectivity. The reaction with other hydroboranes is also described, resulting in reductive Bpin substitution to form new anionic dihydroborate complexes.

Chapter Three describes how $[K(DME)(18\text{-c-}6][ReH_7(Bpin)_3]$, either isolated or prepared *in situ*, is a catalyst for the 1,4-hydroboration of *N*-heteroaromatic substrates under simple operating procedures. A full description of the optimisation of the reaction conditions and substrate scope is presented. A mechanistic investigation of the hydroboration reactivity is outlined and used to elucidate the catalytic cycle of this reaction. The use of other anionic metal-oxo complexes for hydrofunctionalisation catalysis is also discussed.

Chapter Four details the synthesis and characterisation of phosphine-ligated Re boron-polyhydride complexes through the reductive substitution of HBpin from [K(DME)(18-c-6][$ReH_7(Bpin)_3$] with mono- and bidentate phosphine ligands. In particular, the synthesis of σ-borane complex [K(18-c-6)][$ReH_4(\eta^2$-HBpin)(dppp)] is highlighted which, upon protonation, forms the neutral boryl complex [ReH_6(Bpin)(dppp)]. The catalytic activity of [ReH_6(Bpin)(dppp)] in the C–H borylation of heteroaromatics is described, and a full substrate scope and mechanistic study is outlined.

Chapter Five presents a summary of the work presented in this thesis, and Chapter Six outlines the experimental procedures and analytical data for all described compounds and complexes.

Lay Summary

In the modern world we are heavily reliant on the use of bulk and fine chemicals (pharmaceuticals, plastics, agrochemicals) in our daily life. The majority of the processes to manufacture these chemicals require the use of a catalyst, which enables chemical transformations that would otherwise not proceed if the catalyst were not present. This means that the synthesis and evaluation of new catalysts for a variety of chemical transformations is crucial for meeting the needs of industry and society. A category of transformations of particular interest is the formation of organoboron compounds (containing C–B bonds) which are one of the most diverse classes of reagents in organic chemistry. One of the most practical, versatile and powerful ways to achieve this is through the direct conversion of C–H bonds to C–B bonds. To this end, a number of catalysts based on elements across the periodic table have been developed to interact with boron reagents and selectively form the C–B bonds of interest.

However, catalysts based on rhenium have been underexplored in this transformation and relatively little is known about the reactivity of rhenium complexes with boron reagents. This thesis focuses on improving our understanding of how boron reagents react with simple, commercially available rhenium complexes and applying this knowledge to develop catalytic methods for the construction of C–B bonds.

Acknowledgments

I would firstly like to express my thanks and gratitude to my supervisors, Prof. Jason Love and Dr Stephen Thomas, for giving me the opportunity to carry out this PhD. Their support and patience has been invaluable during my time in Edinburgh. I could not have asked for better advisors and mentors. I would also like to thank Dr Vipul Patel and Dr John Pritchard for hosting me at GSK, and Dr James Taylor for hosting me at The University of St Andrews. They gave me the opportunity to work on a broad range of chemistry and have provided continued support.

I am indebted to all members of the Love, Thomas and Arnold groups, past and present, for making my time in the lab/office/pub so enjoyable and entertaining. Thank you to Prof. Carole Morrison (AIRSS/CASTEP) and Prof. Simon Parsons (crystallography) for their guidance, patience and advice during our collaborations. Thank you also to Dr Gary Nichol, Dr Lorna Murray, Dr Juraj Bella, Dr Logan McKay, Dr Faye Cruikshank and Mr. Alan Taylor for their help with instrumentation. I am grateful for the help of Mr. Lloyd Mitchell and Mr. George Steedman in technical services. Thank you to Dr Kevin Jones at St Andrews University for his guidance and advice during the first 6 months of this PhD, and to all other members of the CRITICAT CDT.

I would like to thank my family for their unwavering support and encouragement. In particular I would like to recognise my grandfather, John, who graduated from Edinburgh University in 1952 with a BSc in chemistry and who taught me the value and importance of education. This thesis is dedicated in memory of him.

Finally, I would like to thank my wife and best friend, Rachael, who has been with me through the highs and lows of this PhD. Her love and support has made this all possible.

Abbreviations

$[PPN]^+$ – bis(triphenylphosphine)iminium

9-BBN – 9-borabicyclo[3.3.1]nonane

AcCN – acetonitrile

AIM – atoms in molecules

AIRSS – ab initio random structure searching

Ar - aryl

Bcat – 1,3,2-benzodioxaborole

BCF – tris(pentafluorophenyl)borane

Boc – *tert*-butyloxycarbonyl

Bn – benzyl

Bpin – 4,4,5,5-tetramethyl-1,3,2-dioxaborolane

Bu – butyl

COE - cyclooctene

COSY – correlated spectroscopy

Cp – cyclopentdienyl

Cp^* – 1,2,3,4,5-pentamethylcyclopentadienyl

Cy – cyclohexyl

DABCO – 1,4-diazabicyclo[2.2.2]octane

dcpp – 1,3-bis(dicyclohexylphosphino)propane

DFT – desnity functional theory

DHP – dihydropyridine

Dipp – 2,6-diisopropylphenyl

DMAP – 4-dimethylaminopyridine

DME – dimethoxyethane

DMF – dimethylformamide

DMS – dimethylsulfide

dmpe – 1,2-bis(dimethylphosphino)ethane

dppp – 1,3-bis(diphenylphosphino)propane

dppe – 1,2-bis(diphenylphosphino)ethane

Equiv. – equivalents

esd – estimated standard deviation

ESI – electrospray ionisation

Et – ethyl

FLP – frustrated Lewis pair

GC/MS – gas chromatography/mass spectrometry

Hex – hexyl

HMBC – heteronuclear multiple bond correlation

HRMS – high resolution mass spectrometry

HSQC – heteronuclear single quantum coherence

Ipc – isopenylcamphyl

^{i}Pr – isopropyl

IR – infrared spectroscopy

J – coupling constant

L – ligand

LutHCl – 2,6-lutidinium chloride

Me – methyl

Mes – mesityl

NBO – near bond order

NHC – nucleophilic-heterocyclic carbene

NMR – nuclear magnetic resonance

OTf – triflate

Ph – phenyl

Py – pyridine

^{t}Bu – tertiary-butyl

TetraPhos – 1,1,4,8,11,11-Hexaphenyl-1,4,8,11-tetraphosphaundecane

TM – transition metal

xant – xanthyl

σ-CAM – sigma-complex-assisted metathesis

Publications

A list of publications associated with this thesis:

1) "Recent Advances in the Deoxydehydration of Vicinal Diols and Polyols" L. J. Donnelly, S. P. Thomas, J. B. Love; *Chem. Asian J.*, **2019**, *14*, 3782 – 3790.
2) "Synthesis and Structures of Anionic Rhenium Polyhydride Complexes of Boron-Hydride Ligands and their Application in Catalysis" L. J. Donnelly, S. Parsons, C. A. Morrison, S. P. Thomas, J. B. Love; *Chem. Sci.*, **2020**, *11*, 9994-9999.
3) "C–H Borylation Catalysis of Heteroaromatics by a Rhenium Boryl Polyhydride" L. J. Donnelly, T. Faber, C. A. Morrison, G. Nichol, S. P. Thomas, J. B. Love (*Accepted, ACS Catal.*).

A list of publications arising from collaborations:

1) "Aryl Boronic Acid-Catalysed Dehydrative Substitution of Benzylic Alcohols for C-O Bond Formation" S. Estopiñá-Durán, L. J. Donnelly, E. B. Mclean, B. M. Hockin, A. M. Z. Slawin, J. E. Taylor; *Chem. Eur. J.*, **2019**, *25*, 3950 – 3956.
2) "Aryl Boronic Acid-Catalysed Dehydrative C-C Bond Formation" S. Estopiñá-Durán, E. B. Mclean, L. J. Donnelly, B. M. Hockin, J. E. Taylor; *Org. Lett.*, **2020**, *22*, 7547-7551.

Contents

Chapter One – Introduction

1.1 Transition Metal C–H Functionalisation

A major focus of organometallic chemistry for the past 50 years has been the use of molecular transition metal catalysts for the functionalisation of unactivated C–H bonds.[1] C–H functionalisation mediated by a transition metal refers to reactions where a transition metal complex cleaves a C–H bond and affects a transformation to install a new functional group in place of H (Scheme 1).[2] The step that involves cleavage of the C–H bond is referred to as 'C–H activation' and this step can be classified into several mechanistic types: σ-bond metathesis, oxidative addition, electrophilic activation, Lewis-base assisted metalation or 1,2-addition and σ-CAM.[3-4] Which pathway a transition metal complex will follow is dependent on the nature of the metal centre, ligands, solvents, additives, and the substrate. Classical synthetic organic methods for C–H functionalisation, such as ethane pyrolysis and Friedel-Crafts alkylation, require forcing reaction conditions and suffer from poor chemo-/regioselectivity. The ultimate goal of these transition metal-catalysed systems is to provide useful methods for the preparation of organic molecules for academic and industrial laboratories.

Transition-metal catalysed C-H bond functionalisation

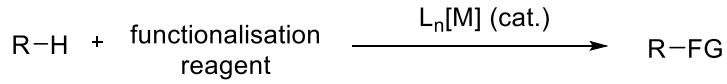

Types of C-H bond activation pathways

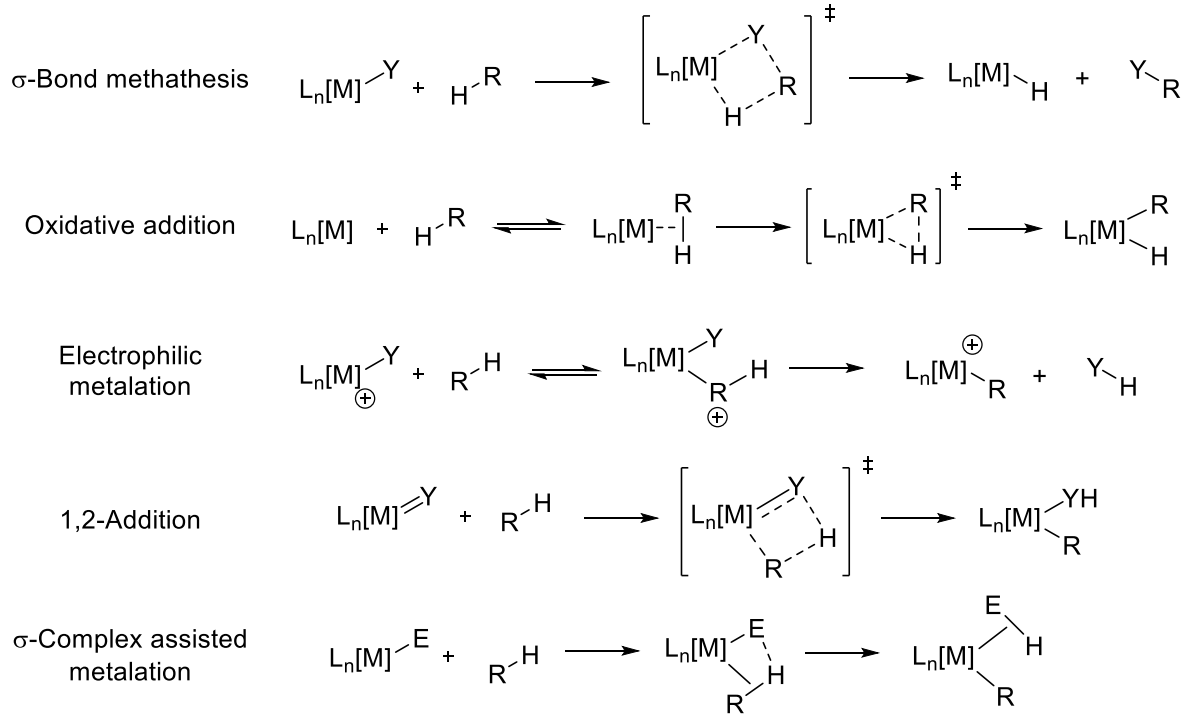

Scheme 1. General scheme for C–H functionalisation and different mechanistic pathways for C–H activation.

The first example of a C–H activation reaction was reported by Chatt and Watson in 1962, where they showed the reduction of $Ru(dmpe)_2Cl_2$ **1** with sodium naphthalenide to produce hydrido complexes *cis*-$Ru(dmpe)_2(H)(napthyl)$ **2** and **3** resulting from the C–H activation of naphthalene (Scheme 2).[5] This was confirmed in a follow-up study through the reaction of **1** with Na in the presence of either benzene, naphthalene, anthracene or phenanthrene to form *cis*-$Ru(dmpe)_2(H)(Aryl)$ complexes. The authors proposed that **1** is reduced to $Ru(dmpe)_2$ **4** by Na, which can oxidatively add to the aryl C–H bond with sterically controlled regioselectivity.[6]

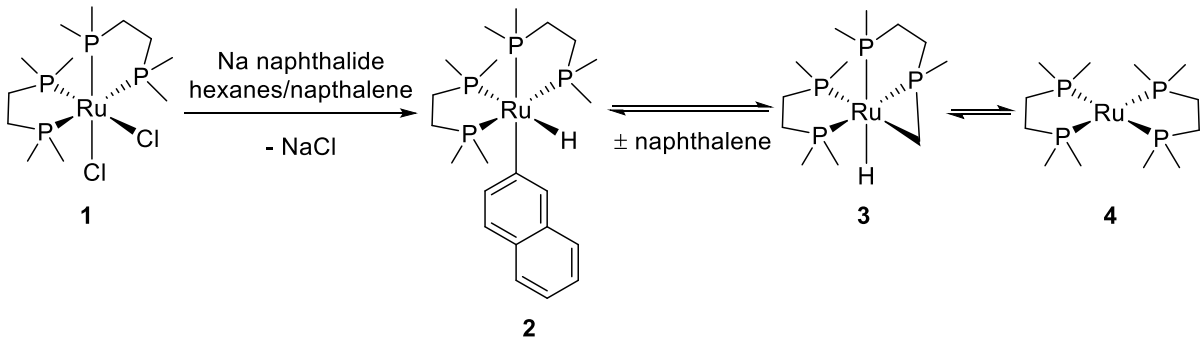

Scheme 2. C–H activation of naphthalene through reduction of **1**.

The subsequent functionalisation of the M–C bond that is formed through C–H activation was not achieved until 1986 by Jones and co-workers through a Ru-catalysed intramolecular cyclisation reaction of 2,6-xylyl isocyanide **5** (Scheme 3).[7] The proposed catalytic cycle begins with the reductive elimination of napthalene from *cis*-Ru(dmpe)$_2$(H)(napthyl) **2** to generate the Ru(0) 16-electron complex Ru(dmpe)$_2$ **4**. Isocyanide coordination directs the metal to the methyl C–H bond, which after phosphine dissociation undergoes oxidative addition. This is followed by 1,1-insertion of the isocyanide into the M–C bond and tautomerisation to the *trans*-2-indolyl species. This isomerises to give the *cis*-2-indolyl isomer that forms the product **6** by reductive elimination, regenerating the active catalyst Ru(dmpe)$_2$ **3** to close the cycle.

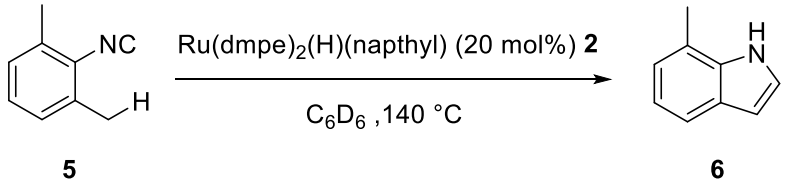

Scheme 3. Intramolecular C–H functionalisation to form indole **6**.

Catalytic intermolecular C–H functionalisation systems that followed were limited to H/D exchange reactions with deuterium gas and alkane dehydrogenation. In 1993, Murai and co-workers reported the Ru-catalysed addition of aromatic C–H bonds to olefins (Scheme 4A).[8] This reaction proceeds by a similar mechanism reported by Jones and uses a ketone substituent on the arene to direct C–H activation to the *ortho* position *via* chelate-assisted oxidative addition to a Ru(0) intermediate. In this context the ketone substituent can be described as a directing group. In 1998, Berry and co-workers reported the dehydrogenative silylation of arenes using a rhodium catalyst **14** and *t*-butylethene **12** as a sacrificial H_2 acceptor (Scheme 4B).[9] The silylation of *m*-xylene **11** gave the *para* functionalised product

exclusively. Monosubstituted benzenes gave a mixture of *meta* and *para* products, with trifluoromethylbenzene giving a 2:1 ratio of *meta*:*para* suggesting that sterics dominate electronic effects in this reaction.

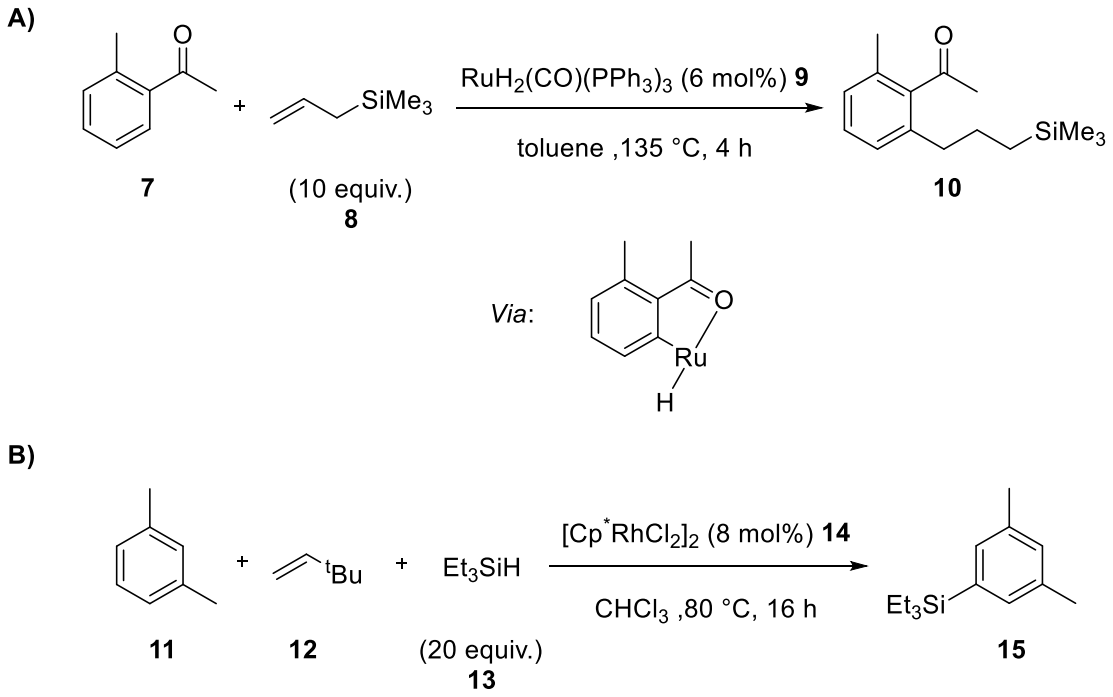

Scheme 4. (A) Alkylation of ketoarene **7** with olefin **8** using a Ru catalyst **9** (B) dehydrogenative silylation of an aromatic C–H bond.

1.2 Transition Metal-Catalysed C–H Borylation

In the last 15-20 years, one class of C–H functionalisation known as C–H borylation has grown from a chemical oddity to a mature catalytic synthetic method.[10-11] This transformation was first noted by Marder and co-workers during the synthesis of Ir-boryl complexes **18** in the presence of arene solvents such as toluene where the formation of organoboronate esters **19** was observed by GC/MS (Scheme 5).[12] This is an attractive transformation as organoboronate esters have a wide variety of uses in synthetic organic chemistry and are traditionally synthesised by addition of Grignard reagents to trialkoxy boronates or by Pd-catalysed coupling reactions.[13]

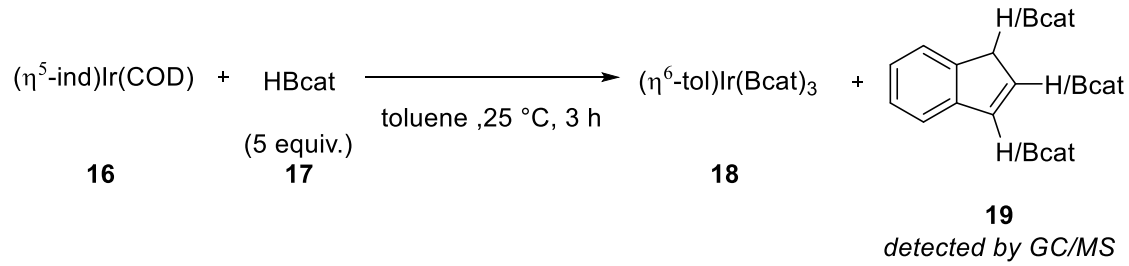

Scheme 5. Detection of stoichiometric borylation of indene by GC/MS in the reaction of **16** with HBcat **17**.

Early examples of transition metal-catalysed C–H borylation were reported for Ru,[14] Rh[15] and Re[16] in the borylation of alkanes. Recent successes include Fe,[17-18] Fe/Cu,[19] Co,[20-23] Pt,[24] and main group systems,[25] however Ir catalysts have proven to the most efficient to date, particularly in the borylation of aromatic C–H bonds. Typically, bidentate bis(phosphines) **22** and **23** (Scheme 6A),[26] 4,4'-di-*tert*-butyl-2,2'-dipyridyl **28** or 1,10-phenanthroline **29** ligands (Scheme 6B)[27] are used in these catalytic systems to give high turnover numbers and sterically controlled regioselectivity. C–H borylation of mono-substituted arene substrates **20** (e.g. toluene) often gives near statistical mixtures of 3- and 4-borylated products. Recent work by Phipps and Smith has shown that ion-pairing can be used to selectively target either the *meta* or *para* positions of arenes.[28-29] Itami and co-workers reported the *para*-selective borylation of mono-substituted arenes by using a very bulky phosphine ligand to control the regioselectivity with steric interactions.[30] Exclusive borylation of the 2-position without the use of directing groups is an ongoing challenge,[31-32] a notable exception is the Co-catalysed borylation of the 2-position of fluoroarenes.[22] Recently, Hartwig and co-workers reported the undirected borylation of primary C(sp^3)–H bonds using a Ir/phenanthroline catalytic system.[33]

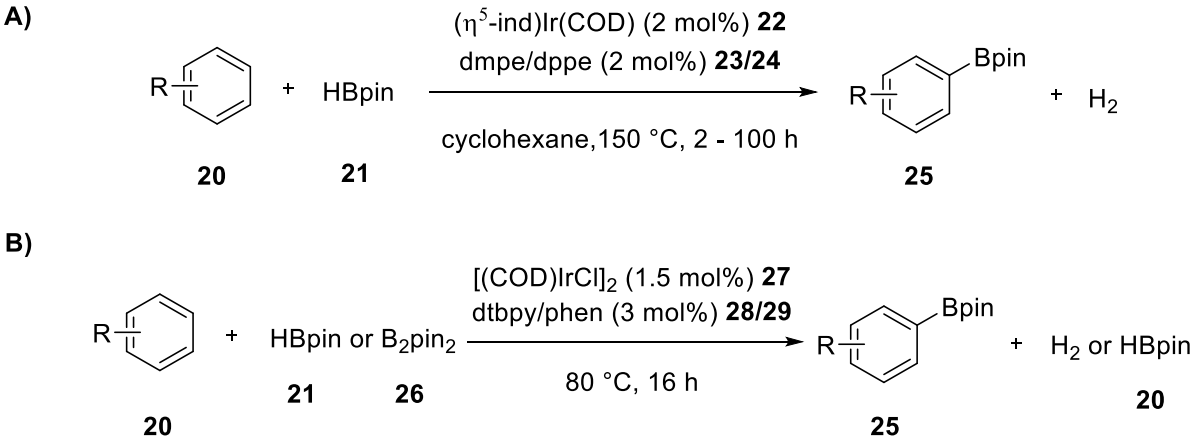

Scheme 6. Ir-catalysed borylation of arenes using A) phosphine ligands **23** and **24** or (B) bipyridine **28** or phenanthroline ligands **29**.

The mechanism of Ir-catalysed C–H borylation is believed to proceed by a 16-electron triboryl intermediate $L_2Ir(Bpin)_3$ **Int-A** generated from an Ir^I precatalyst and HBpin/B_2pin_2 **21**/**26**. This complex activates the arene C–H bond by oxidative addition or the related oxidative hydrogen migration pathway to generate an Ir^V intermediate **Int-B**. Subsequent reductive elimination of the borylated product from Ir^V gives a 16-electron, Ir^{III} diboryl monohydride **Int-C**. Catalyst regeneration begins with oxidative addition of HBpin or B_2pin_2 followed by reductive elimination of H_2 or HBpin (Scheme 7). This was supported by experimental and computational studies,[34] as well as isolation of the catalyst precursors $(dtbpy)Ir(Bpin)_3$,[35] $(dippe)Ir(Bpin)_3$ and $(dcpe)Ir(Bpin)_3$.[36]

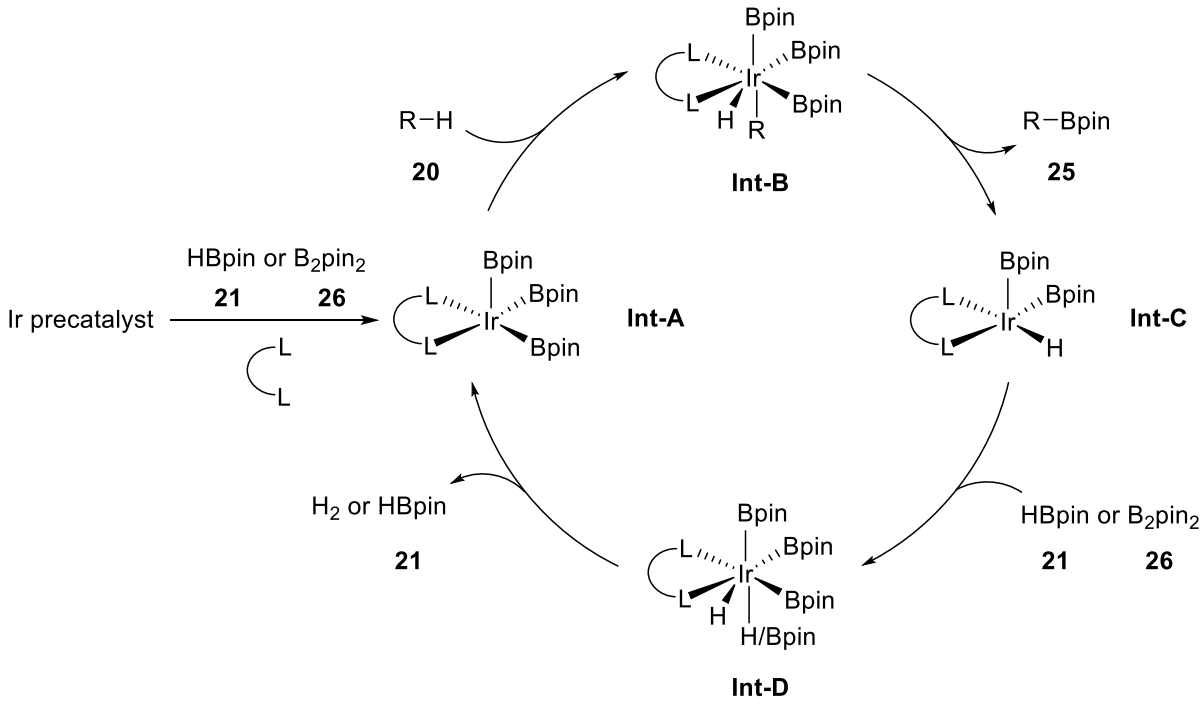

Scheme 7. General mechanism for Ir-catalysed borylation of arenes operating by an Ir^{III}/Ir^{V} redox couple.

1.3 The Bonding Modes of Hydroboranes to Transition Metal Centres

The activation of a B–H bond by a transition metal complex is a key step in catalytic processes such as the borylation of C–H bonds and the hydroboration of unsaturated organic molecules. As such, the synthesis and study of boron-hydride complexes is an area of growing interest where the boron fragment bears alkoxy or alkyl substituents. Transition metals most commonly exist as electrophiles, or Lewis acids, and therefore the formation of bonds between transition metals and ligands of poorly nucleophilic, Lewis acidic donor atoms such as boron has traditionally been viewed as challenging. While, transition metal bonds to p-block elements have been known since the 1800s, transition metal–boron bonds were first proposed in 1963,[37] and the first structurally confirmed complexes that exhibited TM–B interactions were not reported until 1990.[38-39] Early examples were limited in scope due to a lack of synthetic routes for the preparation of these complexes, relying on the salt elimination reactions of anionic metal salts (Scheme 8A) or oxidative addition of electrophilic boron reagents such as haloboranes to electron-rich, low oxidation-state complexes (Scheme 8B).[40]

A) anionic metal salts

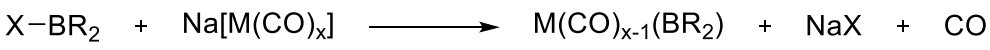

B) low oxidation state transition metal complexes

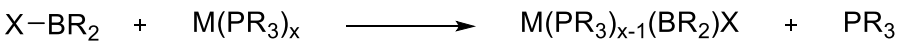

Scheme 8. Early methods to synthesise transition metal boryl complexes.

These reactions led to the formation of complexes that incorporate a two-centre, two-electron TM–B single bond with two additional substituents on the boron atom; ligands of this type are classified as boryl ligands. The pair of electrons involved in ligand-to-metal σ-bonding occupy a formally sp^2-hybridised orbital on the boron atom. This boron atom also possesses an empty p-orbital which can have a π-interaction with the electron-rich metal centre (Figure 1). This interaction is generally considered to be weak, especially when the substituents on boron are π-rich alkoxy (B–OR) or amido (B–NR_2) but can still be significant when rationalising the reactivity of transition metal boryl complexes. Due to the electropositive nature of boron, boryl ligands have a very strong *trans* influence. DFT calculations of a series of platinum(II) boryl complexes show that the *trans* influence of a –Bpin ligand is weaker than a –$SiMe_3$ ligand but stronger than an –alkyl or –H ligand; the greater the p-character of the sp^2-hybridised orbital, the stronger the σ-donor ability and the greater the *trans* influence of the boryl ligand.[41]

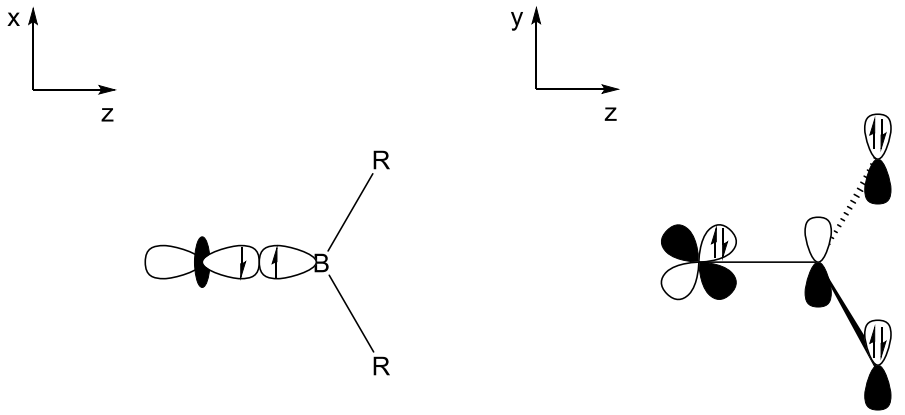

Figure 1. Orbital description of the transition metal-boryl bond – σ donor and π acceptor properties of the boryl ligand.

In more recent years, the most common synthetic route to transition metal boryl complexes is by the oxidative addition of hydroboranes (H–BR_2) or diboranes (R_2B–BR_2) to a transition metal compound.[42-44] This typically involves the use of a low oxidation-state metal precursor with labile ligands that can readily dissociate to form a coordinatively unsaturated, reactive intermediate. Cleavage of the H–BR_2 bond and coordination to a transition metal would form a hydride-boryl species, where the hydride ligand would be defined as a classical hydride. However, this is only one mode of coordination of an H–BR_2 ligand and can be considered an extreme example where the H–BR_2 bond is completely ruptured. The first step of the cleavage of the H–BR_2 bond is coordination to the unsaturated transition metal centre to form a M(η^2-H–BR_2) σ-complex. The bonding description of σ-coordination of a hydroborane is reminiscent of the Chatt-Dewar-Duncanson model for olefin coordination (Figure 2). This involves σ-donation from the σ_{BH} orbital to an empty d-orbital of the metal centre and back-donation from the metal to the antibonding σ^*_{BH} orbital of the H–B bond. The σ-borane ligand is typically described as a three-centre, two-electron bond which is formed without significantly altering the structure of the ligand apart from H–B bond elongation. As discussed previously, boranes have an unoccupied p-orbital on boron, which means that there is an additional interaction in the σ-borane complex due to back-donation from the metal to the empty p-orbital. This interaction is highly dependent on the Lewis acidity of the borane, which is determined by the nature of the substituents on boron.

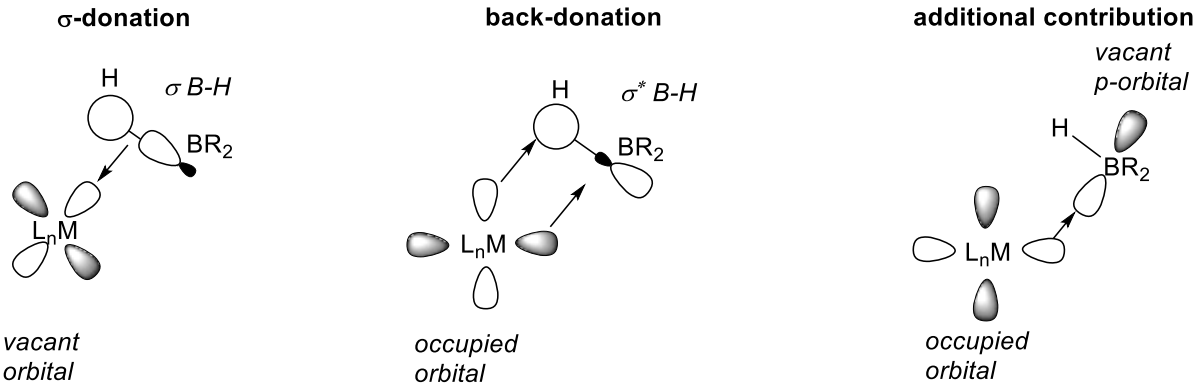

Figure 2. Orbital description of the transition metal σ-borane bond.

In 1996, Hartwig, Eisenstein and co-workers reported the first example of a crystallographically characterised σ-borane complex, $Cp_2Ti(\eta^2\text{-HBcat})_2$ **31**, synthesised through the reaction of HBcat **17** with Cp_2TiMe_2 **30** with evolution of methane **32** and formation of MeBcat **33** (Scheme 9).[45] The solid-state structure of **31** revealed a Ti–B bond length of 2.335(5) Å which is significantly longer than those in the related metallocene boryl

complexes. The B–H distance of 1.25(3) Å is significantly longer than that calculated for free HBcat (1.17 Å),[46] and the Ti–H bond length was 1.74(4) Å which is well within the range of a classical hydride or bridging hydrogen. Computational geometry optimisation of a model structure gave H positions that were in good agreement with the experimental results. The boron atoms are not tetrahedral and lie in a plane with the Ti atom and O atoms of the catecholate ligand. Since this first report, a limited number of related σ-borane complexes have been isolated and characterised.[47-49]

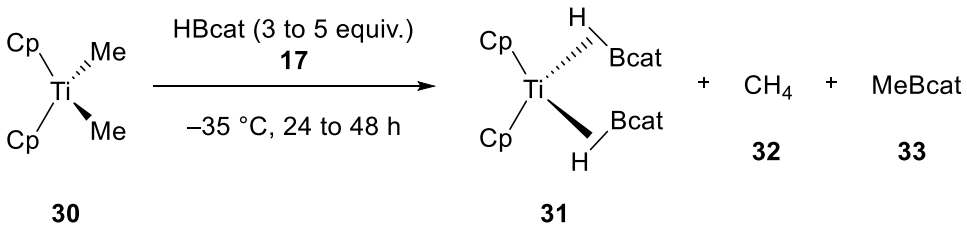

Scheme 9. Synthesis of σ-borane complex **31** from **30**.

1.4 Polyhydride-Borane Complexes

The combination of a H–BR_2 fragment with an $(L)_nMH$ fragment can lead to an even more complex bonding situation. As has been previously discussed, the hydroborane can coordinate to the metal centre as a σ-complex which would result in a hydrido-σ-borane complex, $(L)_nMH(\eta^2\text{-}HBR_2)$. Coordination of the hydride from the M–H bond to the boron atom will lead to the formation of a dihydridoborate ligand, $[H_2BR_2]^-$, which coordinates to the metal through a 3-centre, 3-electron bond $(L)_nM(\kappa^2\text{-}H_2BR_2)$. This motif is commonly observed for hydroboranes with more Lewis acidic boron atoms such as dialkyl boranes. The M–H interaction with the boron p-orbital can also mediate heterolytic cleavage of the H–BR_2 bond which can then undergo oxidation addition to the transition metal centre to form a dihydrido-boryl complex $[(L)_nMH_2(BR_2)]$. For polyhydride complexes the energy barrier for interconversion between these structures is low, which enables rapid interconversion at room temperature and sets up a dynamic equilibrium between these structures (Figure 3).

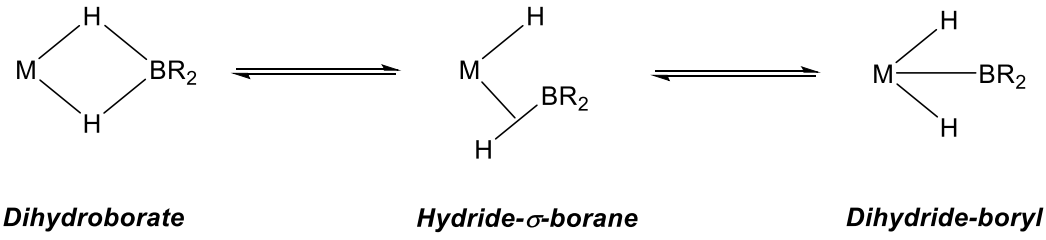

Figure 3. Bonding continuum for hydride-borane complexes.

This rapid interconversion can make structural determination of these complexes challenging using conventional analytical techniques. If the hydrides are rapidly equilibrating on the NMR time scale, then a single resonance will be observed in the ^{1}H NMR spectrum.[50] Low temperature ^{1}H NMR spectroscopy (−40 to −100 °C) can slow the rate of hydride exchange and decoalesce this single resonance into multiple resonances corresponding to each discrete hydride environment.[51] Furthermore, ^{11}B NMR spectroscopy can be a powerful technique for determining the borane bonding mode in these types of complexes.[43] Three-coordinate boryl ligands with alkoxy substituents (e.g. Bpin and Bcat) typically have higher frequency ^{11}B NMR resonances between δ 30 to 70 ppm whereas four-coordinate boron ligands, such as dihydroborates, have lower frequency ^{11}B NMR resonances. Resonances corresponding to σ-boranes lie somewhere between these two extremes, usually closer to boryl resonances, and the observed chemical shift of these resonances is the result of several contributing factors. It can often be difficult to distinguish between boryl and σ-borane resonance based on ^{11}B NMR spectroscopy alone, in these cases ^{1}H-^{11}B HMBC experiments may be used to distinguish between the two bonding modes although any correlation, or lack of, cannot be considered definitive. Structural determination becomes even more challenging when there are multiple boron-centred ligands in the structure with different bonding modes, which can lead to an ^{11}B NMR resonance that is an average of several environments.

The most powerful technique for structural determination is single-crystal X-ray diffraction. The interatomic distance between the transition metal and the boron atom can be used to differentiate between potential bonding modes. M–B distances in boryl complexes are significantly shorter than those in dihydroborate complexes, while those in σ-borane complexes are typically elongated compared to the boryl analogues. However, there are caveats associated with using this technique in the case of hydrido-borane complexes. Although electron density can be located in regions that are consistent with hydride ligands and refined, these positions can at best be described as approximate and can prevent definitive characterisation of B–H/M–H interactions. DFT geometry optimisation of the X-ray coordinates can provide a more reliable representation of the structures of hydride-borane complexes. Neutron diffraction is the most powerful tool for hydrogen location in transition metal hydrides, but high-quality, large single crystals are required and crystalline compounds that are unstable to oxygen, moisture or temperature may not be amenable to this technique.

1.4.1 Group 5 Complexes

Hartwig and De Gala reported the reaction of Cp_2NbH_3 **34** with HBcat **17** and H-9-BBN **36** to form *endo*-Cp_2NbH_2(Bcat) **35** and $Cp_2Nb(H_2$-9-BBN) **37** respectively, with loss of H_2 (Scheme 10A).[52] As expected, **37** adopts a dihydroborate structure, due to the higher Lewis acidity of BBN, which was confirmed by single-crystal X-ray crystallography, ^{1}H and ^{11}B NMR spectroscopy. Complex **35** was shown to rapidly interconvert between dihydroborate and dihydride-boryl structures at room temperature. The solid-state structure of **35** showed a Nb–B distance of 2.292(5) Å which is significantly shorter than the distances of d^0 metallocene dihydroborate complexes and closer to related boryl complexes. Although the hydride positions in this structure are approximate, the B–H distances are 0.4–0.5 Å longer than related d^0 metallocene dihydroborate complexes. The ^{11}B NMR spectrum of **35** displayed a resonance at δ 57 ppm which is similar or downfield to related boryl complexes. This suggests that **35** is more boryl in character than dihydroborate and that the complex has only weak B–H interactions, meaning that **35** is best described as a d^0 Nb(V) boryl complex. The related mono-hydride compound $Cp_2NbH(Bcat)_2$ **39** was synthesised as a minor product in the reaction of HBcat with $Cp_2NbH(CH_2$=CHMe) **38** by Smith and co-workers (Scheme 10B).[53] The ^{11}B NMR spectrum showed two resonances at δ 65 and δ 60 ppm, and two chemically distinct catecholate resonances were observed in the ^{1}H NMR spectrum. Selective ^{1}H{^{11}B} decoupling experiments showed that the hydride is coupled to the boron resonance at δ 60 ppm. This would suggest that one of the Bcat ligands exists as a boryl ligand in an *exo* position, and that the second Bcat ligand is in the *endo* position and is either a boryl with a weak hydride interaction or a σ-borane. The solid-state structure of **39** showed that the Nb centre lies on a C_2 axis and that the chemically inequivalent BCat groups are symmetry related with a Nb–B distance of 2.29(1). The hydrides could not be located due to poor crystal quality.

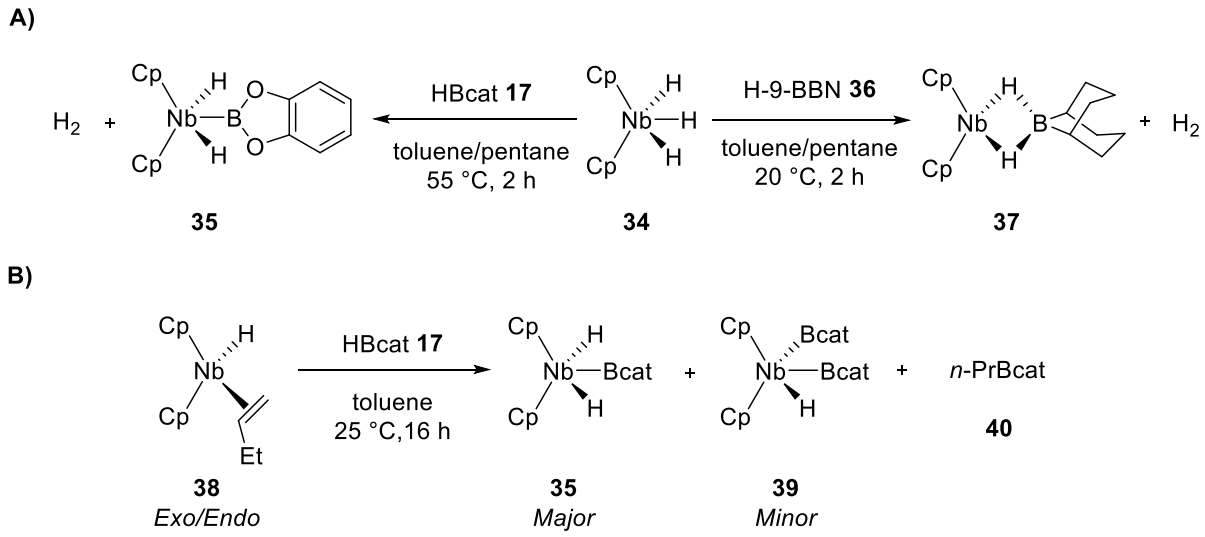

Scheme 10. A) Reaction of niobocene hydride **34** with hydroboranes **17** and **36** to produce **35** and **37** (B) Reaction of **38** with HBcat to form boryl complexes **35** and **39**.

Smith and co-workers synthesised the related $Cp^*_2Nb(H_2Bcat`)$ **43** complex (Bcat` = $BO_2C_6H_3$-3-^{t}Bu) (Scheme 11) in which the boron ligands have increased steric bulk compared to **35** which has a significant effect on the bonding of the H_2BR_2 fragment.[54] Most notably, the Nb–B distance of **43** is 2.348(4) Å, and is elongated compared to **35** suggesting dihydroborate character. The hydride positions were located in the difference Fourier map using low-angle data ($4 < 2\theta < 30$) and the H–Nb–H angle of 58(3)° closely resembles that of other structurally characterised Nb dihydroborate complexes. This suggests that **43** exists as Nb(III) dihydroborate complex and is illustrative of how changes in steric demand of the ligands can change the bonding mode of the borane ligand.

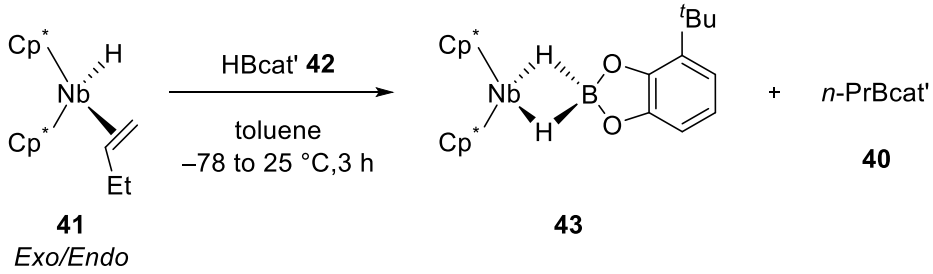

Scheme 11. Steric effects of ligands on borane binding in niobocene complex **43**.

Smith also prepared the related Ta borane complexes $Cp_2TaH_2(Bcat)$ through the reaction of $[Cp_2TaH_2Li]_x$ with ClBcat **45**; *endo* and *exo* isomers were separated by fractional crystallisation from toluene.[53] The *endo* isomer displayed a single hydride resonance in the ^{1}H NMR spectrum that integrates to two protons whereas the *exo* isomer has two hydride

resonances – a doublet at δ −4.20 ppm and a broad signal at δ −5.15 ppm which resolved to a doublet upon ^{11}B decoupling. The solid-state structures of the two isomers revealed similar Ta–B distances of 2.263(6) Å for *exo* and 2.296(11) Å for *endo*, which compare well with the Nb–B distance for **25**. For the *endo* isomer structure, the B–H distances are 1.75(5) Å and 2.11(6) Å which rules out dihydroborate bonding for this complex. While quantitative analysis of the hydride positions in the *exo* isomer structure was not possible, the B–H$_{endo}$ distance appears to be significantly shorter than the distances in the *endo* isomer. These data suggest that the *endo* isomer is best described as a Ta^{V} boryl complex but there is some ambiguity over the bonding mode in the *exo* isomer. The authors proposed a similar Ta^{V} boryl complex but, given the B–H interaction observed by NMR spectroscopy and the lack of qualitative analysis of B–H/Ta–H distances, a Ta^{III} σ-borane complex could not be discounted.

1.4.2 Group 6 Complexes

Hartwig and De Gala also reported the synthesis of the tungstenocene boryl complex, $Cp_2WH(Bcat)$ **46**, from the reaction of $[Cp_2W(H)Li]_4$ **44** and ClBcat **45** (Scheme 12).[55] The solid-state structure of **46** showed a W–B bond distance of 2.190(7) Å and a relatively long B–H distance which suggests that this is a hydrido-boryl complex. The ^{11}B NMR resonance of δ 57 ppm supported the assignment as a W^{IV} boryl. The related diboryl compound $Cp_2W(Bcat`)_2$ was synthesised by irradiation of $Cp_2WH_2$ in the presence of $B_2cat`_2$. Direct comparison of $Cp_2W(Bcat`)_2$ and **46** showed that the ^{11}B NMR resonances and W–B bond distances are similar in both complexes, lending further support to the W^{IV} boryl assignment of **46**.

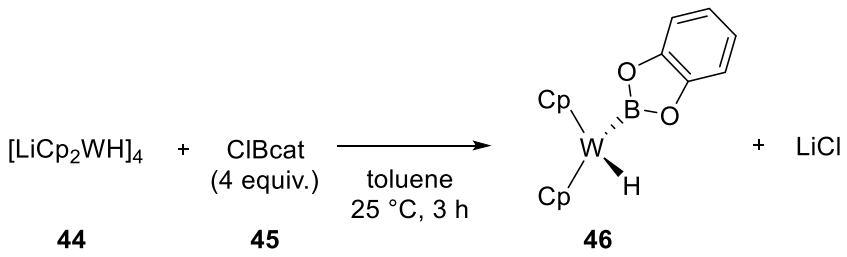

Scheme 12. Synthesis of the tungsten hydridoboryl complex **46** by salt elimination.

While investigating the mechanism of the catalytic hydroboration of nitriles by $(ArN)Mo(H)_2(PMe_3)_3$ **47** Nikonov and co-workers synthesised relevant intermediates bearing boron-centred ligands (Scheme 13).[56] The reaction of **47** with HBpin **21** produced the

dihydroborate complex (ArN)Mo(H_2BPin)(H)(PMe_3)$_3$ **48**, however the analogous reaction with HBcat **17** formed the agostic borane complex Mo(H)$_2$(PMe_3)$_3$(η^3-NAr-HBcat) **49**. Both complexes were unstable in solution and after 16 h at room temperature degraded to form $MoH_4(PMe_3)_4$ **50**.

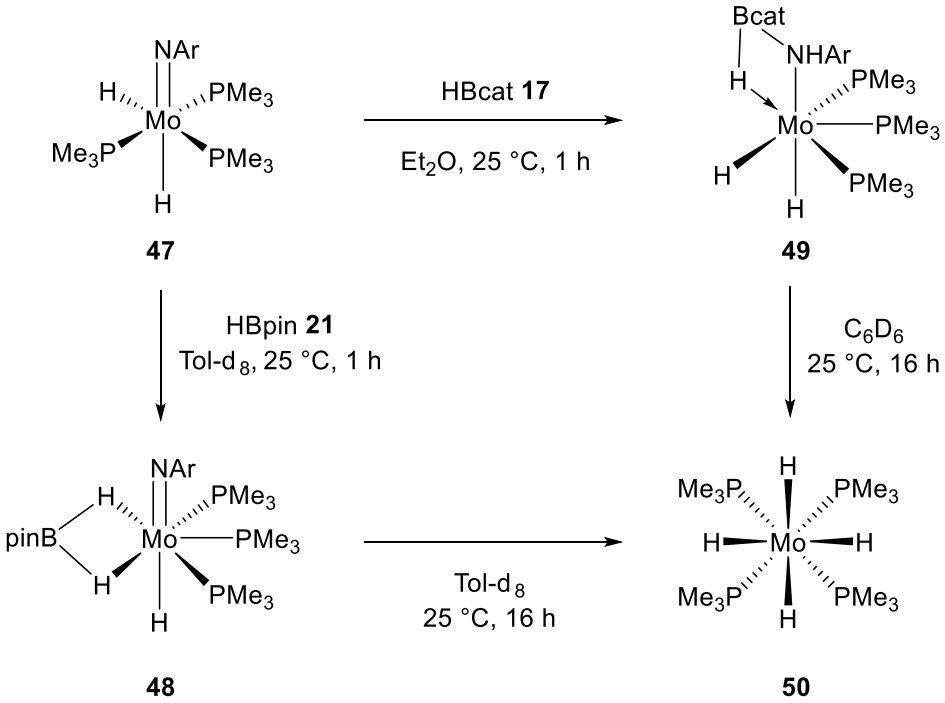

Scheme 13. Reaction of HBpin **21** and HBcat **17** with **47** to form **48** or **49** followed by decomposition to **50**.

1.4.3 Group 8 Complexes

The reaction of hydroboranes with Ru polyhydride complexes has been explored by Sabo-Etienne. The reaction of $RuH_2(\eta^2\text{-}H_2)_2(PCy_3)_2$ **51** with an excess of HBpin **21** resulted in evolution of two equivalents of H_2 and formation of $RuH(H_2Bpin)(HBpin)(PCy_3)_2$ **52** (Scheme 14A).[57] The solid-sate structure showed that the Ru atom adopts a pseudo-octahedral environment, with one Bpin unit bound as a dihydroborate ligand (Ru–B = 2.188(5) Å) and the other as a σ-borane ligand (Ru–B = 2.157(5) Å). In the ^{1}H NMR spectrum at 233 K three hydride resonances were observed in a 2:1:1 ratio. A dihydrogen ligand was ruled out based on relatively large T_{1min} values for all three resonances (~100 ms at 300 MHz). A very broad signal at δ 37 ppm corresponds to an averaged chemical shift for both B environments at room temperature. The reaction of **51** with 1 equivalent of HBpin **21** resulted in an equilibrium between **51** and $RuH_2(\eta^2\text{-}H_2)(HBpin)(PCy_3)_2$ **53** (Scheme 14B), the

latter of which was shown to be an intermediate to the formation of **52**.[58] X-ray crystallography and computational geometry optimisation of **53** showed that the HBpin ligand is a σ-borane and that the σ-H_2 ligand was bound perpendicular to the equatorial plane. The presence of σ-H_2 ligand was supported by its T_{1min} value of 40 ms at 253 K (300 MHz). The analogous HBcat σ-borane complex and H-9-BBN dihydroborate complex were also synthesised and characterised.

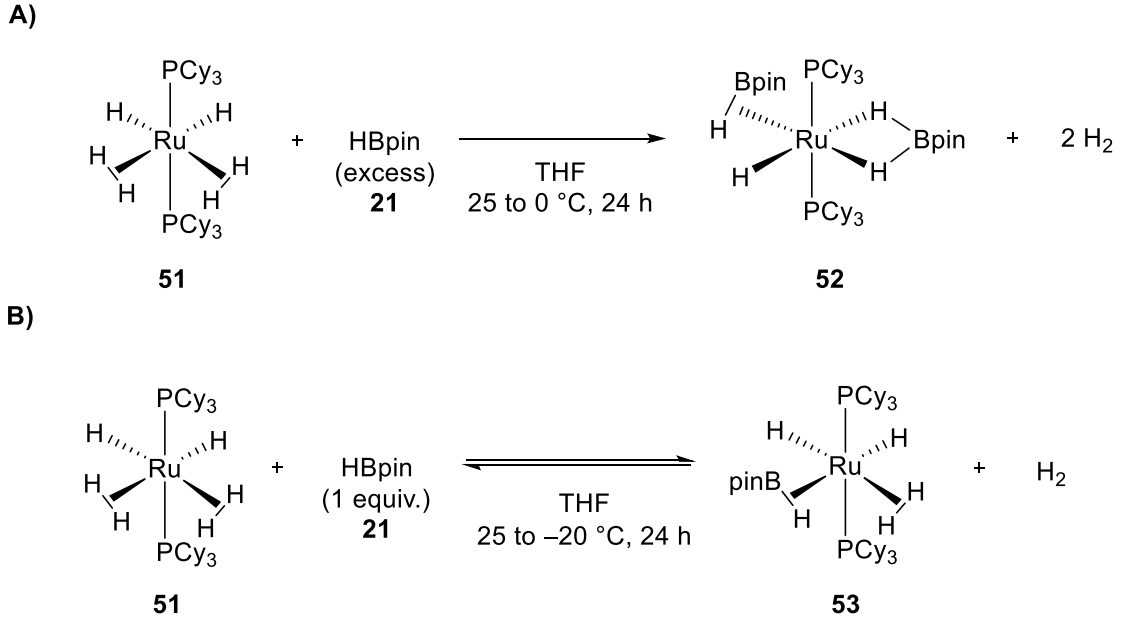

Scheme 14. Selective synthesis of σ-HBpin complexes **52** and **53** controlled by stoichiometry of HBpin **21**.

Complex **51** also reacted with monosubstituted boranes (H_2BR) through displacement of the labile σ-H_2 ligands. The complex $RuH_2(H_2BMes)(PCy_3)_2$ **55** was synthesised either through the reaction of **51** with an equivalent of H_2BMes **54**, or from $RuHCl(\eta^2\text{-}H_2)_2(PCy_3)_2$ **57** and [Li][H_3BMes] **56** (Scheme 15A).[59] This complex was the first example of a borane bound to a transition metal through two σ-B–H bonds, the assignment of which was confirmed by a unusually short Ru–B distance (1.938(4) Å) and a high frequency resonance in the ^{11}B NMR spectrum. Interestingly, the borylene complex $RuHCl(BMes)(PCy_3)_2$ **59** can be formed from the reaction of **58** with H_2BMes **54** followed by removal of H_2 under vacuum (Scheme 15B).[60] In this case, the ^{11}B NMR spectrum showed a broad resonance at δ 106 ppm which is characteristic of a two-coordinate boron atom,[61-62] and the presence of the borylene ligand was confirmed by X-ray crystallography. When a solution of this complex is pressurised

under an atmosphere of H_2 the M=B bond was cleaved to form $RuHCl(H_2BMes)(PCy_3)_2$ **59** which is in equilibrium with $RuHCl(\eta^2\text{-}H_2)_2(PCy_3)_2$.

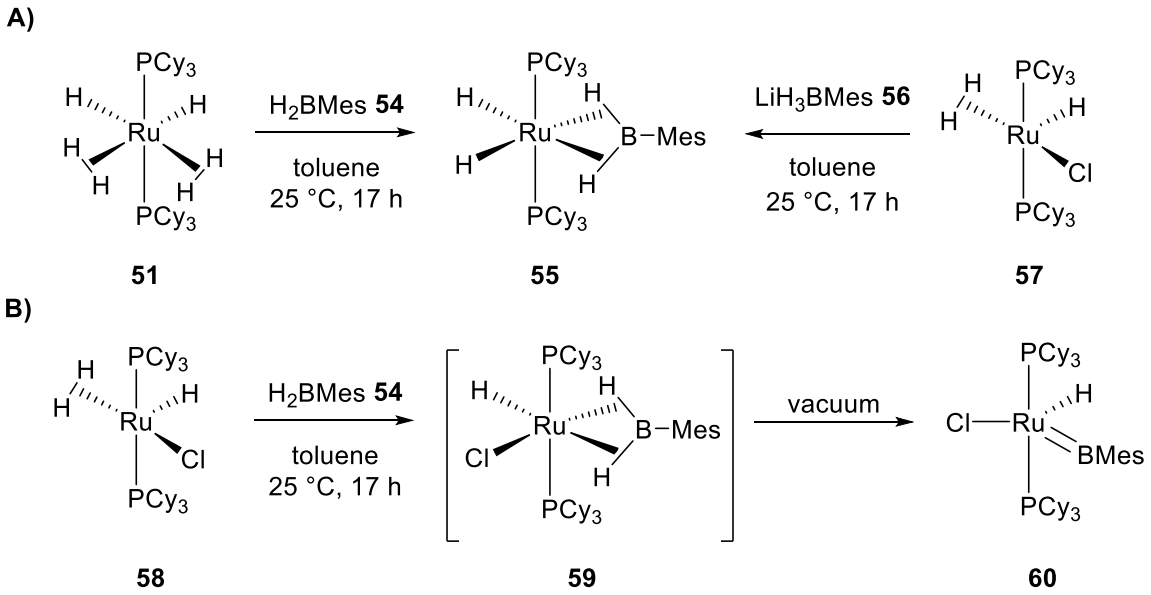

Scheme 15. A) Synthesis of bis-σ-borane complex **55** (B) synthesis of borylene complex **60**.

Esteruelas and co-workers have explored the rich and diverse reactivity of high oxidation-state Os hydride complexes with boranes. $OsH_2Cl_2(P^iPr_3)_2$ **61** can eliminate HCl to form the 14-electron complex $OsHCl(P^iPr_3)_2$ which can abstract a hydride from HBpin **21** and promote ring opening of the pinacol backbone of a second HBpin **21** equivalent to form a σ-borinium complex $OsH_2Cl(HB(Bpin_2))(P^iPr_3)_2$ **62** (Scheme 16).[63] This bonding was supported by X-ray diffraction analysis showing a short Os–B distance of 1.899(7) Å and a single B–H bond of 1.32(5) Å. The presence of three distinct hydride environments was confirmed by three high field resonances in the ^1H NMR spectrum; the ^{11}B NMR spectrum showed a resonance at δ 55 ppm (borinium) and δ 33 ppm (borate).

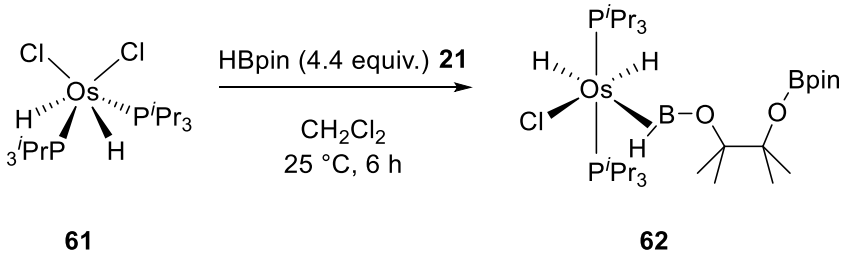

Scheme 16. Synthetic routes to the borinium complex **62**.

However, when $OsH_2(CH_2{=}CHEt)(CO)(P^iPr_3)_2$ **63** was used as a starting material for borane coordination different reactivity was observed (Scheme 17).[64] This compound readily dissociates $CH_2{=}CHEt$ at room temperature and HBpin **21** or HBcat **17** bind as σ-borane ligands to form complexes of the form $OsH_2(\sigma\text{-}HBR_2)(CO)(P^iPr_3)_2$ **64**. $OsH_2(\sigma\text{-}HBpin)(CO)(P^iPr_3)_2$ **64b** underwent borane exchange with HBcat **17** to form $OsH_2(\sigma\text{-}HBcat)(CO)(P^iPr_3)_2$ **64a**, which suggests that the HBcat complex is more stable than the HBpin complex. This can be rationalised by considering the relative ease of π-back-donation from Os to the empty B p-orbital in both complexes; this interaction is competing with π-donation from the oxygen atoms on the boron substituent which is weaker for Bcat as the O electron density in the catecholate is delocalised in the aromatic ring. In the case of **64a**, the addition of a second equivalent of HBcat **17** led to the formation of a boryl-dihydroborate complex **65**. The bonding was supported by X-ray crystallographic analysis with an Os–B distance of 2.244(3) Å for the dihydroborate and an Os–B distance of 2.076(3) Å for the boryl. Two distinct boron environments at 183 K, which appeared at δ 47 ppm (OsBcat) and δ 29 ppm (H_2Bcat), were observed in the ^{11}B NMR spectrum. The hydrides and Bcat units rapidly exchanged on the NMR time scale at room temperature.

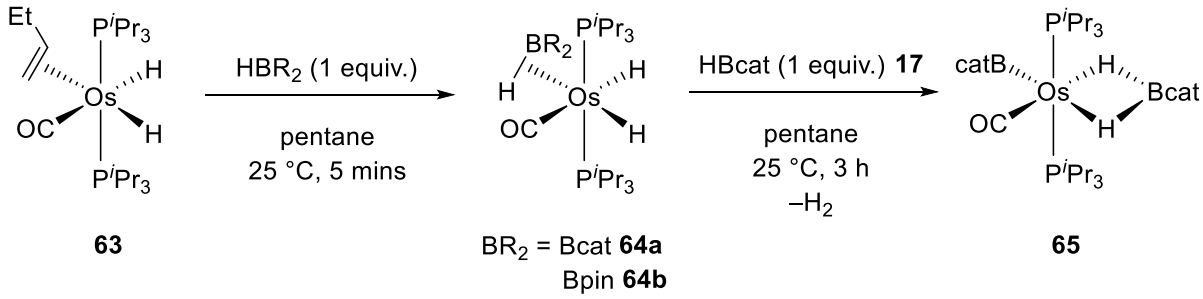

Scheme 17. Synthesis of **64** and **65** by sequential addition of HBcat.

Different reactivity was observed once again when the polyhydride complex $OsH_6(P^iPr_3)_2$ **66** was used as the starting material, where reductive elimination of an equivalent of H_2 enables coordination of borane ligands (Scheme 18).[65] The reaction of **66** with either H-9-BBN **36** or HBpin **21** led to the formation of the dihydroborate complexes $OsH_4(H_2BR_2)(P^iPr_3)_2$ **67**. The hydrides rapidly exchanged at room temperature for both complexes on the NMR time scale, and for $OsH_4(H_2Bpin)(P^iPr_3)_2$ **67b** no decoalescence of NMR signals was observed, even at 183 K. In the case of HBcat **17**, complex **66** reacted with two equivalents of borane to produce an (elongated σ-borane)-{bis(elongated σ)-dihydridoborate}complex **68** *via* an isolable dihydroborate intermediate **67a** (Scheme 9). The η^3-coordination of the

dihydridoborate ligand is an unusual bonding mode that displays two sets of Os–H and B–H bonding interactions, as well as an Os–B interaction. The assignment of this bonding mode was based on X-ray crystallographic analysis that showed a relatively short Os–B bond (2.159(4) Å) which is comparable to Os-boryl distances and is shorter than related Os-dihydroborate distances. This was compounded by relatively short B–H distances (1.58(3) and 1.40(3) Å), which confirms the presence of B–H bonds. Computational AIM analysis showed both Os–H and B–H bond critical points as well as an Os–B bond critical point. This suggests that the H_2Bcat fragment is bound through two σ-B–H bonds to give an Os^{II} species.

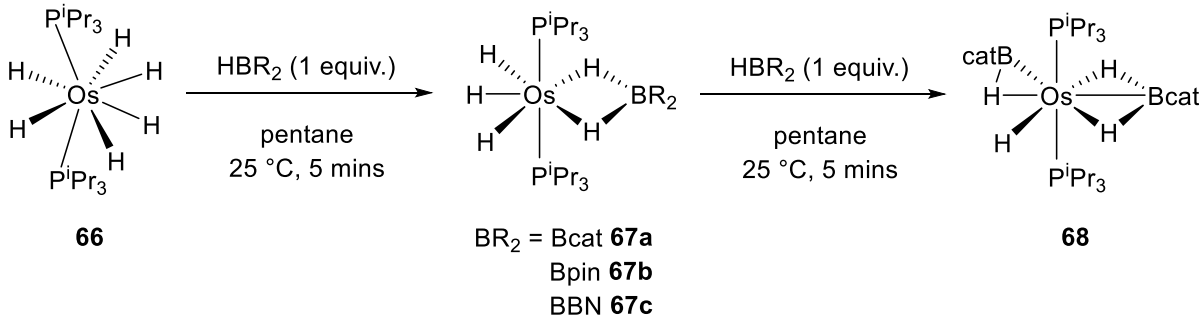

Scheme 18. Synthesis of dihydroborate complexes **67** and (elongated σ-borane)-{bis(elongated σ)-dihydridoborate}complex **68**.

The reactivity of these complexes was tuned further by moving away from simple monophosphine ancillary ligands to POP pincer and NHC ligands. The Os complex [OsCl(η^6-*p*-cymene)(IPr)]OTf **69** of the IPr NHC ligand reacted with HBpin or HBcat to initially form [OsHCl(BR$_2$)(η^6-*p*-cymene)(IPr)]OTf which rapidly undergoes reductive elimination of ClBR$_2$ to form [OsH(η^6-*p*-cymene)(IPr)]OTf; this latter complex reacted with a second equivalent of borane to finally produce dihydridoboryl complexes of the form [OsH$_2$(BR$_2$)(η^6-*p*-cymene)(IPr)]OTf **70** (Scheme 19A).[66] The Bpin complex **70b** was crystallised and analysed by X-ray crystallography, showing a relatively short Os–B distance (2.11(1) Å) and long B–H distances (2.08(5) and 2.09(5) Å), therefore precluding σ-borane or dihydroborate bonding. The use of the pincer ligand xant(P^{i}Pr$_2$)$_2$ (9,9-dimethyl-4,5-bis(di*iso*propylphosphine)xanthene) enabled access to Os^{II} complexes with elongated σ-borane ligands **74** by the reaction of *in situ* formed [OsH$_2$Cl(xant(P^{i}Pr$_2$)$_2$)]BF$_4$ **73** with HBcat **17** or HBpin **21** (Scheme 19B).[67] These complexes were characterised by X-ray crystallography, NMR spectroscopy and computational methods (AIM analysis and NBO analysis).

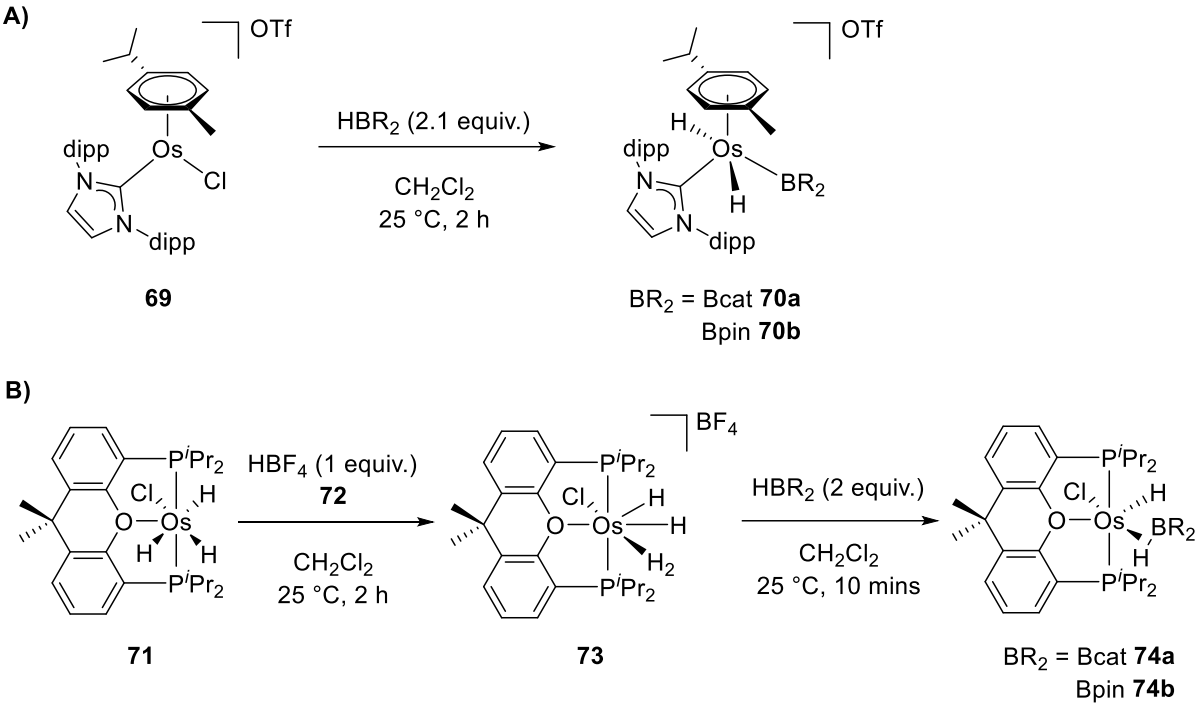

Scheme 19. A) Synthesis of NHC-ligated dihydridoboryl complexes **70** (B) Synthesis of xant(P^iPr_2)$_2$-ligated σ-borane complexes **74**.

1.4.4 Group 9 Complexes

Chirik and co-workers isolated and characterised catalytically relevant Co intermediates formed in the C–H borylation of arenes (Scheme 20).[20-21] The reaction of the Co^I pincer complex (^{iPr}PNP)Co(CH_2SiMe_3) **75** with two equivalents of HBpin **21** resulted in the loss of Me_3SiCH_2Bpin **77** and formation of *trans*-(^{iPr}PNP)CoH_2(Bpin) **76**. This assignment was supported by a single hydride resonance in the ^{1}H NMR spectrum and a resonance at δ 41 ppm in the ^{11}B NMR spectrum for the boryl ligand. X-ray crystallographic analysis provided definitive structural evidence of the *trans* dihydride isomer. This complex was proposed to be a catalyst resting state and readily undergoes reductive elimination of HBpin to enable catalyst turnover.

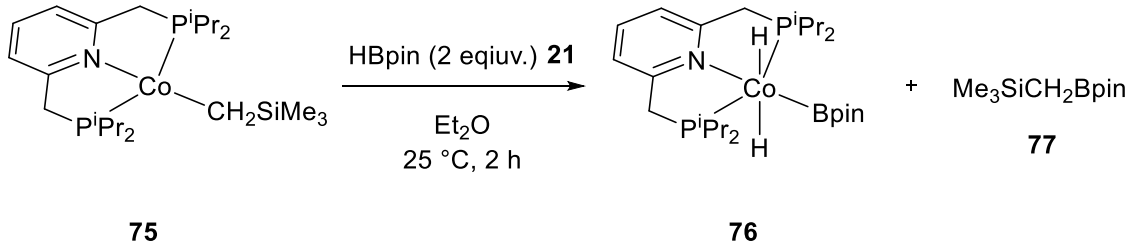

Scheme 20. Oxidative functionalisation of **75** to form dihydridoboryl complex **76**.

Building on the examples of niobium, tantalum, and tungsten metallocene complexes, Hartwig and co-workers synthesised a series of Rh boryl hydride metallocene complexes (Scheme 21). The reaction of $Cp^*RhH_2(SiEt_3)_2$ **78** with excess HBpin **21** at 90 °C or under photoirradiation formed the boryl complex $Cp^*RhH_2(SiEt_3)(Bpin)$ **79**.[68] The solid-state structure showed that the boryl and silyl ligands are mutually *trans* in a four-legged piano stool geometry. In this complex there is the possibility for B–H, H–H and Si–H bonding. The positions of the hydride atoms in the solid-state structure suggested partial B–H bonding, with one hydride 1.74(4) Å from the boron atom. This was supported by a small, scalar coupling between the hydrides and the boron atom in the ^{1}H NMR spectrum, with the two hydride positions averaged on the NMR time scale. Upon addition of P(*p*-tol)$_3$ the major product was $Cp^*RhH(SiEt_3)(P(p\text{-tol})_3)$ **81** with dissociation of an equivalent of HBpin **21** instead of H_2 or $HSiEt_3$ **13**.

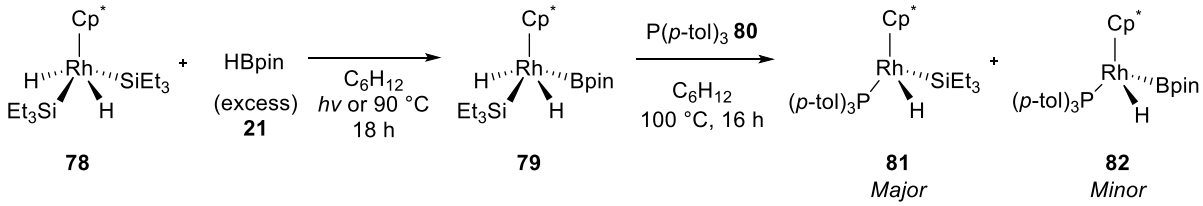

Scheme 21. Silane/borane substitution to form **79** and subsequent reaction with P(*p*-tol)$_3$ **80**.

Similarly, the reaction of $Cp^*Rh(\eta^4\text{-}C_6Me_6)$ **83** with HBpin **21** under photochemical conditions generated $Cp^*RhH_2(Bpin)_2$ **84** which reacted in neat HBpin **21** to form the tris(boryl) complex $Cp^*RhH(Bpin)_3$ **85** and H_2 (Scheme 22A).[69] There are several potential geometries and bonding modes that these complexes can adopt (Scheme 22B and 22C). X-ray crystallographic analysis and the calculated structure of **84** showed a *trans* structure with a significant B–H interaction between each boryl group and a *cis* hydride. Similarly, for **85** the hydride is positioned significantly closer to one boryl over the other two. These complexes could either be described as $Rh^{I/III}$ with σ-HBpin ligands or Rh^V with hydride and boryl ligands. Both complexes reacted with PEt_3 in a similar fashion to **79** to form the relevant phosphine-coordinated complex with elimination of HBpin.

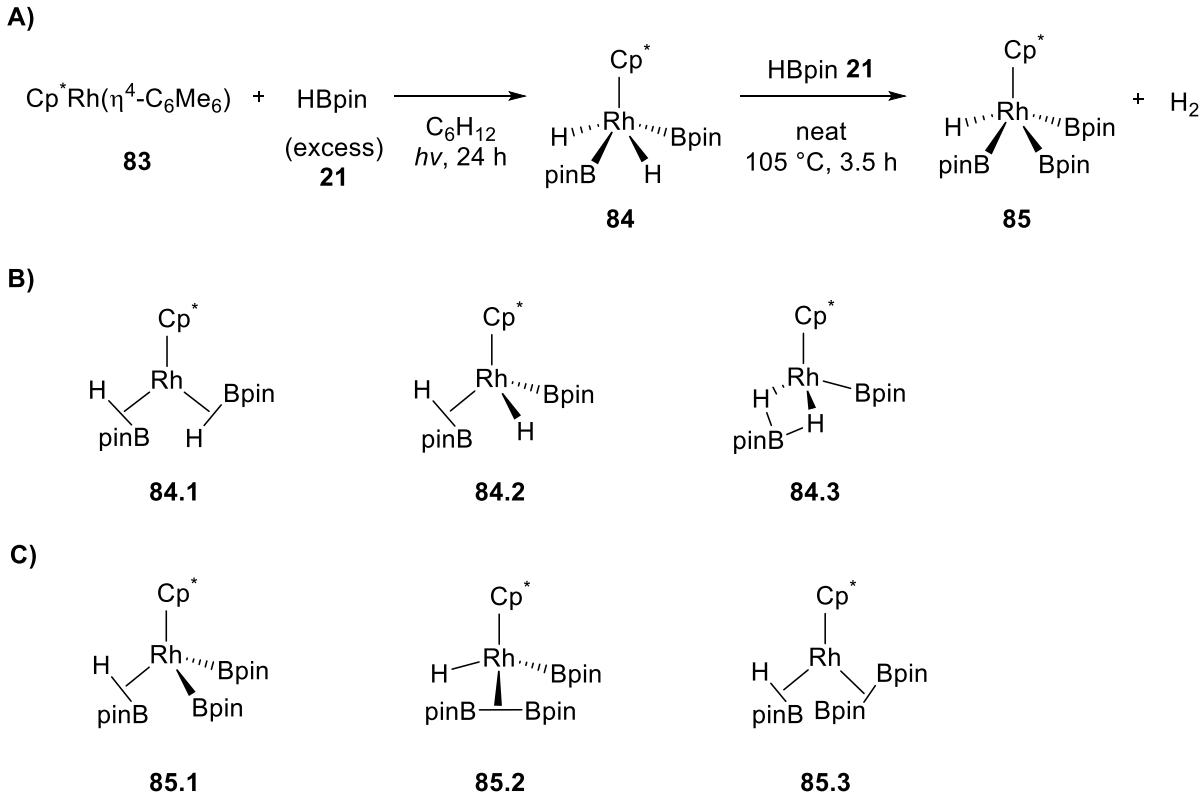

Scheme 22. A) Synthesis of **84** and **85** by sequential addition of HBpin (B) alternative possible bonding modes of **84** (C) alternative possible bonding modes of **85**.

Budzelaar and co-workers reported the synthesis of hydrido borane complexes bearing a β-diketiminate ligand (^{Me}BDI) (Scheme 23).[70] (^{Me}BDI)Rh(COE) **86** was generated *in situ* from $[Rh(COE)_2Cl]_2$ and (^{Me}BDI)Li(THF) which was then reacted with 3 equivalents of HBpin **21** to form (^{Me}BDI)Rh(HBpin)$_2$ **87**. This solid-state structure of this complex showed one short B–H contact per boron atom with no distinction between σ-HBpin and hydrido boryl bonding modes. The mixed-ligand complex (^{Me}BDI)Rh($HSiEt_3$)(HBpin) **89** was synthesised by addition of an equivalent of **87** to (^{Me}BDI)Rh($HSiEt_3$)$_2$ **88** whereupon the borane and silane

ligands exchanged. In this complex one hydride ligand was located with a close contact to the boron atom over the silicon atom.

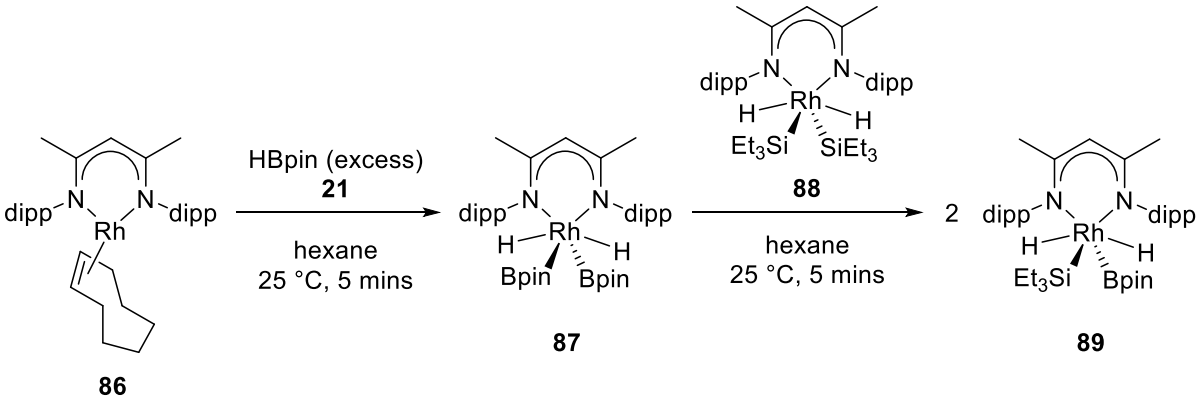

86 87 89

Scheme 23. Reaction of **86** with HBpin to form **87** and subsequent ligand exchange with **88**.

As discussed previously, in the last 20 years Ir complexes have emerged as efficient catalysts for the C–H borylation of organic substrates, and as such a number of Ir hydride borane complexes have been synthesised and studied as intermediates in these catalytic processes. In 1999, Smith and co-workers showed that products of C–H activation, $Cp^*IrH(PMe_3)(R)$, reacted with hydroboranes to form C–B bonds and hydrido boryl complexes (Scheme 24A).[71] The reaction of $Cp^*IrH(PMe_3)(Cy)$ **90** with excess HBpin **21** led to the formation of CyBpin **92**, CyH **93** and $Cp^*IrH(PMe_3)(Bpin)$ **91**. The ^{11}B NMR resonance at δ 33 ppm suggests that complex **91** has significant σ-borane character. Unfortunately, the authors were unable to obtain crystalline material, so the solid-state structure was not determined. Hartwig and co-workers used Cp^*IrH_4 **94** as a precursor to a series of hydride borane complexes, either through the reaction with excess hydroborane or deprotonation with BuLi **95** and subsequent reaction of $[Li][Cp^*IrH_4]$ **96** with haloboranes (Scheme 24B).[72] The complexes, $Cp^*IrH_3(Bpin)$ **97a** and $Cp^*IrH_3(Bcat)$ **97b**, were formulated as hydride boryl complexes based on NMR spectroscopic and X-ray crystallographic analysis. In contrast, $Cp^*IrH_3(BCy_2)$ **97c** was formulated as a dihydroborate complex based on a resonance at δ 72 ppm in the ^{11}B NMR spectrum; however, this is significantly downfield compared to related dihydroborate complexes, which suggests some boryl character. The reaction of **97a** with excess HBpin **21**

produced the diboryl complex **98**, but in this case no single crystals of this complex were obtained and therefore assignment as a boryl species was tentative.

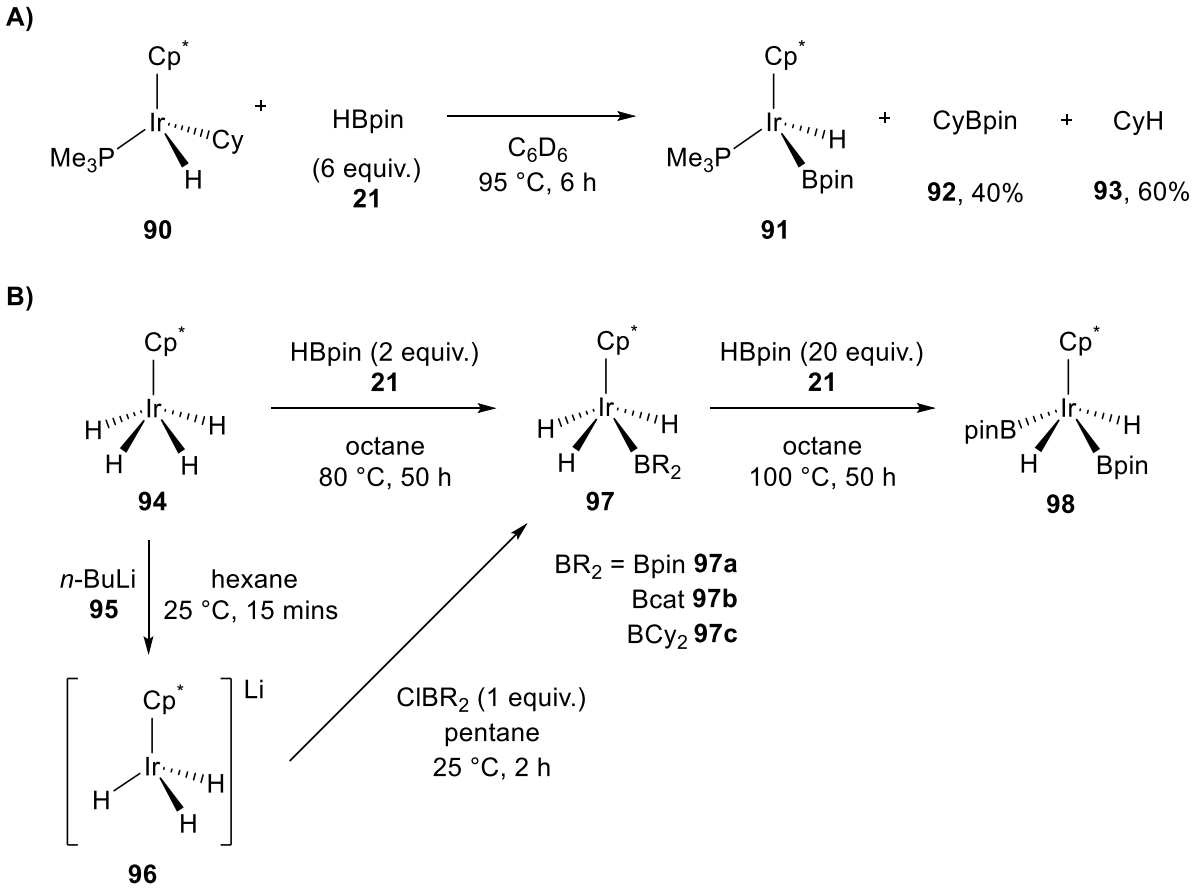

Scheme 24. A) Stoichiometric B–C bond formation and synthesis of **91** (B) Synthesis of Ir boryl and borohydride complexes **97** and **98** from polyhydride precursor **94**.

Smith and Maleczka demonstrated the utility of bis(phosphine) Ir tris(boryl) complexes in C–H borylation catalysis and an in-depth study of the Ir intermediates formed under catalytic conditions showed that a range of hydride borane complexes were operative.[73] Addition of an equivalent of HBpin **21** to (dippe)Ir(Bpin)$_3$ **99** set up an equilibrium between this complex and the borylene complex (dippe)Ir(H)(Bpin)$_2$(BOCMe$_2$CMe$_2$OBpin) **100**, which was formed by ring-opening of the pinacol backbone of HBpin (Scheme 25A). This latter compound displayed three resonances in the ^{11}B NMR spectrum: the resonance for the borate environment at δ 20 ppm; a resonance at δ 39 ppm corresponded to the boryl ligands; the borylene resonance was located downfield at δ 55 ppm. When **99** was subjected to a 10-fold excess of HBpin **21** at −35 °C, the new complex (dippe)IrH$_3$(Bpin$_2$) **101** was formed (Scheme 25B). In the X-ray structure, there are two independent molecules in the unit cell which differ in orientation of the Bpin ligand relative to the phosphines; one isomer is *cis*/*cis* and the other

is *cis*/*trans*. In solution, the Bpin and hydride positions are proposed to be rapidly exchanging at room temperature. These structures were geometry optimised using computational methods, and both isomers are best represented as Ir^{III} dihydridoboryl complexes bearing a σ-borane ligand. The reaction of **99** with H_2 at −45 °C produced (dippe)Ir(η^2-H_2)(Bpin)$_3$ **102** which was not isolated in high analytical purity but was characterised by NMR spectroscopy. The reaction of **101** with H_2 at room temperature produced (dippe)IrH_3(HBpin) **103** and single crystals were obtained (Scheme 25C). Once again, the X-ray coordinates were optimised using computational methods and suggested that the structure is best represented as an Ir^{III} trihydride complex bearing a σ-borane ligand. Further reaction with H_2 led to the formation of a dimeric complex (dippe)IrH_2(μ-H)]$_2$ **104**.

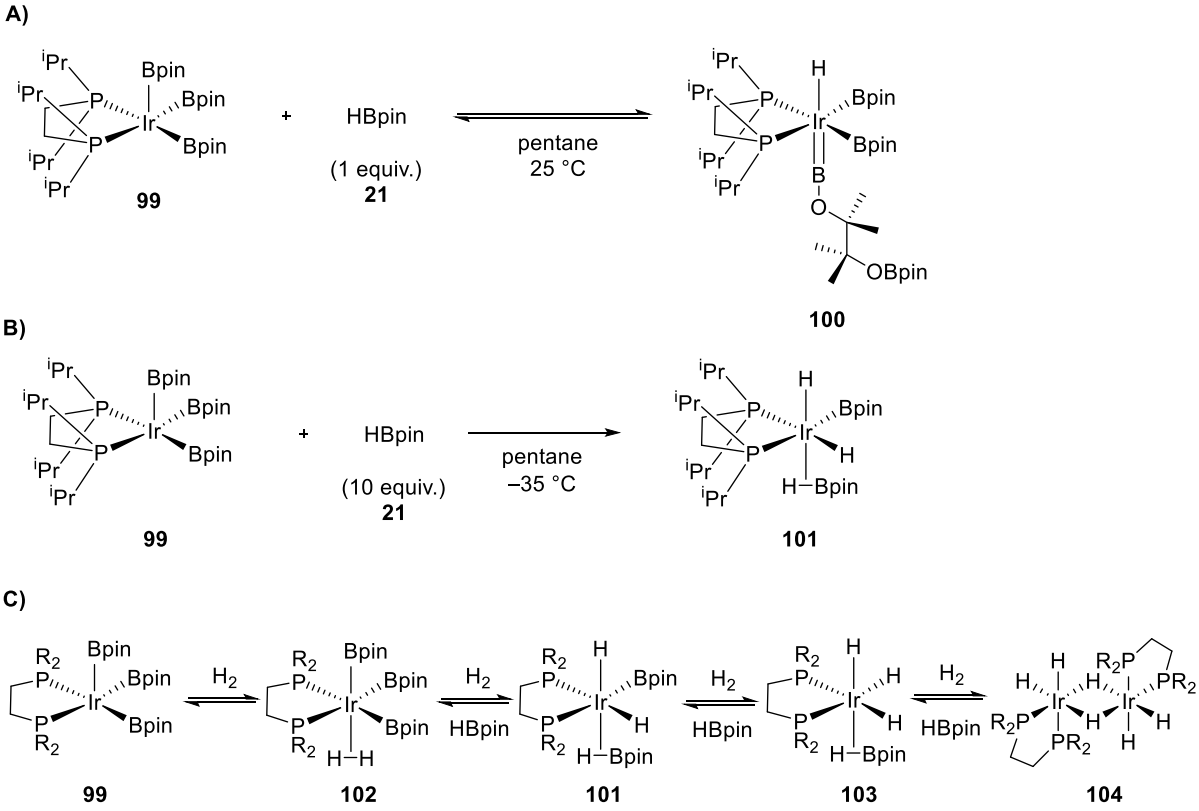

Scheme 25. A) Synthesis of borylene complex **100** (B) Reaction of **99** with 1 equivalent of HBpin **21** (C) Stepwise substitution of HBpin **21** with H_2.

Heinekey and co-workers reported that (^{t}BuPOCOP)IrH_2 **105** reacted with HBpin **21** at 0 °C to initially form (^{t}BuPOCOP)IrH_3(Bpin) **106** which slowly evolved H_2 at room temperature to produce (^{t}BuPOCOP)Ir(HBpin) **107** (Scheme 26).[74] The authors were unable to isolate **106**, and *in situ* characterisation by NMR spectroscopy could not conclusively distinguish between an Ir^v hydrido boryl complex or an Ir^{III} hydride σ-borane complex. The ^{11}B NMR

resonance of δ 37 ppm would suggest that the boron atom has some σ-borane character. The solid-state structure of **107** showed a relatively short Ir–B distance of 2.082(5) Å which suggests that the Bpin ligand has significant boryl character; however, a close B–H distance of 1.61(6) Å led the authors to characterise it as an Ir^{III} hydride σ-borane complex. This was supported by an upfield ^{11}B NMR resonance of δ 29.7 ppm, which is not significantly shifted from the resonance for free HBpin (δ ~28 ppm). Ozerov and co-workers have synthesised and characterised a series of related complexes which match well with the solid-state structures and NMR spectroscopic analysis reported by Heinekey.[75]

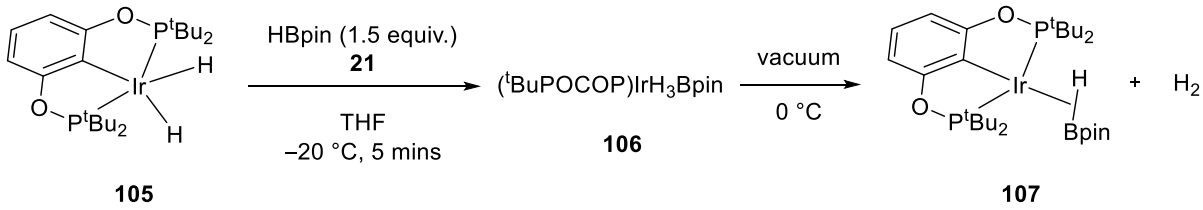

Scheme 26. Synthesis of **106** from dihydride complex **105** and elimination of H_2 under vacuum to form **107**.

Chirik and co-workers synthesised an Ir analogue of the Co complexes previously mentioned to directly compare catalytic activity.[21] The complex (PNP)IrH_2(Bpin) **112** was prepared by reacting $[Ir(COE)_2Cl]_2$ **108** with the PNP ligand **109** and an excess of HBpin **21** followed by reaction of the intermediate with $NaHBEt_3$ **111** (Scheme 27). The solid-state structure showed a short Ir–B distance of 1.923(2) Å and large separations between the hydrides and the B atom (2.25(2) and 2.31(2) Å) which means that **112** is best described as an Ir^{III} dihydride boryl complex.

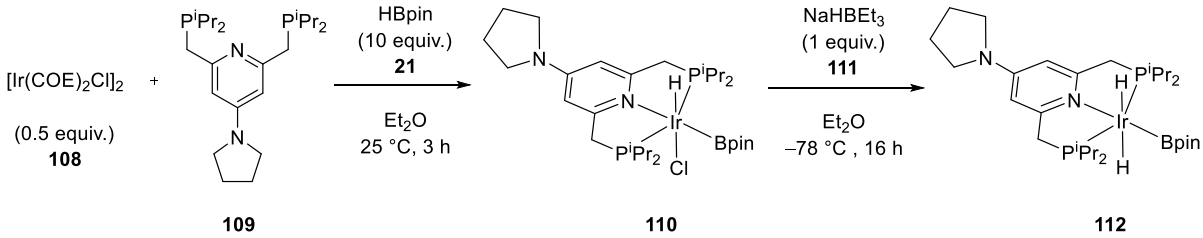

Scheme 27. Synthesis of Ir^{III} dihydridoboryl complex **112**.

Esteruelas and co-workers investigated the use of POP pincer ligands in Ir-catalysed C–H borylation catalysis (Scheme 28).[76] During this investigation they examined the sequential reactivity of $IrH_3\{\kappa^3$-P,O,P-[xant(P^iPr_2)$_2$]} **113** with two equivalents of HBpin **21**. The addition of one equivalent of HBpin **21** led to the formation of the monoboryl complex

$IrH_2(Bpin)\{\kappa^3$-P,O,P-[xant($P^iPr_2)_2$]} **114** and H_2. The solid-state structure of this complex showed an Ir–B distance of 1.994(3) Å and the ^{11}B NMR spectrum showed a resonance broad at δ 34.2 ppm. Addition of a second equivalent of HBpin **21** produced the diboryl complex $IrH(Bpin)_2\{\kappa^3$-P,O,P-[xant($P^iPr_2)_2$]} **115** which exhibited a broad resonance at δ 38.4 ppm in the ^{11}B NMR spectrum. These complexes were both active catalysts for the C–H borylation of arenes.

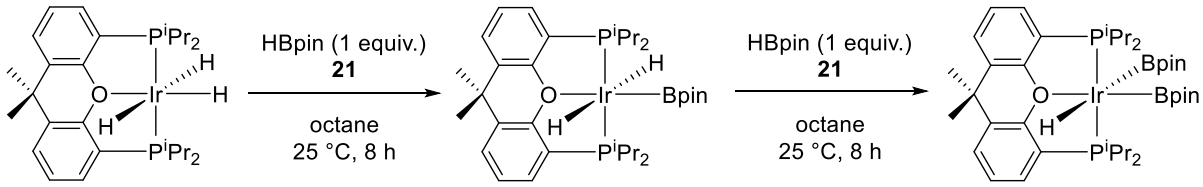

Scheme 28. Sequential reaction of **113** with 2 equivalents of HBpin **21** to form the monoboryl complex **114** and diboryl complex **115**.

1.5 High-Valent Metal-Oxo Activation of Si/B–H Bonds

High-valent metal-oxo complexes are traditionally associated with oxo-transfer reactions and oxidation catalysis,[77-78] most notably oxo-molybdenum[79] and oxo-rhenium complexes[80-81] have been employed as catalysts for the oxidation of alkenes, sulfides and pyridines to the corresponding epoxides, sulfoxides and *N*-oxides. In the last 15-20 years, these complexes have been reinvented as catalysts for the reduction of unsaturated organic molecules. In 2003, Toste and co-workers reported that a high-valent oxo-Re complex catalysed the hydrosilylation of carbonyl compounds.[82] This reaction is proposed to proceed by [2+2] addition of the silane Si–H bond to the Re=O bond of $ReIO_2(PPh_3)_2$ **117** to form a siloxyrhenium hydride intermediate **Int-A**. This intermediate then reacts with the carbonyl substrate to generate the silyl ether product (Scheme 29).[83-84] Toste also reported an asymmetric variant of this reaction using a enantioenriched (CN-box)Re-oxo catalyst for the asymmetric reduction of ketones and imines.[85-86] Royo and co-workers reported similar reactivity for the dioxomolybdenum complex MoO_2Cl_2 in the hydrosilylation of aldehydes and ketones.[87] The mechanism for this reaction was proposed based on DFT calculations which again involves the [2+2] addition of the silane to MoO_2Cl_2 to form $MoCl_2H(O)(OSiR_3)$.[88]

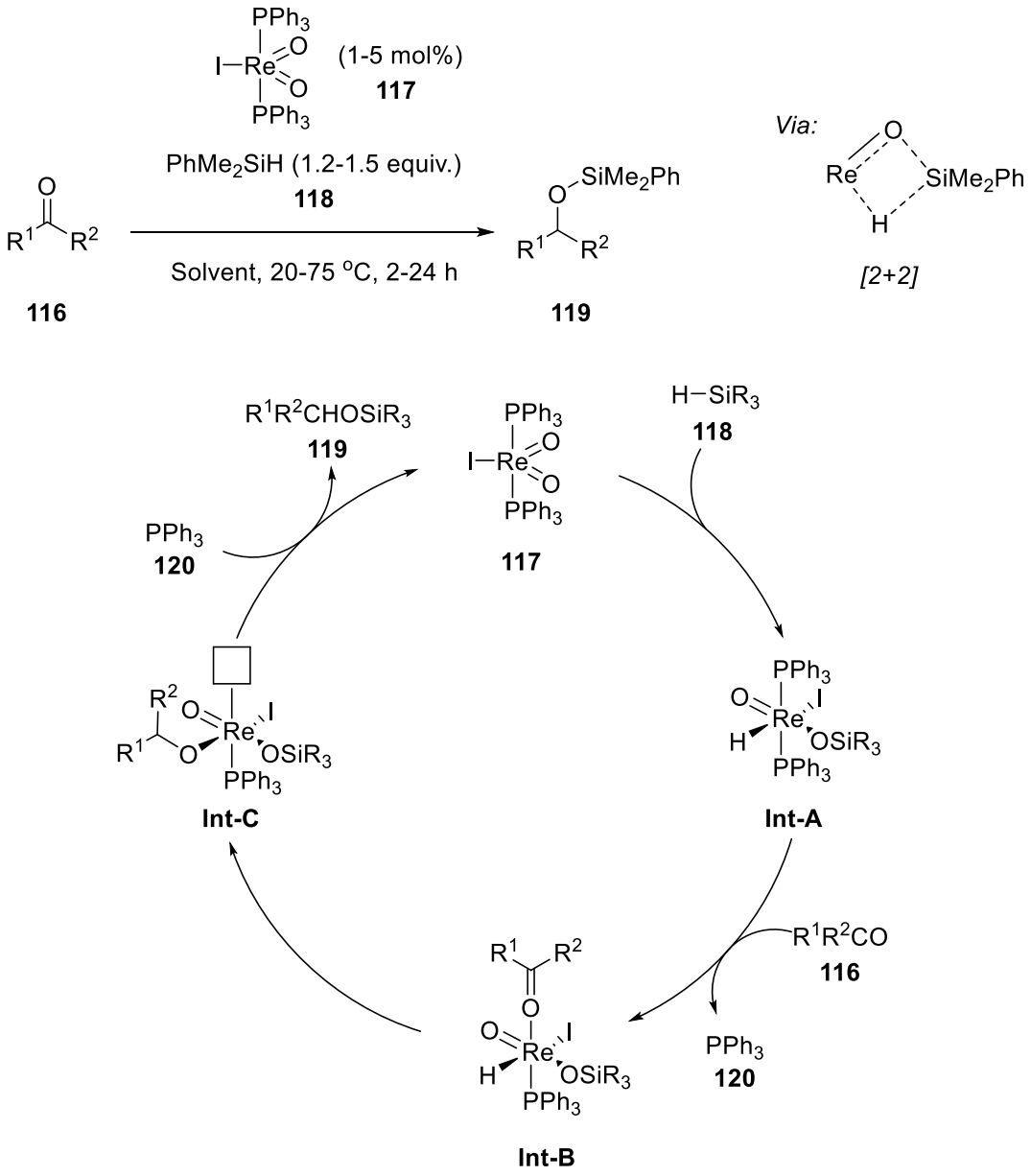

Scheme 29. Hydrosilylation of carbonyls catalysed by Re-oxo complex **117** and the proposed catalytic cycle.

Recently, Love and co-workers have shown that the simple perrhenate salt, $[N(hexyl)_4][ReO_4]$ **121**, can act as an efficient catalyst for the reduction of organic carbonyls and carbon dioxide to the corresponding alcohols by activation of hydrosilanes (Scheme 30).[89] DFT analysis of the reaction mechanism for CO_2 reduction indicated that the perrhenate anion acts as a Lewis base and activates the silicon centre forming a pentavalent silicate intermediate, and CO_2 activation occurs directly at the Si–H bond with no formation of a Re–H species. The $[N(hexyl)_4][ReO_4]$ **121** catalyst has also been shown to be effective in the *N*-methylation of amines using CO_2 as a C1 feedstock; additionally the perrhenate is

easily recyclable by transfer from the organic phase to the aqueous phase by addition of base (e.g. NaOH), mitigating the cost of using rhenium. The catalyst is air- and moisture stable, so can be used in 'bench-top' procedures.

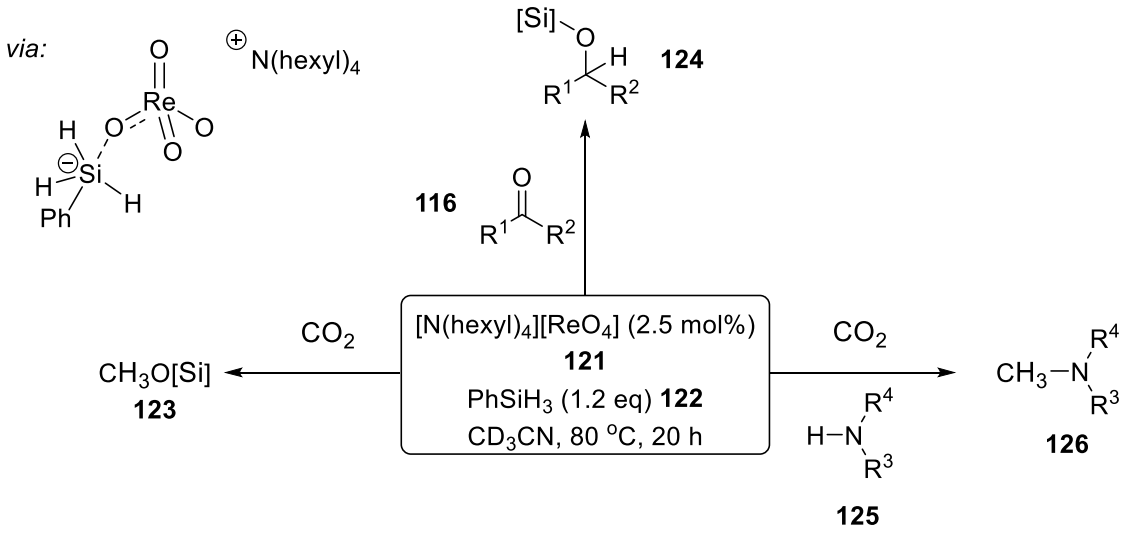

Scheme 30. Hydrosilylation of carbonyls and CO_2 catalysed by [Nhex$_4$][ReO$_4$] **121**.

The reactivity of high oxidation-state metal-oxo compounds towards hydroboration has been reported previously but is much less well established than hydrosilylation reactions. Fernandes and co-workers have shown that several Re-oxo catalysts can reduce sulfoxides using hydroboranes (HBcat **17** and HBpin **21**).[90] The complex $ReIO_2(PPh_3)_2$ **117** was studied in detail as a catalyst for this reaction, and the stoichiometric reaction between **117** and HBpin **21** or HBcat **17** was found to produce the boroxy rhenium hydride complex (Scheme 31).[91] This suggests that B–H bonds are activated by this catalyst by a [2+2] addition similar to that proposed by Toste for the activation of silanes. This pathway was supported by computational studies of the sulfoxide reduction mechanism where initially the phosphine ligands are substituted by sulfoxide molecules, followed by addition of one HBcat **17** molecule to form the hydride species **127a**. Subsequent reduction of the sulfoxide to a sulfide leads to the formation of a Re(VII) species which is then reduced by a second HBcat **17** molecule to liberate H_2 and $O(Bcat)_2$. The active catalyst is then reformed by coordination of a new sulfoxide molecule.

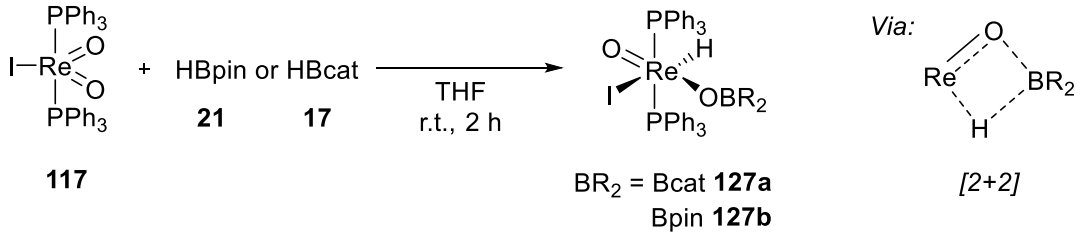

Scheme 31. Reaction of **117** with HBpin **21** or HBcat **17** to form the boroxy hydride complexes **127a** or **127b**.

Mösch-Zanetti and co-workers synthesised a Mo^{VI} oxido imido adduct **130** from BCF **129** and [MoO(N^tBu)L_2] **128** and have shown its FLP-type reactivity in Si–H bond activation (Scheme 32A).[92-93] The reaction of the adduct with an excess of R_3SiH **131** resulted in heterolytic cleavage of the Si–H bond to form a cationic Mo^{VI} species [Mo($OSiR_3$)(N^tBu)L_2][$HB(C_6F_5)_3$] **132**. Upon addition of benzaldehyde to a solution of **132** in C_6D_6 nucleophilic addition of hydride is observed and insertion of benzaldehyde into the B–H bond. This species then slowly converted to **130** and the silyl ether. In a related study, Arnold and co-workers have shown that the Re^V oxo imido complex O(NDipp)Re(η^2-DHF)(BDI) **133** can activate a B–C bond to form a Re^V aryl borinate complex through 1,2-addition across the Re=O bond (Scheme 32B).[94]

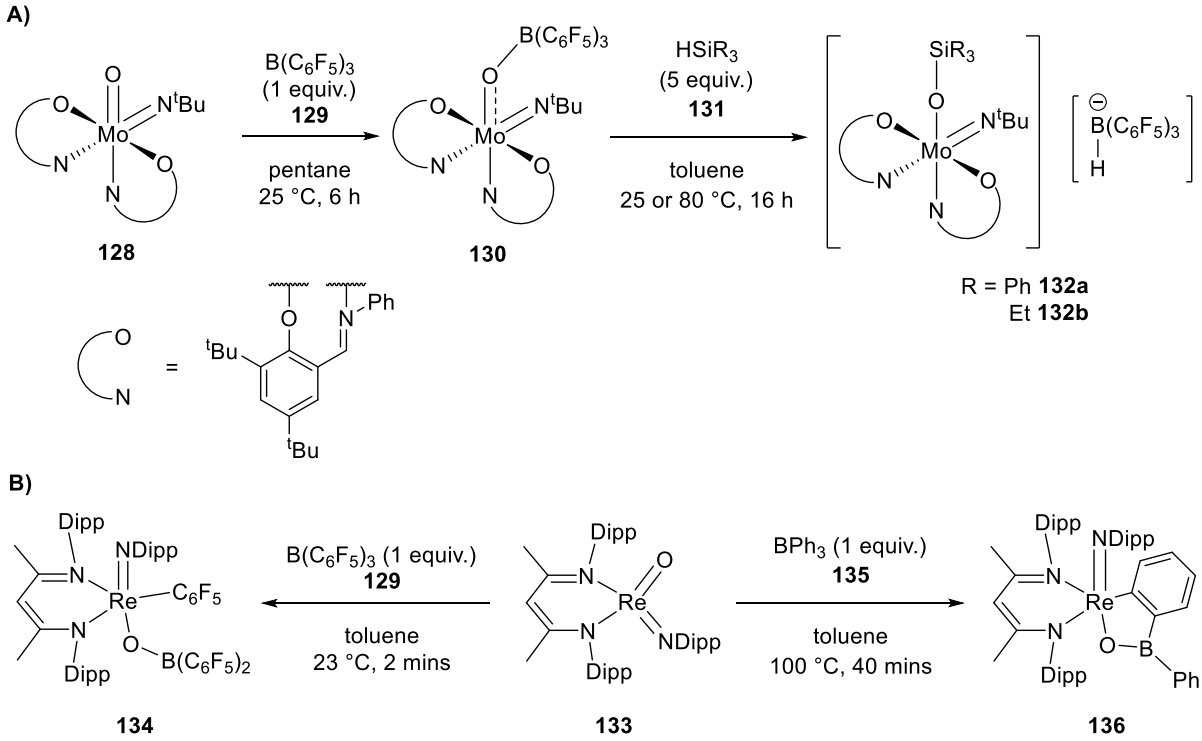

Scheme 32. A) FLP-type Si–H bond activation by BCF **129** and a Mo-oxo complex **128** (B) C–B bond activation by a Re-oxo complex **133**.

1.6 Rhenium Hydride Complexes

Polyhydride complexes are typically described as discrete mononuclear or polynuclear complexes containing from 2 to 9 hydride ligands covalently bound to each metal and are generally formed by transition metals from the second and third rows of the periodic table, from Group V to Group IX.[95] The uniquely small steric requirement of the hydride ligand means that it is ideal for higher coordinate transition metal complexes (coordination number = 7 to 9) and these complexes are typically stabilised by bulky phosphine or NHC ligands. Of these examples rhenium shows some of the richest and most diverse polyhydride chemistry since reports on the isolation and characterisation of K_2ReH_9 from the reduction of [K][ReO_4] with alkali metals in the 1960s.[96-97] The majority of reported Re polyhydrides are synthesised by the reaction of Re halides or oxides with main group hydrides such as $NaBH_4$ **138** or $LiAlH_4$ **140** (Scheme 33).[98-99] Characterisation of Re polyhydrides can be challenging for a variety of reasons. The small amount to which hydride ligands contribute to the overall molecular weight render elemental analysis and gas evolution studies unreliable. Similar to hydride-borane complexes, spectroscopic and crystallographic methods are needed to fully

characterise Re polyhydrides, and the 18-electron rule is a useful method for arriving at the correct formula.

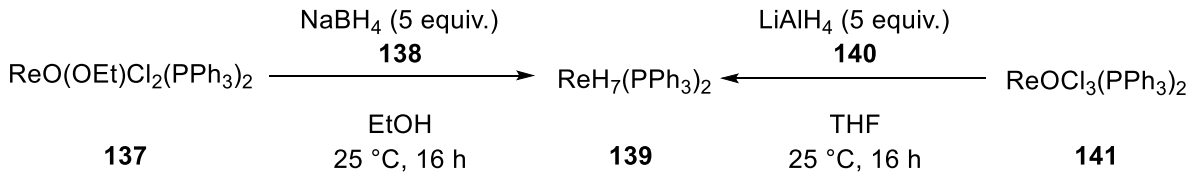

Scheme 33. Typical methods to synthesise Re polyhydride complex **139**.

As has been discussed previously, the presence of multiple hydride ligands bound to a transition metal centre means that they can be bound as classical hydrides with terminal M–H bonds or as nonclassical hydrides where two hydrides are bound as an η^2-H_2 ligand. One can distinguish between these bonding modes by using the T_{1min} NMR spectroscopy method developed by Crabtree and co-workers,[100] or by using crystallographic methods in combination with computational methods that have become more useful in the last two decades.[101] In fact, T_1 inversion recovery experiments have led to the reassignment of $ReH_7(PPh_3)_2$ **139** as a Re^{VII} classical hydride complex to $ReH_5(\eta^2\text{-}H_2)(PPh_3)_2$ bearing a non-classical dihydrogen ligand given a measured T_{1min} value of 110 ms at 200 K.[102]

Again, like hydride-borane complexes, the hydride and dihydrogen ligands in Re polyhydride complexes exchange positions around the central Re atom, this exchange is thermally activated and takes place with activation barriers that are much lower than those involved for the movements of the rest of the ligands. The reactivity of Re polyhydrides is largely determined by their ability to generate vacant coordination sites by liberation of H_2, either thermally or photochemically. The Re–H bond in polyhydrides is relatively unpolarised despite the formal high oxidation-states of these compounds (+4 to +7), and the metal bears a charge closer to that of the free metal. Comparing $ReCl_3(PMe_2Ph)_3$, which was arbitrarily assigned an oxidation-state of 3.0, to XPS studies on $ReH_5(PMe_2Ph)_3$ gave a measured oxidation-state of 1.9. This leads to Re polyhydrides exhibiting chemistry that is more similar to low oxidation-state transition metal complexes where the d-orbitals are not contracted and play a full role.

The reaction of $ReH_7(PR_3)_2$ with two-electron donors such as amines, phosphines and arsines led to substitution of an equivalent of H_2 and coordination of the donor ligand to give products of the form $ReH_5(PR_3)_2L$.[95] Complexes bearing bidentate phosphines are significantly more thermally stable than complexes bearing monodentate phosphines. This

was demonstrated by Felkin and Pascard where they showed that **139** reacts with 2,3-dimethylbutadiene **142** at 65 °C in 10 mins to form the diene trihydride **143** (Scheme 34A).[103] Whereas, $ReH_7(dppe)$ **144** did not react with dienes under the same conditions and required deprotonation with KO^{t}Bu **145** and methylation with Me_2SO_4 **146** to presumably form $ReH_6(Me)(dppe)$, which readily loses methane to form the unsaturated $ReH_5(dppe)$ which can coordinate a diene (Scheme 34B).

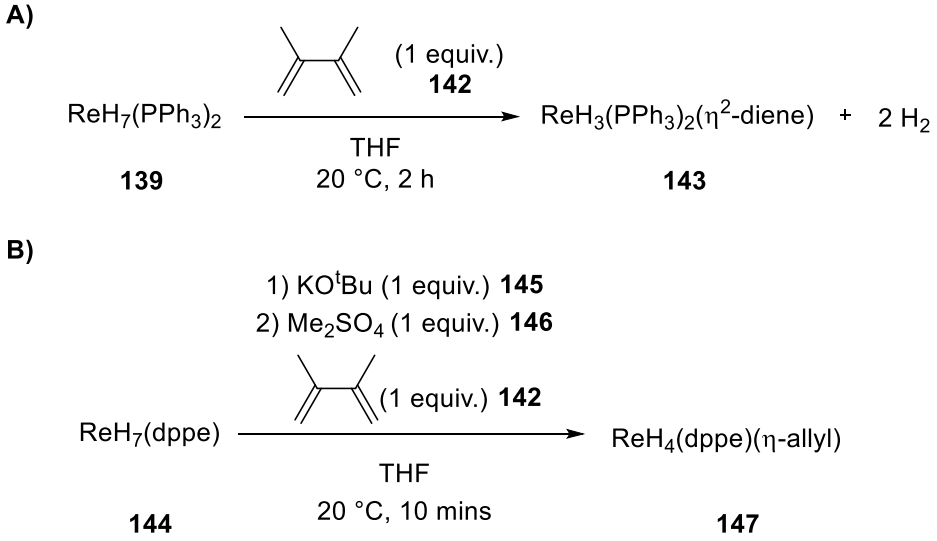

Scheme 34. A) Activation of dienes by **139** (B) Activation of dienes by **144** through a deprotonation, methylation and elimination strategy.

Crabtree and co-workers showed that **139** reacts with hydrosilanes **131** at room temperature over 24 – 36 h to form the relevant Re silyl complexes $ReH_6(SiR_3)(PPh_3)_2$ **148** with loss of an equivalent of H_2 (Scheme 35).[104] Although these complexes exhibited a single hydride resonance at 298 K in the ^{1}H NMR spectrum, this resonance decoalesced to two separate resonances in a ratio of 2:4 at 198 K. The solid-state structure of **148a** showed a short Si–H distance of 1.76 and 1.92 Å between the Si atom and two hydrides, which suggests a possible two-electron three-centre bonding mode of the SiH_2 unit. No further reactivity has been described for these silyl complexes.

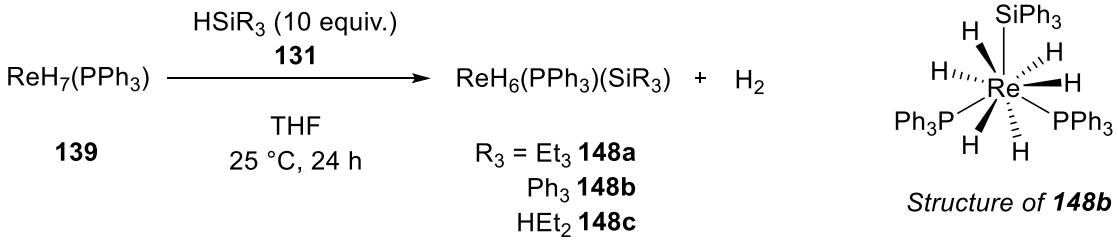

Scheme 35. Silane activation by **139** to produce silyl complexes **148**.

Re polyhydrides are also capable of activating C–H bonds, and this is best exhibited by $ReH_7(PCy_3)_2$ **149** which when heated in C_6D_6 at 60 – 80 °C exchanged hydrogen with deuterium (Scheme 36).[105] Deuterium was not only incorporated as hydride ligands but also selectively at the C2 and C3 positions of the cyclohexyl rings, where only one of the hydrogens at each carbon was exchanged. Therefore, this complex can activate both [sp^2] and [sp^3] C–H bonds. The H/D exchange also occurred in cyclohexane solvent using 1 atm of D_2 at 55 °C. Both reactions are likely to proceed by formation of the highly reactive transient species $ReH_5(PCy_3)_2$ **150** followed by coordination of D_2 or C_6D_6 and oxidative addition of the D–D or C–D bond.

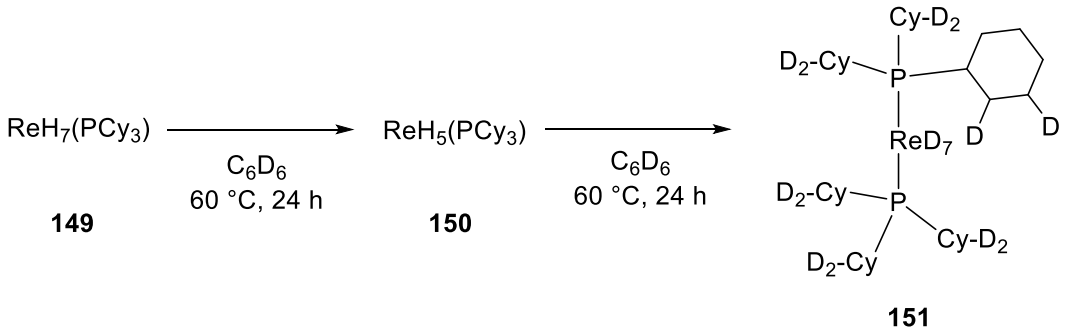

Scheme 36. H/D Exchange on the cyclohexyl substituents of **149**.

This C–H activation chemistry was further studied by Moehring and co-workers by reaction of **139** and a series of benzylic imines (Scheme 37).[106] This resulted in *ortho*-metalation of the aromatic ring with the imine acting as a directing group through coordination of the nitrogen atom to the Re centre, with the release of two equivalents of H_2.

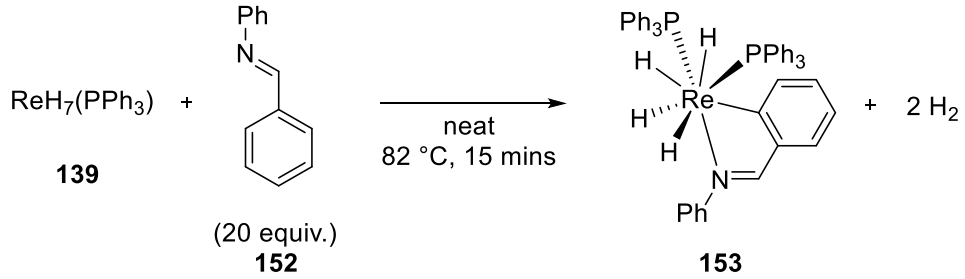

Scheme 37. C–H activation of **152** by **139** to form the metalated product **153**.

More recently, Ozerov and co-workers synthesised a Re hexahydride complex bearing a PCP pincer ligand (Scheme 38).[107] This was prepared from the reaction of (PCP^{i}Pr)ReOCl$_2$ **154** with LiAlH$_4$ **140** and H/D exchange was observed when (PCP^{i}Pr)ReH$_6$ **155** was dissolved in C_6D_6 at room temperature. Complex **155** reacted with strong donor ligands such as DMAP **157** with release of an equivalent of H_2 and coordination of the ligand. The catalytic applications of Re polyhydrides includes alkane dehydrogenation,[108] dehydrogenative coupling,[109-111] and alkene polymerisation.[112]

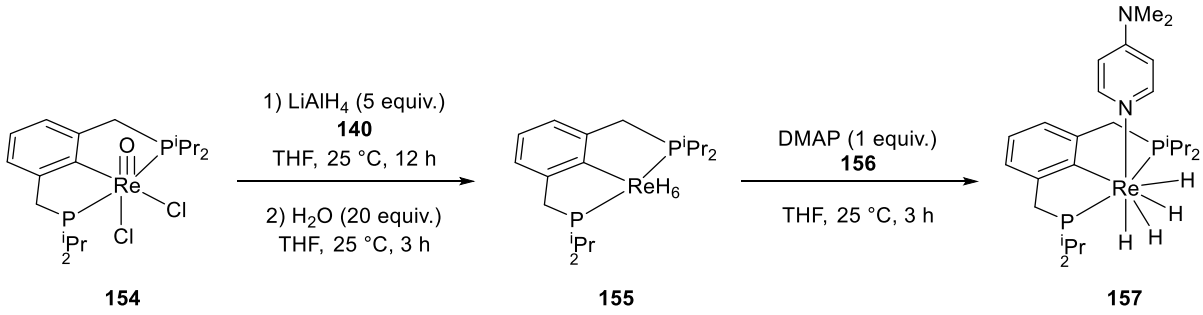

Scheme 38. Formation of Re polyhydride **155** and subsequent reaction with DMAP **156** to form **157**.

1.7 Rhenium Complexes with Boron-Centred Ligands

There have been few reports of Re complexes bearing boron-centred ligands in the literature (not including BH_3 and BH_4^-, and in all these complexes Re is in the +1 oxidation-state (Figure 4). The first example came from Morris and co-workers in 1993 when they synthesised the dihydroborate complex **158** through the reaction of ReCl$_3$(TetraPhos) with LiBHEt$_3$ in THF.[113] The solid-state structure of **158** showed a Re–B distance of 2.340(7) Å. Berke and co-workers have shown that the reaction of *mer*-Re(CO)$_2$(PMe$_3$)$_3$H with H-9-BBN **36** formed the related dihydroborate complex Re(CO)(PMe$_3$)$_3$(H$_2$-9-BBN) **159**.[114] Hartwig and co-workers have synthesised the σ-borane complex Cp*Re(CO)$_2$(HBpin) **160** which was

prepared from Cp*Re(CO)$_2$(Bpin)$_2$ by methanolysis at room temperature after 2 h in benzene.[115] X-ray crystallographic analysis of the complex was not obtained, however the ^{11}B NMR spectrum showed a resonance at δ 46 ppm and a broad resonance at −11.06 ppm in the ^{1}H NMR spectrum, which are indicative of Re–B and Re–H bonds respectively. This complex was demonstrated as a catalyst for the photochemical C–H borylation of alkanes.[16] Hartwig also synthesised a pentacarbonyl boryl complex ReCO$_5$(Bcat) **161** through the reaction of Na[ReCO$_5$] with ClBcat **45** at room temperature in toluene.[116] The ^{11}B NMR spectrum of this complex showed a resonance at δ 44 ppm, and it was shown to be active in the stoichiometric C–H borylation of benzene. Aldridge and co-workers took a different approach to those listed above and used a nucleophilic boron reagent (THF)$_2$Li{B(NDippCH)$_2$} to form the boryl complex (OC)$_5$Re{B(NDippCH)$_2$} **162** by reaction with the related acyl ester complex.[117]

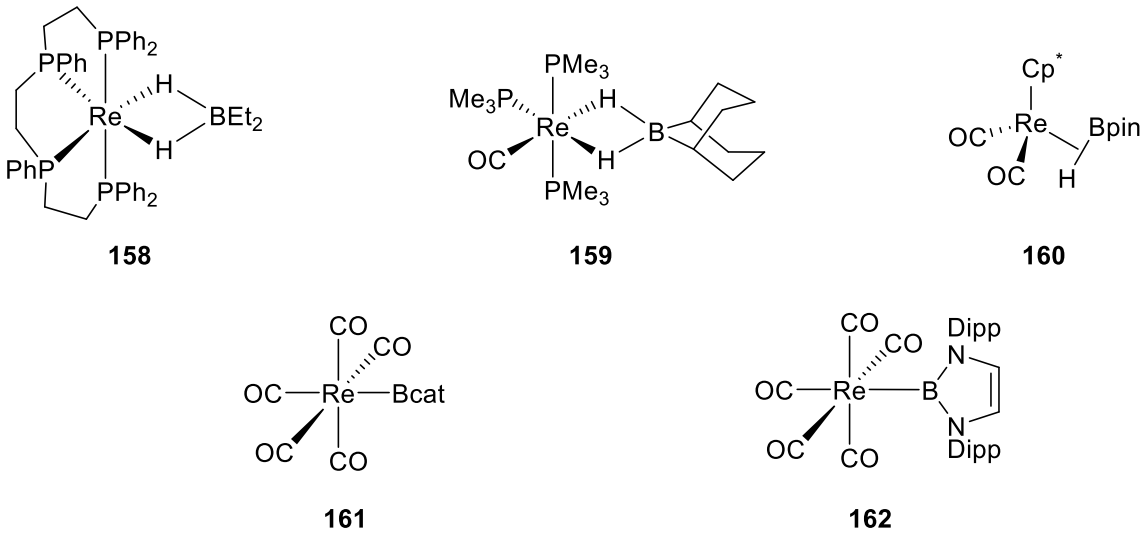

158 **159** **160**

161 **162**

Figure 4. Reported Re complexes with boron-centred ligands.

1.8 Aims of this thesis

As outlined in Chapter 1, previous methods to synthesise transition metal complexes bearing hydride ligands and boron-centred ligands has relied on the addition of hydroboranes to reactive low oxidation-state complexes or to high oxidation-state polyhydride complexes. These synthetic routes suffer from a number of drawbacks which hinder their practical everyday use: 1) the use of air/moisture sensitive reagents 2) the use of non-commercially available prefunctionalised transition metal complexes as starting materials 3) a lack of generality for the synthesis of hydride borane complexes. In the specific case of Re complexes bearing boron-centred ligands the current examples are limited to complexes in

the +1 oxidation-state and the reactivity of these complexes is limited, with only one example of application in catalysis.

The primary aim of the research presented in thesis is to investigate the activation of hydroboranes by commercially available, high oxidation-state, anionic metal-oxo complexes to produce novel transition metal polyhydride complexes bearing boron-centred ligands. This can be divided into several secondary aims:

- Synthesise a series novel transition metal polyhydride complexes bearing boron-centred ligands and characterise them by using NMR spectroscopy, single-crystal X-ray diffraction and computational methods.
- Investigate the coordination chemistry of these complexes with different ligand systems and their reactivity with stoichiometric reagents.
- Explore the uses of these complexes as catalysts in the hydroboration of unsaturated organic molecules or in the C–H borylation of arenes.
- Study the mechanisms of these catalytic reactions by use of NMR analysis for *in situ* reaction monitoring and kinetic investigations of both stoichiometric and catalytic reactions.

1.9 References

1. Hartwig, J. F., *J. Am. Chem. Soc.* **2016**, *138*, 2-24.
2. Crabtree, R. H., *J. Chem. Soc., Dalton Trans.*. **2001**, 2437-2450.
3. Balcells, D.; Clot, E.; Eisenstein, O., *Chem. Rev*. **2010**, *110*, 749-823.
4. Wencel-Delord, J.; Dröge, T.; Liu, F.; Glorius, F., *Chem. Soc. Rev*. **2011**, *40*, 4740-4761.
5. Chatt, J.; Hart, F. A.; Watson, H. R., 490. *J. Chem. Soc.* **1962**, 2537-2545.
6. Chatt, J.; Davidson, J. M., *J. Chem. Soc.* **1965**, 843-855.
7. Jones, W. D.; Kosar, W. P., *J. Am. Chem. Soc.* **1986**, *108*, 5640-5641.
8. Murai, S.; Kakiuchi, F.; Sekine, S.; Tanaka, Y.; Kamatani, A.; Sonoda, M.; Chatani, N., *Nature* **1993**, *366*, 529-531.
9. Ezbiansky, K.; Djurovich, P. I.; LaForest, M.; Sinning, D. J.; Zayes, R.; Berry, D. H., *Organometallics* **1998**, *17*, 1455-1457.
10. Mkhalid, I. A. I.; Barnard, J. H.; Marder, T. B.; Murphy, J. M.; Hartwig, J. F., C−H *Chem. Rev*. **2010**, *110*, 890-931.

11. Xu, L.; Wang, G.; Zhang, S.; Wang, H.; Wang, L.; Liu, L.; Jiao, J.; Li, P., *Tetrahedron* **2017**, *73*, 7123-7157.

12. Nguyen, P.; Blom, H. P.; Westcott, S. A.; Taylor, N. J.; Marder, T. B., *J. Am. Chem. Soc.* **1993,** *115*, 9329-9330.

13. Fyfe, J. W. B.; Watson, A. J. B., *Chem* **2017**, *3*, 31-55.

14. Murphy, J. M.; Lawrence, J. D.; Kawamura, K.; Incarvito, C.; Hartwig, J. F., *J. Am. Chem. Soc.* **2006**, *128*, 13684-13685.

15. Chen, H.; Schlecht, S.; Semple, T. C.; Hartwig, J. F., *Science* **2000**, *287*, 1995.

16. Chen, H.; Hartwig, J. F., *Angew. Chem. Int. Ed.* **1999**, 3391-3393.

17. Dombray, T.; Werncke, C. G.; Jiang, S.; Grellier, M.; Vendier, L.; Bontemps, S.; Sortais, J.-B.; Sabo-Etienne, S.; Darcel, C., *J. Am. Chem. Soc.* **2015,** *137*, 4062-4065.

18. Britton, L; Docherty, J. H.; Dominey, A. P.; Thomas, S. P., *Molecules* **2020**, *25*, 905.

19. Mazzacano, T. J.; Mankad, N. P., *J. Am. Chem. Soc.* **2013**, *135*, 17258-17261.

20. Obligacion, J. V.; Semproni, S. P.; Chirik, P. J., *J. Am. Chem. Soc.* **2014**, *136*, 4133-4136.

21. Obligacion, J. V.; Semproni, S. P.; Pappas, I.; Chirik, P. J., *J. Am. Chem. Soc.* **2016**, *138*, 10645-10653.

22. Pabst, T. P.; Obligacion, J. V.; Rochette, É.; Pappas, I.; Chirik, P. J., *J. Am. Chem. Soc.* **2019**, *141*, 15378-15389.

23. Agahi, R.; Challinor, A. J.; Dunne, J.; Docherty, J. H.; Carter, N. B.; Thomas, S. P., *Chem. Sci.* **2019**, *10*, 5079-5084.

24. Furukawa, T.; Tobisu, M.; Chatani, N., *J. Am. Chem. Soc.* **2015**, *137*, 12211-12214.

25. Légaré, M.-A.; Courtemanche, M.-A.; Rochette, É.; Fontaine, F.-G., *Science* **2015**, *349*, 513.

26. Cho, J.-Y.; Tse, M. K.; Holmes, D.; Maleczka, R. E.; Smith, M. R., *Science* **2002**, *295*, 305.

27. Boller, T. M.; Murphy, J. M.; Hapke, M.; Ishiyama, T.; Miyaura, N.; Hartwig, J. F., *J. Am. Chem. Soc.* **2005**, *127*, 14263-14278.

28. Davis, H. J.; Mihai, M. T.; Phipps, R. J., *J. Am. Chem. Soc.* **2016,** *138*, 12759-12762.

29. Mihai, M. T.; Williams, B. D.; Phipps, R. J., *J. Am. Chem. Soc.* **2019,** *141*, 15477-15482.

30. Saito, Y.; Segawa, Y.; Itami, K., *J. Am. Chem. Soc.* **2015,** *137*, 5193-5198.

31. Ishiyama, T.; Isou, H.; Kikuchi, T.; Miyaura, N., *Chem. Commun.* **2010,** *46*, 159-161.

32. Kawamorita, S.; Ohmiya, H.; Hara, K.; Fukuoka, A.; Sawamura, M., *J. Am. Chem. Soc.* **2009,** *131*, 5058-5059.

33. Oeschger, R.; Su, B.; Yu, I.; Ehinger, C.; Romero, E.; He, S.; Hartwig, J., *Science* **2020,** *368*, 736.

34. Tamura, H.; Yamazaki, H.; Sato, H.; Sakaki, S., *J. Am. Chem. Soc.* **2003**, *125*, 16114-16126.

35. Ishiyama, T.; Takagi, J.; Ishida, K.; Miyaura, N.; Anastasi, N. R.; Hartwig, J. F., *J. Am. Chem. Soc.* **2002**, *124*, 390-391.

36. Chotana, G. A.; Vanchura, B. A.; Tse, M. K.; Staples, R. J.; Maleczka, J. R. E.; Smith, M. R., *Chem. Commun.* **2009**, 5731-5733.

37. Nöth, H.; Schmid, G., *Angew. Chem. Int. Ed.* **1963**, *2*, 623-623.

38. Baker, R. T.; Ovenall, D. W.; Calabrese, J. C.; Westcott, S. A.; Taylor, N. J.; Williams, I. D.; Marder, T. B., *J. Am. Chem. Soc.* **1990**, *112*, 9399-9400.

39. Knorr, J. R.; Merola, J. S., *Organometallics* **1990**, *9*, 3008-3010.

40. Schmid, G., *Angew. Chem. Int. Ed.* **1970**, *9*, 819-830.

41. Zhu, J.; Lin, Z.; Marder, T. B., *Inorg. Chem.* **2005**, *44*, 9384-9390.

42. Braunschweig, H.; Kollann, C.; Rais, D., *Angew. Chem. Int. Ed.* **2006,** *45*, 5254-5274.

43. Braunschweig, H.; Dewhurst, R. D.; Schneider, A., *Chem. Rev.* **2010**, *110*, 3924-3957.

44. Zhao, Q.; Dewhurst, R. D.; Braunschweig, H.; Chen, X., *Angew. Chem. Int. Ed.* **2019**, *58*, 3268-3278.

45. Hartwig, J. F.; Muhoro, C. N.; He, X.; Eisenstein, O.; Bosque, R.; Maseras, F., *J. Am. Chem. Soc.* **1996**, *118*, 10936-10937.

46. Rablen, P. R.; Hartwig, J. F., *J. Am. Chem. Soc.* **1996**, *118*, 4648-4653.

47. Perutz, R. N.; Sabo-Etienne, S., *Angew. Chem. Int. Ed.* **2007**, *46*, 2578-2592.

48. Alcaraz, G.; Sabo-Etienne, S., *Coord. Chem. Rev.* **2008**, *252*, 2395-2409.

49. Alcaraz, G.; Grellier, M.; Sabo-Etienne, S., *Acc. Chem. Res.* **2009**, *42*, 1640-1649.

50. Heinekey, D. M.; Payne, N. G.; Sofield, C. D., *Organometallics* **1990**, *9*, 2643-2645.

51. Scorzelli, A. G.; Macalush, B. E.; Naik, D. V.; Moehring, G. A., *Inorganica Chim. Acta* **2021**, *516*, 120120.

52. Hartwig, J. F.; De Gala, S. R., *J. Am. Chem. Soc.* **1994**, *116*, 3661-3662.

53. Lantero, D. R.; Miller, S. L.; Cho, J.-Y.; Ward, D. L.; Smith, M. R., *Organometallics* **1999**, *18*, 235-247.

54. Lantero, D. R.; Ward, D. L.; Smith, M. R., *J. Am. Chem. Soc.* **1997**, *119*, 9699-9708.

55. Lantero, D. R.; Motry, D. H.; Ward, D. L.; Smith, M. R., *J. Am. Chem. Soc.* **1994**, *116*, 10811-10812.

56. Khalimon, A. Y.; Farha, P. M.; Nikonov, G. I., *Dalton Trans.* **2015**, *44*, 18945-18956.

57. Montiel-Palma, V.; Lumbierres, M.; Donnadieu, B.; Sabo-Etienne, S.; Chaudret, B., *J. Am. Chem. Soc.* **2002**, *124*, 5624-5625.

58. Lachaize, S.; Essalah, K.; Montiel-Palma, V.; Vendier, L.; Chaudret, B.; Barthelat, J.-C.; Sabo-Etienne, S., *Organometallics* **2005**, *24*, 2935-2943.

59. Alcaraz, G.; Clot, E.; Helmstedt, U.; Vendier, L.; Sabo-Etienne, S., *J. Am. Chem. Soc.* **2007**, *129*, 8704-8705.

60. Alcaraz, G.; Helmstedt, U.; Clot, E.; Vendier, L.; Sabo-Etienne, S., *J. Am. Chem. Soc.* **2008**, *130*, 12878-12879.

61. Braunschweig, H.; Burzler, M.; Kupfer, T.; Radacki, K.; Seeler, F., *Angew. Chem. Int. Ed.* **2007**, *46*, 7785-7787.

62. Coombs, D. L.; Aldridge, S.; Jones, C.; Willock, D. J., *J. Am. Chem. Soc.* **2003**, *125*, 6356-6357.

63. Esteruelas, M. A.; Fernández-Alvarez, F. J.; López, A. M.; Mora, M.; Oñate, E., *J. Am. Chem. Soc.* **2010**, *132*, 5600-5601.

64. Esteruelas, M. A.; López, A. M.; Mora, M.; Oñate, E., *Organometallics* **2015**, *34*, 941-946.

65. Babón, J. C.; Esteruelas, M. A.; Fernández, I.; López, A. M.; Oñate, E., *Inorg. Chem.* **2018**, *57*, 4482-4491.

66. Buil, M. a. L.; Esteruelas, M. A.; Fernández, I.; Izquierdo, S.; Oñate, E., *Organometallics* **2013**, *32*, 2744-2752.

67. Esteruelas, M. A.; Fernández, I.; García-Yebra, C.; Martín, J.; Oñate, E., *Organometallics* **2017**, *36*, 2298-2307.

68. Cook, K. S.; Incarvito, C. D.; Webster, C. E.; Fan, Y.; Hall, M. B.; Hartwig, J. F., *Angew. Chem. Int. Ed.* **2004**, *43*, 5474-5477.

69. Hartwig, J. F.; Cook, K. S.; Hapke, M.; Incarvito, C. D.; Fan, Y.; Webster, C. E.; Hall, M. B., *J. Am. Chem. Soc.* **2005**, *127*, 2538-2552.

70. Zhang, N.; Sherbo, R. S.; Bindra, G. S.; Zhu, D.; Budzelaar, P. H. M., *Organometallics* **2017**, *36*, 4123-4135.

71. Iverson, C. N.; Smith, M. R., *J. Am. Chem. Soc.* **1999**, *121*, 7696-7697.

72. Kawamura, K.; Hartwig, J. F., *J. Am. Chem. Soc.* **2001**, *123*, 8422-8423.

73. Ghaffari, B.; Vanchura, B. A.; Chotana, G. A.; Staples, R. J.; Holmes, D.; Maleczka, R. E.; Smith, M. R., *Organometallics* **2015**, *34*, 4732-4740.

74. Hebden, T. J.; Denney, M. C.; Pons, V.; Piccoli, P. M. B.; Koetzle, T. F.; Schultz, A. J.; Kaminsky, W.; Goldberg, K. I.; Heinekey, D. M., *J. Am. Chem. Soc.* **2008**, *130*, 10812-10820.

75. Press, L. P.; Kosanovich, A. J.; McCulloch, B. J.; Ozerov, O. V., *J. Am. Chem. Soc*. **2016**, *138*, 9487-9497.

76. Esteruelas, M. A.; Martínez, A.; Oliván, M.; Oñate, E., *Chem. Eur.J*. **2020**, *26*, 12632 –12644.

77. Chen, Z.; Yin, G., *Chem. Soc. Rev*. **2015**, *44*, 1083-1100.

78. Gunay, A.; Theopold, K. H., *Chem. Rev*. **2010**, *110*, 1060-1081.

79. Kühn, F. E.; Santos, A. M.; Abrantes, M., *Chem. Rev*. **2006**, *106*, 2455-2475.

80. Owens, G. S.; Arias, J.; Abu-Omar, M. M., *Catal. Today* **2000**, *55*, 317-363.

81. Romão, C. C.; Kühn, F. E.; Herrmann, W. A., *Chem. Rev*. **1997**, *97*, 3197-3246.

82. Kennedy-Smith, J. J.; Nolin, K. A.; Gunterman, H. P.; Toste, F. D., *J. Am. Chem. Soc*. **2003**, *125*, 4056-4057.

83. Nolin, K. A.; Krumper, J. R.; Pluth, M. D.; Bergman, R. G.; Toste, F. D., *J. Am. Chem. Soc.* **2007**, *129*, 14684-14696.

84. Chung, L. W.; Lee, H. G.; Lin, Z.; Wu, Y.-D., *J. Org. Chem.* **2006**, *71*, 6000-6009.

85. Nolin, K. A.; Ahn, R. W.; Toste, F. D., *J. Am. Chem. Soc.* **2005**, *127*, 12462-12463.

86. Nolin, K. A.; Ahn, R. W.; Kobayashi, Y.; Kennedy-Smith, J. J.; Toste, F. D., *Chem. Eur. J.* **2010**, *16*, 9555-9562.

87. Reis, P. M.; Romão, C. C.; Royo, B., *Dalton Trans.* **2006**, 1842-1846.

88. Costa, P. J.; Romão, C. C.; Fernandes, A. C.; Royo, B.; Reis, P. M.; Calhorda, M. J., *Chem. Eur. J.* **2007**, *13*, 3934-3941.

89. Morris, D. S.; Weetman, C.; Wennmacher, J. T. C.; Cokoja, M.; Drees, M.; Kühn, F. E.; Love, J. B., *Catal. Sci. Technol.* **2017**, *7*, 2838-2845.

90. Fernandes, A. C.; Fernandes, J. A.; Romão, C. C.; Veiros, L. F.; Calhorda, M. J., *Organometallics* **2010**, *29*, 5517-5525.

91. Fernandes, A. C.; Fernandes, J. A.; Almeida Paz, F. A.; Romao, C. C., *Dalton Trans.* **2008**, 6686-6688.

92. Zwettler, N.; Walg, S. P.; Belaj, F.; Mösch-Zanetti, N. C., *Chem. Eur. J.* **2018**, *24*, 7149-7160.

93. Zwettler, N.; Mösch-Zanetti, N. C., *Chem. Eur. J.* **2019**, *25*, 6064-6076.

94. Lohrey, T. D.; Cortes, E. A.; Bergman, R. G.; Arnold, J., *Inorg. Chem.* **2020**, *59*, 7216–7226

95. Hlatky, G. G.; Crabtree, R. H., *Coord. Chem. Rev.* **1985**, *65*, 1-48.

96. Ginsberg, A. P.; Miller, J. M.; Cavanaugh, J. R.; Dailey, B. P., *Nature* **1960**, *185*, 528-529.

97. Abrahams, S. C.; Ginsberg, A. P.; Knox, K., *Inorg. Chem.* **1964**, *3*, 558-567.

98. Malatesta, L.; Freni, M.; Valenti, V.,, *Gazz. Chim. Ital.* **1964**, *94*, 1278.

99. Chatt, J.; Coffey, R. S., *J. Chem. Soc. A* **1969**, 1963-1972.

100. Hamilton, D. G.; Crabtree, R. H., *J. Am. Chem. Soc.* **1988,** *110* 4126-4133.

101. Maseras, F.; Lledós, A.; Clot, E.; Eisenstein, O., *Chem. Rev.* **2000**, *100*, 601-636.

102. Luo, X. L.; Crabtree, R. H., *J. Am. Chem. Soc.* **1990**, *112*, 4813-4821.

103. Baudry, D.; Boydell, P.; Ephritikhine, M.; Felkin, H.; Guilhem, J.; Pascard, C.; Dau, E. T. H., *J. Chem. Soc., Chem. Commun.* **1985**, 670-671.

104. Luo, X. L.; Baudry, D.; Boydell, P.; Charpin, P.; Nierlich, M.; Ephritikhine, M.; Crabtree, R. H., *Inorg. Chem.* **1990**, *29*, 1511-1517.

105. Zeiher, E. H. K.; DeWit, D. G.; Caulton, K. G., *J. Am. Chem. Soc.* **1984**, *106*, 7006-7011.

106. Moehring, G. A.; Williams, C. C.; Buford, J.; Kaviani, M.; Sulko, J.; Fanwick, P. E., *Inorg. Chem.* **1998**, *37*, 3848-3852.

107. Kosanovich, A. J.; Reibenspies, J. H.; Ozerov, O. V., *Organometallics* **2016**, *35*, 513-519.

108. Aoki, T.; Crabtree, R. H., *Organometallics* **1993**, *12*, 294-298.

109. Takaya, H.; Ito, M.; Murahashi, S.-I., *J. Am. Chem. Soc.* **2009**, *131*, 10824-10825.

110. Jin, H.; Xie, J.; Pan, C.; Zhu, Z.; Cheng, Y.; Zhu, C., *ACS Catal.* **2013**, *3*, 2195-2198.

111. Schleker, P. P. M.; Honeker, R.; Klankermayer, J.; Leitner, W., *ChemCatChem* **2013**, *5*, 1762-1764.

112. Batsanov, A. D.; Howard, J. A. K.; Love, J. B.; Spencer, J. L., *Organometallics* **1995**, *14*, 5657-5664.

113. Jia, G.; Lough, A. J.; Morris, R. H., *J. Organomet. Chem* **1993**, *461*, 147-156.

114. Liu, X.-Y.; Bouherour, S.; Jacobsen, H.; Schmalle, H. W.; Berke, H., *Inorganica Chim. Acta* **2002**, *330*, 250-267.

115. Schlecht, S.; Hartwig, J. F., *J. Am. Chem. Soc.* **2000**, *122*, 9435-9443.

116. Waltz, K. M.; Muhoro, C. N.; Hartwig, J. F., *Organometallics* **1999**, *18*, 3383-3393.

117. Frank, R.; Howell, J.; Tirfoin, R.; Dange, D.; Jones, C.; Mingos, D. M. P.; Aldridge, S., *J. Am. Chem. Soc.* **2014**, *136*, 15730-15741.

Chapter Two – Perrhenate Deoxygenation

2.1 Perrhenate Deoxygenation using HBpin

2.1.1 Potassium 18-Crown-6 Complexes

As has been described in Chapter One, ReO_4^- is able to activate hydrosilanes toward the catalytic hydrosilylation of carbonyl compounds. DFT analysis of the reaction mechanism for CO_2 reduction indicated that the perrhenate anion acts as a Lewis base and activates the silicon centre forming a pentavalent silicate intermediate, and CO_2 activation occurs directly at the Si-H bond with no formation of a Re–H species. In contrast, it was envisaged that the reaction of a hydroborane with ReO_4^- may result in the addition of the B–H bond across the Re=O bond to form a boroxy hydride complex in a similar manner to that described by Fernandes.[1-2] The reaction between [K][ReO_4] **163^{K}** and HBpin **21** in the presence of 18-crown-6 (18-c-6) **164** formed the new boron polyhydride complex [K(18-c-6)$_2$][ReH_7(Bpin)$_3$] **165$^{(18\text{-}c\text{-}6)}$**, O(Bpin)$_2$ **166**, and H_2 as a result of the complete deoxygenation of [K][ReO_4] **163^{K}**. Recrystallization of the reaction mixture from toluene/DME allowed isolation of the product [K(DME)(18-c-6)][ReH_7(Bpin)$_3$] **165^{DME}** in 56% yield as colourless needles (Scheme 39).

Scheme 39. Deoxygenation of [K][ReO_4] **163^{K}** using HBpin **21** to produce **165$^{(18\text{-}c\text{-}6)}$**.

The ^{1}H NMR spectrum of **165^{DME}** in d_8-toluene exhibited a singlet hydride resonance at −7.22 ppm integrating to 7 hydrogens which remained sharp upon cooling to 173 K. The ^{11}B NMR spectrum showed a single broad resonance at 45.6 ppm which, similarly to the ^{1}H NMR resonances, was unchanged at low temperature. The IR spectrum of **165^{DME}** showed weak and broad absorptions that are attributable to Re–H stretches between 2000 and 1750 cm^{-1}. Single-crystal X-ray diffraction was carried out on a two-domain aggregate crystal of **165^{DME}** from which diffraction images were integrated for both domains using two orientation matrices. The solid-state structure showed that two of the Bpin ligands (B1, B1‘) are related by a C_2-symmetry axis and, along with B2, adopt a *psuedo*-trigonal arrangement at the Re atom (B1–Re1–B2 = 118.6(2)°, B1–Re1–B1′ = 122.9(5)°) with similar Re1–B1

(2.198(10) Å) and Re1–B2 (2.174(14) Å) distances (Figure 6A); these distances compare well with other high oxidation-state boron-hydride complexes.[3-6] The hydrides could not be located with confidence from difference maps. As such, in collaboration with Prof. Carole Morrison, possible hydride positions were identified using AIRSS with the positions of the heavier atoms derived from the crystal structure and constraints on prospective hydride positions to ensure neither H_2 was formed nor unwanted K–H interactions occurred.[7-8] This approach generated a series of structures with various combinations of hydride, boryl, σ-borane, and hydroborate ligands (Figure 5). The seven hydrogen atoms around the Re centre in $[ReH_7(Bpin)_3]^-$ **165** were located in a non-biased way through a series of AIRSS/CASTEP geometry optimisation calculations. The model comprised the anion located inside a 15 $Å^3$ cubic box alongside a non-coordinating $[K]^+$ to maintain charge neutrality of the periodic boundary condition box. AIRSS constructed the initial models by positioning the hydrogen atoms randomly on a sphere of radius 1.6-1.85 Å centred on the Re coordinate. Two further constraints were imposed on the initial hydrogen atom placement, to ensure a minimum separation of 1.1 Å between the hydrogen atoms (to prevent possible formation of H_2) and 1.5 Å between the hydrogen atoms and the potassium centre (to prevent loss of hydrogen around the Re centre through the formation of K-H bonds). Over 30 random input structures were generated in this way, and optimised using CASTEP (version 16) for full atom optimisation (basis set energy cut-off: 750 eV; functional: PBE; dispersion correction: TS; pseudopotentials: on-the-fly; geometry optimisation criteria: energy tolerance: 5×10^{-4} eV, maximum force tolerance: 5×10^{-2} eV $Å^{-1}$ atomic displacement tolerance: 5×10^{-2} Å). The relative energies of the resulting optimised structures are arranged, from lowest to highest (Figure 5A) alongside images of the minima obtained (Figure 5B).

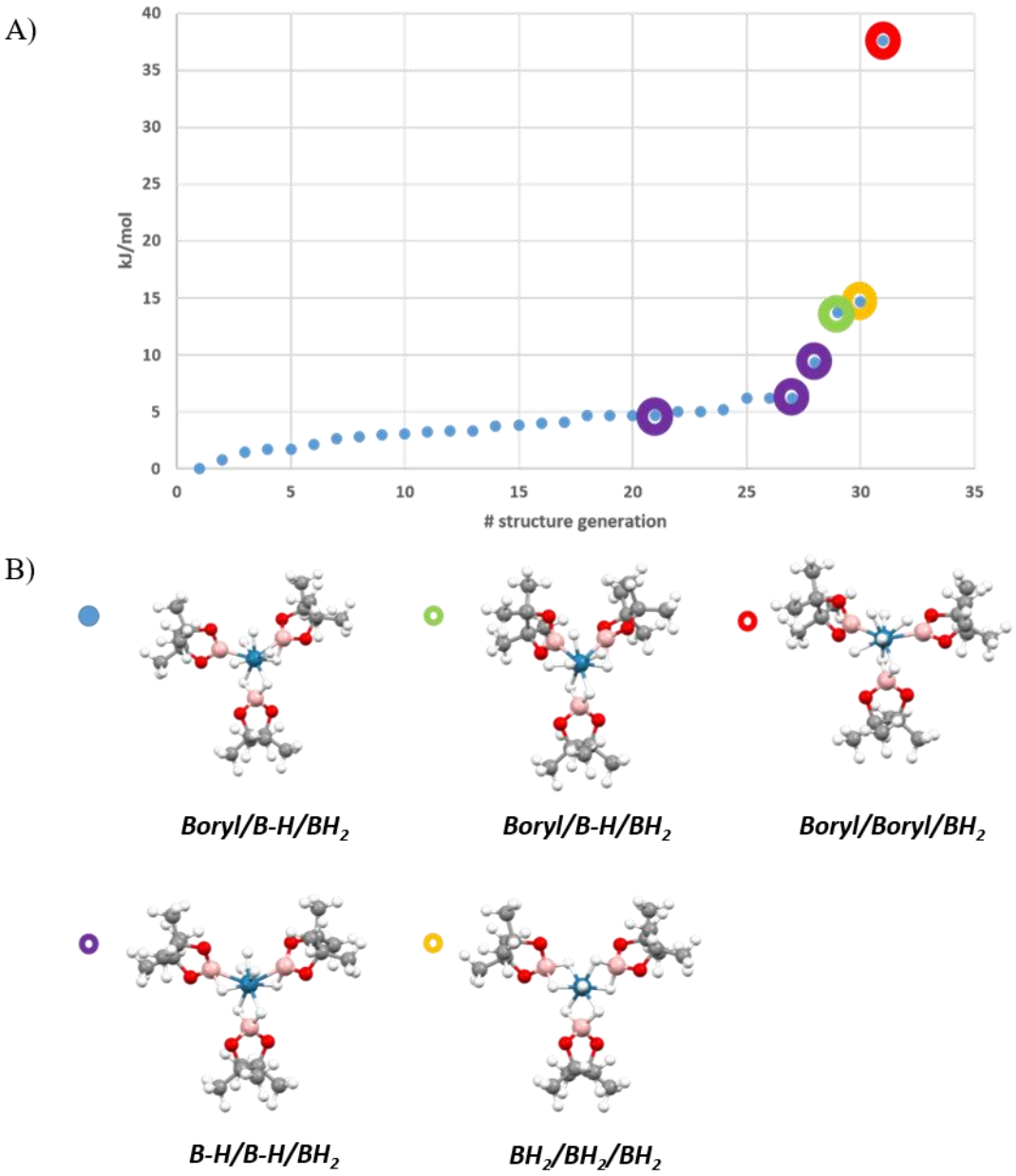

Figure 5. (A) Relative energies of the optimised structures of $[ReH_7(Bpin)_3]^-$ **165**, generated through randomising the initial positions of the seven hydrogen atoms around the Re centre, and (B) the five minima obtained.

The first point to observe is that all (bar six) of the optimised structures obtained conform to one structure type in which the Re is coordinated by one bridging dihydroborate ligand and one σ-borane ligand, leaving three equatorial hydrides and one axial terminal hydride at a formally Re^V centre. The repetition of this basic structural motif, which spans over an energy range of no more than 6 kJ mol^{-1}, present variations in the three B–B–B angles (which typically present as ca. 110, 115 and 130 ± 5°). The next most stable minimum, which was

found 5-10 kJ mol^{-1} above the lowest energy structure comprises one bridging dihydroborate ligand and two σ-borane ligands, leaving three (equatorial) Re–H bonds; the biggest variations between these structures again rests with the B–B–B angles, which adopt similar ranges to that noted above. The three remaining highest energy structures each have single multiplicity. The first at +14 kJ mol^{-1} is very similar to the lowest energy motif but with two equatorial and two axial terminal Re–H bonds; the second at +15 kJ mol^{-1} comprises three bridging dihydroborate ligands and one axial Re–H bond; the final and highest energy structure at +38 kJ mol^{-1} has just one bridging dihydroborate and five terminal Re–H bonds (three equatorial, two axial), and thereby represents a Re(VII) centre.

The higher energy structures featuring two boryl or three dihydroborate ligands were discounted, leaving a series of closely related, low-energy structures within 5 kJ mol^{-1} comprising three different bonding modes for the boron ligands: a dihydroborate (B2); a σ-borane (B1); a boryl (B3); and four terminal hydrides (Figure 6B). In collaboration with Prof. Simon Parsons this model was then used to place the hydrides in the crystal structure refinement (Figure 6A); while refinement is successful there is only a very minor enhancement to its quality. The geometry optimized and crystal structures show significant differences in the Re1–B2 distances (calc[d] 2.334 Å *c.f.* X-ray 2.175 Å) and the B1–Re1–B1'/B3 angles (calc[d] 130.2° *c.f.* X-ray 122.9°) which might arise from disorder in the crystal structure of the anion such that its geometrical parameters are averages.

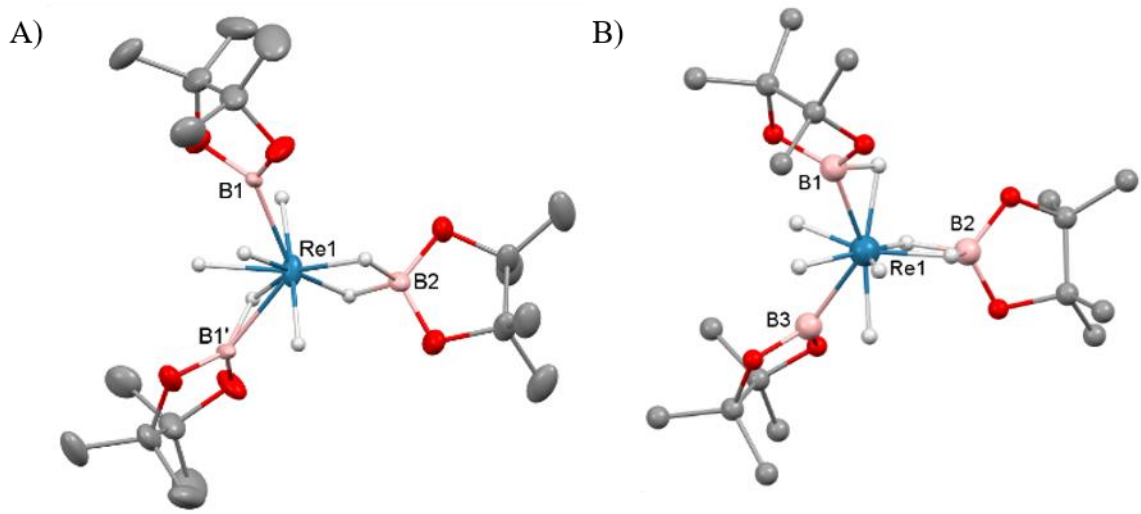

Figure 6. (A) Solid-state structure of **165**^{DME} (B) calculated structure of **165**. For clarity, the cation $[K(DME)(18\text{-c-}6)]^+$ and all hydrogen atoms except for the Re hydrides are omitted from the X-ray crystal structure; displacement ellipsoids are drawn at 50% probability. Selected distances (Å): Re1-B1 2.198(10); Re1-B2 2.174(14). Selected angles (°): B2-Re1-B1 118.6(2); B1-Re1-B1' 122.9(5). The crystallographic C2 symmetry is reflected in the heavy atom positions but not the hydride positions.

Also, the calculated structure portrays a formal Re(V) oxidation-state, whereas the short Re–B distances in the crystal structure and the ^{11}B NMR data are consistent with more boryl character and suggest a Re(VII) oxidation-state. It is therefore evident that rapid hydride/boron ligand rearrangement occurs as seen with other transition metal hydrides,[9-10] potentially by a σ-CAM mechanism,[11] resulting in a range of energetically similar structures (Scheme 40).[12]

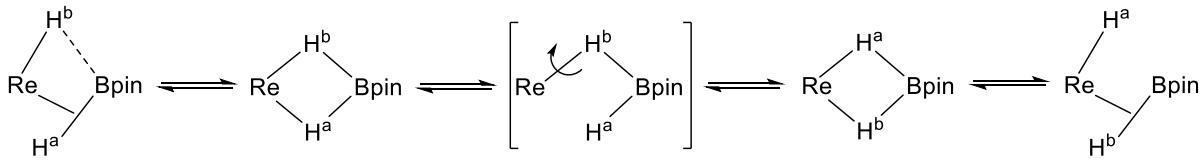

Scheme 40. Hydride rearrangement in **165** by a σ-CAM mechanism.

Dissolution of **165**^{DME} in d_8-THF resulted in a different ^{1}H NMR spectrum to that seen in d_8-toluene, showing a major signal at −7.74 ppm and a minor signal at −7.32 ppm that slightly increases in intensity over the course of 72 h (Figure 7), and these signals showed no coupling in the COSY NMR spectrum, suggesting the existence of two distinct Re–H species.

This feature was concomitant with the formation of free HBpin and the growth of a second signal at 41.9 ppm in the ^{11}B NMR spectrum (Figure 8). These spectra suggest that an equivalent of HBpin dissociates upon dissolution of **165^{DME}** in donor solvents to form the related rhenium boron-polyhydride, [K(DME)(18-c-6)][ReH$_6$(Bpin)$_2$(L)] **167^{THF}**, where L in this instance is THF (Scheme 41); decomposition of the two Re species to an insoluble material also occurred over time (see below). This ease of ligand exchange may be important in terms of the catalytic activity of **165** (see Chapter 3).

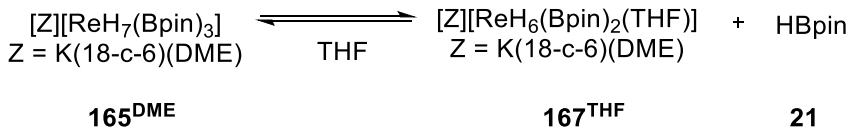

Scheme 41. Equilibrium established between **165^{DME}** and **167^{THF}** when **165^{DME}** upon dissolution in donor solvents such as THF.

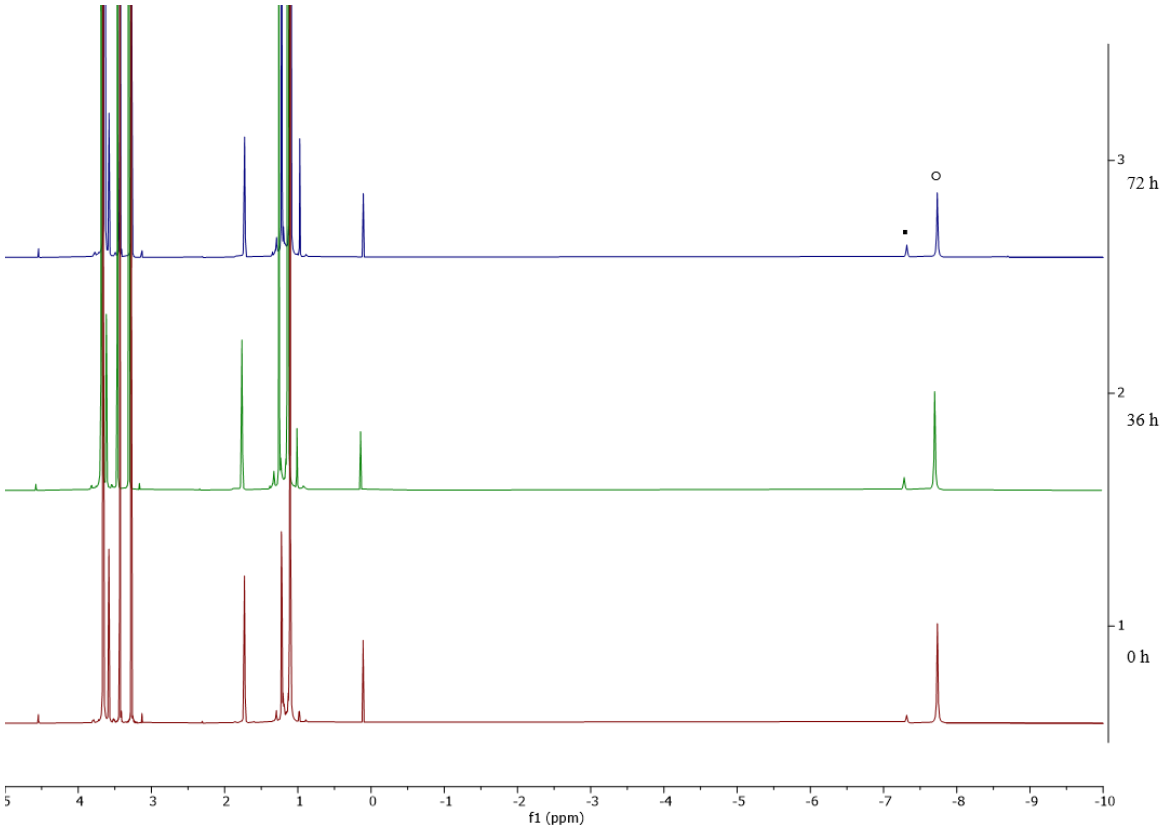

Figure 7. ^{1}H NMR spectrum of **165^{DME}** in THF-d$_8$. Assignment: ▪ **167^{THF}**, ○ **165^{DME}**.

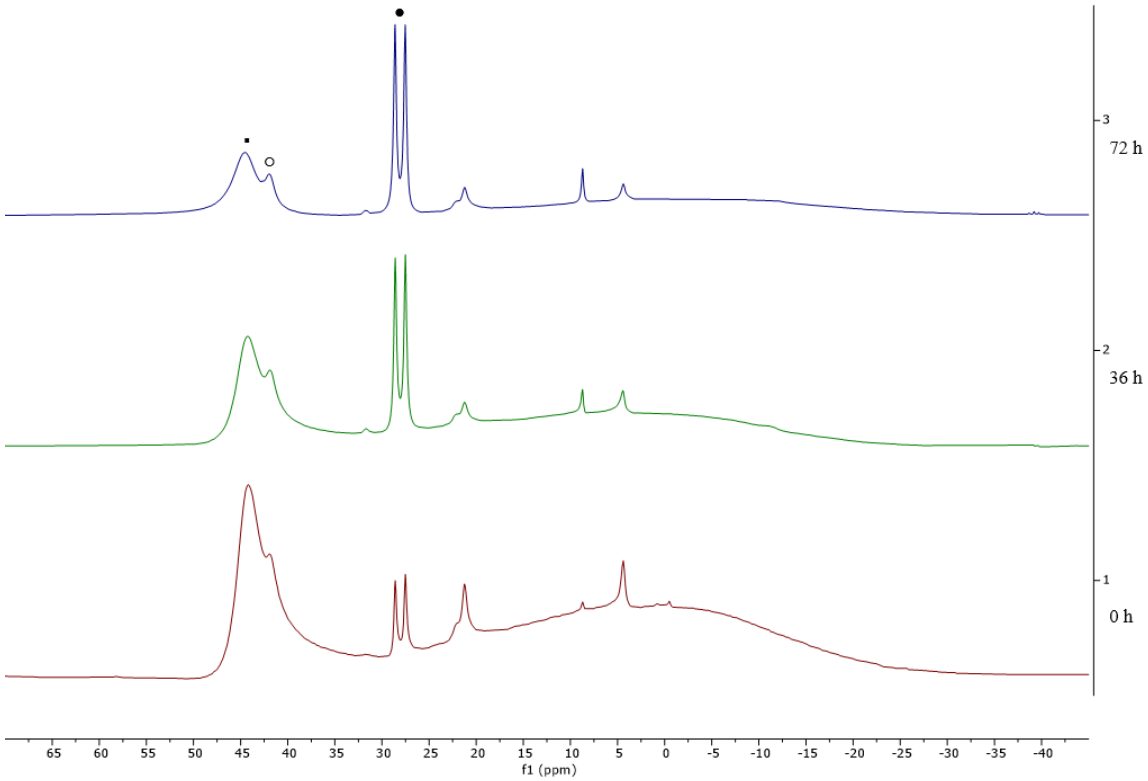

Figure 8. ^{11}B NMR spectrum of **165^{DME}** in THF-d$_8$. Assignment: ▪ **165^{THF}**, ○ **167^{DME}**, ● HBpin **21**.

2.1.2 Ammonium Salts

Initial NMR-scale stoichiometric reactions of [N(hexyl)$_4$][ReO$_4$] **163^{Nhex}** with HBpin **21** in C_6D_6 produced two hydride signals in the ^{1}H NMR spectrum at −6.16 and −6.46 ppm. The ^{11}B NMR spectrum of the reaction solution showed five different boron environments with signals observed at 45.6 (**165^{Nhex}**), 31.6, 21.9 (**166**), 4.9 and −0.4 ppm, with that at 21.9 ppm being the major signal. When this dark brown solution was allowed to stand at room temperature for 3 days, colourless crystals formed concomitant with decomposition of [N(hexyl)$_4$][ReH$_7$(Bpin)$_3$] **165^{NHex}**. This colourless material was identified as the 3-centre boronate complex [N(hexyl)$_4$][BpinO(Bpin)$_2$] **168** by single-crystal X-ray crystallography (Figure 9). The R-factor is quite high (0.1861) for the refined structure of **168**, and the cause of this appears to be associated with significant disorder in the [N(hexyl)$_4$]$^+$ that could not be adequately modelled even after imposing restraints. As the [BpinO(Bpin)$_2$]$^-$ anion was modelled well, reliable information about connectivity can be derived from this model. The ^{11}B NMR spectrum of this compound in C_6D_6 showed a signal at 4.9 ppm which matches well with the previously reported salt [^{t}Bu$_3$PNH$_2$][(Bpin(OBpin)$_2$].[13]

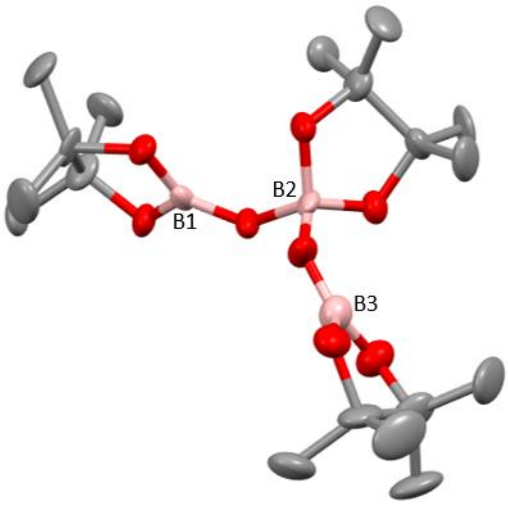

Figure 9. Solid-state structure of **168**. For clarity, the cation $[N(hexyl)_4]^+$ and all hydrogen atoms are omitted from the X-ray crystal structure; displacement ellipsoids are drawn at 50% probability.

On scale-up of this reaction using benzene as the solvent, stoichiometric C–H borylation of benzene was observed, forming PhBpin (See 1.1.3). HD formation was also observed in NMR-scale reactions, with a triplet at 4.43 ppm appearing in ^{1}H NMR spectrum, which indicates C–D activation of the solvent and H/D exchange, and which was confirmed by ^{2}D NMR studies. To avoid these C–H activation side reactions, subsequent mechanistic studies were performed in d_8-THF or proteo-solvents (THF, Et_2O, hexane, cyclohexane) with strong C–H bonds. For NMR-scale reactions conducted in THF, three singlets at −7.17, −7.32 and −7.74 ppm were observed in the ^{1}H NMR spectrum, the ^{11}B NMR spectrum of the reaction solution displayed four different boron environments with signals observed at 43.0, 32.2, 21.9 (**166**) and 4.69 (**168**) ppm; the signal at 43.0 ppm matches reported resonances for Re–Bpin/Bcat environments.[14-16]

During the reaction of $[NBu_4][ReO_4]$ with HBpin at −20 °C for 30 mins in neat conditions, the new complex $[NBu_4][ReH_n(Bpin)_2]$ crystallised adventitiously and the X-ray crystal structure was determined (Figure 10). While the R-factor was slightly high (0.0541), likely due to significant disorder in the $[NBu_4]^+$ cation that could not be adequately modelled, it is clear that only two boron ligands are present. Due to the poor quality of these data the hydride positions were not located. It is proposed that this complex is $[NBu_4][ReH_8(Bpin)_2]$ **167^{H2}** bearing a σ-H_2 ligand given that there is no coordinating solvent in the crystal structure. When these colourless crystals were dissolved in d_8-THF, a small amount of dark

solid precipitated and the ^{1}H and ^{11}B NMR spectra showed a mixture of $[NBu_4][ReH_7(Bpin)_3]$ **165^{NBu}** and $[NBu_4][ReH_6(Bpin)_2(THF)]$ **167**. It is proposed that a mixture of these two compounds forms initially during the reaction of $[Z][ReO_4]$ **163** with HBpin **21** in donor solvents such as THF, but $[Z][ReH_6(Bpin)_2(L)]$ **167** converts into $[Z][ReH_7(Bpin)_3]$ **165** in a large excess of HBpin.

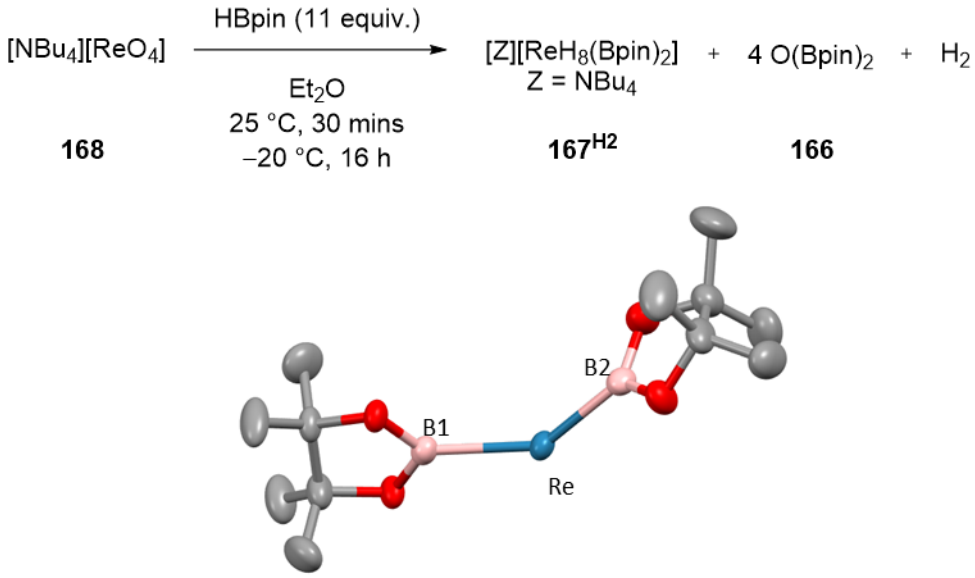

Figure 10. The reaction of $[NBu_4][ReO_4]$ with HBpin to form **167^{H2}** and solid-state structure of **167^{H2}**. For clarity, the cation $[NBu_4]^+$ and all hydrogen atoms are omitted from the X-ray crystal structure; displacement ellipsoids are drawn at 50% probability.

Isolation of high purity products with alkylammonium countercations was challenging due to their high solubility in common organic solvents and their lack of crystallinity. In order to obtain high purity crystalline material $[PPN]^+$ was used as the countercation, due to its reputation for forming highly crystalline salts. $[PPN][ReO_4]$ **163^{PPN}** was synthesised in high yield by a salt metathesis reaction between $[K][ReO_4]$ **163^{K}** and [PPN][Cl] **169** and was used in stoichiometric reactions with HBpin **21** in THF. A broad singlet at −7.19 ppm was observed in the ^{1}H NMR spectrum of the reaction mixture and the ^{11}B NMR spectrum showed three different boron environments at 31.9 and 21.5 (**166**) ppm. After partial purification of the dark brown reaction mixture, the only species remaining by ^{11}B NMR spectroscopy was the singlet at 31.9 ppm and residual $O(Bpin)_2$ **166**. The resonance at 31.9 ppm is indicative of an Ar–Bpin environment, suggesting that the PPN cation has been borylated, and further evidence for this was observed in the ^{1}H and ^{13}C NMR spectra. Therefore, this reaction appears to provide multiple products with no chemoselectivity over

which C–H bond is borylated. This reactivity hindered the isolation of pure crystalline material. C–H borylation of the PPN cation was not observed by NMR spectroscopy during cation exchange of [K(DME)(18-c-6)][$ReH_7(Bpin)_3$] **165^{DME}** and [PPN][Cl] **169** and there was no observed shift in hydride and Re–B signals.

2.2 Stoichiometric reactivity

[K(DME)(18-c-6)][$ReH_7(Bpin)_3$] **165^{DME}** is stable indefinitely in the solid-state when stored under N_2 or Ar at −20 °C but decomposes with loss of H_2 and HBpin **21** over 3-5 days in ethereal solvents at room temperature to give an insoluble and unidentified dark-brown solid. In contrast, [K(DME)(18-c-6)][$ReH_7(Bpin)_3$] **165^{DME}** reacted cleanly with aromatic solvents such as toluene over 3 days at room temperature to form the aryl boronic esters and an insoluble, dark-brown rhenium species. Toluene **170** underwent C–H borylation with high regioselectivity for the *meta* C–H over the *para* C–H (81:19) (Scheme 42). To the best of our knowledge, this is the highest reported *meta* selectivity observed for the stoichiometric or catalytic C–H borylation of toluene.[17] This reaction is likely to proceed by a similar mechanism reported for [$Ir(Bpin)_3(L)_2$] complexes which undergo σ-CAM activation of the arene C–H bond, where L is a bisphosphine, bipyridine or phenanthroline ligand.[18-19] This is the first example of a high oxidation-state rhenium complex mediating C(sp^2)–H borylation, contrasting with the two previous examples that use complexes of lower oxidation-states for C(sp^3/sp^2)–H borylation.[14, 20]

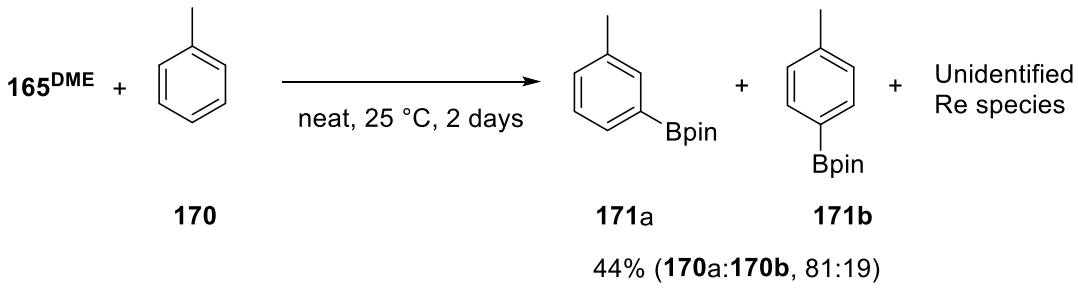

Scheme 42. Stoichiometric C–H borylation of toluene **170** by **165^{DME}**.

In addition to C–H functionalization, **165^{DME}** also underwent borane exchange. Reaction of [K(DME)(18-c-6)][$ReH_7(Bpin)_3$] **165^{DME}** with 4 equivalents of H-9-BBN **36** formed the new tetrahydroborate complex [K(DME)(18-c-6)][Re(κ^2-H-9-BBN)$_4$] **172** in 82% yield, along with three equivalents of HBpin (Scheme 43). The solid-state structure of **172** revealed dihydroborate ligands in a tetrahedral geometry at the Re atom (average B–Re–B = 109.1°). The hydrides were located in the difference Fourier map and display an average B–H bond

length of 1.284(2) Å, with the average Re–B distance of 2.296(2) Å similar to those seen in the optimised structure of [K(DME)(18-c-6)][$ReH_7(Bpin)_3$] **165^{DME}** and to related dihydroborate complexes.[21-23]

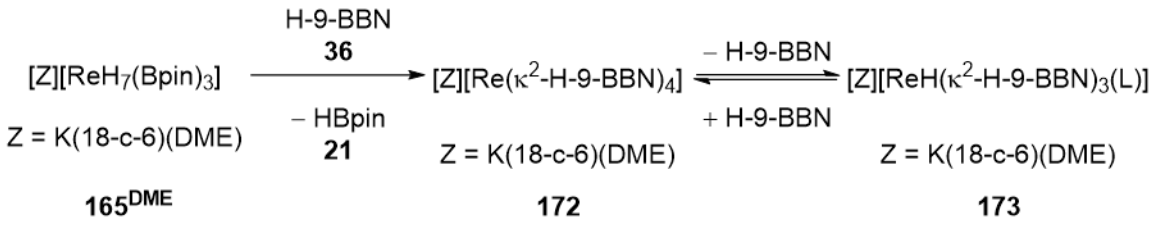

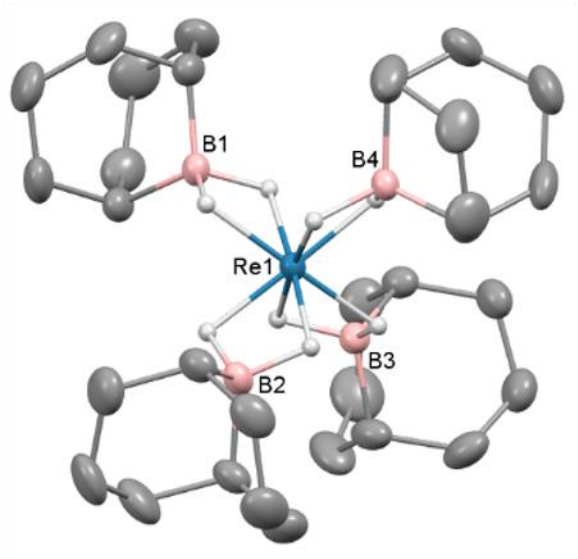

Scheme 43. Borane exchange of **165^{DME}** with H-9-BBN **36** to form **172** which readily dissociates an equivalent of H-9-BBN **36** upon dissolution in donor solvents to form **173** and the solid-state structure of **172**. For clarity, the cation $[K(DME)(18\text{-c-}6)]^+$ and all hydrogen atoms except for the Re hydrides are omitted; displacement ellipsoids are drawn at 50% probability. Selected distances (Å): B-H (avg.) 1.284(2); Re-B (avg.) 2.296(2); Re-H (avg.) 1.731(2). Selected angles (°): H-B-H (avg.) 94.8(3); H-Re-H (avg.) 66.23(3).

The IR spectrum of **172** did not display any absorptions attributable to Re–H stretches which further supports a borohydride bonding motif. Complex **172** is insoluble in aromatic and alkane solvents. On dissolution in d_8-THF, the ^{1}H NMR spectrum showed two hydride signals at −9.02 ppm (s, br), −9.80 ppm (s) which have a combined integration of 8 protons (Figure 11). As H-9-BBN monomer was seen in the ^{11}B NMR spectrum, it is evident that substitution of H-9-BBN by THF occurs to form a mixture of complex **172** and presumably the THF-adduct [K(DME)(18-c-6)][Re((κ^2-H-9-BBN)$_3$(THF)] **173** (Figure 12). Upon addition of 1 equivalent of H-9-BBN to a solution of crystalline **172**, the ratio of **172** to **173** increased from 61:39 to 97:3. A coinciding decrease occured in the signal at 52.7 ppm and an

increase in the signal at 29.4 ppm in the ^{11}B NMR spectrum. In contrast, addition of 2 equivalents of DABCO to a solution of **172** gave **173** as the only hydridic species in the ^{1}H NMR spectrum (Figure 13), with the only signals in the ^{11}B NMR spectrum at 52.7 ppm and the DABCO•H-9-BBN adduct at 2.38 ppm (Figure 14). A minor unknown species was also formed upon dissolution of **172** in d_8-THF that displayed a sharp singlet at 57.4 ppm in the ^{11}B NMR spectrum that diminished upon addition of either DABCO or H-9-BBN.

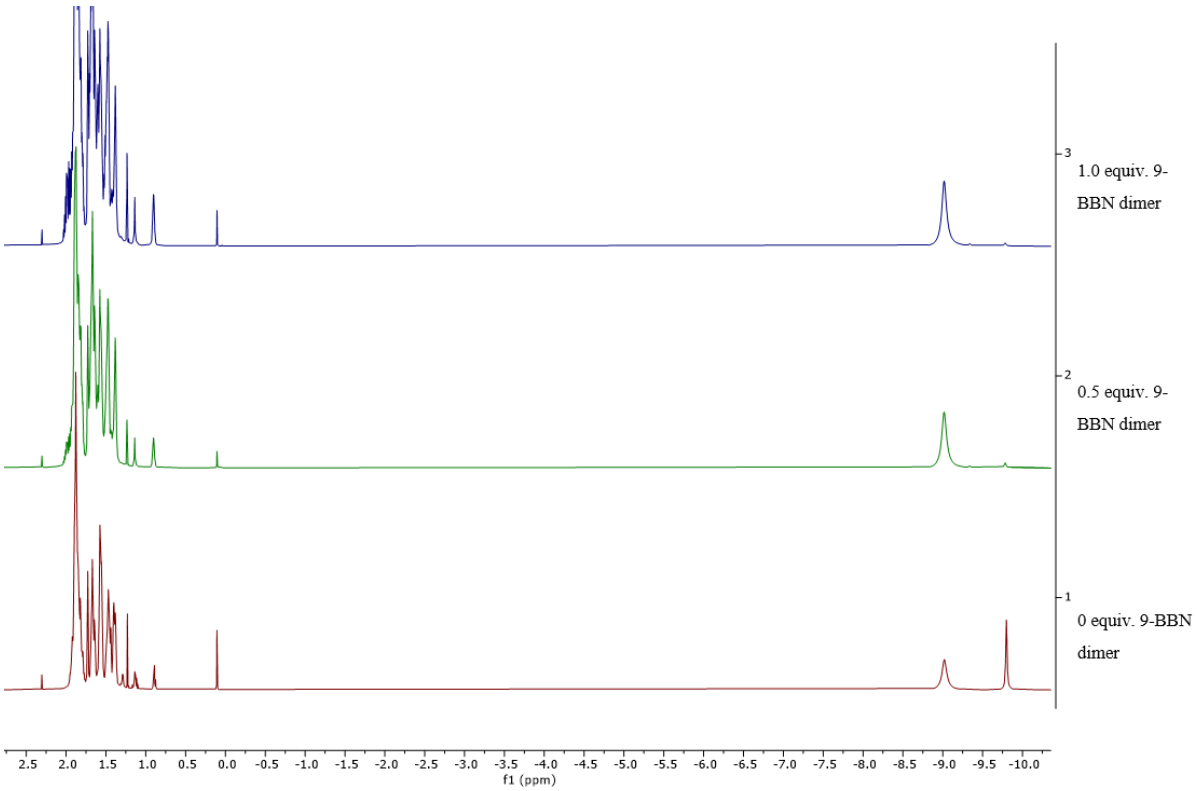

Figure 11. ^{1}H NMR spectrum of addition of H-9-BBN dimer to **172** in THF-d_8.

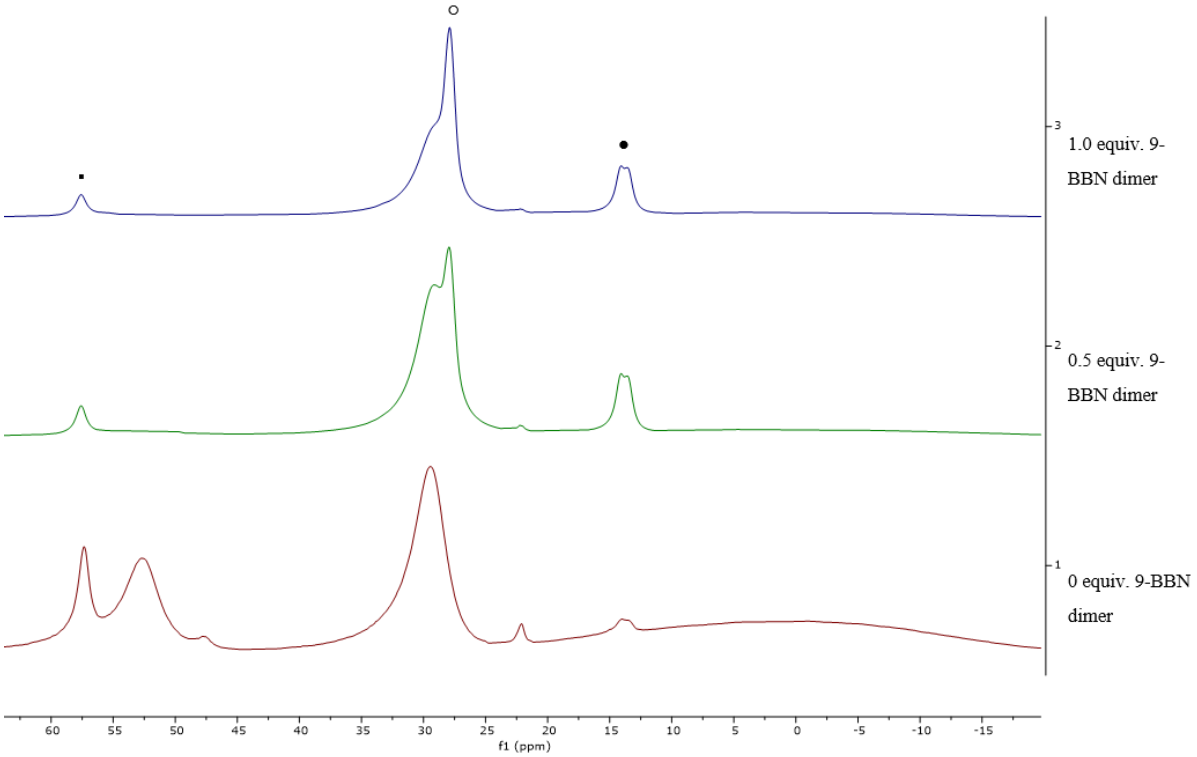

Figure 12. ^{11}B NMR spectrum of addition of H-9-BBN dimer to **172** in THF-d_8. ▪ Unknown, ○ H-9-BBN dimer, ● H-9-BBN monomer.

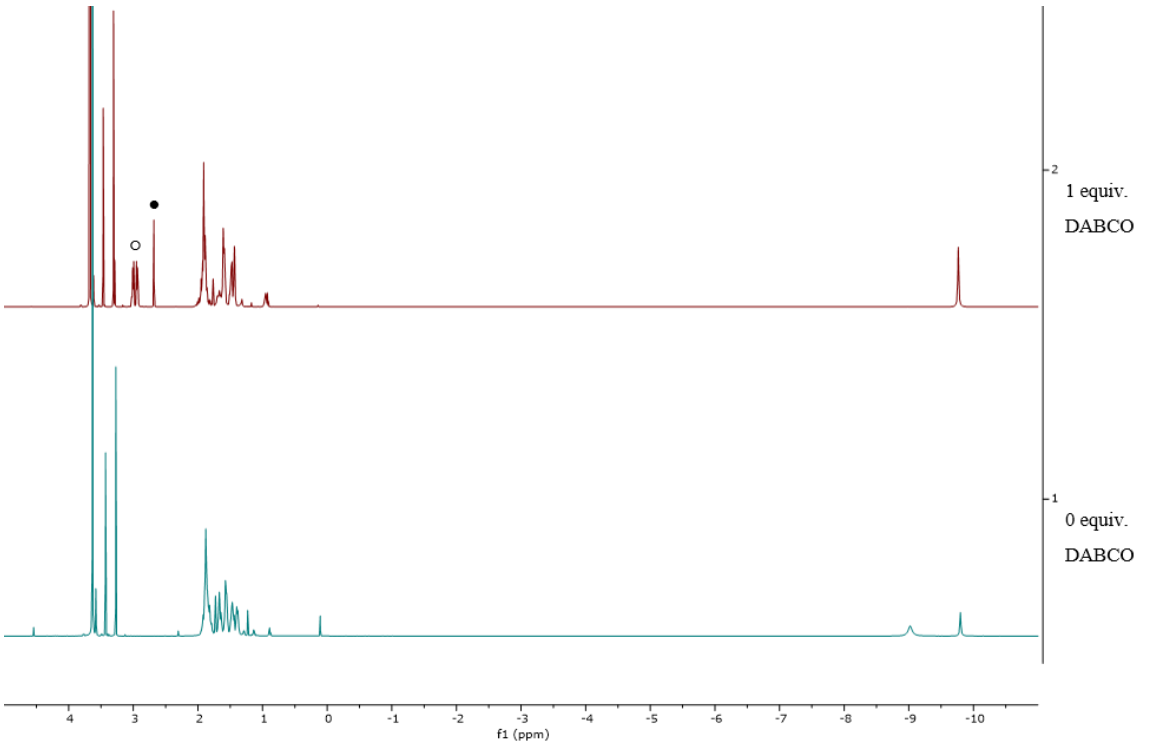

Figure 13. ^{1}H NMR spectrum of addition of DABCO to **172** in THF-d_8. ○ DABCO•H-9-BBN adduct, ● Free DABCO.

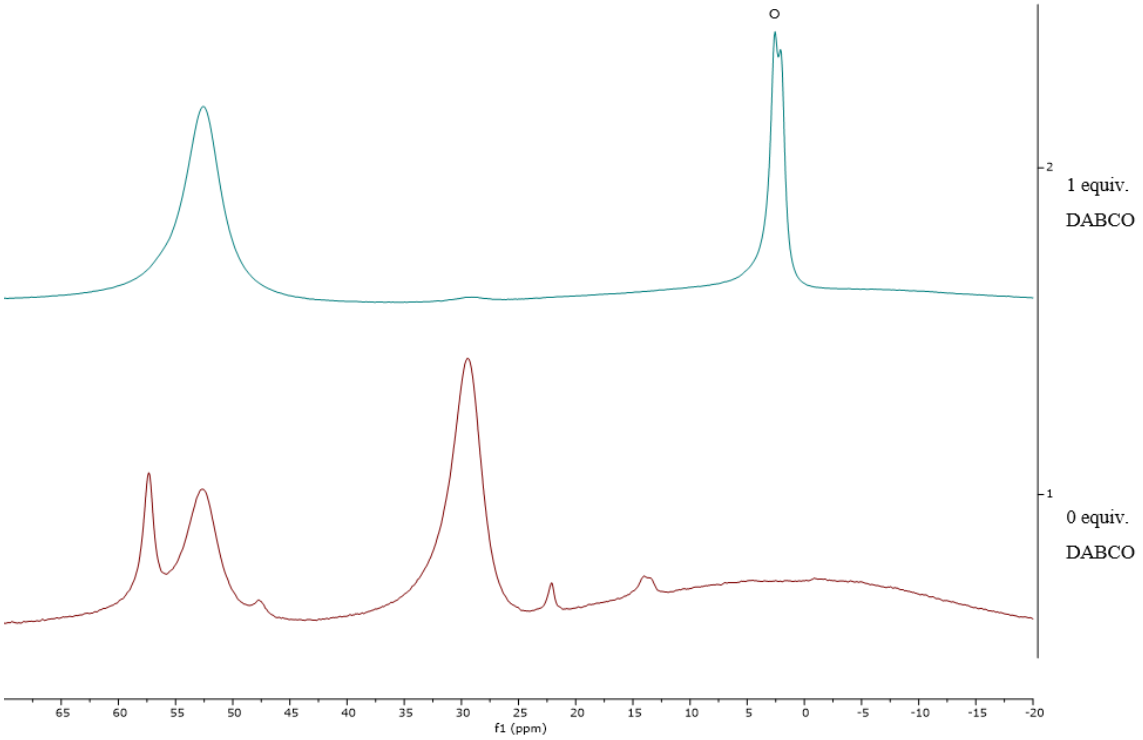

Figure 14. ^{1}H NMR spectrum of addition of DABCO to **172** in THF-d_8. ○ DABCO•H-9-BBN adduct.

The reaction between $HBCy_2$ **174** and $[K(DME)(18\text{-c-}6)][ReH_7(Bpin)_3]$ $\mathbf{165^{DME}}$ also resulted in HBpin **21** substitution but in this case only by 3 equivalents, forming $[K(DME)(18\text{-c-}6)][ReH(\kappa^2\text{-}H_2BCy_2)_3]$ **175** in 73% yield. The ^{1}H NMR spectrum of **175** in d_8-THF showed a single hydride signal at −11.12 ppm and a single resonance in the ^{11}B NMR spectrum at 51.1 ppm. The difference in borane formulation between **172** and **175** is presumably due to the increased steric bulk of the cyclohexyl substituents of $HBCy_2$ **174** compared with the cyclononane backbone of **36**, preventing a fourth $HBCy_2$ **174** equivalent binding to the complex.

2.3 Perrhenate deoxygenation using other boranes

Deoxygenation of perrhenate was also achieved using other hydroboranes (Scheme 44). The addition of solid $[K][ReO_4]$ $\mathbf{163^K}$ to a stirred solution of 18-c-6 **164** and the appropriate hydroborane in toluene at room temperature formed **172** for H-9-BBN **36** and **175** for $HBCy_2$ **174**, respectively, and is complementary reactivity to the borane exchange reactions discussed previously. Using HBcat **17** resulted in a complex mixture of products in the ^{11}B NMR spectrum including BH_3 and BH_4^-, when the reaction was carried out in toluene, THF, or without solvent; nucleophile-initiated decomposition of HBcat **17** to form BH_3 and

hydroborate species is well documented.[24]. No reaction was observed by addition of H_3B•DMS **175** to [K][ReO_4]. Other non-commercially available hydroboranes were synthesised and trialled in this reaction to examine the effects of changing the steric and electronic properties of the substituents on boron. The diamino borane **176** was shown to be unreactive in the deoxygenation reaction,[25] presumably due to the significant electron donation of the amine substituents to the B p-orbital. The sterically bulky dialkoxy borane **177** was also unreactive,[26] giving an indication of the steric constraints of this reactivity. The enantioenriched borane (−)-Ipc_2BH **178** was synthesised and was also found to be unreactive in the deoxygenation reaction which could be due to the deborylation of α-pinene upon dissolution of crystalline (−)-Ipc_2BH dimer.[27]

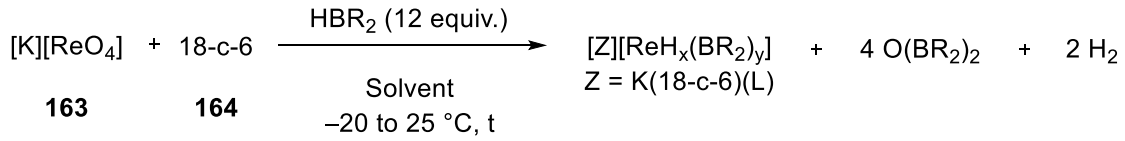

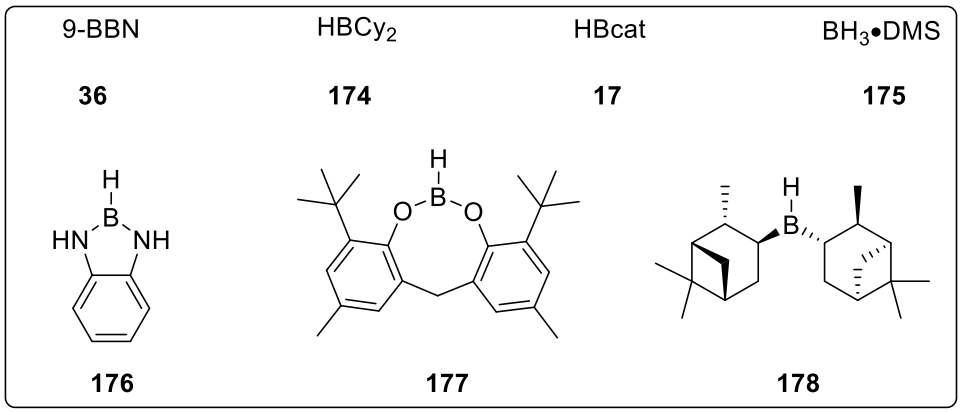

Scheme 44. Perrhenate deoxygenation with other boranes.

2.4 Perrhenate deoxygenation mechanism

Perrhenate is considered to be a weak nucleophile and is often used as a non-coordinating anion in molecular inorganic chemistry. However, the Love Group have shown by DFT calculations that perrhenate can coordinate to Lewis acidic Si atoms of hydrosilanes to activate them towards hydride transfer to CO_2.[28] Analogous reactivity has been observed with boranes. Green and co-workers have shown that simple ammonium and phosphonium perrhenate salts can form adducts with BCF **129** through coordination of an oxo ligand to the B atom; in this case no cleavage of the B–C bond is observed.[29] Arnold and co-workers have shown that other Re-oxo catalysts are able to cleave this bond through a similar intermediate

where the oxo coordinates to BCF **129**.[30] Fernandes and co-workers reported the [2+2] addition of hydroboranes to Re-oxo complexes which was proposed to proceed by addition of the oxo ligand to B to form a tetrahedral boron intermediate which can then transfer a hydride to Re. This reactivity is reminiscent of the activation of HBpin **21** by alkoxide salts to generate a hydridic boron 'ate' complex that, when generated *in situ,* can be used to reduce transition metal pre-catalysts.[31] None of these examples of Re-oxo reactivity show complete rupture of the Re=O bond to form a deoxygenated product, as has been observed for the reaction of $[ReO_4]^-$ with HBpin. The Re=O bond of $[ReO_4]^-$ is relatively labile, as demonstrated by its oxygen atom transfer chemistry,[32-33] and can be considered more nucleophilic than the majority of neutral Re-oxo complexes which may be the characteristics that enable deoxygenation by HBpin **21**.

Based on this previous work and experimental observations, the following potential pathways are proposed for $[ReO_4]^-$ deoxygenation (Scheme 45). The initial step is most likely coordination of the Re=O to the B atom of HBR_2, followed by [2+2] addition of HBR_2 across the Re=O bond. This Re boroxy-hydride intermediate could then react with a second equivalent of HBR_2 to eliminate $O(BR_2)_2$ and form a dihydride intermediate **Int-A** which could either eliminate H_2 to form $[ReO_3]^-$ **Int-B**, which has been proposed as an intermediate in DODH catalysis, from which further steps involving iterative $H_2/O(BR_2)_2$ elimination and HBR_2 addition would eventually lead to the formation of the exhaustively deoxygenated product.

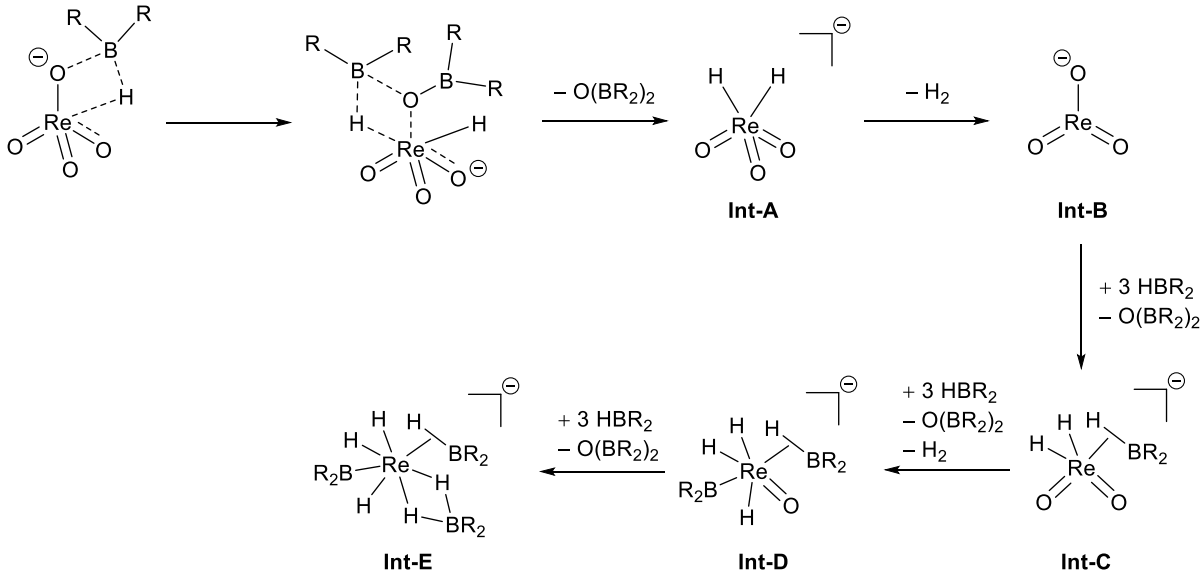

Scheme 45. Proposed mechanistic pathway for the deoxygenation of $[ReO_4]^-$ by hydroboranes.

2.5 References

1. Fernandes, A. C.; Fernandes, J. A.; Almeida Paz, F. A.; Romao, C. C., *Dalton Trans.* **2008**, 6686-6688.

2. Fernandes, A. C.; Fernandes, J. A.; Romão, C. C.; Veiros, L. F.; Calhorda, M. J., *Organometallics* **2010**, *29*, 5517-5525.

3. Zhang, N.; Sherbo, R. S.; Bindra, G. S.; Zhu, D.; Budzelaar, P. H. M., *Organometallics* **2017**, *36*, 4123-4135.

4. Cook, K. S.; Incarvito, C. D.; Webster, C. E.; Fan, Y.; Hall, M. B.; Hartwig, J. F., *Angew. Chem. Int. Ed.* **2004**, *43*, 5474-5477.

5. Hartwig, J. F.; Cook, K. S.; Hapke, M.; Incarvito, C. D.; Fan, Y.; Webster, C. E.; Hall, M. B., *J. Am. Chem. Soc.* **2005**, *127*, 2538-2552.

6. Callaghan, P. L.; Fernández-Pacheco, R.; Jasim, N.; Lachaize, S.; Marder, T. B.; Perutz, R. N.; Rivalta, E.; Sabo-Etienne, S., *Chem. Commun.* **2004**, 242-243.

7. Pickard, C. J.; Needs, R. J., *J. Condens. Matter Phys.* **2011**, *23*, 053201.

8. Clark, S. J.; Segall, M. D.; Pickard, C. J.; Hasnip, P. J.; Probert, M. I. J.; Refson, K.; Payne, M. C., *Z. Kristallogr. Cryst. Mater.* **2005**, *220*, 567.

9. Kawamura, K.; Hartwig, J. F., *J. Am. Chem. Soc.* **2001**, *123*, 8422-8423.

10. Ghaffari, B.; Vanchura, B. A.; Chotana, G. A.; Staples, R. J.; Holmes, D.; Maleczka, R. E.; Smith, M. R., *Organometallics* **2015**, *34*, 4732-4740.

11. Perutz, R. N.; Sabo-Etienne, S., *Angew. Chem. Int. Ed.* **2007**, *46*, 2578-2592.

12. Sieffert, N.; Kendrick, T.; Tiana, D.; Morrison, C. A *Dalton Trans.* **2015**, *44*, 4259-4270.

13. Hawkeswood, S.; Stephan, D. W., *Dalton Trans.* **2005**, 2182-2187.

14. Chen, H.; Hartwig, J. F., *Angew. Chem. Int. Ed.* **1999**, *38*, 3391-3393.

15. Waltz, K. M.; Muhoro, C. N.; Hartwig, J. F., *Organometallics* **1999**, *18*, 3383-3393.

16. Schlecht, S.; Hartwig, J. F., *J. Am. Chem. Soc.* **2000**, *122*, 9435-9443.

17. Kato, T.; Kuriyama, S.; Nakajima, K.; Nishibayashi, Y., *Chem. Asian J.* **2019**, *14*, 2097-2101.

18. Boller, T. M.; Murphy, J. M.; Hapke, M.; Ishiyama, T.; Miyaura, N.; Hartwig, J. F., *J. Am. Chem. Soc.* **2005**, *127*, 14263-14278.

19. Tamura, H.; Yamazaki, H.; Sato, H.; Sakaki, S., *J. Am. Chem. Soc.* **2003**, *125*, 16114-16126.

20. Murai, M.; Omura, T.; Kuninobu, Y.; Takai, K., *Chem. Commun.* **2015**, *51*, 4583-4586.

21. Ding, E.; Du, B.; Meyers, E. A.; Shore, S. G.; Yousufuddin, M.; Bau, R.; McIntyre, G. J., *Inorg. Chem.* **2005**, *44*, 2459-2464.

22. Liu, X.-Y.; Bouherour, S.; Jacobsen, H.; Schmalle, H. W.; Berke, H., *Inorganica Chim. Acta* **2002**, *330*, 250-267.

23. Ding, E.; Du, B.; Liu, F.-C.; Liu, S.; Meyers, E. A.; Shore, S. G., *Inorg. Chem.* **2005**, *44*, 4871-4878.

24. Bage, A. D.; Hunt, T. A.; Thomas, S. P., *Org. Lett.* **2020**, *22*, 4107-4112.

25. Hadebe, S. W.; Robinson, R. S., *Eur. J. Org. Chem.* **2006**, *2006*, 4898-4904.

26. Lang, A.; Nöth, H.; Thomann-Albach, M., *Chemische Berichte* **1997**, *130*, 363-370.

27. Fürstner, A.; Bonnekessel, M.; Blank, J. T.; Radkowski, K.; Seidel, G.; Lacombe, F.; Gabor, B.; Mynott, R., *Chem. Eur. J.* **2007**, *13*, 8762-8783.

28. Morris, D. S.; Weetman, C.; Wennmacher, J. T. C.; Cokoja, M.; Drees, M.; Kühn, F. E.; Love, J. B., *Catal. Sci. Technol.* **2017**, *7*, 2838-2845.

29. Barrado, G.; Doerrer, L.; L. H. Green, M.; A. Leech, M., *J. Chem. Soc., Dalton Trans.* **1999**, 1061-1066.

30. Lohrey, T. D.; Cortes, E. A.; Bergman, R. G.; Arnold, J., *Inorg. Chem.* **2020**

31. Peng, J.; Thomas, S. P., *Synlett* **2020**, *31*, 1140-1146.

32. Donnelly, L. J.; Thomas, S. P.; Love, J. B., *Chem. Asian J.* **2019**, *14*, 3782-3790.
33. Dethlefsen, J. R.; Fristrup, P., *ChemSusChem* **2015**, *8*, 767-775.

Chapter Three – Hydrofunctionalisation Catalysis

3.1 Perrhenate-Catalysed Hydroboration

3.1.1 Substrate Screening

As has been described in Chapter 1, the reactivity of high oxidation-state metal-oxo compounds towards hydroboration has been reported previously but is much less well established than hydrosilylation reactions. Previously reported results within the Love group have shown that a perrhenate precatalyst can activate HBpin **21** towards the hydroboration of aldehydes under air and using 'wet' solvents (Scheme 1).[1] To mitigate the loss of HBpin **21**, due to the reaction with H_2O to form $O(Bpin)_2$ **166**, an excess of HBpin was used to give full conversion of starting material.

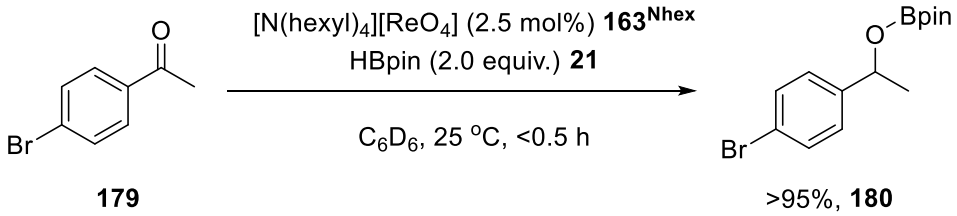

Scheme 46. Hydroboration of **179** using $[N(hexyl)_4][ReO_4]$ **163^{Nhex}**.

This result provided the basis to subject a range of organic compounds containing unsaturated bonds to these unoptimised hydroboration conditions (Table 1). Interestingly, HBpin **21** appears to be more reactive than silanes in perrhenate-catalysed hydrofunctionalisation.[2] Pyridine **181** was successfully reduced to the *N*-boryl-dihydropyridine **182** in good yield and selectivity for the 1,4-product **182a** over the 1,2-product **182b** (entry 1). Benzonitrile **183** was reduced to the corresponding aminoborane **184** in moderate yield (entry 2) and styrene **185** underwent hydroboration to give a 1:1 mixture of the *anti*-Markovnikov **186** and Markovnikov **187** products (entry 3). In contrast, phenylacetylene **188** exhibited poor conversion to the corresponding alkenyl boronic ester product **189** and styrene **185** (entry 4). In all of these reactions the conversion was low due to competitive consumption of HBpin through its reaction with water to give $O(Bpin)_2$ **166** as a side-product, as these reactions were performed open to air and in 'wet' solvents. In the analogous reactions with hydrosilanes only trace conversion to the hydrosilylated products were observed even after extended reaction times at 80 °C.

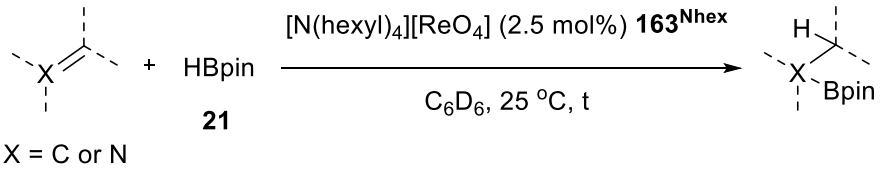

Entry	Substrate	HBpin equiv.	Time (hours)	Products (yields)
1	 **181**	1.05	20	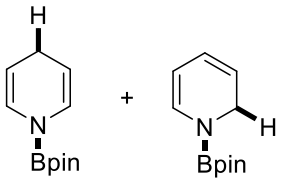 **182a** **182b** 64%, 95:5
2	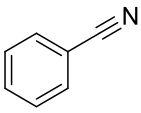 **183**	2.1	20	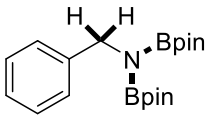 50%, **184**
3	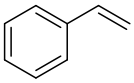 **185**	1.05	4	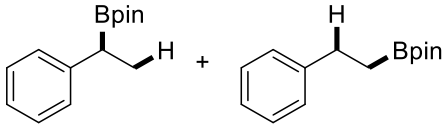 **186** **187** 82%, 51:49
4	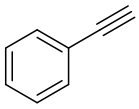 **188**	2.1	4	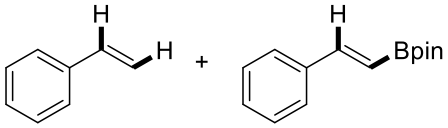 **185** **189** 11%, 55:45

Table 1. $[N(hexyl)_4][ReO_4]$ **163**^{Nhex} - catalysed hydroboration of unsaturated organic compounds. Reactions conducted in C_6D_6, 25 °C., 0.2 mmol scale, 2.5 mol% [Re] catalyst. % Yields determined by ^1H NMR (10 µL of mesitylene as internal standard).

3.1.2 Catalytic Hydroboration of *N*-Heterocycles

The most interesting of these results was the hydroboration of pyridine **181** (Table 1, Entry 1). The dearomatisation of *N*-heteroaromatic compounds is a challenging and synthetically useful transformation that can provide access to key structural motifs present in many bioactive molecules.[3] Dihydropyridines (DHPs) are widely prevalent in nature, and are useful building blocks in synthetic organic chemistry for the synthesis of pharmaceuticals and natural products (Figure 15). DHPs are also applied as a hydride transfer reagents for the reduction of organic molecules.[4] As a result, many stoichiometric methods for the synthesis of these molecules have been developed, such as the Hantzsch DHP synthesis and nucleophilic addition to pyridinium salts.[5] However, these reactions suffer from forcing conditions, poor regio- and chemoselectivity, and poor atom economy.

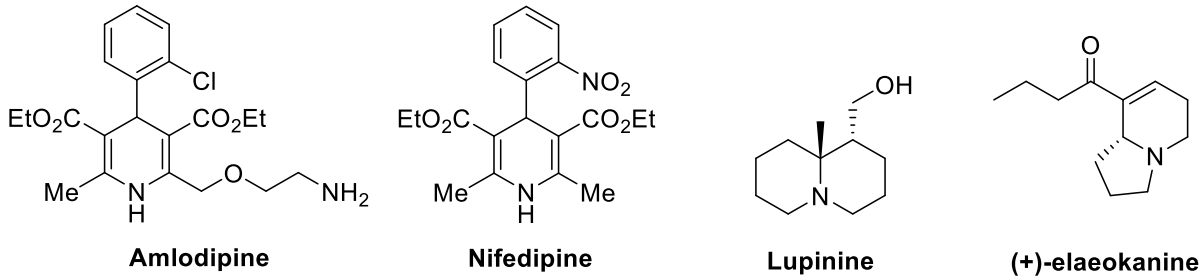

Figure 15. Drug molecules and natural products containing de-aromatised pyridine moieties.

Hill and co-workers reported that a magnesium complex **190** catalysed pyridine hydroboration to form a mixture of 1,2 and 1,4-hydroboration products (Scheme 47).[6] This system showed poor chemoselectivity, with aldehyde, ester and nitrile functionalities all being reduced. In recent years, alternative catalysts have been reported for the selective hydroboration of pyridines, including 1,2 selective reactions using Mg,[7-8] Zn,[9] Fe (**192**),[10] Ni,[11] Rh[12], Th[13] and La (**191**)[14] catalysts. Suginome and co-workers developed a stoichiometric de-aromatisation of pyrazine,[15] and the Fontaine group demonstrated the use of BH_3 as a catalyst for the hydroboration of indoles.[16] Chang and co-workers have shown that simple NHC compounds can catalyse the hydroboration of *N*-heteroaromatics with high selectivity for the 1,2-DHP products.[17]

A number of catalyst have also been used to favour the 1,4-hydroboration product. Wang reported the first example of a metal-free approach giving high regioselectivity and excellent functional group tolerance using an organoborane catalyst (**193**),[18] and Wright has shown that

the commercially available boronium salt $[NH_4][BPh_4]$ was also a competent catalyst, although with reduced regioselectivity and functional group tolerance.[19] Park and Chang have shown that metal alkoxides can be used to generate BH_3 from HBpin **21** *in situ* which acts as a catalyst for this transformation forming 1,4-DHP products with high selectivity.[20] Kinjo and co-workers have synthesised a highly active and regioselective diazaphosphenium catalyst for 1,4-hydroboration with excellent functional group tolerance (cyano, alkene, alkyne and ketone functionalities),[21] and Speed has shown that a similar organophosphorus complex can act as competent 1,4-hydroboration catalyst; in this latter case, low yields were seen in several cases and required electron-withdrawing substituents in the 3-position of the pyridines to be effective.[22] So and co-workers showed that a silyliumylidene cation was an active catalyst for the 1,4-hydroboration of *N*-heteroaromatics.[23] Lin and co-workers developed a Zr/Hf MOF that was an effective catalyst for this transformation even at low catalyst loadings (0.2 mol%); however, a high reaction temperature was required (90 ^{o}C) and the reaction proceeded with relatively poor regioselectivity.[24] Work by Gunanathan and co-workers showed that the simple precatalyst $[Ru(p\text{-cymene})Cl_2]_2$ was effective in the selective 1,4-hydroboration of a range of pyridine derivatives, under solvent-free conditions with high regioselectivity.[25] Findlater and co-workers have recently shown that the air-stable and commercially available $Ni(acac)_2$ was an effective catalyst for the de-aromatisation of a range of pyridines, even for a number of 2- and 4-substituted pyridines that are not reactive in other catalyst systems.[26] Mankad and co-workers developed a cooperative heterobimetallic Cu/Fe system for the 1,4-hydroboration of pyridines.[27] These protocols provide a range of catalysts and reaction conditions to control the regioselectivity and chemoselectivity of the hydroboration reaction.[28-30]

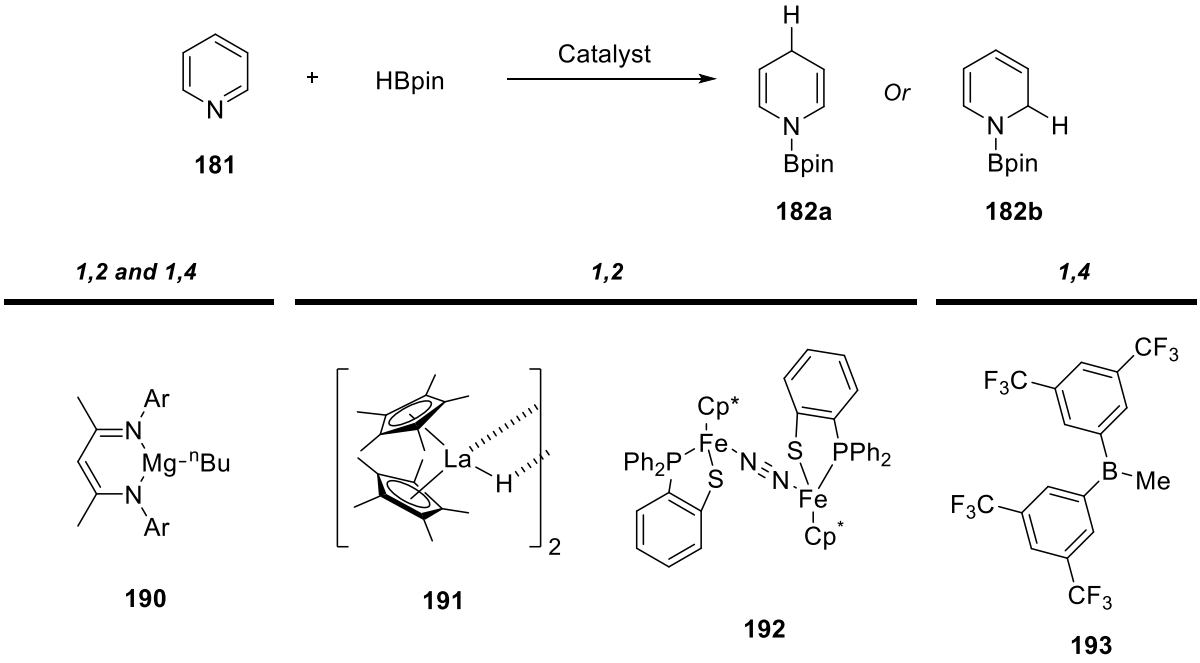

Scheme 47. Representative examples of the catalytic hydroboration of pyridine **181**.

While effective, many of these catalytic protocols suffer from using highly oxygen and moisture sensitive precatalysts, with preparation and isolation of the precatalysts being conducted in a glovebox under an inert atmosphere, typically from multi-step syntheses. This severely limits the ability of these procedures to be used in industrial processes and makes them less attractive for broad application in academia. This provided an impetus to use $[N(hexyl)_4][ReO_4]$ as a precatalyst to develop an air- and moisture-tolerant protocol for the selective dearomatisation of *N*-heterocycles. It is notable that the Re-oxo complex $[(PPh_3)_2Re(O)_2I]$ **117** was recently tested by Westcott as a catalyst for the hydroboration of quinoline **194**, but the reaction proceeded with poor regioselectivity and chemoselectivity and the reactivity was not fully explored (Scheme 48).[31] No de-aromatisation of pyridine **181** itself was seen using this catalyst, so it is likely that the substrate scope for *N*-heterocycle hydroboration would be narrow.

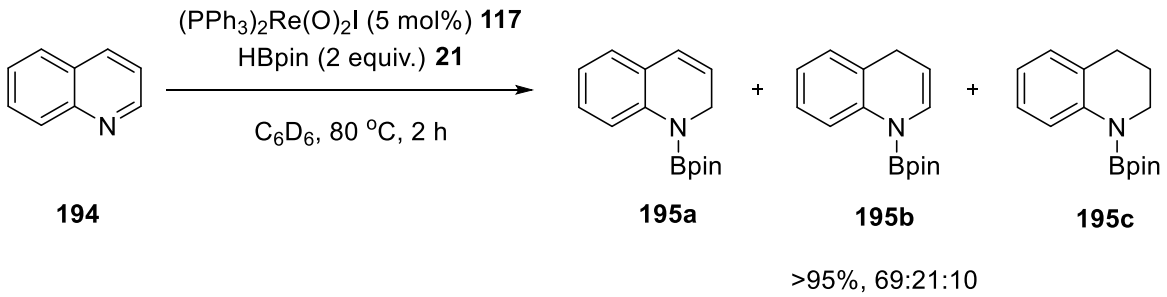

Scheme 48. Hydroboration of quinoline by **117**.

3.1.3 Perrhenate-Catalysed Hydroboration of *N*-Heterocycles

Using [N(hexyl)$_4$][ReO$_4$] **163^{Nhex}** (2.5 mol%) as catalyst and HBpin **21** (1.5 equiv.) to conduct a screen of anhydrous deuterated reaction solvents for pyridine hydroboration under an inert atmosphere showed that d_8-toluene, d_6-benzene and d_8-THF were all suitable to form the 1,4-hydroboration **182a** product in quantitative yields with high regioselectivity over the 1,2-product **182b** (95:5) in all cases after 16 h at room temperature. Reactions in d_7-DMF and d_3-AcCN provided complex mixtures of products, potentially due to reduction of the solvent. 1.5 Equivalents of HBpin **21** was required to achieve full consumption of pyridine. This gave optimised conditions of [N(hexyl)$_4$][ReO$_4$] **163^{Nhex}** (2.5 mol%) as a pre-catalyst with HBpin **21** (1.5 equiv.) at room temperature in C_6D_6 (Table 2, entry 1). Changing catalyst to [N(butyl)$_4$][ReO$_4$] **163^{NBu}** gave identical results, but shorter chain alkylammonium cations (e.g. Me, Et and Pr) gave trace conversion of **181** presumably due to the reduced solubility of these salts (Entry 2). Using the benzyl ammonium salt [N(butyl)$_3$Bn][ReO$_4$] **163^{NBn}** as the catalyst resulted in very poor conversion which could be due to catalyst deactivation by borylation of the benzyl ammonium cation, though this was not directly observed (Entry 3). The phosphonium salts [P(butyl)$_3$Ph][ReO$_4$] **163^{PBu}** and [PPN][ReO$_4$] **163^{PPN}** also gave poor conversion to the DHP products (Entry 4 and 5). The neutral Re-oxo complexes Re_2O_7 and ReO_4SiPh_3 were also shown to have significantly reduced activity under these conditions (Entry 6 and 7). Changing boron sources to H-9-BBN **36**, HBcat **17** or BH_3•THF **175** also resulted in reduced yields (Entry 8 to 10). Increasing the temperature to 80 °C resulted in an increased rate of reaction, with the reaction complete after 6 h (Entry 11).

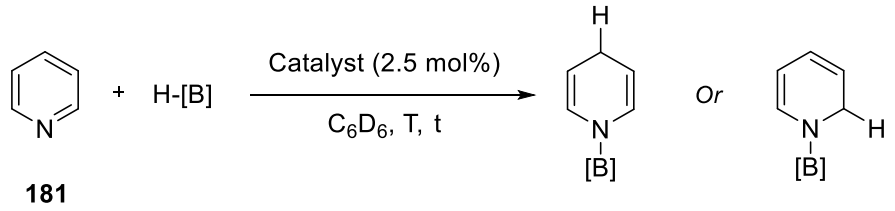

Entry	Catalyst	Borane	T (°C)	1,4/1,2[b]	Yield[b]
1	$[N(hexyl)_4][ReO_4]$	HBpin	25	95:05:00	>95%
2	$[N(butyl)_4][ReO_4]$	HBpin	25	95:05:00	>95%
3	$[N(butyl)_3Bn][ReO_4]$	HBpin	25	95:05:00	8%
4	$[P(butyl)_3Ph][ReO_4]$	HBpin	25	95:05:00	19%
5	$[PPN][ReO_4]$	HBpin	25	N/A	0%
6	ReO_4SiPh_3	HBpin	25	71:29:00	28%
7	Re_2O_7	HBpin	25	N/A	<5%
8	$[N(hexyl)_4][ReO_4]$	9-BBN	25	100:00:00	25%
9	$[N(hexyl)_4][ReO_4]$	HBcat	25	N/A	<5%
10	$[N(hexyl)_4][ReO_4]$	BH_3 THF	25	N/A	<5%
11[c]	$[N(hexyl)_4][ReO_4]$	HBpin	80	95:05:00	>95%

Table 2. Optimisation of hydroboration catalysis conditions. [a]Reaction conditions: pyridine (0.20 mmol), borane (0.40 mmol, 2 equiv.), catalyst (2.5 mol%, 0.005 mmol), mesitylene (internal standard, 10 μL, 0.053 mmol) in 0.4 mL C_6D_6 for 16 h. [b]Regioselectivity and yields were determined by ^{1}H NMR spectroscopy from the crude reaction mixture using mesitylene as an internal standard. [c]Reaction complete after 6 h.

With the optimised conditions in hand, the substrate scope of this system was explored for a range of *N*-heteroaromatics (Scheme 49). The hydroboration of benzannulated substrates all reacted with good yields and regioselectivities, with quinoline **194**, isoquinoline **196** and acridine **197** giving the hydroborated products. 3-Methylpyridine **198**, 3-phenylpyridine **199** and 2,6-lutidine **200** all reacted with good yields and regioselectivities. *N*-Methylbenzimidazole **201** was hydroborated to the corresponding DHP product in high yield. Substrates bearing an electron-withdrawing group such as methyl-3-pyridinecarboxylate **202** were tolerated in the reaction with no observable reduction of the ester group and relatively short reaction times; however, the major product in this case was the 1,6-DHP. 3-

Methoxypyridine **203** was reduced with poor regioselectivity and required an extended reaction time. Interestingly, in the presence of 1 equivalent of HBpin **21**, 3-acetylpyridine **204** was selectively reduced to the corresponding alkoxy boronic ester with no formation of the DHP product observed.

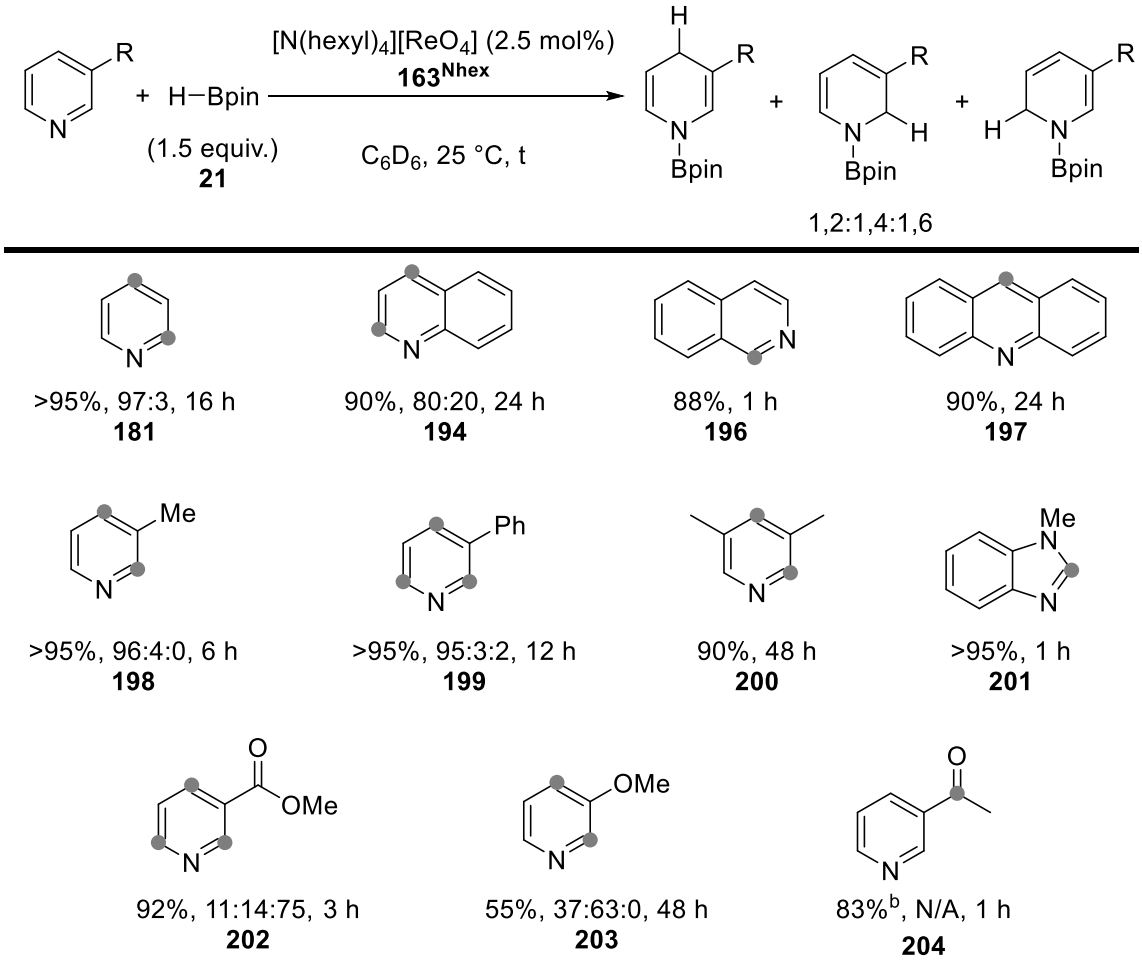

Scheme 49. Catalytic hydroboration of *N*-heteroaromatics using $[N(hexyl)_4][ReO_4]$ as a pre-catalyst and HBpin. For **204** reduction was observed exclusively at the carbonyl when 1 equivalent of HBpin was used. • Indicates position of hydride addition.

In exploring the substrate scope of this reaction, a number of functional groups and substitution patterns were found to be incompatible (Figure 16). Functional groups such as NO_2, alkynyl and cyano **205**-**207** were not tolerated due to competitive hydroboration of these groups to give complex product mixtures. Halo-substituted pyridines **208**-**210**, apart from fluoro-pyridines gave no significant conversion to DHP products presumably due to deactivation of the catalyst through reaction with the C–X bond. Boc-protected amine **211** and stannyl **212** *meta*-substituted pyridines position showed no formation of DHP products

but complex mixtures of products, and 3,3-bipyridyl **213** exhibited no reactivity. *para*- and *ortho*-Substituted pyridines showed poor reactivity with no significant conversion to DHP products **214**-**219**, apart from 4-methoxy pyridine **220** which gave the 1,2-product in low yield.

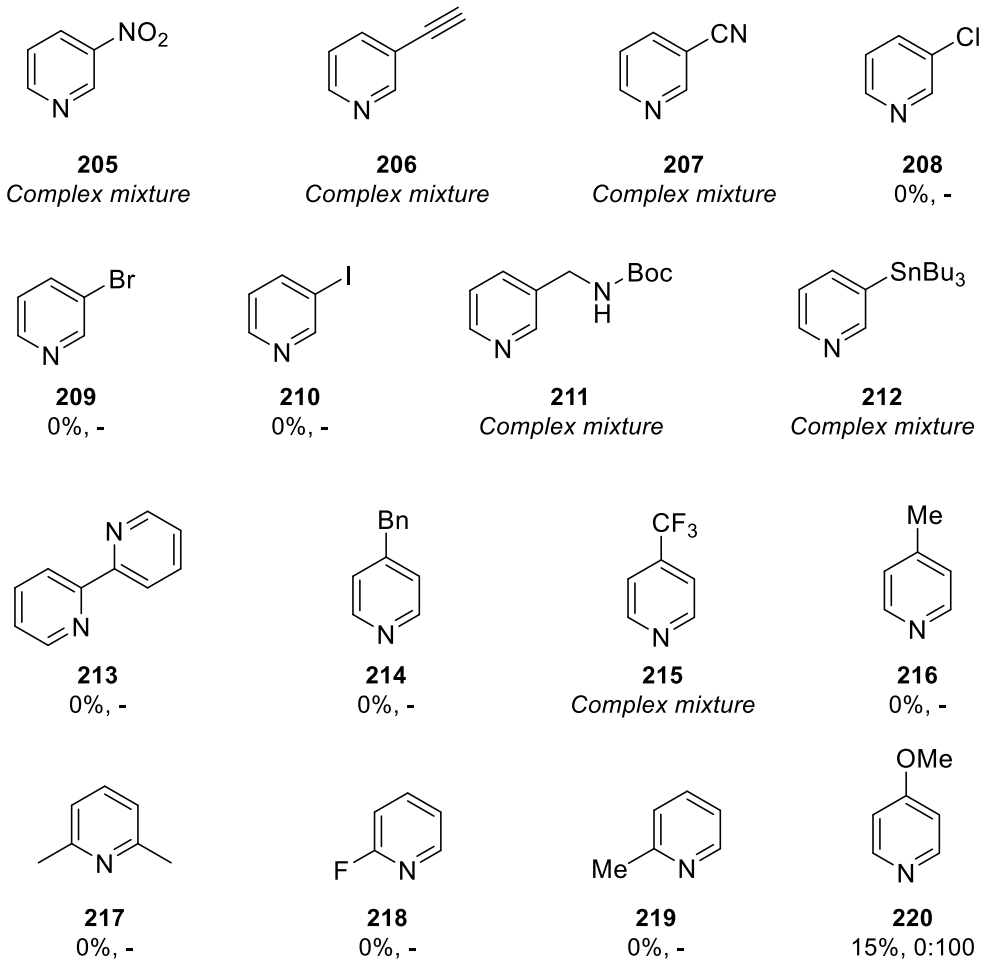

Figure 16. Unsuccessful substrates for 1,4-hydroboration.

The DHP products themselves are moisture-sensitive, undergoing protodeboronation and subsequent rearomatisation, requiring rigorously anaerobic and water-free conditions (i.e., glovebox /Schlenk techniques) for isolation. Therefore, to have a truly moisture-tolerant protocol the products of the reaction need to be 'bench-stable' and easily isolable. This can be achieved by one-pot procedures where the DHP products are further functionalised to amides and Diels-Alder products.[13, 18]

The isolated borane heptahydride complex [K(18-c-6)(DME)][$ReH_7(Bpin)_3$] **165^{DME}** was also a competent, albeit sluggish, catalyst for this reaction giving comparable yields and regioselectivity to the catalyst generated *in situ* after 3 days in d_8-THF, a feature which may

be a consequence of its reduced solubility. However, when **165**$^{\mathbf{DME}}$ was dissolved in d_5-pyridine both **165**$^{\mathbf{DME}}$ and [K(18-c-6)(DME)][$ReH_6(Bpin)_2(py)$] **167**$^{\mathbf{Py}}$ were observed in the ^1H and ^{11}B NMR spectra. When monitored over 96 h, the gradual consumption of **165**$^{\mathbf{DME}}$ and **167**$^{\mathbf{Py}}$ was observed along with the formation of multiple new hydride signals in the ^1H NMR spectrum which eventually resolved into a singlet at −2.63 ppm (Figure 17). Multiple hydride signals were also observed during catalysis using **163**$^{\mathbf{NHex}}$**,** suggesting that similar species are formed from the *in situ* reaction of perrhenate and HBpin. In the ^{11}B NMR spectrum a signal at 23.9 ppm was observed to increase in intensity over time and is indicative of N–Bpin bond formation (Figure 18). The signal at 16.6 ppm corresponds to an unknown compound and the signal at 7.44 ppm is either $[H_2Bpin]^-$ or a boronium ion of the form $[(pyridine)_2(Bpin)]^+$.[19-20]

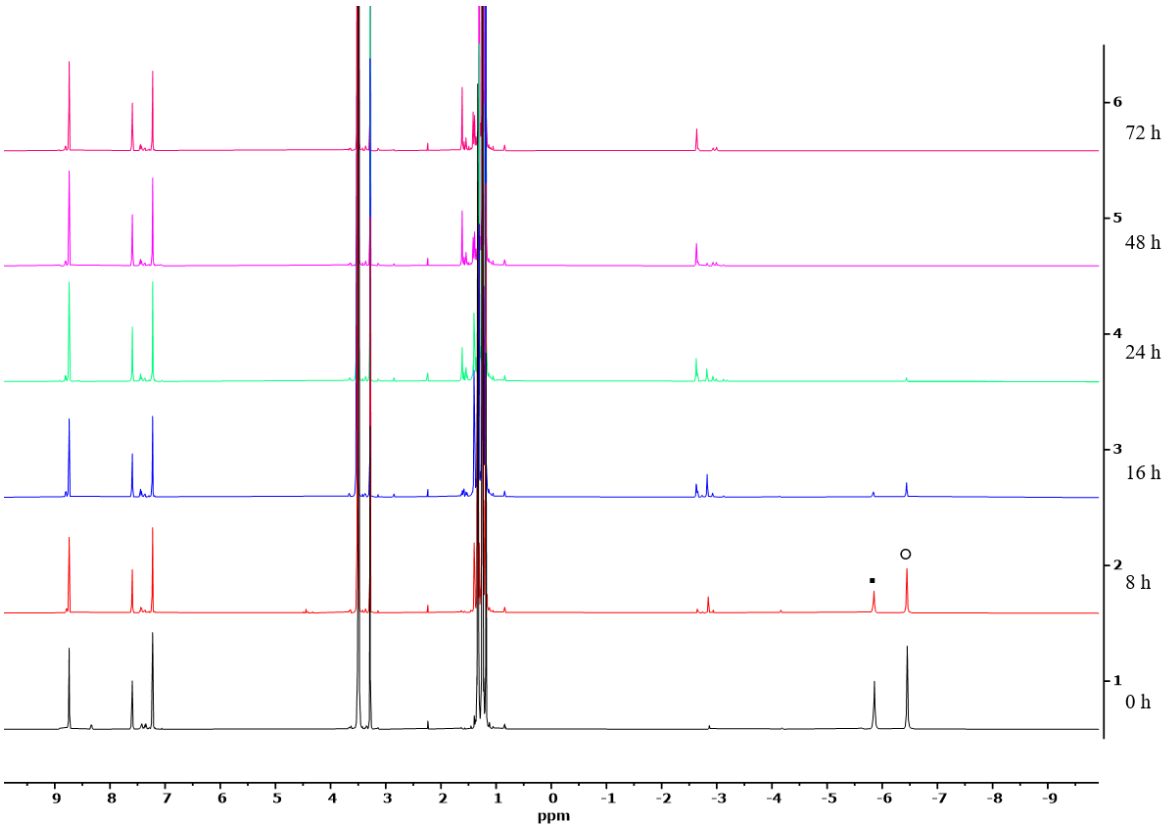

Figure 17. ^1H NMR spectrum of **165**$^{\mathbf{DME}}$ in pyridine-d_5. Assignment: ▪ **165**$^{\mathbf{DME}}$, ○ **167**$^{\mathbf{Py}}$.

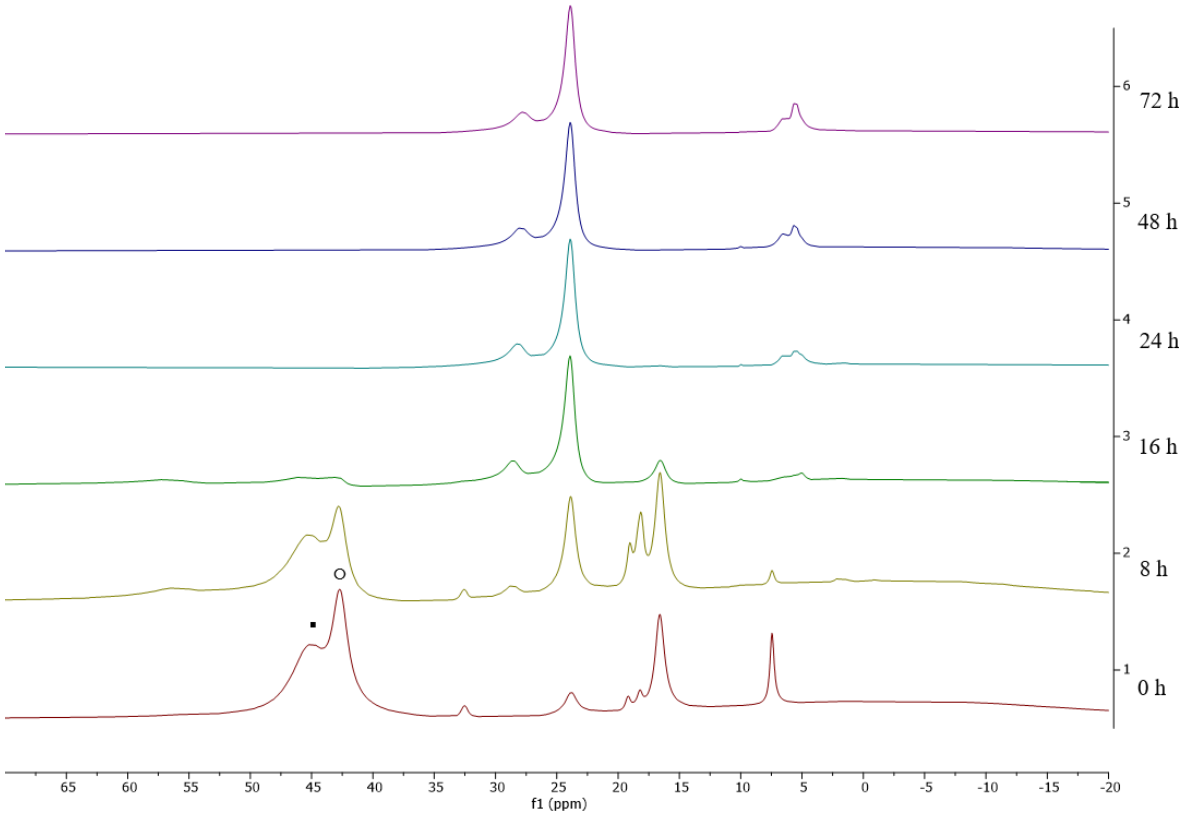

Figure 18. ^{11}B NMR spectrum of **165^{DME}** in pyridine-d_5. Assignment: ▪ **165^{DME}**, ○ **167^{Py}**.

These observations suggest that **165^{DME}** serves as a reservoir for the more reactive, bis(boron) hydride complex **167^{Py}** through substitution of HBpin by the pyridine substrate. Subsequent boration is likely to proceed by an inner-sphere mechanism of hydride transfer to the activated pyridine substrate; however, the 1,4-selectivity seen is unusual for a transition metal hydride catalyst (Scheme 50). Typically, transition metal hydrides proceed by an inner-sphere mechanism and undergo 1,2-hydrometallation of the C=N bond.[29] For some substrates, methyl-3-pyridinecarboxylate **202** and 3-methoxypyridine **203**, a mixture of 1,2-, 1,4- and 1,6- products were observed which suggests that these functionalities may act as directing groups for 1,2- and 1,6-addition.

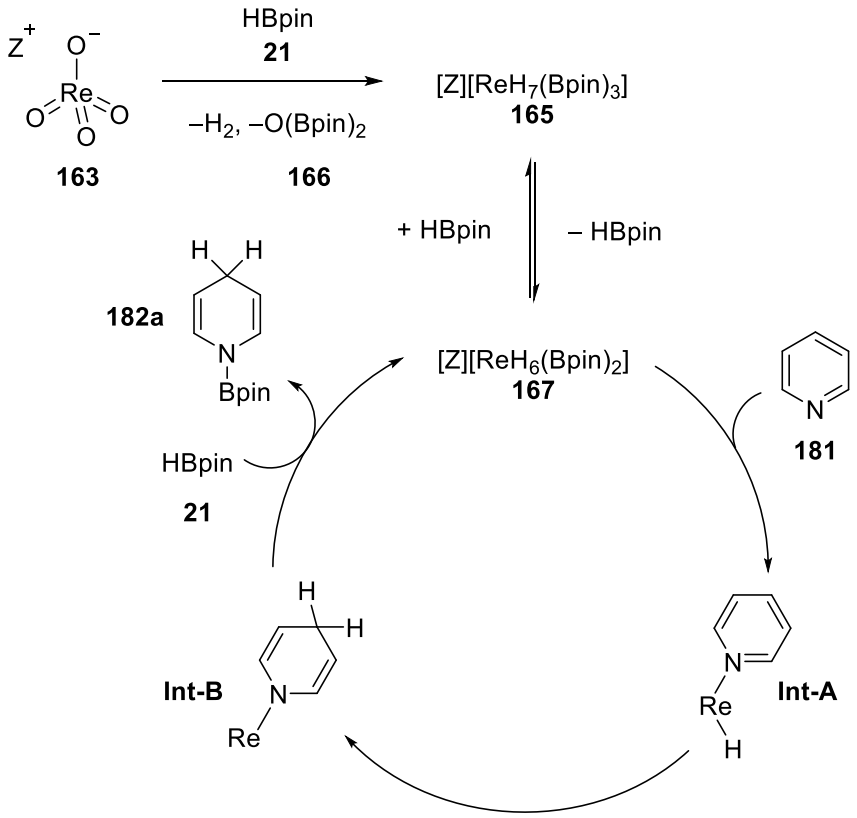

Scheme 50. Proposed catalytic cycle for the inner-sphere hydroboration of pyridine **181**.

No DHP products were seen when using [K(DME)18-c-6][Re(κ_2-H_2BBN)$_4$] **172** as a catalyst at room temperature in d_8-THF. However, dissociation of an equivalent of H-9-BBN **36** to form the pyridine•H-9-BBN adduct (δ −1.22 ppm in the ^{11}B NMR spectrum) and a new hydride species (δ −6.25 ppm in the ^{1}H NMR spectrum) was observed and, upon heating at 70 °C for 4 hours, 90% conversion of pyridine to reduced products was achieved. In this case, the 1,4-DHP isomer **182a** was the major product and two minor over-reduction products were identified as the tetrahydropyridine and fully reduced piperidines containing C–B bonds, as supported by a signal at 31.9 ppm in the ^{11}B NMR spectrum. A possible mechanism for this transformation would involve pyridine hydroboration catalysed by **172** to form the 1,4-DHP followed by hydroboration of these products by free H-9-BBN **36** or **172** to tetrahydropyridines/piperidines and potentially followed by BBN-Bpin exchange to form new C–Bpin bonds (Scheme 51).[32-35]

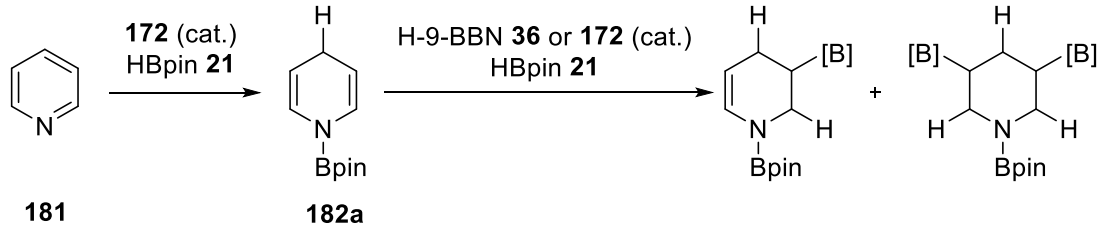

Scheme 51. Pyridine hydroboration catalysed by **172** and potential overreduction products.

3.2 Catalytic Reactivity of Other Metal-Oxo Complexes

In light of the catalytic activity for hydroboration shown by **165**$^{\mathbf{DME}}$, the reactivity of other simple metal-oxo anions (MnO_4^-, VO_3^-, RuO_4^-) towards hydrofunctionalisation was explored. The manganese and vanadium complexes $[N(butyl)_4][MnO_4]$ **222** and $[N(butyl)_4][VO_3]$ **223**, respectively, were synthesised and trialled as catalysts in the hydroboration and hydrosilylation of 3-methoxyacetophenone **221**.[36-37] Both complexes were shown to be efficient catalysts in these transformations, with reaction times below 1 hour and quantitative NMR yields against mesitylene as an internal standard (Scheme 52).

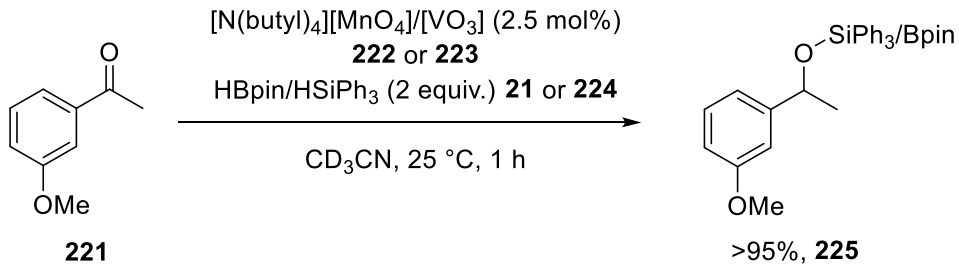

Scheme 52. Catalytic ketone reduction using **222** or **223**.

Neither **222** nor **223** were effective catalysts for the hydrofunctionalisation of more challenging substrates such as alkenes and pyridines under standard reaction conditions or at elevated temperatures (80 °C). Stoichiometric reactions of **222** or **223** with hydroboranes or hydrosilanes did not result in the observable formation of new hydridic species. In both cases a rapid colour change from either purple **222** or colourless **223** to dark brown was observed, with concomitant formation of H_2 when the reaction was undertaken in 'wet' solvents. Stoichiometric reactions of Ph_3SiH **224** or HBpin **21** with either complex did not result in the observable formation of hydride complexes. Lickiss and co-workers investigated the stoichiometric oxidation of hydrosilanes by $[K][MnO_4]$ which resulted in the formation of silanols with MnO_2 and KOH as by-products.[38] Nikonov and co-workers have shown that the hydrosilylation of aldehydes and ketones can be catalysed by KOH through the formation of

hypervalent silicate intermediates.[39] In the reaction of **222** or **223** with Ph_3SiH **224**, the formation of Ph_3SiOH was observed in the ^{29}Si NMR spectrum of the reaction mixture, and in the reaction with HBpin **21** the formation of ROBpin products was observed in the ^{11}B NMR spectrum. This would suggest that the hydrosilylation/hydroboration catalysis is operating through the KOH pathway, rather than through the formation of catalytically active Mn/V-H species.

$[NPr_4][RuO_4]$ **227**, otherwise known as the Griffith-Ley reagent, is a well-documented catalyst for the oxidation of alcohols to the corresponding aldehyde or ketone.[40] Salt **227** was shown to be a highly active catalyst in the hydroboration of acetophenone **226**. In pyridine **181** hydroboration, **227** gave the 1,4-product selectively, but a complex mixture of potential over-reduction products was also observed by multiple minor signals between 6 and 3 ppm in the ^1H NMR spectrum (Scheme 53).

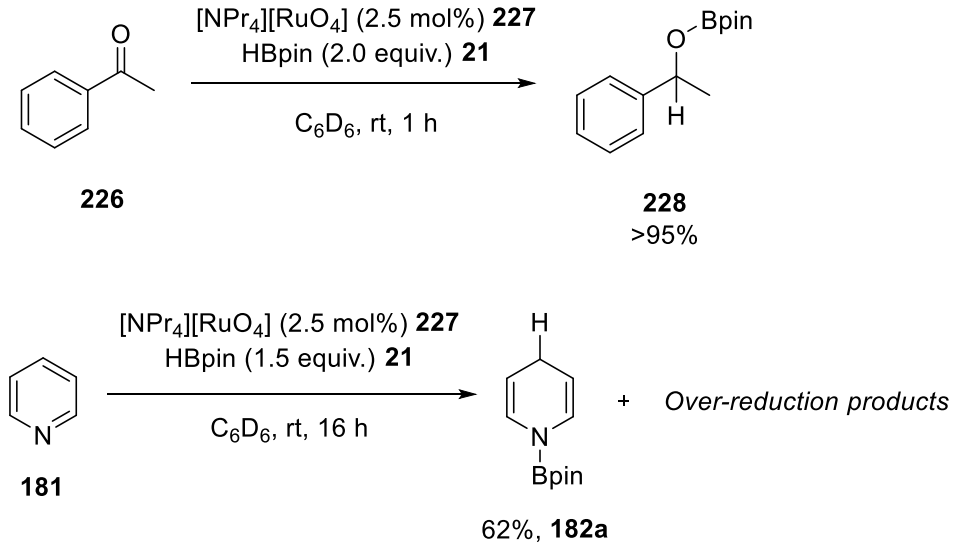

Scheme 53. Catalytic acetophenone **226** and pyridine **181** reduction using **227**.

This reactivity suggests that RuO_4^- reacts with hydroboranes in a similar manner to ReO_4^- to form catalytically active Ru polyhydride-borane species. Stoichiometric reactions of **227** with HBpin **21** in DME rapidly produced a single major Ru hydride with boryl/σ-borane bonding indicated by a signal at −9.52 ppm in the ^1H NMR spectrum and a signal at 38.4 ppm in the ^{11}B NMR spectrum.[41] This complex was short-lived, decomposing to NMR silent Ru products over 6 hours at room temperature, presumably through the reaction of the Ru polyhydride-borane complex with $O(Bpin)_2$ **166** in a similar manner to that observed for reactions of HBpin with $[NR_4][ReO_4]$ salts. The reaction of H-9-BBN **36** with **227** proceeded in a similar manner and a hydride signal at −12.63 ppm in the ^1H NMR spectrum was seen,

but no obvious dihydroborate or Ru–B signal was observed in the ^{11}B NMR spectrum. An attempt to form an isolable Ru complex similar to the strategy used for ReO_4^- through the reaction between [K][RuO_4] **227** with neat HBpin **21** in the presence of 18-c-6 **164** produced a dark green insoluble pyrophoric solid; however, further analysis of this material did not provide any structural information. It was envisaged that further functionalisation of the *in situ* formed Ru polyhydride-borane complex was required to form an isolable complex. To this end, a series of phosphine ligands were reacted with the *in situ* formed species from **227** and attempts were made to isolate the phosphine-ligated products (Scheme 54).

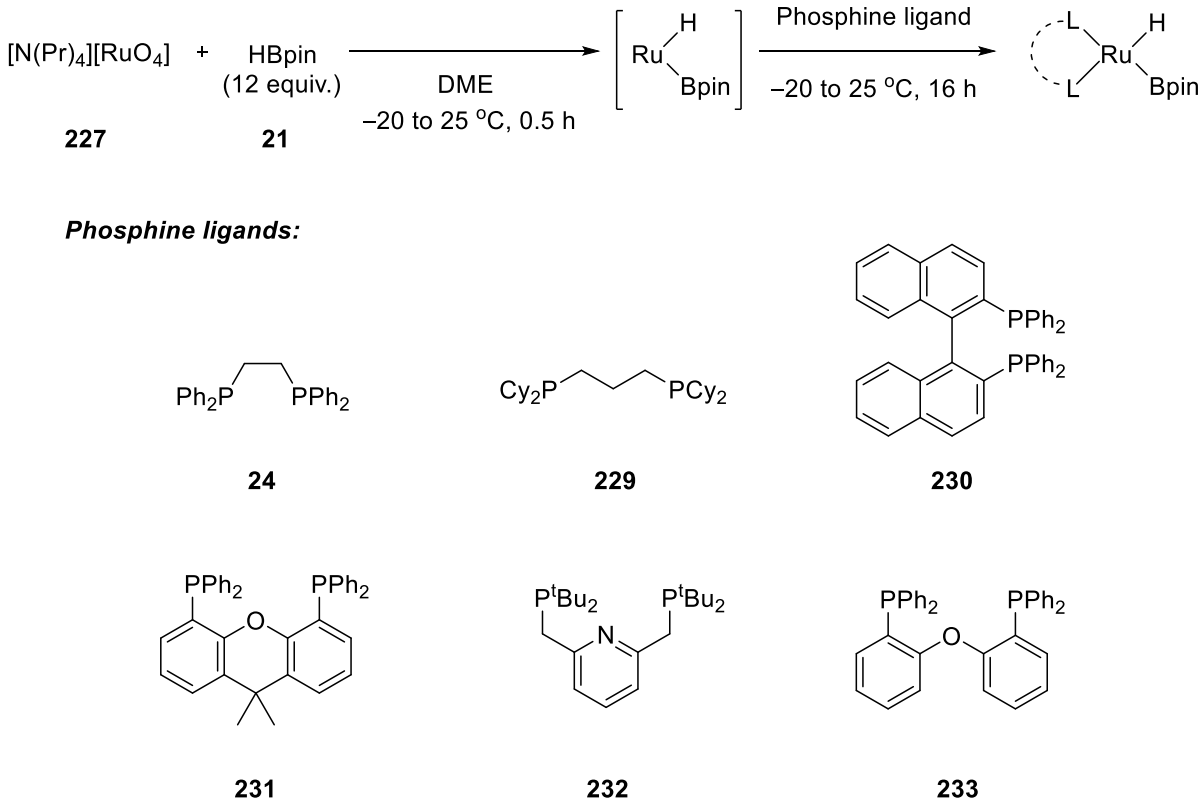

Scheme 54. Screen of phosphine ligands to coordinate to the Ru-H intermediate.

^{1}H NMR analysis of the reaction mixtures from the reaction of phosphines **24** and **229** to **231** showed the unselective formation of multiple different phosphine-ligated hydride complexes. The reaction with the PNP ligand **232** resulted in full conversion to two major hydrides indicated by broad singlet resonances at −5.02 ppm and at −12.07 ppm in the ^{1}H NMR spectrum; this was supported by related broad singlets in the ^{31}P NMR spectrum at 95.3 and 94.8 ppm. A signal at 37.8 ppm in the ^{11}B NMR was indicative of a Ru–B bond and was shifted from that of the parent complex (38.4 ppm). After 48 h the integration between the two hydride signals was unchanged. Unfortunately, it was not possible to isolate the major

product of this reaction in high purity. The reaction between **227**, HBpin **21**, and the POP ligand **233** resulted in the formation of a single major complex indicated by a resonance at −9.61 (m) ppm in the ^{1}H NMR, and two broad signals at 41.3 (s) and 35.3 (d, J = 63.1 Hz) in the ^{31}P NMR spectrum. No obvious Ru–B signal was observed in the ^{11}B spectrum. The Ru dihydride complex **234** was crystallised from the reaction mixture as pale yellow plates in 11% yield and the X-ray crystal structure showed the *cis*-bis(diphosphine) complex, *cis*-$ReH_2(DPEPhos)_2$ in which the phosphine and hydride ligands display a distorted octahedral geometry at the Re centre (Figure 19).[42] The two hydrides were located in the difference Fourier map and refined freely. Complex **234**, is neutral and Ru has been reduced from Ru^{VII} to Ru^{II} in this reaction, which contrasts with the results for the deoxygenation of ReO_4^- by hydroboranes. Although **234** does not contain a Ru–B bond, this complex provides evidence that RuO_4^- can undergo exhaustive deoxygenation to form hydride complexes. The Ru complexes are evidently more sensitive than the analogous Re complexes and will require further optimisation of the reaction conditions in order to isolate complexes with and without phosphine ligands.

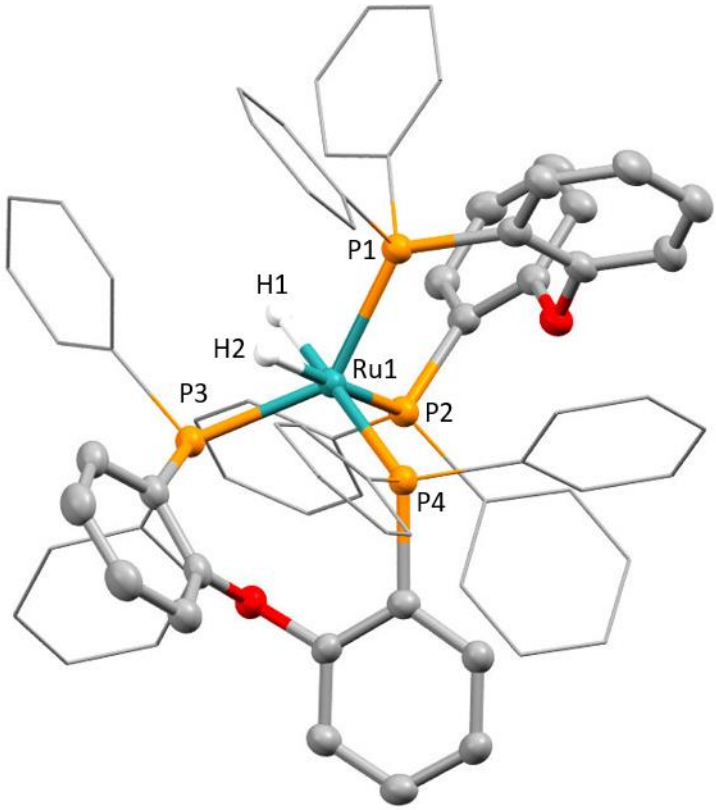

Figure 19. The X-ray crystal structure of **234** (all hydrogen atoms except for the Re hydrides are omitted; displacement ellipsoids are drawn at 50% probability). X-ray crystal structure selected distances (Å) and angles (°): Ru1-H 1.59(4) avg.; Ru1-P1 2.312(1); Ru1-P2 2.3648(7); Ru1-P3 2.3205(7); Ru1-P5 2.4172(9); P2-Ru1-P1 98.78(3); P3-Ru1-P4 102.39; P4-Ru1-P1 101.71(3), P4-Ru1-P2 104.05(3), P2-Ru1-H1 82(1), P1-Ru1-H2 82(1), P3-Ru1-H1 76(1), P4-Ru1-H2 88(1).

3.3 References

1. Morris, D. S., Unpublished Work.

2. Morris, D. S.; Weetman, C.; Wennmacher, J. T. C.; Cokoja, M.; Drees, M.; Kühn, F. E.; Love, J. B., *Cat. Sci. Tech.* **2017,** *7*, 2838-2845.

3. Sharma, V. K.; Singh, S. K., *RSC Adv.* **2017,** *7*, 2682-2732.

4. Ouellet, S. G.; Walji, A. M.; Macmillan, D. W. C., *Acc. Chem. Res.* **2007,** *40*, 1327-1339.

5. Bull, J. A.; Mousseau, J. J.; Pelletier, G.; Charette, A. B., *Chem. Rev.* **2012,** *112*, 2642-2713.

6. Arrowsmith, M.; Hill, M. S.; Hadlington, T.; Kociok-Köhn, G.; Weetman, C., *Organometallics* **2011,** *30*, 5556-5559.

7. Intemann, J.; Lutz, M.; Harder, S., *Organometallics* **2014,** *33*, 5722-5729.

8. Liu, X.; Li, B.; Hua, X.; Cui, D., *Organic Letters* **2020**, *22*, 4960–4965.

9. Lortie, J. L.; Dudding, T.; Gabidullin, B. M.; Nikonov, G. I., *ACS Catal.* **2017,** *7*, 8454-8459.

10. Zhang, F.; Song, H.; Zhuang, X.; Tung, C.-H.; Wang, W., *J. Am. Chem. Soc*. **2017,** *139*, 17775-17778.

11. Liu, J.; Chen, J.-Y.; Jia, M.; Ming, B.; Jia, J.; Liao, R.-Z.; Tung, C.-H.; Wang, W., *ACS Catal*. **2019**, 3849-3857.

12. Oshima, K.; Ohmura, T.; Suginome, M., *J. Am. Chem. Soc*. **2012,** *134*, 3699-3702.

13. Liu, H.; Khononov, M.; Eisen, M. S., *ACS Catal*. **2018,** *8*, 3673-3677.

14. Dudnik, A. S.; Weidner, V. L.; Motta, A.; Delferro, M.; Marks, T. J., *Nature Chem.* **2014,** *6*, 1100.

15. Oshima, K.; Ohmura, T.; Suginome, M., *Chem. Commun.* **2012,** *48*, 8571-8573.

16. Jayaraman, A.; Misal Castro, L. C.; Desrosiers, V.; Fontaine, F.-G., *Chem. Sci.* **2018**, *9*, 5057-5063.

17. Jeong, J.; Heo, J.; Kim, D.; Chang, S., *ACS Catal.* **2020,** *10*, 5023-5029.

18. Fan, X.; Zheng, J.; Li, Z. H.; Wang, H., *J. Am. Chem. Soc*. **2015,** *137*, 4916-4919.

19. Keyzer, E.; Kang, S.; Hanf, S.; Wright, D. S., *Chem. Commun.* **2017**, *53*, 9434-9437.

20. Jeong, E.; Heo, J.; Park, S.; Chang, S., *Chem. Eur. J*. **2019,** *25*, 6320-6325.

21. Rao, B.; Chong, C. C.; Kinjo, R., *J. Am. Chem. Soc*. **2018,** *140*, 652-656.

22. Hynes, T.; Welsh, E. N.; McDonald, R.; Ferguson, M. J.; Speed, A. W. H., *Organometallics* **2018,** *37*, 841-844.

23. Leong, B.-X.; Lee, J.; Li, Y.; Yang, M.-C.; Siu, C.-K.; Su, M.-D.; So, C.-W., A *J. Am. Chem. Soc.* **2019**, *141*, 17629-17636.

24. Ji, P.; Feng, X.; Veroneau, S. S.; Song, Y.; Lin, W., *J. Am. Chem. Soc*. **2017,** *139*, 15600-15603.

25. Kaithal, A.; Chatterjee, B.; Gunanathan, C., *Org. Lett.* **2016,** *18*, 3402-3405.

26. Tamang, S. R.; Singh, A.; Unruh, D. K.; Findlater, M., *ACS Catal.* **2018,** *8*, 6186-6191.

27. Yu, H.-C.; Islam, S. M.; Mankad, N. P., *ACS Catal.* **2020**, 3670-3675.

28. Park, S.; Chang, S., *Angew. Chem. Int. Ed.* **2017,** *56*, 7720-7738.

29. Park, S., *ChemCatChem* **2020,** *12*, 3170-3185.

30. Chong, C. C.; Kinjo, R., *ACS Catal*. **2015,** *5*, 3238-3259.

31. Arevalo, R.; Vogels, C. M.; MacNeil, G. A.; Riera, L.; Perez, J.; Westcott, S. A., *Dalton Trans.* **2017,** *46*, 7750-7757.

32. Arase, A.; Hoshi, M.; Mijin, A.; Nishi, K., *Synth. Commun.* **1995,** *25*, 1957-1962.

33. Shirakawa, K.; Arase, A.; Hoshi, M., *Synthesis* **2004,** *2004*, 1814-1820.

34. Nieto-Sepulveda, E.; Bage, A. D.; Evans, L. A.; Hunt, T. A.; Leach, A. G.; Thomas, S. P.; Lloyd-Jones, G. C., *J. Am. Chem. Soc*. **2019,** *141*, 18600-18611.

35. Docherty, J. H.; Nicholson, K.; Dominey, A. P.; Thomas, S. P., *ACS Catal*. **2020,** *10*, 4686-4691.

36. Sala, T.; Sargent, M. V., *J. Chem. Soc., Chem. Commun.* **1978,** 253-254.

37. Day, V. W.; Klemperer, W. G.; Yagasakl, A., *Chem. Lett.* **1990,** *19*, 1267-1270.

38. Lickiss, P. D.; Lucas, R., *J. Organomet. Chem.* **1996**, *521*, 229-234.

39. Revunova, K.; Nikonov, G. I., *Chem. Eur. J.* **2014**, *20*, 839-845

40. Griffiths, W. P.; Ley, S. V.; Whitcombe, G. P.; White, A. D., *J. Chem. Soc., Chem. Commun.* **1987**, 1625-1627.

41. Montiel-Palma, V.; Lumbierres, M.; Donnadieu, B.; Sabo-Etienne, S.; Chaudret, B., *J. Am. Chem. Soc*. **2002**, 124, 5624-5625.

42. Cybulski, M. K.; Beattie, N. A.; Macgregor, S. A.; Mahon, M. F.; Whittlesey, M. K., *Chem. Eur. J.* **2020**, *26*, 11141-11145.

Chapter Four – Phosphine Complexes

4.1 Phosphine-Ligated Complexes

4.1.1 Ligand Screen

As has been described in Chapter Two, [K(DME)(18-c-6)][$ReH_7(Bpin)_3$] **165^{DME}** underwent stoichiometric C(sp^2)-H borylation of toluene **170** with high *meta*-selectivity, unfortunately, attempts to adapt these conditions for catalytic C–H borylation by addition of stoichiometric boron reagents or sacrificial H_2 acceptors were unsuccessful. It was therefore envisaged that strongly σ-donating, neutral ligands such as phosphines would help to stabilise the high oxidation-state hydrido-boryl complexes involved in C–H bond activation and subsequent C–B bond formation. Rhenium-catalysed C–H borylation has, to the best of our knowledge, only been reported using low oxidation-state complexes. For example, Hartwig and co-workers reported the C–H borylation of alkanes and arenes using $Cp^*Re(CO)_3$ **236** and B_2pin_2 **26** under photochemical conditions and an atmosphere of CO (Scheme 55A).[1] Murai and Takai reported the C(sp^3)–H borylation of tertiary amines at the α-position, facilitated by a pyridyl directing group under thermal conditions using [$ReBr(CO)_3(THF)]_2$ **239** as the catalyst and H-9-BBN **36** as the boron source (Scheme 55B).[2] However, no examples of C(sp^2)–H borylation of arenes were reported using this catalyst system.

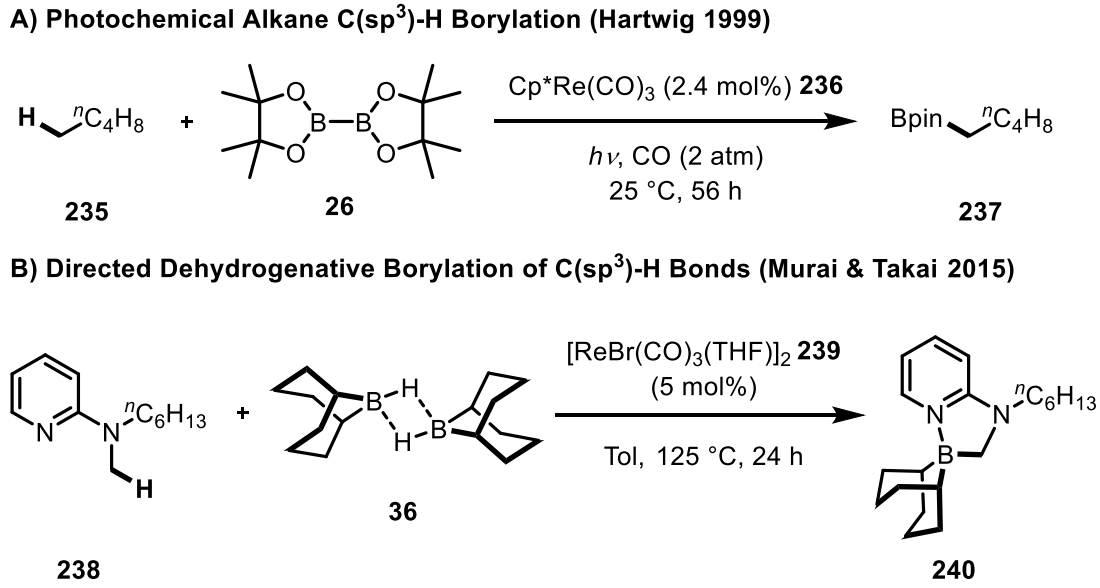

Scheme 55. Examples of rhenium-catalysed borylation C–H bonds.

Given the chemistry of rhenium polyhydride phosphine complexes,[3] a screen of a range of phosphine ligands for coordination to complex **165^{DME}** was conducted and the progress of the reactions were monitored by NMR spectroscopy (^{1}H, ^{11}B and ^{31}P) (Scheme 56). The reactions were conducted in toluene, THF or DME at low temperatures to control the selectivity of the phosphine ligation. Moderate to excellent conversion of **165^{DME}** was observed for phosphines PCy_3 **241**, PPh_3 **120**, dcpp **229** and dppp **242** forming the monodentate or bidentate complexes. Bulky monodentate phosphines XPhos **243** and CyJohnPhos **244** as well as bidentate phosphine ^{t}BuXantPhos **245** did not show any observable coordination to Re and in these reactions **165^{DME}** slowly decomposed to insoluble or NMR silent products through the pathways discussed in Chapter 2. The major products from the reactions with polydentate ligands **24** and **246** to **250** were the monoligated complexes which were formed in varying quantities depending on the ligand but generally with poor conversion of **165^{DME}**. Heating these reactions did not result in the formation of the desired bi/tridentate complexes and instead resulted in either decomposition to NMR silent products or the formation of complex mixtures of products. The reaction of polydentate ligands **233** and **251** to **254** resulted in the formation of a complex mixture of products. From this screen, it was concluded that the choice of phosphine ligand is limited by both the steric and electronic properties of the ligand as well as its denticity. Sterically bulky monodentate or polydentate phosphines are not suitable for this reaction. Ligands with free N–H bonds undergo N–H borylation and lead to unselective coordination to Re. The selectivity of ligand coordination appears to be sensitive to the flexibility of the ligand as exemplified by comparing the reaction outcomes using **242**, **24** and **247**.

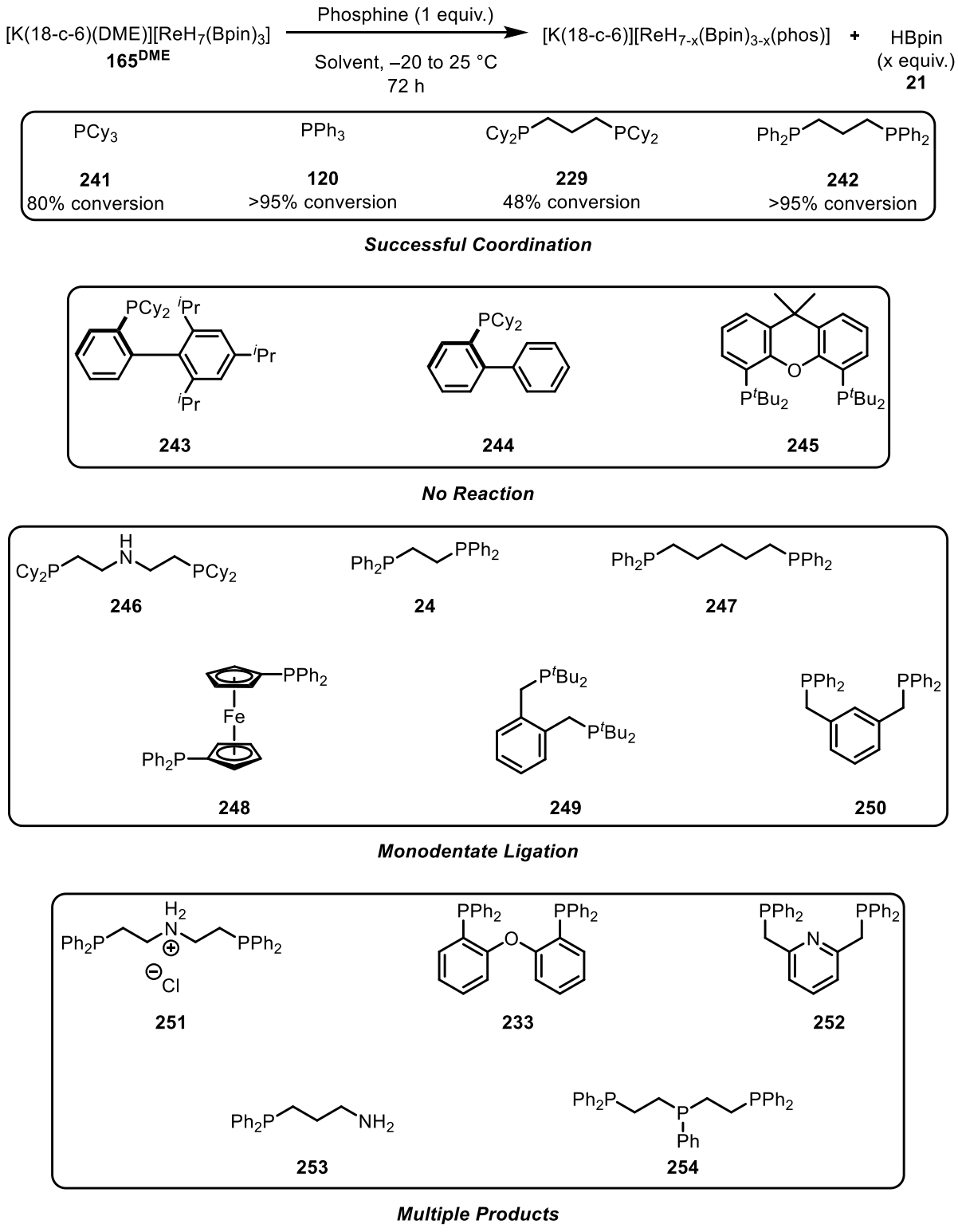

Scheme 56. Screen of phosphine ligands for coordination to **165**$^{\mathbf{DME}}$. Conversions were calculated from integration of ^{31}P NMR signals.

Non-phosphine ligands were also trialed in this reaction (Scheme 57). The reaction of 4,4′-di-*tert*-butyl-2,2′-dipyridyl **28** was sluggish with 85% conversion to a new major boron-hydride

species with a resonance at −3.82 ppm in the ^{1}H NMR spectrum and a corresponding boryl signal at 58.2 ppm in the ^{11}B NMR spectrum after 96 h. This complex was stable under vacuum but it was not possible to isolate it cleanly from the reaction mixture. The reaction of **165^{DME}** with 3,4,7,8-tetramethyl-1,10-phenanthroline **29** was very slow, with only 6% conversion to a new boron-hydride species with a resonance at −3.78 ppm in the ^{1}H NMR spectrum and a corresponding boryl signal at 57.3 ppm in the ^{11}B NMR spectrum after 24 h.

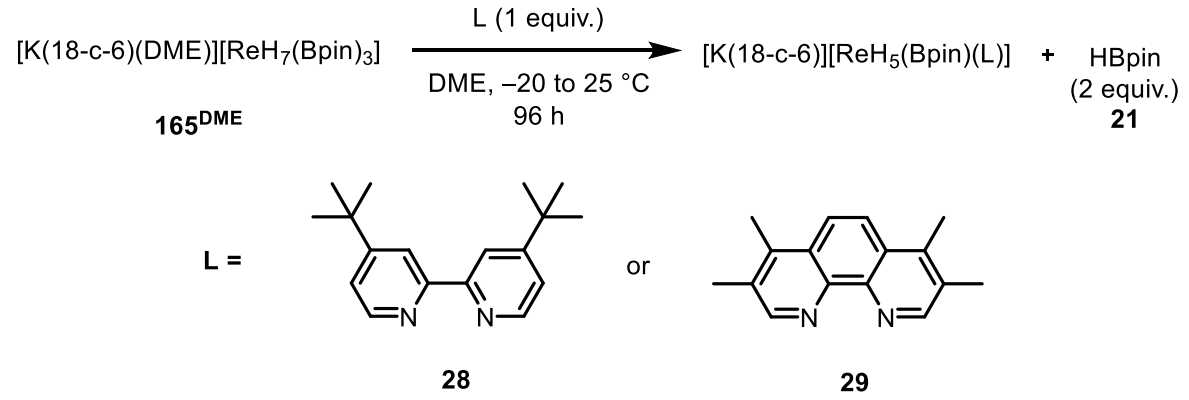

Scheme 57. The reaction of *N*-donor ligands with **165^{DME}**.

Attempts to form any of these phosphine and *N*-donor complexes through the reaction of [K][ReO_4] **163^{K}**, 18-c-6 **164** and HBpin **21** in the presence of the appropriate ligand was unsuccessful. In all cases a complex mixture of boron-hydride species was produced through unselective coordination of the ligand to any potential intermediate formed during the deoxygenation of perrhenate.

4.1.2 Structure and Reactivity of Phosphine-Ligated Complexes

Further studies were focused on reactions using phosphines **241**, **120**, **229** and **242** given the successful coordination of these ligands. The cyclohexyl-substituted phosphines **241** and **229** reacted significantly more slowly than the phenyl-substituted phosphines **120** and **242**. In all these cases, ligand coordination was concomitant with liberation of equivalents of HBpin, as observed by the appearance of a doublet resonance at ~28 ppm in the ^{11}B NMR spectra. However, for all 4 ligands a resonance corresponding to a Re–Bpin environment was observed at the completion of the reaction which was shifted downfield by 8 – 10 ppm from the resonance corresponding to **165^{DME}**, indicating that at least one Bpin group remained coordinated. In all cases, monodentate ligation was relatively fast (under 16 hours) whereas for phosphines **229** and **242** conversion from monodentate to bidentate phosphine coordination required extended reaction times (up to 72 h). This suggests that the first

equivalent of HBpin which is substituted is much more labile than the second equivalent. This was observed by monitoring the time course of the reaction between **165^{DME}** and **242** by NMR spectroscopy in d_8-toluene which revealed full conversion of **165^{DME}** to a monodentate complex (major) and a bidentate complex (minor) after 2 h. The monodentate complex corresponds to a doublet at −7.67 ppm in the ^{1}H NMR spectrum and a broad resonance at 52.9 ppm in the ^{11}B NMR spectrum. This monodentate complex then slowly converted to the bidentate complex over the course of 72 h which was characterised by a triplet at −7.84 ppm in the ^{1}H NMR spectrum and a broad resonance at 53.7 ppm in the ^{11}B NMR spectrum. Correlation between the hydride signals and two signals at 24.3 and 12.4 ppm in the ^{31}P NMR spectrum were observed in the ^{1}H-^{31}P HMBC NMR spectrum.

Attempts to isolate the products from these reactions proved challenging, as the products decomposed rapidly upon removal of the reaction solvent under vacuum. NMR spectroscopic analysis of the residue showed a complex mixture of phosphine-bound hydride complexes. This could result from the dissociation of HBpin or H_2 to form an unstable 16-electron complex which reacts unselectively with itself or with the solvent. Therefore, these complexes **255** to **258** were characterised *in situ* from the reaction mixture (Table 3). All complexes showed correlation between the phosphine resonances and the hydride resonances in the ^{1}H-^{31}P HMBC NMR spectrum; however, no correlation was observed between the B resonances and the hydride resonances in the ^{1}H-^{11}B HMQC NMR spectrum. In all cases, the ^{31}P resonances are broad and for complex **257** the hydride resonance was also broad, which is likely due to the quadrupolar effect of the ^{11}B nuclei. None of the hydride or phosphine resonances sharpen or decoalesce when cooled to cryogenic temperatures (0 to −80 °C), emphasising the highly fluxional nature of the hydride and Bpin ligands.

Complex	Solvent	^{1}H NMR Hydride Signal (ppm)	^{11}B NMR Re-B Signal (ppm)	^{31}P NMR (ppm)
[K(18-c-6)][$ReH_6(Bpin)_2(PPh_3)$] **255**	d_8-Toluene	−7.72 (d, J = 15.0 Hz, 6H)	52.3 (s)	36.1 (s (br))
[K(18-c-6)][$ReH_6(Bpin)_2(PCy_3)$] **256**	d_8-THF	−8.60 (d, J = 15.9 Hz, 6H)	53.6 (s)	47.9 (s (br))
[K(18-c-6)][ReH_5(Bpin)(dcpp)] **257**	d_8-Toluene	−8.16 (s (br), 5H)	53.1 (s)	33.8 (s (br))
[K(18-c-6)][ReH_5(Bpin)(dppp)] **258**	d_8-THF	−8.16 (t, J = 11.8 Hz, 5H)	53.8 (s)	11.9 (s (br))

Table 3. NMR data for phosphine-ligated complexes **255** to **258**.

When DME is used as the reaction solvent, [K(18-c-6)][$ReH_4(\eta^2$-HBpin)(dppp)] **258** was isolated by crystallisation from the reaction mixture as large yellow blocks which were also unstable once removed from the mother liquor. The X-ray crystal structure of **258** (Figure 20) revealed a rhenium pentahydride anion in which the P and B atoms are arranged in a distorted T-shape geometry with an elongated Re–B bond (Re1-B1 = 2.149(4) Å) which could reflect contributions from σ-borane structures due to the close B1-H1 distance (1.48(4) Å).[4] The hydrides were located in the difference Fourier map and refined freely. The structure also exhibited a close Re–H…K contact (H5-K1 = 2.74(5) Å), which is similar to the those seen in other potassium salts of rhenium polyhydride anions.[5] The bite angle of the phosphine ligand is 93.28(3)° and the average P-Re distance is 2.3518(9) Å.

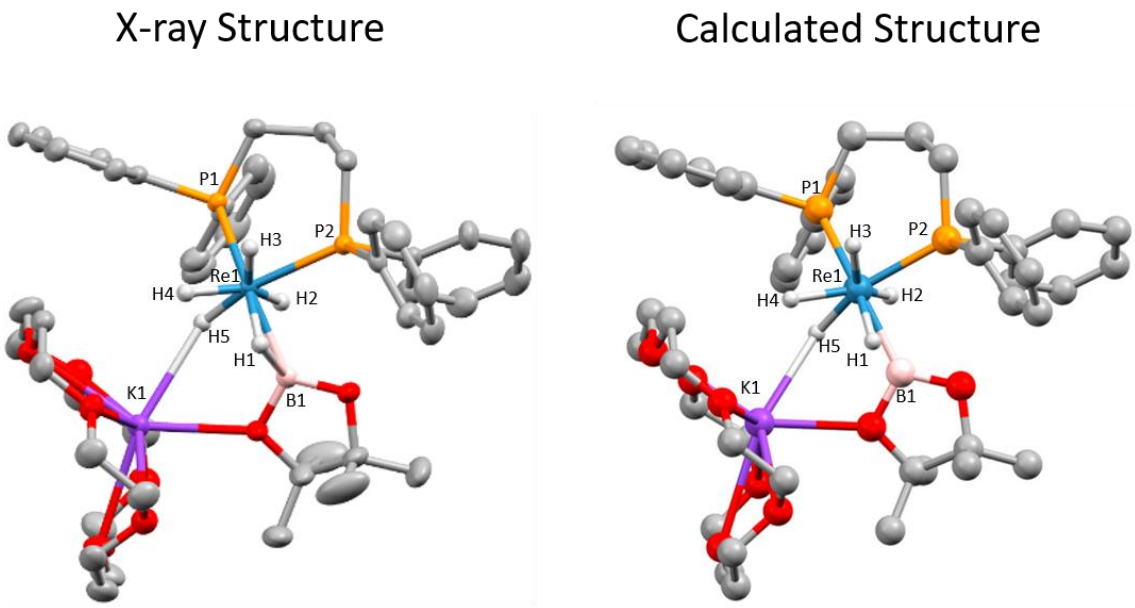

Figure 20. The X-ray crystal structure (left) and calculated structure (right) of **258** (all hydrogen atoms except for the Re hydrides are omitted; displacement ellipsoids are drawn at 50% probability). X-ray crystal structure selected distances (Å) and angles (°): Re1-B1 2.149(4); Re1-H 1.54(4) avg.; B1-H1 1.48(4); H5-K1 2.74(5); H4-K1 3.19(5); Re1-P1 2.3571(9).; Re1-P2 2.3465(9); P2-Re1-P1 93.28(3); P2-Re1-B1 141.5(1); B1-Re1-P1 91.36(9).

The usual caveats of locating hydrides with confidence from the X-ray structure apply here. As such, possible hydride positions were identified using AIRSS/CASTEP with the initial positions of the heavier atoms derived from the crystal structure and geometric constraints on prospective initial hydride positions to ensure H_2 is not formed.[6-7] This approach generated a series of structures with various combinations of hydride, boryl, σ-borane, and hydroborate

ligands that were then ranked in order of increasing energy (Figure 21A). Of the data set of 26 optimised structures generated, the same lowest energy geometry was obtained 18 times which was demonstrated in an overlay image of three of these structures randomly selected from the low energy plateau (Figure 21B). This structure suggests two bridging hydrogen atoms between the Re and K sites, and one bridging hydrogen atom between the Re and B sites, making this formally a σ-borane complex. Breaking this bridging hydrogen bond, to create a structure with two Re–H–K linkages and three Re–H terminal bonds gave the structure found some +32 kJ/mol above the low energy plateau (Figure 21C). All remaining higher energy structures contained just one Re–H–K linkage, and differed in the location of the remaining four Re–H terminal bonds. Finally, overlaying the global minimum structure with the crystal structure geometry (Figure 21D) showed a strong correlation, with all heavy atoms and all hydrogen atoms in good alignment. The only significant difference between the lowest energy structures the X-ray structure was a closer K1-H4 contact (2.956 Å compared to 3.19(5) Å). The calculated structure contains an elongated B1-H1 distance compared with the solid-state structure (1.522 Å comparted to 1.48(4) Å), although this bond distance remains in the range reported for σ-borane complexes and is within one esd range of the X-ray structure (Figure 20).[4, 8] The hydride positions are consistent with those from the X-ray structure, indicating a high level of confidence for their assignment.

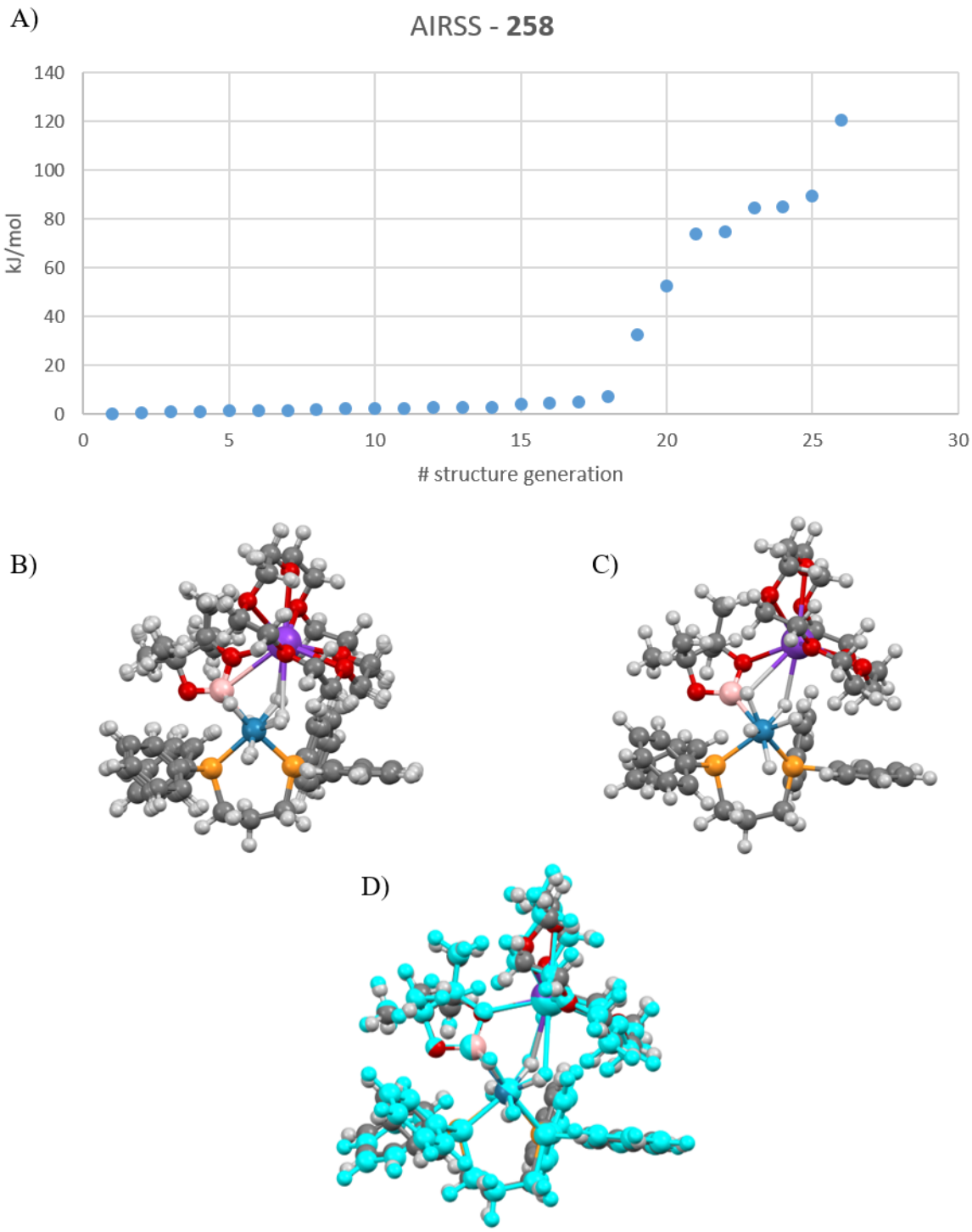

Figure 21. (A) Energy ranking of 26 optimised structures of **258** found by AIRSS (B) Structure overlay of the three of the lowest energy structures for **258** (C) Structural overlay of the **258** structures ca. +32 kJ/mol above the global minimum structure (D) Structural overlay of the lowest energy 2 structure (in cyan) and the molecular structure derived from the crystal structure.

4.1.3 Structure and Reactivity of Neutral dppp Complex

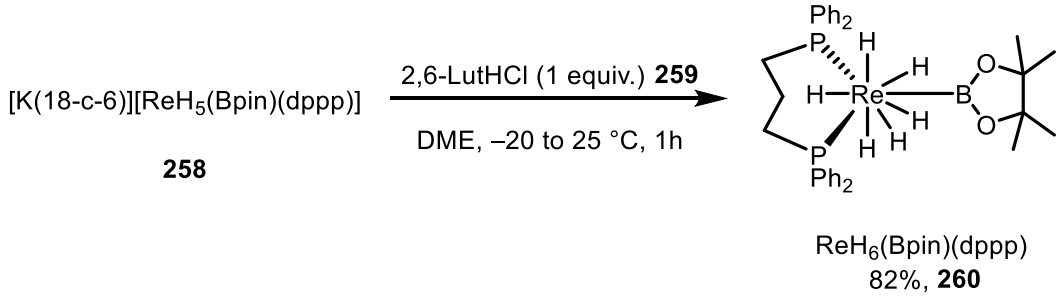

Scheme 58. Protonation of **258** to produce the neutral complex **260**.

Due to the limited stability of **258** and the difficulty in isolating high purity material, it was reacted with 1 equivalent of 2,6-lutidinium chloride **259** which resulted in protonation without H_2 evolution to form the neutral hexahydridoboryl complex [ReH_6(Bpin)(dppp)] **260** (Scheme 58). The ^{1}H NMR spectrum of **260** displayed a triplet at −5.57 ppm for 6 hydrides and the ^{31}P NMR spectrum exhibited a broad signal at 6.24 ppm. As with **258**, these resonances were unchanged at −80 °C. A broad signal at 47.3 ppm was seen in the ^{11}B NMR spectrum of **260** and corresponds to a Re–Bpin environment. Single-crystal X-ray diffraction analysis of **260** showed the P and B atoms arranged in a distorted trigonal planar geometry (Figure 22). The hydrides were located in the difference Fourier map and displayed an average Re–H bond length of 1.50(3) Å which is comparable to other terminal hydride bond lengths.[9] The Re–B bond length is 2.188(3) Å and B1-H1 distance is 1.69(3) Å, both of which are within the range of other high oxidation-state, elongated σ-borane or hydrido boryl complexes.[4, 10] The phosphine bite angle (96.22(3)^{o}) is similar to pentahydride anion **258** however the P-Re distances are slightly elongated (2.4071(9) Å).

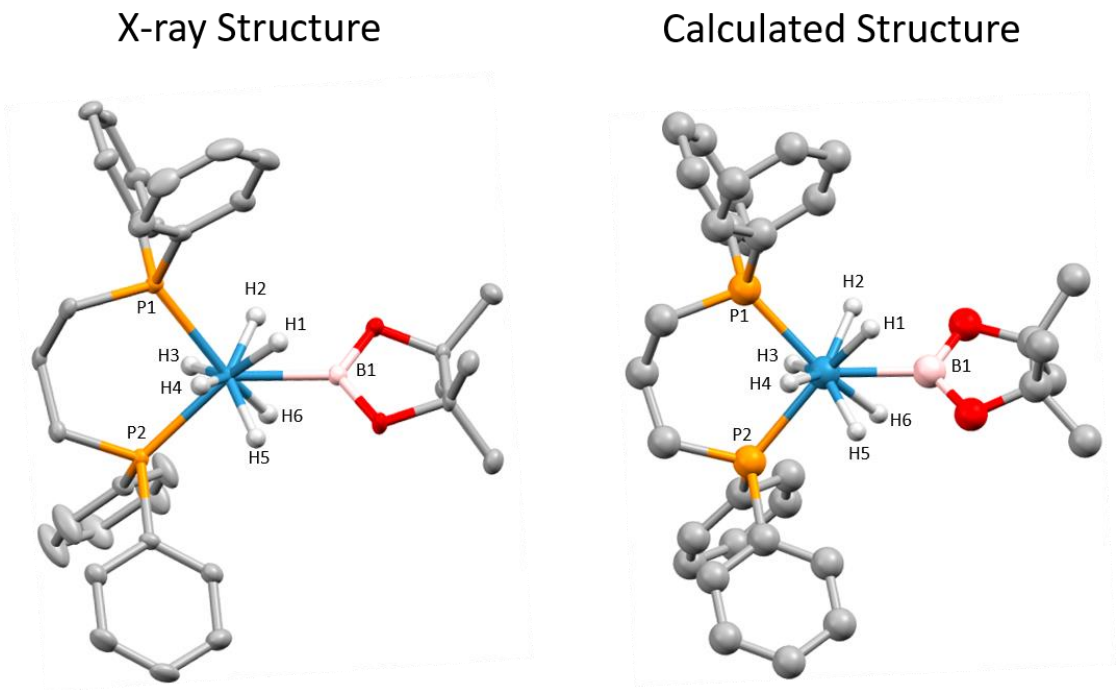

Figure 22. The X-ray crystal structure (left) and calculated structure (right) of **260** (toluene solvate and all hydrogen atoms except for the Re hydrides are omitted; displacement ellipsoids are drawn at 50% probability). X-ray crystal structure selected distances (Å) and angles (°): Re1-B1 2.188(3); Re1-H 1.50(3) avg., B1-H1 1.69(3), Re1-P1 2.4053(9); Re1-P2 2.4106(9); P2-Re1-P1 96.22(3); P1-Re1-B1 127.9(1); P2-Re1-B1 135.9(1).

Once again, possible hydride positions were identified using AIRSS where, from a data set of 24 optimised structures (Figure 23A), a series of 21 closely related, low-energy structures (within 5 kJ mol^{-1}) were obtained which is demonstrated in an overlay image of ten of these structures randomly selected from the low energy plateau (Figure 23B). The remaining three structures lie 42-50 kJ/mol above the global minimum structure and refer to a different boryl structure compared to the global minimum structure with potential μ^2-H_2 bonding (H1…H5 = 1.096 Å) (Figure 23C). A visual overlay with the global minimum structure with the X-ray geometry showed a convincing match (Figure 23D). Given the long B1-H1 distances in both the solid-state and calculated structures and that the crystals of **260** were colourless, it is evident that **260** is best described as a boryl hexahydride complex (i.e., Re^{VII}).

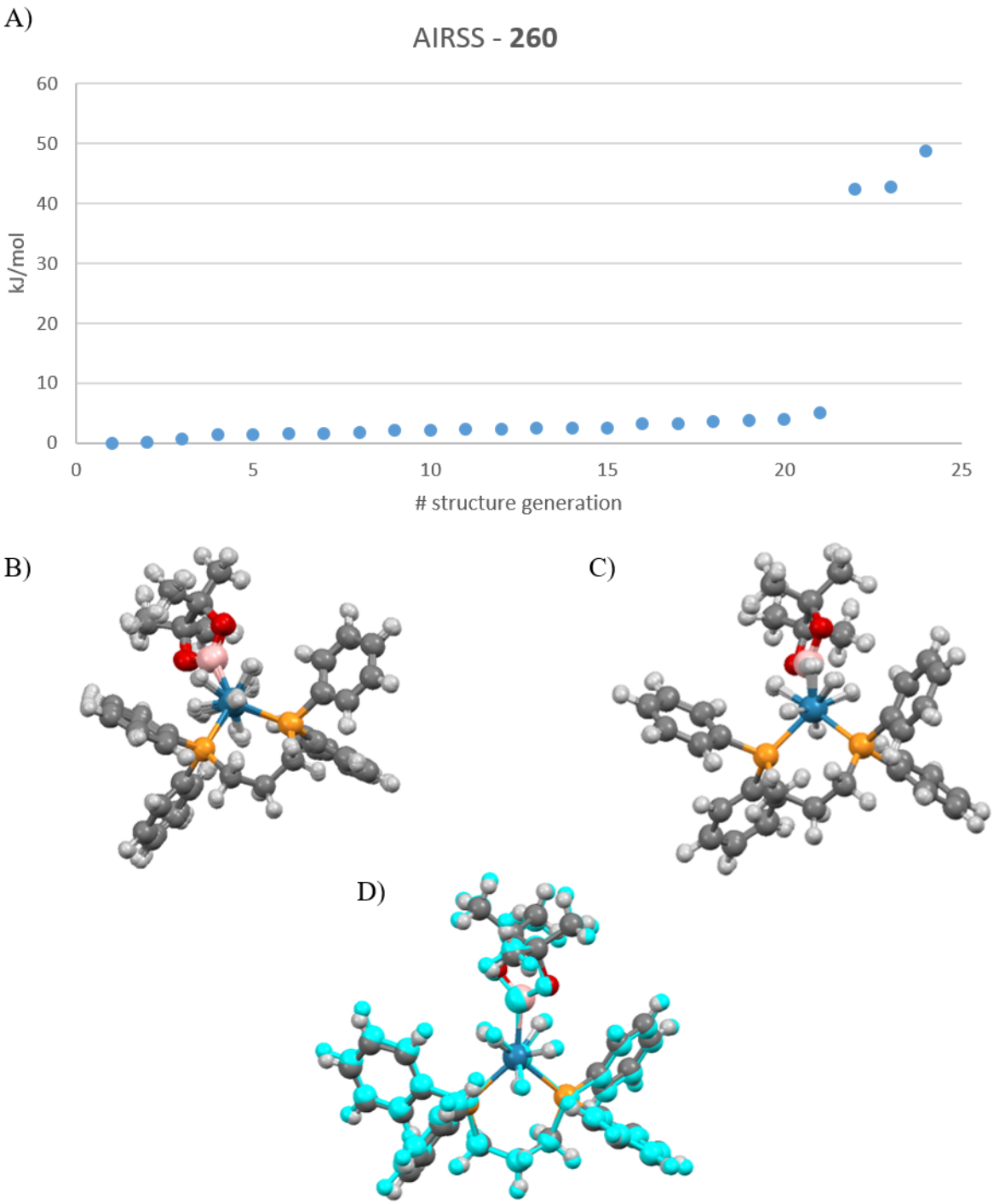

Figure 23. (A) Energy ranking of 24 optimised structures of **260** found by AIRSS (B) Structure overlay diagram of the ten lowest energy structures obtained for **260** by AIRSS (C) Structure overlay of the three highest energy structures of **260** found by AIRSS (D) Structure overlay diagram of the lowest energy structure found by AIRSS (in cyan) and the crystal structure geometry of **260**.

Boryl complex **260** is remarkably stable in both the solid-state and in solution, with no observable decomposition after 4 weeks in the crystalline form or in solutions of C_6D_6, d_8-

toluene and d_8-THF at room temperature. It was also found to be stable in the crystalline form when exposed to air, with no observable decomposition after 4 weeks. This is in sharp contrast to all the boron-hydride complexes previously synthesised that are highly air, temperature and pressure sensitive. Complex **260** was inert to borane substitution with H-9-BBN **36** or HBcat **17**, and was inert to substitution with hydrosilanes at room temperature. No reaction was observed with B_2pin_2 **26**, in contrast to related Ir complexes.[11] The complex was inactive for catalytic pyridine **181** hydroboration in C_6D_6 at 80 °C with no observable formation of DHP products by ^{1}H NMR spectroscopy.

4.2 C–H Borylation Catalysis

4.2.1 Reaction Discovery and Optimisation of Reaction Conditions

The ready synthesis of this well-defined Re(VII) boryl complex **260** prompted its exploration as a catalyst for the C(sp^2) –H borylation of arenes (Table 2). Optimised conditions were established for the C–H borylation of 2-methylfuran **261** using 2 mol% of **260** and 1.5 equivalents of HBpin in THF at 80 °C for 16 h (Table 4); this gave the borylated furan **262** in high yield and regioselectivity for the C5–Bpin regiosiomer **262a** over the C4–Bpin regiosiomer **262b** (>95% conversion, 95:5). This reaction was equally efficient when conducted in DME, cyclohexane or dioxane. No reaction was observed using B_2pin_2 **26** as the boron source for this transformation. Increasing the catalyst loading resulted in an enhanced conversion to **262** and lowering the loading of HBpin **21** from 1.5 equivalents to 1 equivalent decreased conversion. In contrast, catalytic borylation reactivity was not observed using the anionic complexes $\mathbf{165^{DME}}$ or **258** showing that the neutral, phosphine-coordinated complex **260** displays significant differences in reactivity.

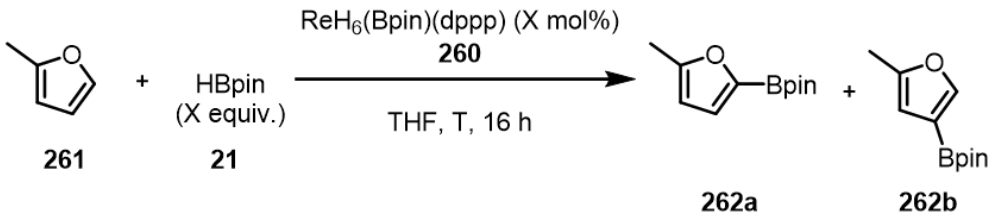

Entry	Catalyst mol%	HBpin equiv.	T (°C)	Yield[a]
1	2	1	50	23%
2	2	1	80	74%
3	2	1.5	80	>95%
4	0	1.5	80	<5%
5	1	1.5	80	55%
6	5	1.5	80	>95%

Table 4. Optimisation of C–H borylation reaction conditions. [a]Yields were determined by ^{1}H NMR spectroscopy from the crude reaction mixture using mesitylene as an internal standard. Regioselectivity of **262a** and **262b** products was consistently 95:5.

4.2.2 Substrate Scope

Mono- and disubstituted furans **261** and **263** were tolerated under these reaction conditions with good selectivity for the C5–Bpin regiosiomer. Furan **264** reacted with 3 equivalents of HBpin to give the doubly borylated products exclusively. Thiophene substrates were also converted to borylated products although the yields were lower than those seen for furans. Thiophene **265** gave a mixture of 2-boryl and 2,5-diboryl thiophenes. Monosubstituted thiophenes **266** – **268** were converted with high selectivity for the 5-boryl products. 3,4-Ethylenedioxythiophene **269** and 2,2'-bithiophene **270** gave a mixture of monosubstituted (major) and disubstituted (minor) boronic ester products. Extended reactions times did not lead to any further appreciable conversion to the disubstituted products. *N*-Unsubstituted pyrroles and indoles **271** – **275** were tolerated and gave high yields and regioselectivities, with no observed formation of N–Bpin bonds. Notably, substrates containing carbon halide bonds (C–Cl/Br) **274** and **275** favoured C–H borylation over Miyaura-type borylation of the C–X bond.

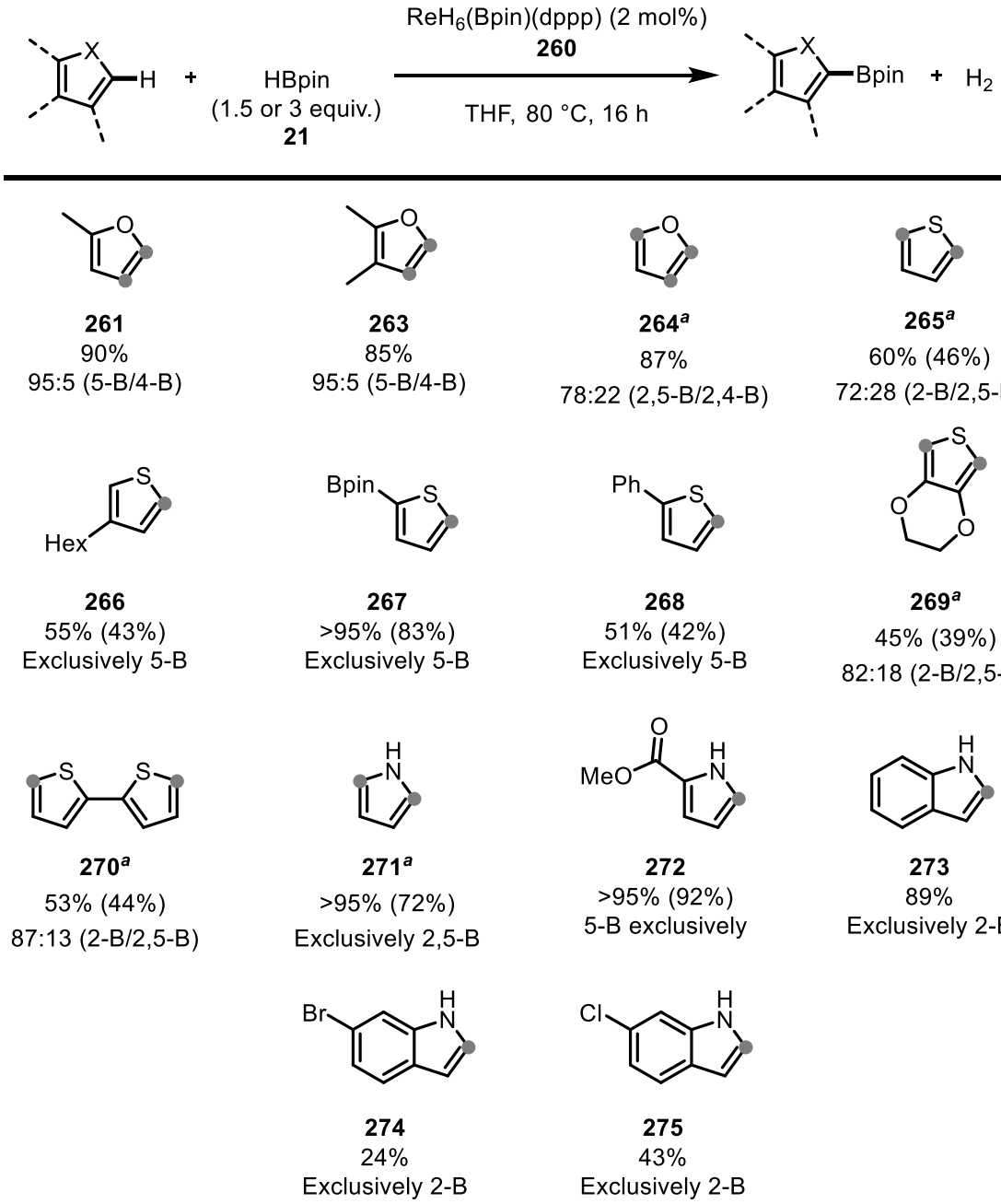

Scheme 59. Substrate scope for the catalytic dehydrogenative C–H borylation of heteroarenes. NMR yields determined by ^{1}H NMR spectroscopy by integration against mesitylene, isolated yields in parentheses.[a] 3 equivalents of HBpin. • Indicates position of borylation.

N–Methyl and *N*–Boc protected pyrroles and indoles gave trace conversion, suggesting that the steric effect, rather than electronic effect, of *N*-substitution inhibits the reaction or that the N–H bonds plays a role in activating pyrroles and indoles.[12] Similarly, di *ortho*-substituted heteroaromatics showed significantly reduced conversion to the boronic ester products with borylation occurring at the 4-position. Expanding the scope of the reaction to carboarenes or

pyridines was unsuccessful, giving trace conversion to the desired borylated products. This could be due to the increased aromaticity of these substrates and/or the decreased p*K*a of the C–H bonds. Alkyne, nitrile, imine and ketone functional groups were not tolerated under these reaction conditions, instead undergoing competitive hydroboration.

4.2.3 Mechanistic Investigation

The time course of a catalytic borylation using **260** was monitored by ^{1}H NMR spectroscopy in d_8-THF (Figure 24). Over 16 h, the hydride signal at −6.08 ppm corresponding to complex **260** diminished and two new signals at −6.27 (t) and −6.34 (p) ppm were observed. Both signals correspond to catalyst deactivation and are identified as arising from the heptahydride complex [ReH_7(dppp)] **276** and the dinuclear octahydride complex [ReH_4(dppp)]$_2$ **277**, respectively.

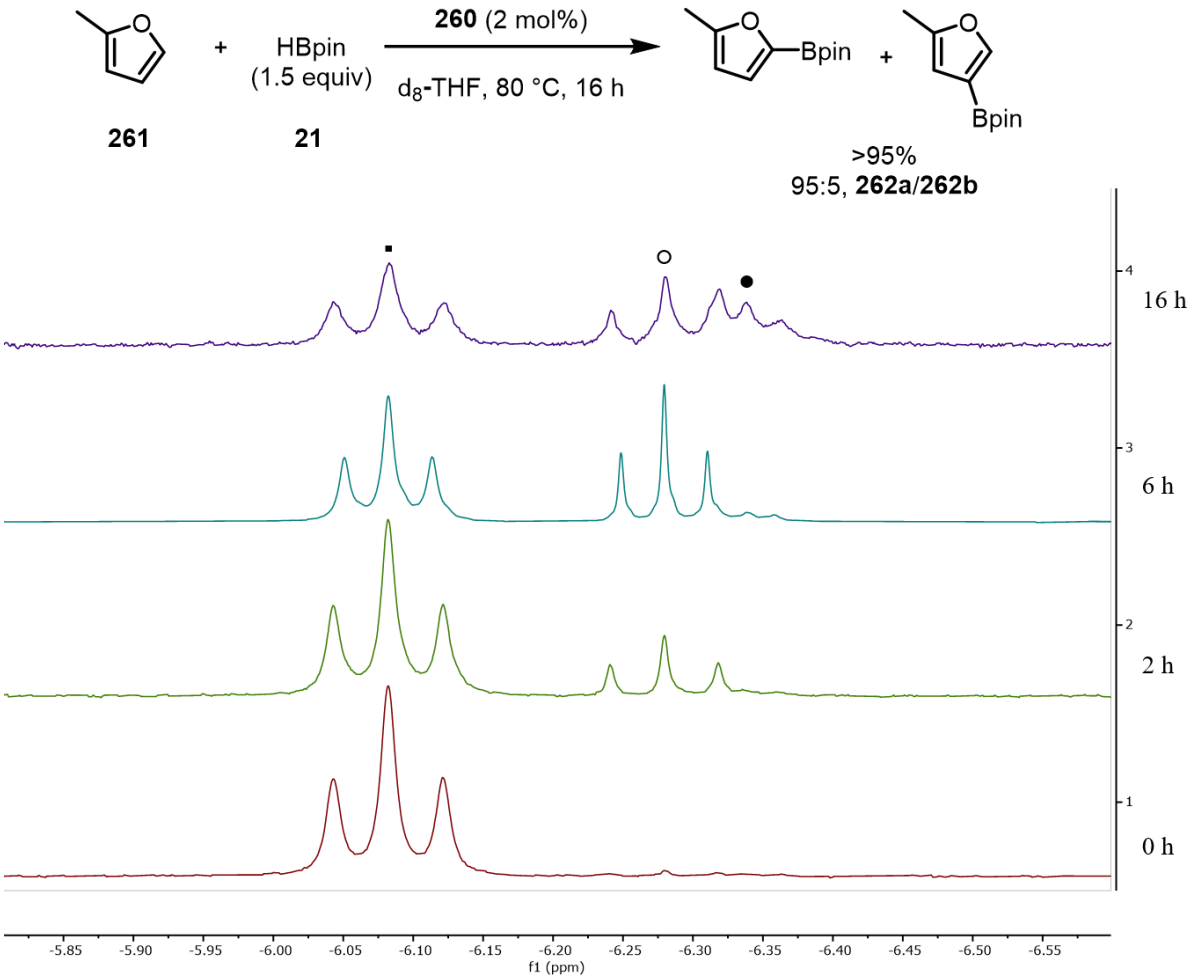

Figure 24. Analysis by ^{1}H NMR spectroscopy of the Re hydride species formed during the catalytic C–H borylation of 2-methylfuran **261**. ▪ **260**, ○ **276**, ● **277**.

The heptahydride complex **276** has been previously reported and was synthesised independently to confirm this assignment. The complex was originally reported to be inert to H_2 loss when heated under reflux in THF in the presence of PPh_3, pyridine and hydrosilanes.[13] Interestingly, we found that **276** acts as a catalyst for C–H borylation, albeit at a significantly reduced rate compared with **260**, achieving only 48% NMR yield after 16 h (Scheme 60).

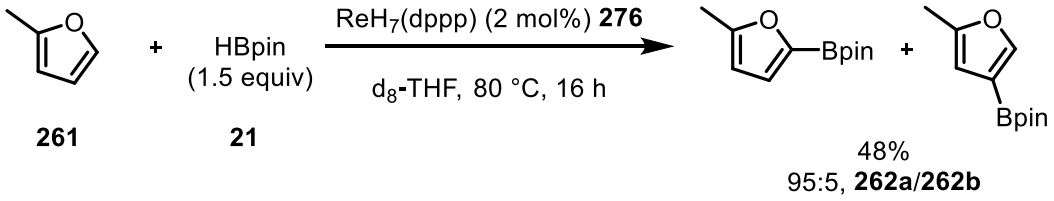

Scheme 60. C–H borylation of **261** with **276** as the catalyst

Complex **276** is presumably formed during standard catalytic conditions from boryl complex **260** by coordination of H_2, liberated during the C–H borylation of the substrate, to the transiently formed ReH_5(dppp). When heptahydride **276** was heated in the presence of an excess of HBpin **21** a small amount of boryl complex **260** was seen in the ^{1}H NMR spectrum, along with dinuclear **277** and an unknown complex **278** which has a hydride resonance at −8.52 ppm (Scheme 61).

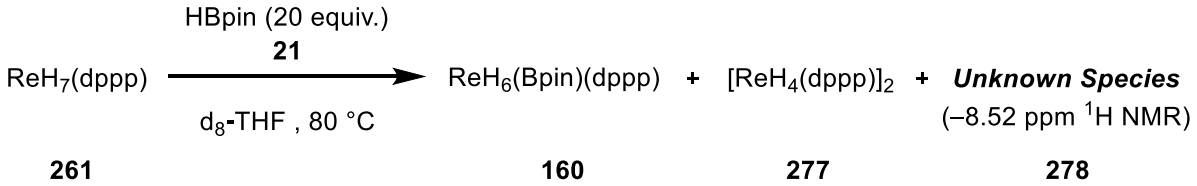

Scheme 61. Reaction of **276** with an excess of HBpin

The dinuclear complex **277** was the sole product formed on heating **260** or **276** at 80 °C in toluene and crystallised directly from the reaction mixture (Scheme 62). The ^{1}H NMR spectrum of isolated **277** matched the signals corresponding to the hydride resonance at −6.34 (quin.), observed under standard catalytic conditions. It should be noted that the formation of **277** by heating **260** at 80 °C for 16 hours in toluene resulted in stoichiometric borylation of toluene to give a 74:26 regioisomeric mixture of the *meta* and *para* borylated products in 48% NMR yield against an internal standard. In contrast to **276**, *in situ* ^{1}H/^{11}B/^{31}P NMR spectroscopy showed that dinuclear complex **277** is inactive in C–H borylation catalysis and inert to hydride substitution by HBpin **21**, reinforcing its role in a deactivation pathway.

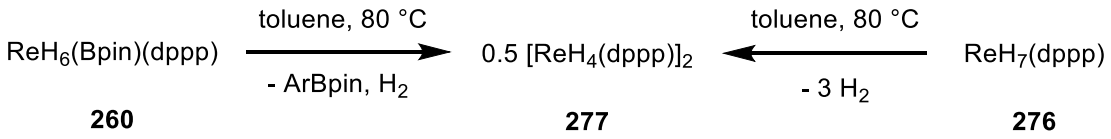

Scheme 62. Synthesis of binuclear complex **277** from **276** and **260**.

The X-ray crystal structure of **277**¸ which exhibited two chemically equivalent but crystallographically independent molecules in the asymmetric unit (Figure 25), confirms that it is a dimeric complex with four bridging hydrides between the Re atoms and two terminal hydrides on each Re atom; the hydride atoms were located in the difference Fourier map and refined freely. Similar dinuclear complexes have been synthesised bearing monodentate or tridentate phosphines;[9, 14-15] however, to the best of our knowledge, complex **277** is the first example with a bidentate phosphine. The average Re-Re distance 2.5341 Å is comparable to other related dimeric complexes and the average phosphine ligand bite-angle (97.16(3)^{o}) and average Re-P distance (2.323(1) Å) are similar to complexes **258** and **260**.

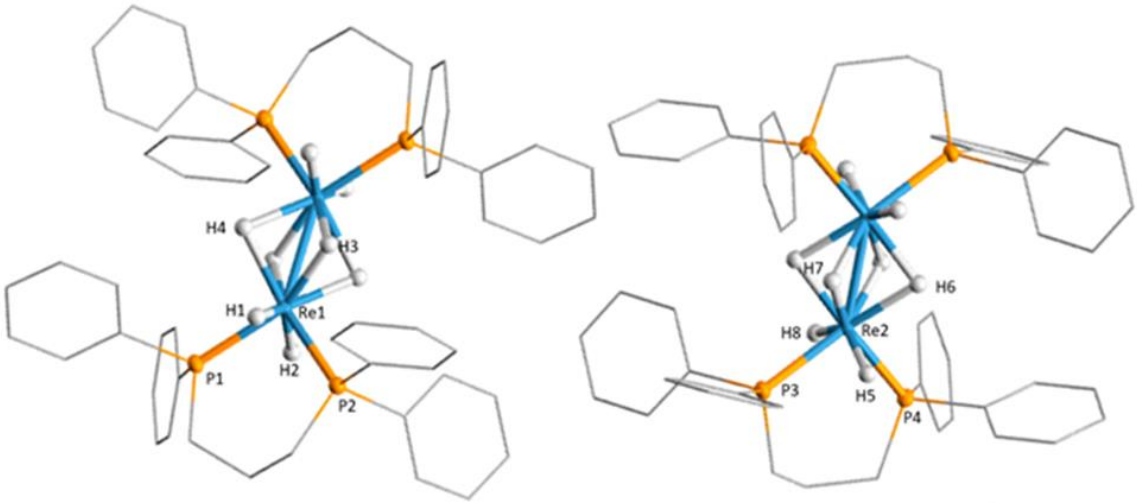

Figure 25. Solid-state structure of **277**. For clarity, all hydrogen atoms (except hydrides) are omitted and displacement ellipsoids are drawn at 50% probability. X-ray crystal structure selected distances (Å) and angles (^{o}): Re1-Re1' 2.5383(5); Re1-H1 1.47(3); Re1-H2 1.48(6); Re1-H3 1.95(1); Re1-H4 1.95(4); Re1-P1 2.327(1); Re1-P2 2.3265(8); H1-Re1-H2 129(3); H3-Re1-H4 65(2); P1-Re1-P2 96.62(3); Re2-Re2' 2.5299(5); Re2-H5 1.47(2); Re2-H6 1.94(3); Re2-H7 1.95(5); Re2-H5 1.47(3); Re2-P3 2.322(1); Re2-P4 2.318(1); H5-Re2-H6 131(2); H7-Re2-H8 65(2); P3-Re2-P4 97.70(3).

To assess the effect of H_2 evolution during catalysis, the borylation of 3-hexylthiophene **266** was conducted under standard conditions in a Teflon-tapped NMR tube and compared to a

reaction performed under static vacuum to enable H_2 formed during the reaction to escape into the head-space of the NMR tube. The progress of both reactions and Re hydride speciation was monitored by *in situ* ^{1}H NMR spectroscopy. Firstly, comparing the yield of borylated product **279** in each reaction over time it is clear that both reactions appear to follow the same profile until ~240 mins time-point, where they diverge and we can see that the rate of reaction for the standard reaction is slower than that of the reaction under partial static vacuum (Scheme 63). At 1000 mins the final yield of **279** is 37% for the standard reaction and 44% for the vacuum reaction, indicating the deleterious effect of H_2 on the reaction.

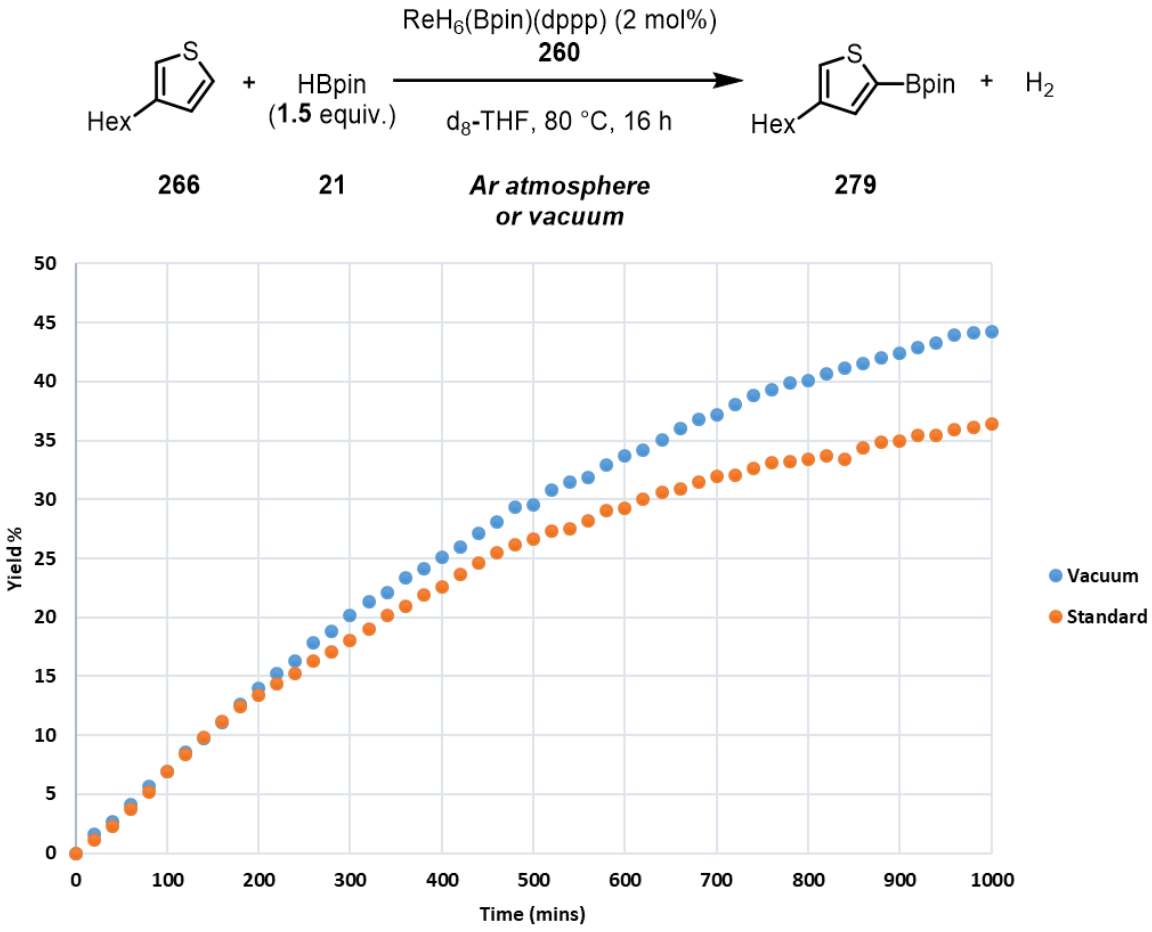

Scheme 63. Reaction progress monitoring of the C–H borylation of **260** under standard and static vacuum conditions.

The speciation of the Re hydride species present in the reaction mixtures could be quantified by integration of the relevant hydride signals in the ^{1}H NMR spectra. Comparing the speciation in the standard and vacuum reactions it is evident that the standard reaction has a much higher proportion of heptahydride **276**, as one would expect given the higher

concentration of H_2 in this reaction compared to the vacuum reaction (Figure 26). Given the decreased catalytic activity of heptahydride **276** compared to boryl **260**, this increased concentration of **276** would support the observed decreased rate in the standard reaction. The standard reaction also appears to have a higher relative concentration of dimer **277** compared to the vacuum reaction, which would support the lower rate of reaction by loss of active Re hydride species through this deactivation pathway. These results also correlate with the evolution of H_2 (4.55 ppm in the ^{1}H NMR spectra) during the course of the reaction, with a consistently lower concentration of H_2 in solution in the vacuum reaction compared to the standard reaction.

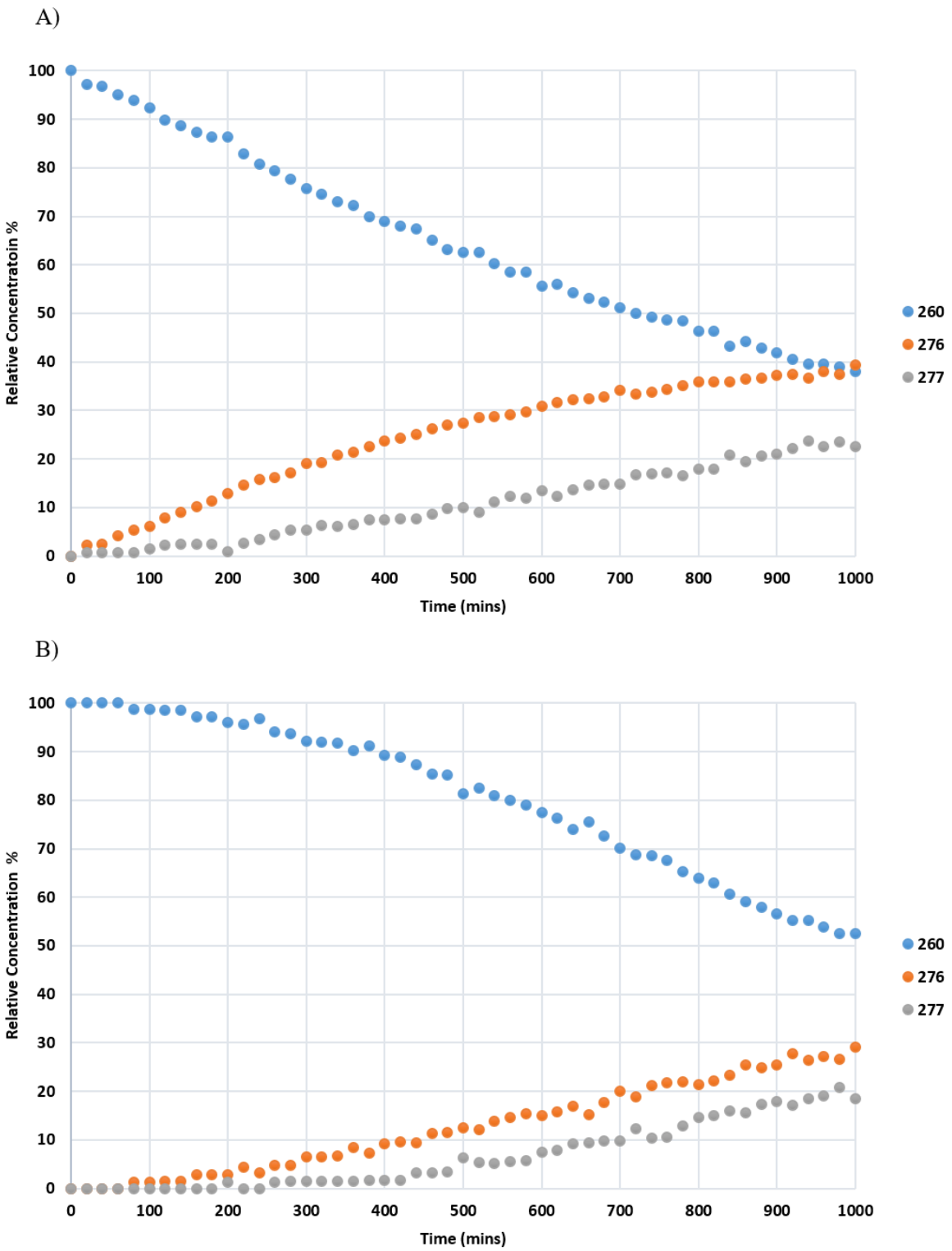

Figure 26. (A) Reaction progress monitoring of hydride speciation under (A) standard conditions and (B) vacuum conditions.

As has been discussed in Chapter One, the reactivity of Re polyhydrides is largely determined by their ability to generate vacant coordination sites by liberation of H_2, either

thermally or photochemically, and they have been shown to participate in C–H bond activation chemistry. It is likely that complex **260** participates in a similar manner to activate the C–H bonds of the heteroarenes. However, under catalytic conditions there is potential for the boryl complex **260** to sequentially lose equivalents of H_2 and add equivalents of HBpin **21** to form higher-order boryl complexes which may be catalytically relevant. To investigate this, a solution of the boryl complex **260** and HBpin **21** (20 equiv.) in d_{12}-cyclohexane was heated at 80 °C and monitored by NMR spectroscopy. After 3 h a broad singlet was seen at −8.50 ppm in the ^{1}H NMR spectrum corresponding to unidentified phosphine-ligated Re hydride complex **278**, as well as several minor signals between −6.00 and −7.50 ppm; H_2 evolution was also observed (singlet at 4.55 ppm) (Figure 27). The formation of **278** did not coincide with an obvious Re–B resonance in the ^{11}B NMR spectrum, however this may be obscured by the large HBpin **21** signal (doublet at 28.2 ppm). A similar, but shorter-lived complex was seen if the reaction was undertaken in d_8-THF, but it was not present in observable quantities under standard catalytic conditions. It was not possible to isolate complex **278** and it appeared to be unstable under vacuum.

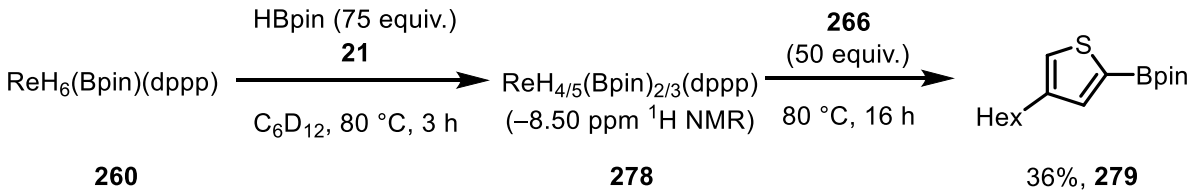

Scheme 64. Formation of unknown species **278** from the reaction of **260** with an excess of HBpin and subsequent catalytic borylation of **266**.

The unknown complex **278** was active in the catalytic borylation of 3-hexylthiophene **266**: complex **278** was generated *in situ* by the reaction between **260** and HBpin **21** for 3 h in d_{12}-cyclohexane, after which addition of **266** and further heating for 16 h resulted in the borylated product **279** in 36% yield (Scheme 64). After 20 mins heating in the presence of thiophene **266** complex **278** was near fully consumed and the only major hydride species was **260** (Figure 27). From this point, the reaction followed a similar profile to standard catalytic reaction conditions using **260**. Complex **278** is only observed in significant quantities in the presence of a large excess of HBpin and in the absence of substrate, therefore, it may only be formed transiently under standard catalytic conditions. These results would suggest that **278** is likely a higher-order boryl species and this would align with the mechanism proposed for

related iridium boryl catalysts which proceed through the formation of tris-boryl intermediates from low oxidation-state Ir pre-catalysts under catalytic conditions.[16-18]

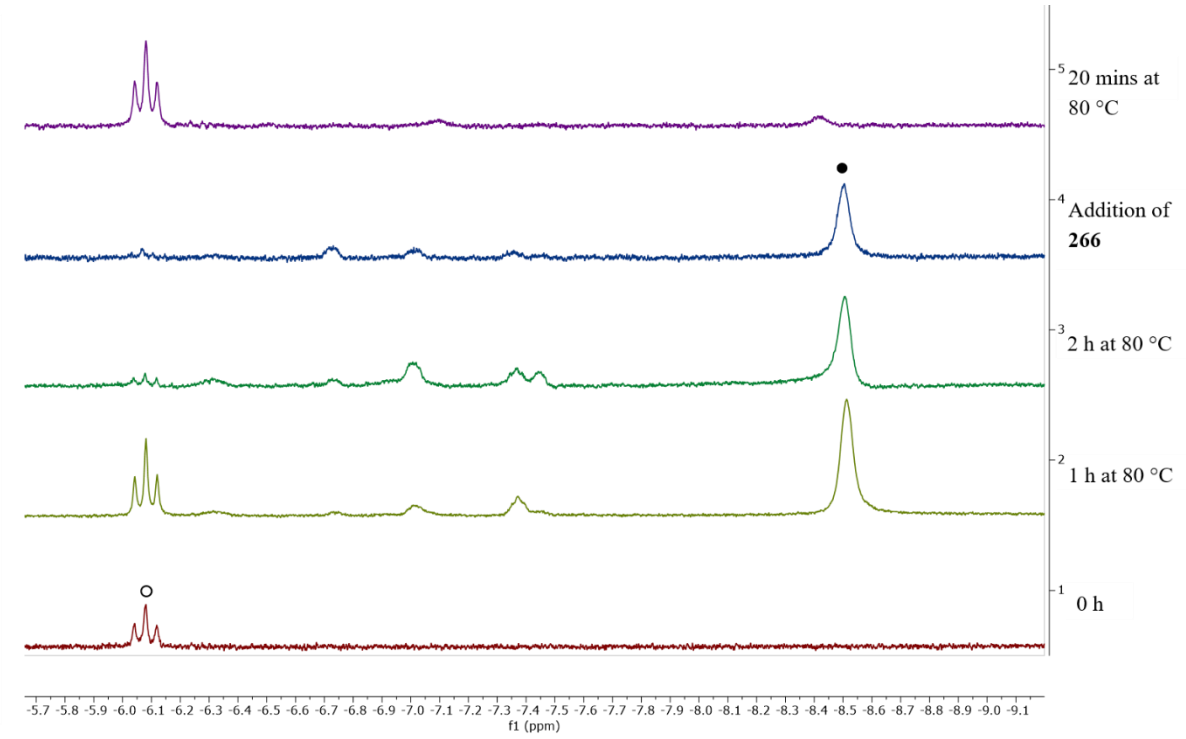

Figure 27. ^{1}H NMR spectra of in situ formation of **278** from HBpin **21** and **260** followed by addition of thiophene **266**. ○ **260**, ● **278**.

Based on these results two catalytic cycles are proposed with complex **278** either as an off-cycle intermediate present in very low concentrations (Scheme 65) or as an on-cycle, catalytically active intermediate that is consumed as quickly as it is formed (Scheme 66). Considering the first cycle: (1) Elimination of an equivalent of H_2 from pre-catalyst **260** forms a coordinatively unsaturated boryl complex **Int-1A**; (2) oxidative addition of the arene substrate gives a Re aryl intermediate **Int-1B**; (3) reductive elimination of the boronic ester product and formation of a coordinatively unsaturated pentahydride complex **Int-1C**; (4) addition of an equivalent of HBpin **21** and elimination of H_2 reforms **Int-1A**. The reaction of pre-catalyst **260** with an excess of HBpin **21** will lead to the formation of the higher-order boryl **278**. The reaction of **260** with H_2 will form heptahydride **276**. Catalyst deactivation can occur through the dimerization of **260** or **276** to form **277**.

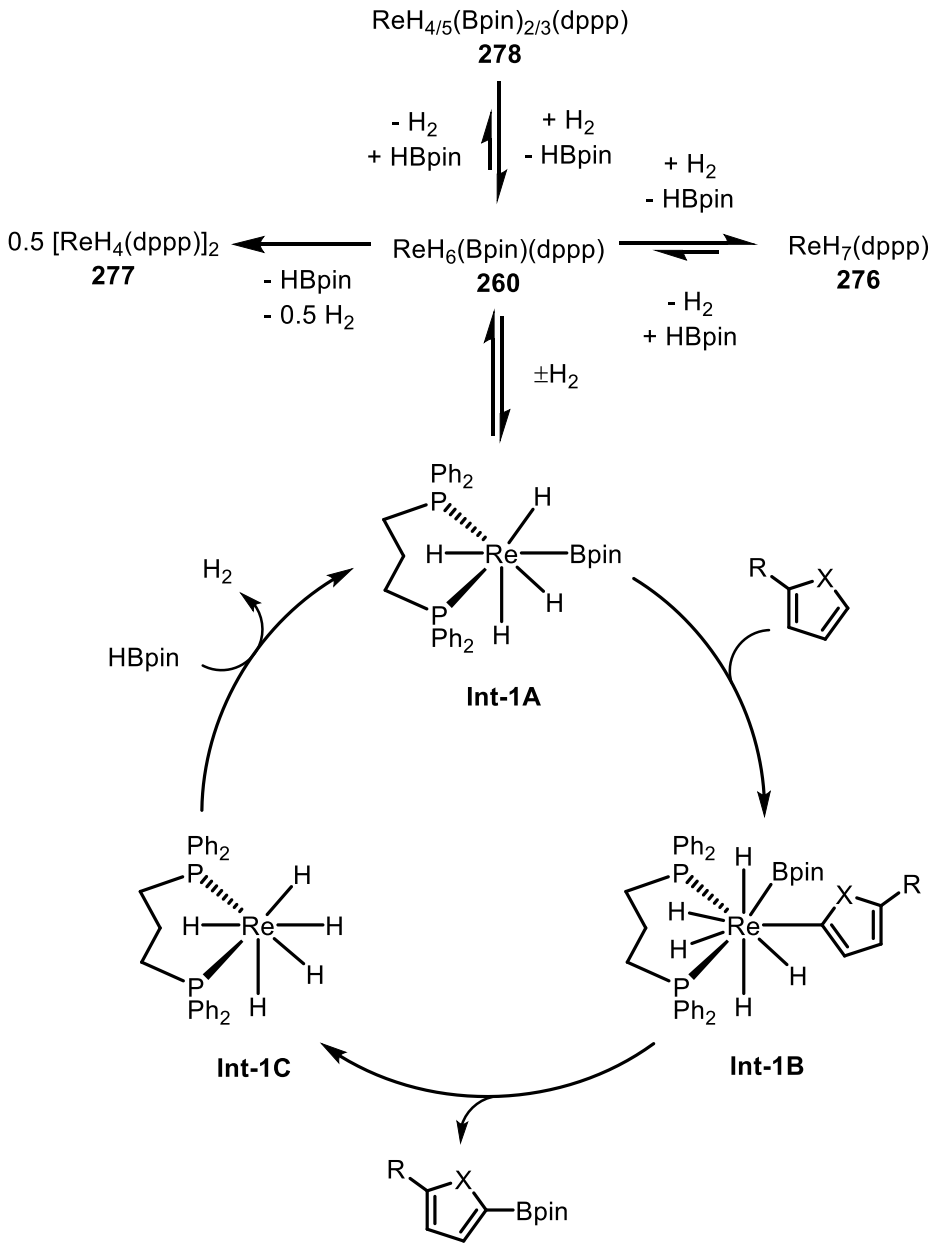

Scheme 65. Proposed catalytic cycle for the C–H borylation of heteroarenes with **278** as an off-cycle intermediate.

Now considering the second cycle where **278** is an on-cycle intermediate: (1) Elimination of equivalents of H_2 from pre-catalyst **260** and addition of HBpin forms the higher-order boryl complex **278**; (2) elimination of H_2 and oxidative addition of the arene substrate gives a Re aryl intermediate **Int-2A**; (3) reductive elimination of the boronic ester product and formation of a coordinatively unsaturated mono- or bisboryl complex **Int-2B**; (4) addition of an equivalent of HBpin **21** and elimination of H_2 reforms **278**.

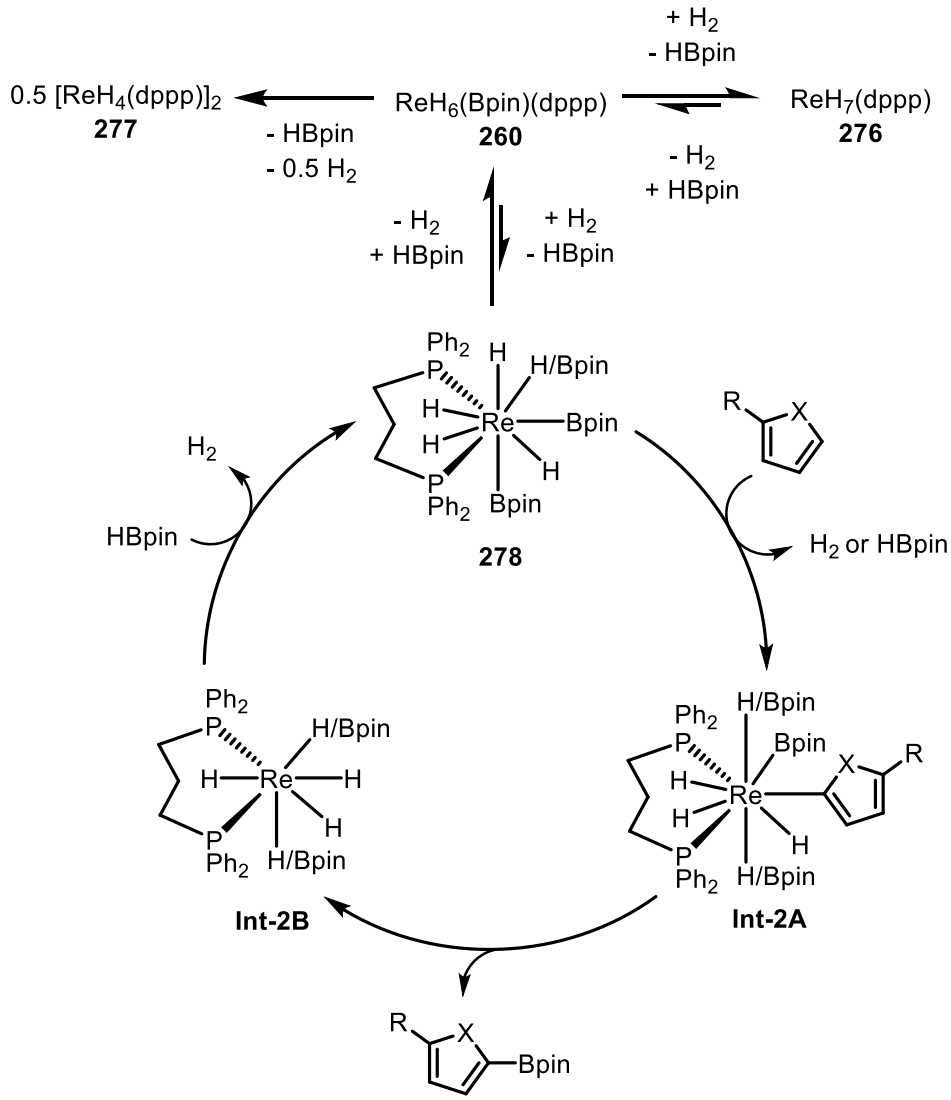

Scheme 66. Proposed catalytic cycle for the C–H borylation of heteroarenes with **278** as an on-cycle intermediate.

4.3 References

1. Chen, H.; Hartwig, J. F., Catalytic, *Angew. Chem. Int. Ed.* **1999**, *38*, 3391-3393.
2. Murai, M.; Omura, T.; Kuninobu, Y.; Takai, K., *Chem. Commun.* **2015**, *51*, 4583-4586.
3. Hlatky, G. G.; Crabtree, R. H., *Coord. Chem. Rev.* **1985**, *65*, 1-48.
4. Esteruelas, M. A.; Fernández, I.; García-Yebra, C.; Martín, J.; Oñate, E., *Organometallics* **2017**, *36*, 2298-2307.
5. Abdur-Rashid, K.; Lough, A. J.; Morris, R. H., *Can. J. Chem.* **2001**, *79*, 964-976.
6. Pickard, C. J.; Needs, R. J., *J. Condens. Matter Phys.* **2011**, *23*, 053201.

7. Clark, S. J.; Segall, M. D.; Pickard, C. J.; Hasnip, P. J.; Probert, M. I. J.; Refson, K.; Payne, M. C., *Z. Kristallogr. Cryst. Mater.* **2005**, *220*, 567.

8. Hebden, T. J.; Denney, M. C.; Pons, V.; Piccoli, P. M. B.; Koetzle, T. F.; Schultz, A. J.; Kaminsky, W.; Goldberg, K. I.; Heinekey, D. M., *J. Am. Chem. Soc.* **2008**, *130*, 10812-10820.

9. Kosanovich, A. J.; Reibenspies, J. H.; Ozerov, O. V., *Organometallics* **2016**, *35*, 513-519.

10. Hartwig, J. F.; Cook, K. S.; Hapke, M.; Incarvito, C. D.; Fan, Y.; Webster, C. E.; Hall, M. B., *J. Am. Chem. Soc.* **2005**, *127*, 2538-2552.

11. Cho, J.-Y.; Tse, M. K.; Holmes, D.; Maleczka, R. E.; Smith, M. R., *Science* **2002**, *295*, 305.

12. Tian, Y.-M.; Guo, X.-N.; Wu, Z.; Friedrich, A.; Westcott, S. A.; Braunschweig, H.; Radius, U.; Marder, T. B., *J. Am. Chem. Soc.* **2020**, *142*, 13136-13144.

13. Luo, X. L.; Crabtree, R. H., *J. Am. Chem. Soc.* **1990**, *112*, 4813-4821.

14. Cotton, F. A.; Luck, R. L., *Inorg. Chem.* **1989**, *28*, 4522-4527.

15. Bau, R.; Carroll, W. E.; Teller, R. G.; Koetzle, T. F., *J. Am. Chem. Soc.* **1977**, *99*, 3872-3874.

16. Tamura, H.; Yamazaki, H.; Sato, H.; Sakaki, S., *J. Am. Chem. Soc.* **2003**, *125*, 16114-16126.

17. Boller, T. M.; Murphy, J. M.; Hapke, M.; Ishiyama, T.; Miyaura, N.; Hartwig, J. F., *J. Am. Chem. Soc.* **2005**, *127*, 14263-14278.

18. Vanchura, I. I. B. A.; Preshlock, S. M.; Roosen, P. C.; Kallepalli, V. A.; Staples, R. J.; Maleczka, J. R. E.; Singleton, D. A.; Smith, I. I. I. M. R., *Chem. Commun.* **2010**, *46*, 7724-7726.

Chapter Five – Conclusions and Outlook

An operationally simple procedure for the synthesis of the reactive rhenium(VII) boron-polyhydride anion **165** by exhaustive deoxygenation of the bench-stable and commercially available perrhenate anion ReO_4^- **163** with HBpin **21** was developed. The structure of **165^{DME}** was analysed by X-ray crystallography and NMR spectroscopy revealing the presence of seven hydride ligands and three Bpin units that are highly fluxional at room temperature. Further evaluation of the structure by AIRSS identified the presence of hydride, boryl, σ-borane, and dihydroborate ligands. This is a rare of example of a high oxidation-state, transition metal complex of a boron-hydride ligand and the synthesis provides a new level of practicality compared to traditional routes to polyhydride and borane complexes. Initial attempts were made to elucidate the mechanism of the deoxygenation reaction, but the isolation and analysis of potential reaction intermediates is challenging due to the high sensitivity of these complexes. Future studies of the reaction mechanism would benefit from computational techniques such as DFT to compare and contrast potential reaction pathways.

Anion **165** exhibited diverse reactivity including the catalytic hydroboration of *N*-heteroaromatics, stoichiometric C–H borylation, and borane ligand substitution. This complex, either isolated or prepared *in situ*, was a catalyst for the 1,4-hydroboration of *N*-heteroaromatic substrates under simple operating procedures. Mechanistic studies revealed an equilibrium between **165** and **167** through dissociation of HBpin which appears to be an important step in the catalytic cycle of *N*-heterocycle hydroboration. **165** was also a reagent for the stoichiometric C–H borylation of toluene which displayed high *meta* regioselectivity. Unfortunately, attempts to adapt this stoichiometric reactivity to a catalytic protocol through optimisation of the reaction conditions were unsuccessful. The reaction of **165^{DME}** with H-9-BBN **36** or $HBCy_2$ **174** resulted in Bpin substitution to form the new anionic tetra(dihydroborate) complexes **172** and **175** for which the hydride positions were clearly identified by X-ray crystallography. Like **165**, these dihydroborate complexes could also be synthesised directly from perrhenate through an exhaustive deoxygenation pathway. The deoxygenation method used to generate these isolable yet reactive boron-hydride complexes is direct and straightforward and initial attempts to expand this chemistry to RuO_4^- demonstrates the ability to form hydride complexes such as **234**, highlighting the potential for other, more earth-abundant, metal-oxo compounds (WO_4^{2-} and MoO_4^{2-}) to undergo exhaustive deoxygenation with hydroboranes. If successful, the resulting boron hydride

complexes may have interesting structures and reactivity as well as useful applications in hydroboration and C–H borylation catalysis.

The reaction of **165^{DME}** with phosphine and *N*-donor ligands resulted in the reductive substitution of one or two equivalents of HBpin **21** and coordination of the ligand to Re. In most cases this reaction was either sluggish or unselective, producing a mixture of new hydride complexes. However, the reaction of **165^{DME}** with dppp produced an anionic complex **258** through substitution of two equivalents of HBpin **21**. Complex **258** and other related phosphine complexes were unstable once isolated from the reaction mixture. Combined X-ray crystallographic and DFT studies showed that **258** is best described as a σ-borane complex and this was supported by *in situ* NMR spectroscopy of the reaction mixture. Protonation of **258** produced the neutral boryl complex **260** which was characterised as a Re(VII) boryl complex. Compared with **258**, complex **260** was remarkably stable in both the solid-state and in solution. This work has the potential to inform further ligand screens to synthesise and isolate a range of related compounds. This could provide further information on how the ligand environment affects the bonding mode of HBpin and its associated reactivity.

The boryl complex **260** acted as a catalyst for the dehydrogenative C(sp^2)–H borylation of a variety of heteroarenes, including furan, thiophene, pyrrole and indole derivatives. In the majority of cases the C–H bond α to the heteroatom was borylated, which is consistent with related catalytic reactions mediated by high oxidation-state Ir complexes. An investigation of the mechanism of this reaction identified potential reactive intermediates and deactivation pathways which were tracked over the time scale of the reaction. Catalyst inhibition occurred through coordination of evolved H_2 to Re to form the heptahydride complex **276** which, while active as a C–H borylation catalyst, reacted at a significantly reduced rate. Catalyst deactivation occurs through a dimerisation reaction that forms the binuclear octahydride complex **277** which was isolated and fully characterised. The catalytic C–H borylation reaction either proceeds *via* formation of a coordinatively unsaturated monoboryl complex or formation of higher-order, bis- and tris-boryl complexes through sequential addition of HBpin. This work represents a new application of high oxidation-state Re complexes in C–H functionalisation catalysis and may have applications to related transformations, for example C–H silylation and germylation. Exploration of ligand scaffolds other than phosphines may ultimately enable the catalytic C–H borylation of more challenging C(sp^2)–H bonds of carboarenes and pyridines, and C(sp^3)–H bonds of alkanes.

Chapter Six – Experimental

6.1 General Experimental

Reaction set-up: The syntheses of all air- and moisture-sensitive compounds were undertaken using standard Schlenk techniques. Vacuum Atmospheres and MBraun glove boxes were used to manipulate and store air- and moisture-sensitive compounds under an atmosphere of dried and deoxygenated dinitrogen or Ar. All glassware was dried in an oven at 160 °C, allowed to cool under 1×10^{-3} mbar vacuum, and then purged with nitrogen. All glassware was cleaned using base (KOH, *i*PrOH) and acid (HCl_{aq}) baths. All reported reaction temperatures correspond to external bath temperatures. Room temperature (r.t) was approximately 25 °C.

NMR Spectroscopy: ^{1}H, $^{13}C\{^{1}H\}$, ^{11}B and $^{31}P\{^{1}H\}$ NMR spectra were recorded on Bruker AVA400, AVA500, or PRO500 spectrometers at 298 K. Chemical shifts are reported in parts per million. All ^{1}H NMR and $^{13}C\{^{1}H\}$ NMR spectra were referenced relative to $SiMe_4$ through a resonance of the employed deuterated solvent or proteo impurity of the solvent; C_6D_6 (7.16 ppm), d_8-toluene (7.09, 7.01, 6.97, 2.08 ppm), d_5-pyridine (7.19, 7.55, 8.71 ppm), C_6D_{12} (1.38 ppm) and d_8-THF (3.58, 1.72 ppm) for ^{1}H NMR spectra; C_6D_6 (128.0 ppm), d_8-toluene (137.48, 128.87, 127.96, 125.13, 20.43 ppm), d_5-pyridine (123.5, 135.5, 149.5 ppm), C_6D_{12} (26.4 ppm) and d_8-THF (67.21, 25.31 ppm) for $^{13}C\{^{1}H\}$ NMR spectra. ^{11}B NMR spectra were referenced using an external standard of $BF_3(OEt_2)$. Multiplicities are indicated by app. (apparent), br. (broad), s (singlet), d (doublet), t (triplet), q (quartet), quin. (quintet), sext. (sextet), sept. (septet), non. (nonet). Coupling constants, *J*, are reported in Hertz and rounded to the nearest 0.1 Hz. Integration is provided and assignments are indicated. ^{1}H and ^{13}C assignments are corroborated through 2-D NMR experiments (COSY, HSQC, HMBC) where applicable.

Infrared Spectroscopy: Infra-red (IR) spectra were recorded on a Shimadzu IRAffinity-1 spectrometer (serial no. A213749) spectrometer. Relevant peaks are reported in cm^{-1}.

Elemental Analysis: Elemental analyses were determined by Mr. Stephen Boyer at the London Metropolitan University or by Elemental Microanalysis Ltd and measured in duplicate.

Single-Crystal X-ray Crystallography: Single-crystal X-ray data was collected using an Excalibur Eos diffractometer, fitted with a CCD area detector and using MoKα radiation at 120.0(1) K or using an Oxford Diffraction Supernova instrument at 120.0(1) K, fitted with a CCD area detector using Mo Kα radiation. Structures were solved using ShelXT by direct methods or intrinsic phasing and refined using a full-matrix least-squares refinement on $|F|^2$ using ShelXL.[1-2] All programs were used within the Olex suite.[3] All hydrogens atoms were placed geometrically and refined by using a riding model, with the exception of the hydrides in compounds **165^{DME}**, **172**, **234**, **258**, **260** and **277** which were located in the difference Fourier map and were isotropically refined with restraints as appropriate.

Solvents: Solvents for air- and moisture sensitive techniques were degassed and purified by passage through activated alumina towers and stored over 4 Å molecular sieves. Pyridine was dried by refluxing in a N_2 atmosphere, over molten potassium metal on a still for four consecutive days; it was then collected and stored over 4 Å molecular sieves in a Young's tap fitted flask. Deuterated solvents were purchased from Cambridge Isotopes. C_6D_6, d_8-toluene, d_5-pyridine, C_6D_{12} and d_8-THF were boiled over potassium, freeze−pump−thaw degassed and vacuum-transferred prior to use. Reaction solvents tetrahydrofuran (THF) (Fisher, HPLC grade), ether (Et_2O) (Fisher, BHT stabilized ACS grade), and dichloromethane (CH_2Cl_2) (Fisher, unstabilized HPLC grade) were dried by percolation through two columns packed with neutral alumina under a positive pressure of argon. Reaction solvent ethanol (absolute, VWR) was used as received. Solvents for filtration, transfers, chromatography, and recrystallization were dichloromethane (CH_2Cl_2) (ACS grade, amylene stabilized), diethylether (Et_2O) (Fisher, BHT stabilized ACS grade), ethyl acetate (EtOAc) (Fisher, ACS grade), hexane (Optima), methanol (MeOH) (ACS grade), pentane (ACS grade), and petroleum ether (40–60°C, ACS grade).

Reagents: HBpin was purchased from Sigma Aldrich and freeze−pump−thaw degassed and vacuum-transferred and stored at −20 °C in an Ar-filled glovebox prior to use.
All other reagents were purchased from Sigma Aldrich, Alfa Aesar, Acros Organics, Tokyo Chemical Industries UK, Fluorochem, Fisher Scientific UK and Apollo Scientific or synthesised within the laboratory and used without further purification.
The compounds $HBCy_2$ **174**,[4] Aminoborane **176**,[5] Alkoxyborane **177**,[6] Ipc_2BH,[7], $[N(hexyl)_4][ReO_4]$,[8] $[N(butyl)_4][ReO_4]$,[8] ReO_4SiPh_3,[9] $[N(butyl)_4][MnO_4]$,[10] $N(butyl)_4][VO_3]$[11] and ReH_7(dppp) **276**[12] were prepared according previously reported methods.

Chromatography: Column chromatography was carried out on a Teledyne ISCO CombiFlash NextGen 300+ using RediSep Rf normal phase silica flash columns (12, 25, 40, or 80 g; 20-40 microns) or performed 'by hand' on silica gel (Merck Kielselgel 60, 40-63 μm). Analytical thin-layer chromatography was performed on aluminium-backed silica plates (Merck 60 F254). Product spots were visualised by UV light at 254 nm, and subsequently developed using potassium permanganate solution if appropriate.

Computational Details: The Re-H hydrogen atoms in complexes **165^{DME}**, **258** and **260** were located in a non-biased way through a series of AIRSS/CASTEP geometry optimisation calculations.[13-14] The models, derived from the crystal structure coordinates, stripped of coordinating solvate molecules (in the case of **165^{DME}**) and hydrogen atoms around the Re site were placed inside a 17 Å^3 box. AIRSS constructed the initial models by positioning the hydrogen atoms randomly on a sphere of radius 1.6-1.85 Å centred on the Re coordinate. One further constraint was imposed on the initial hydrogen atom placement, to ensure a minimum separation of 1.1 Å between the hydrogen atoms, to prevent possible formation of H_2. Over twenty random structures for each complex were generated in this way and optimised using CASTEP (version 19.11) for full atomic optimisation (basis set energy cut-off: 750 eV; DFT functional: PBE; dispersion correction: TS; pseudopotentials: on-the-fly; geometry optimisation criteria: energy tolerance: 5×10^{-4} eV, maximum force tolerance: 0.1 eV Å^{-1} atomic displacement tolerance: 5×10^{-2} Å).

6.2 Synthesis of Complexes

Synthesis of [K(DME)(18-c-6)][ReH$_7$(Bpin)$_3$] (165^{DME})

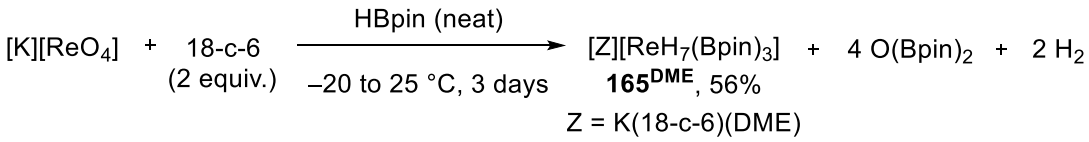

HBpin (15 mL) was added to [K][ReO_4] (1.00 g, 3.5 mmol) and 18-crown-6 (1.86 g, 7 mmol) and stirred at room temperature. After 5 days, the HBpin was evaporated under vacuum (recovered HBpin was recycled for further use) to give a light brown solid. Et_2O (20 mL) was added to the crude solid at 0 °C and the mixture was stored at −20 °C for 16 h to precipitate a light brown solid, which was isolated by filtration and dried under vacuum. The solids were dissolved in DME (30 mL) the solution was stored at −20 °C for 16 h to give colourless crystals of **165^{DME}** which were collected by cannula filtration at 0 °C, washed with cold Et_2O

(5 mL) and dried under vacuum to give **165^{DME}** as a colourless solid (1.90 g, 56 %) which was indefinitely stable when stored at −20 °C in a glovebox. Elemental analysis. Calculated for $C_{34}H_{77}B_3KO_{14}Re$ (Mr = 968.48 g mol^{-1}): C, 42.20; H, 8.02 %. Found: C, 42.22; H, 7.98 %. ^{1}H NMR (500 MHz, toluene-d_8): δ_H 3.37 (s, 24H), 3.31 (s, 4H), 3.12 (s, 6H), 1.23 (s, 36H), -7.21 (s, 7H). ^{13}C{^{1}H} NMR (126 MHz, toluene-d_8): δ_C 81.7, 72.3 , 70.0, 58.6, 25.2. ^{11}B[^{1}H] NMR (toluene-d_8, 300 K): δ ^{11}B NMR (160 MHz, toluene-d_8): δ_B 45.0, 31.3 (Ar-Bpin), 28.6 (d, J = 117.8 Hz, HBpin). IR (ATR): ν 1950 (br.w, Re-H), 1850 (br.w, Re-H). Due to the volatility of the DME ligand bound to potassium the integration for the DME signals in the ^{1}H NMR spectrum is low and the elemental analysis is low in C.

Synthesis of [NBu$_4$][ReH$_8$(Bpin)$_2$] (167^{H2})

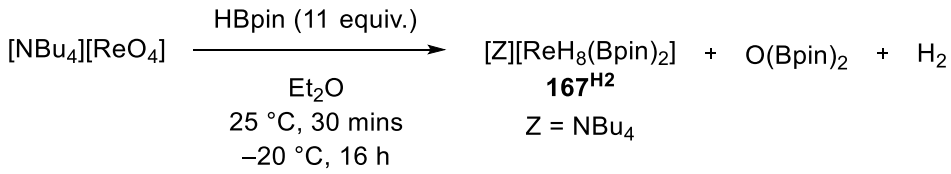

HBpin (588 μL) was added to a solution of [N(butyl)$_4$][ReO$_4$] (1.00 g, 3.5 mmol) and stirred at room temperature for 10 minutes. The crude reaction mixture was dissolved in Et_2O (1.5 mL) and was stored at −20 °C for 16 h to produce **167^{H2}** as small colourless crystals. Crystalline **167^{H2}** decomposes rapidly at room temperature and as such we were unable to isolate pure material for full characterisation. The solid-state structure of **167^{H2}** was determined by single-crystal X-ray diffraction. A major hydridic signal at δ -7.21 ppm was observed in the ^{1}H NMR spectrum for **167^{H2}** in THF which decomposed after to give a dark brown solid. δ ^{11}B NMR (128 MHz, THF) δ 42.4, 28.5 (d, J = 173.7 Hz, HBpin), 21.6 (O(Bpin)$_2$).

Synthesis of [PPN][ReO$_4$] (163^{PPN})

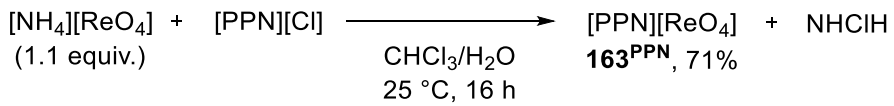

[PPN][Cl] (0.78 g, 1.36 mmol) and [NH$_4$][ReO$_4$] (0.40 g, 1.49 mmol) were dissolved in mixture of $CHCl_3$ (20 mL) and H_2O (20 mL). The mixture was stirred at room temperature for 16 h. The two layers were separated and the aqueous layer was extracted with $CHCl_3$ (3 x 20 mL). The combined organic layers were dried over $MgSO_4$, filtered and the solvent removed under vacuum to give **163^{PPN}** as a colourless solid (0.76 g, 71%). Elemental analysis

calculated for $C_{36}H_{30}NO_4P_2Re$ (Mr = 789.12 g mol^{-1}): C, 54.82; H, 3.83; N, 1.78 %. Found: C, 54.87; H, 3.85; N, 1.76 %. ^{1}H NMR (400 MHz, $CDCl_3$) δ 7.66 (ddq, *J* = 9.0, 5.4, 1.7 Hz, 6H), 7.54 – 7.40 (m, 24H). ^{13}C NMR (126 MHz, $CDCl_3$) δ 133.90 (d, *J* = 1.8 Hz), 132.35 – 131.99 (m), 129.82 – 129.33 (m), 126.99 (dd, *J* = 108.0, 2.0 Hz). ^{31}P NMR (162 MHz, $CDCl_3$) δ 21.12.

Synthesis of [P(butyl)$_3$Ph][ReO$_4$] (163^{PBu})

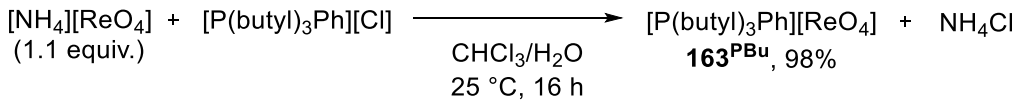

[P(butyl)$_3$Ph][Cl] (0.31 g, 1.00 mmol) and [K][ReO$_4$] (0.32 g, 1.10 mmol) were dissolved in mixture of $CHCl_3$ (10 mL) and H_2O (10 mL). The mixture was stirred at room temperature for 16 h. The two layers were separated and the aqueous layer was extracted with $CHCl_3$ (3 x 10 mL). The combined organic layers were dried over $MgSO_4$, filtered and the solvent removed under vacuum to give **163^{PBu}** as a colourless solid (0.52 g, 98%). Elemental analysis calculated for $C_{18}H_{32}O_4PRe$ (Mr = 530.16 g mol^{-1}): C, 40.82; H, 6.09 %. Found: C, 40.80; H, 6.04 %. ^{1}H NMR (500 MHz, $CDCl_3$) δ 7.82 – 7.69 (m, 5H), 2.55 (ddd, *J* = 12.6, 9.2, 6.1 Hz, 6H), 1.59 – 1.45 (m, 12H), 0.96 (t, *J* = 6.9 Hz, 9H). ^{13}C NMR (126 MHz, $CDCl_3$) δ 134.6 (d, J = 3.0 Hz), 131.7 (d, J = 8.6 Hz), 130.4 (d, J = 11.8 Hz), 117.5 (d, J = 79.6 Hz), 23.7 (d, J = 12.5 Hz), 23.6, 19.2 (d, J = 48.8 Hz), 13.3. ^{31}P NMR (162 MHz, $CDCl_3$) δ 29.61.

Synthesis of [K(DME)(18-c-6)][Re(κ$_2$-H$_2$BBN)$_4$] (172)

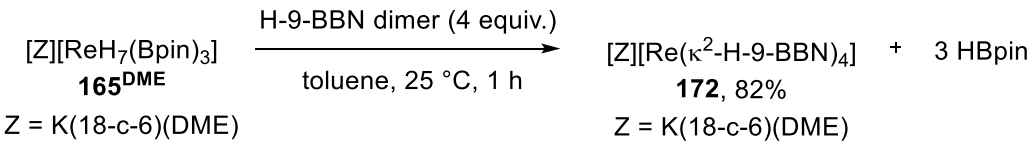

Solid H-9-BBN dimer (101 mg, 0.412 mmol) was added to a solution of **165^{DME}** (100 mg, 0.103 mmol) in toluene (3 mL) with stirring at room temperature. After 1 hour, a red precipitate and a light red solution formed. The mixture was filtered and the solids were dried under vacuum after which they were dissolved in DME (1 mL) and hexane was layered on to the solution. After 48 hours, large red crystals formed and these were collected by filtration and dried under vacuum to give the desired product **172** as a red solid (90.6 mg, 82 %). This compound exists in equilibrium with a related Re(BBN)$_3$ species when dissolved in donor solvents such as THF through dissociation of one equivalent of H-9-BBN. Elemental analysis. Calculated for $C_{48}H_{98}B_4KO_8Re$ (Mr = 1072.68 g mol^{-1}): C, 53.79; H, 9.22 %.

Found: C, 53.85; H, 9.24 %. ^{1}H NMR (500 MHz, THF-d_8): δ_H 3.63 (s, 24H), 3.43 (s, 4H), 3.27 (s, 6H), 1.99 – 1.77 (m, 28H), 1.66 (m, 8H), 1.56 (m, 10H), 1.46 (m, 8H), 1.43 – 1.36 (m, 6H), -9.02 (s, 4.86H), -9.80 (s, 3.14H). ^{11}B NMR (160 MHz, THF-d_8): δ_B 57.4 (unknown), 52.7 (**173**), 29.4 (**172**), 13.80 (9-BBN Monomer). IR (ATR): No clear Re-H stretches. Due to the volatility of the DME ligand bound to potassium the integration for the DME signals in the ^{1}H NMR spectrum is low and the elemental analysis is low in C.

Synthesis of [K(DME)(18-c-6)][ReH(κ^2-H$_2$BCy$_2$)$_3$] (175)

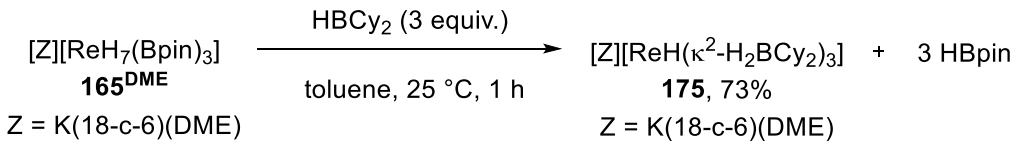

$HBCy_2$ (55.0 mg, 0.309 mmol) was added to a solution of **165^{DME}** (100 mg, 0.103 mmol) in toluene (3 mL) with stirring at room temperature. After 1 hour, a red solution formed. The solvent was removed under vacuum to give the crude product as a red solid. The crude product was dissolved in DME (2 mL), filtered and hexane (1 mL) was layered onto the filtrate. The mixture was stored at −20 °C. After 1 week, large red crystals formed and these were collected by filtration and dried under vacuum to give the desired product **175** as a red solid (84.2 mg, 73 %). Elemental analysis. Calculated for $C_{52}H_{107}B_3KO_8Re$ (Mr = 1118.74g mol^{-1}): C, 55.86; H, 9.65 %. Found: C, 55.24; H, 9.41 %. ^{1}H NMR (500 MHz, THF-d_8) δ 3.64 (s, 24H), 3.43 (s, 4H), 3.27 (s, 6H), 1.67 – 1.63 (m, 12H), 1.58 (m, 18H), 1.30 – 1.13 (m, 30H), 0.93 – 0.80 (m, 6H), -11.12 (s, 7H). ^{11}B NMR (128 MHz, THF-d_8) δ 51.1. ^{13}C NMR (126 MHz, THF-d_8) δ 72.9, 71.4, 59.1, 35.0, 30.2, 29.0, 26.0.

General procedure for perrhenate deoxygenation with 9-BBN and HBCy$_2$

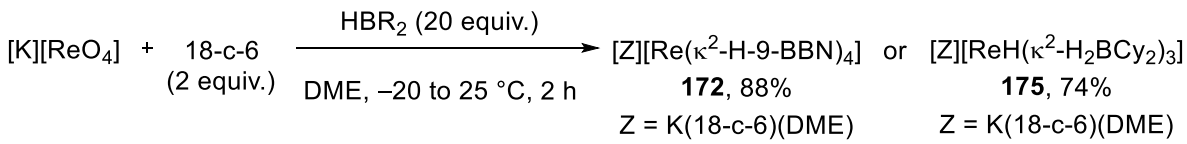

To a mixture of [K][ReO$_4$] (100 mg, 0.35 mmol) and 18-crown-6 (186 mg, 0.70 mmol) in DME (2 mL) the appropriate borane (4.2 mmol) was added at room temperature with stirring. After 2 h, the reaction mixture was analysed by ^{1}H and ^{11}B NMR spectroscopy to determine whether boron hydride complexes had been formed. Successful reactions were concentrated under vacuum, redissolved in DME (2 mL) and filtered. Hexane (2 mL) was layered onto the filtrate and the mixture was stored at −20 °C. After 1 week, red crystals formed which were

isolated by filtration and dried under vacuum to give **172** (330 mg, 88%) and **175** (290 mg, 74%) respectively.

Synthesis of *cis*-(DPEphos)$_2$RuH$_2$ (234)

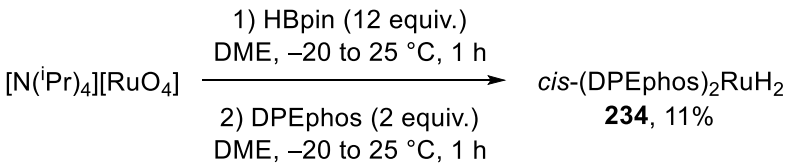

HBpin (825.8 µL, 5.68 mmol) was added to a slurry of [N(*i*Pr)$_4$][RuO$_4$] (100 mg, 0.285 mmol) in DME (2 mL) with stirring at −20 °C. The reaction was allowed to warm to room temperature over 1 hour. The reaction mixture was cooled to −20 °C and DPEphos (306 mg, 0.569 mmol) was added with stirring. The reaction was allowed to warm to room temperature and was stirred for 16 h. The mixture was filtered and the solids were extracted with DME (2 x 1 mL). Hexane was layered on the DME solution and the mixture was stored at −20 °C. After 2 weeks, yellow crystals formed and these were collected by filtration and dried under vacuum to give the desired product **234** as a light yellow solid (37.0 mg, 11 %). ^{1}H NMR (500 MHz, Benzene-d_6) δ 7.77 (s, 2H), 7.67 (s, 2H), 7.37 – 7.25 (m, 2H), 7.01 (m, 6H), 6.91 – 6.76 (m, 10H), 6.74 (dt, *J* = 7.7, 1.9 Hz, 1H), 6.66 (t, *J* = 7.5 Hz, 2H), 6.57 (td, *J* = 7.5, 1.4 Hz, 1H), 6.49 (ddd, *J* = 8.4, 7.3, 1.7 Hz, 1H), 6.38 (td, *J* = 7.5, 1.2 Hz, 1H), 6.23 – 6.19 (m, 1H), -9.81 (m, 2H). ^{31}P NMR (202 MHz, Benzene-d_6) δ 41.4, 35.1 (d, *J* = 63.1 Hz). Elemental analysis was consistently low in H and C, suggests the presence of NMR silent impurities.

Synthesis of [K(18-c-6)][ReH$_5$(Bpin)(PPh$_3$)] (255)

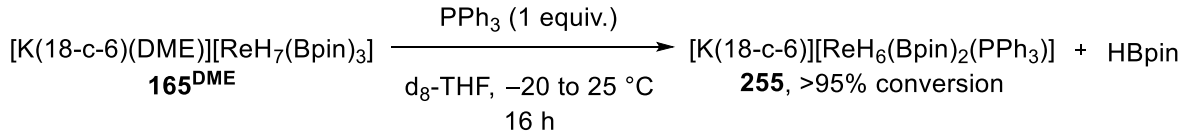

To a solution of [K(DME)(18-c-6)][ReH$_7$(Bpin)$_3$] **165^{DME}** (20 mg, 0.021 mmol) in d$_8$-THF (0.5 mL) was added PPh$_3$ (5.51 mg, 0.021 mmol) at −20 °C. The reaction was allowed to warm to room temperature slowly with stirring for 72 h to give a yellow solution. The product **255** was unstable in the solid-state and therefore was characterised by *in situ* NMR from the reaction mixture. ^{1}H NMR (500 MHz, THF-d_8) δ 7.76 (ddd, *J* = 9.8, 7.4, 2.4 Hz, 6H), 7.18 – 7.07 (m, 9H), 3.58 (s, 24H), 1.03 (s, 24H), -7.72 (d, *J* = 15.0 Hz, 6H). ^{11}B NMR (160 MHz, THF-d_8) δ 52.4. ^{13}C NMR (126 MHz, THF-d_8) δ 145.2 (d, *J* = 40.0 Hz), 136.0 (d,

J = 11.3 Hz), 128.4, 127.3 (d, J = 9.0 Hz), 81.4, 71.0, 25.4. ^{31}P NMR (202 MHz, THF-d_8) δ 36.02.

Synthesis of [K(18-c-6)][ReH$_6$(Bpin)(PCy$_3$)] (256)

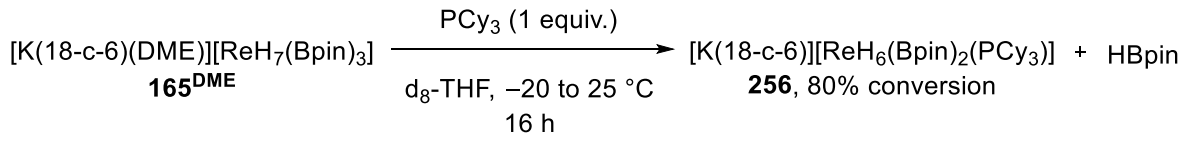

To a solution of [K(DME)(18-c-6)][ReH$_7$(Bpin)$_3$] **165^{DME}** (20 mg, 0.021 mmol) in d$_8$-THF (0.5 mL) was added PCy$_3$ (5.97 mg, 0.021 mmol) at −20 °C. The reaction was allowed to warm to room temperature slowly with stirring for 72 h to give a yellow solution. The product **256** was unstable in the solid-state and therefore was characterised by *in situ* NMR from the reaction mixture. ^{1}H NMR (500 MHz, THF-d_8) δ 3.65 (s, 24H), 2.11 (d, J = 13.1 Hz, 3H), 1.83 – 1.39 (m, 12H), 1.29 – 1.21 (m, 8H), 1.12 (s, 12H), -8.60 (d, J = 15.9 Hz, 6H). ^{11}B NMR (160 MHz, THF-d_8) δ 53.6. ^{13}C NMR (126 MHz, THF-d_8) δ 80.0, 39.7 (d, J = 20.4 Hz), 31.7 (d, J = 18.6 Hz), 31.2 (d, J = 12.9 Hz), 30.0, 28.2 (d, J = 9.6 Hz), 27.6 (d, J = 9.1 Hz), 25.68. ^{31}P NMR (202 MHz, THF-d_8) δ 47.9.

Synthesis of [K(18-c-6)][ReH$_5$(Bpin)(dcpp)] (257)

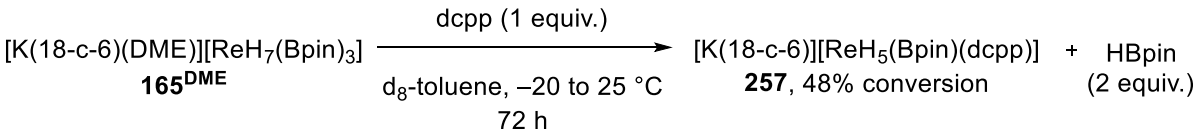

To a solution of [K(DME)(18-c-6)][ReH$_7$(Bpin)$_3$] **165^{DME}** (20 mg, 0.021 mmol) in d$_8$-toluene (0.5 mL) was added dcpp (9.17 mg, 0.021 mmol) at −20 °C. The reaction was allowed to warm to room temperature slowly with stirring for 72 h to give a yellow solution. The product **257** was unstable in the solid-state and therefore was characterised by *in situ* NMR from the reaction mixture. ^{1}H NMR (500 MHz, Toluene-d_8) δ 3.47 (s, 24H), 2.26 (d, J = 13.0 Hz, 6H), 1.98 – 1.69 (m, 24H), 1.57 – 1.19 (m, 16H), 1.33 (s, 12H) -8.16 (d, J = 16.8 Hz, 5H). ^{11}B NMR (160 MHz, Toluene-d_8) δ 53.0. ^{31}P NMR (202 MHz, Toluene-d_8) δ 33.8. Overlapping signals in ^{1}H and ^{13}C NMR spectra of **257** and unreacted dcpp mean that definitive assignment of resonances is not possible.

Synthesis of [K(18-c-6)][ReH$_5$(Bpin)(dppp)] (258)

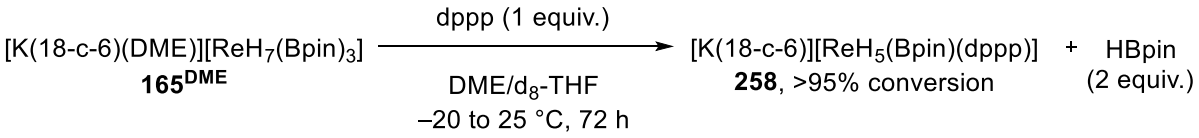

To a solution of [K(DME)(18-c-6)][ReH$_7$(Bpin)$_3$] **165^{DME}** (200 mg, 0.21 mmol) in DME (3 mL) was added a solution of 1,3-bis(diphenylphosphino)propane (dppp) (86.6 mg, 0.21 mmol) in DME (2 mL) at −20 °C. The reaction was allowed to warm to room temperature slowly with stirring for 72 h to give a red solution. The reaction mixture was filtered. Hexane (5 mL) was layered on to the filtrate and this solution was stored at −20 °C for 5 days. The resulting yellow crystals were unstable upon drying under vacuum or at ambient pressure/temperature, therefore **258** was characterised by *in situ* NMR from the reaction mixture in d$_8$-THF. However, these crystals were suitable for analysis by single-crystal X-ray diffraction. ^{1}H NMR (500 MHz, THF-d_8) δ 7.95 – 7.85 (m, 8H, Ar-*H*), 7.10 – 7.03 (m, 8H, Ar-*H*), 7.03 – 6.96 (m, 4H, Ar-*H*), 3.49 (s, 24H, (18-c-6)-*H*), 2.72 – 2.58 (m, 4H, P-C*H*$_2$-CH$_2$), 1.68 – 1.49 (m, 2H, CH$_2$-C*H*$_2$-CH$_2$), 1.23 (s, 12H, (Bpin)-*H*), −8.16 (t, J = 11.8 Hz, 5H, Re-*H*). ^{13}C{^{1}H} NMR (126 MHz, THF-d_8) δ 147.8 (d, *J* = 32.8 Hz, Ar), 134.3 (t, *J* = 6.3 Hz, Ar), 127.5 (Ar), 127.1 (t, *J* = 4.0 Hz, Ar), 84.0 (O-*C*-(CH$_3$)$_2$), 70.9 (18-c-6), 38.0 (d, *J* = 29.3 Hz, P-*C*H$_2$-CH$_2$), 25.6 (O-C-(*C*H$_3$)$_2$), 22.0 (d, *J* = 3.8 Hz, CH$_2$-*C*H$_2$-CH$_2$). ^{11}B NMR (160 MHz, THF-d_8) δ 53.8. ^{31}P NMR (202 MHz, THF-d_8) δ 11.85.

Synthesis of ReH$_6$(Bpin)(dppp) (260)

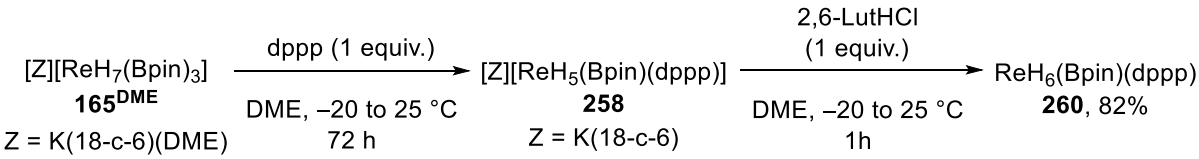

To a solution of [K(DME)(18-c-6)][ReH$_7$(Bpin)$_3$] **165^{DME}** (200 mg, 0.21 mmol) in DME (2 mL) was added a solution of dppp (86.6 mg, 0.21 mmol) in DME (2 mL) at −20 °C. The reaction was allowed to warm to room temperature slowly with stirring for 72 h to give a yellow solution. A solution of 2,6-lutidinium chloride (30.2 mg, 0.21 mmol) in DME (2 mL) was added to the reaction mixture at −20 °C with stirring for 1 h to give a brown solution. The solvent was removed under vacuum and toluene (1 mL) was added to the residue. The mixture was filtered and hexane (5 mL) was layered on to the filtrate. This solution was stored at −20 °C for 5 days whereupon colourless crystals suitable for X-ray diffraction were collected by filtration and dried under vacuum to give **260** (126 mg, 82%). Elemental analysis. Calculated for $C_{33}H_{44}BO_2P_2Re$ (Mr = 732.25 g mol^{-1}): C, 54.17; H, 6.06 %. Found:

C, 53.92; H, 6.02 %. ^{1}H NMR (500 MHz, C_6D_6) δ 7.90 – 7.63 (m, 8H, Ar-*H*), 7.04 – 6.85 (m, 12H, Ar-*H*), 2.11 (qd, J = 5.8, 1.7 Hz, 4H, P-C*H*$_2$-CH$_2$), 1.73 – 1.50 (m, 2H, CH$_2$-C*H*$_2$-CH$_2$), −5.41 (t, J = 15.7 Hz, 6H, Re-*H*). ^{13}C{^{1}H} NMR (126 MHz, C_6D_6) δ 141.4 – 140.5 (m, Ar), 133.0 (t, J = 6.3 Hz, Ar), 129.5 (Ar), 128.4 (Ar), 83.0 (O-*C*-(CH$_3$)$_2$), 34.5 – 33.3 (m, P-*C*H$_2$-CH$_2$), 25.2 (O-C-(*C*H$_3$)$_2$), 21.6 (d, J = 3.8 Hz, CH$_2$-*C*H$_2$-CH$_2$). ^{31}P NMR (202 MHz, C_6D_6) δ 6.24. ^{11}B NMR (160 MHz, C_6D_6) δ 47.2.

Synthesis of $Re_2H_8(dppp)_2$ (277)

Procedure A:

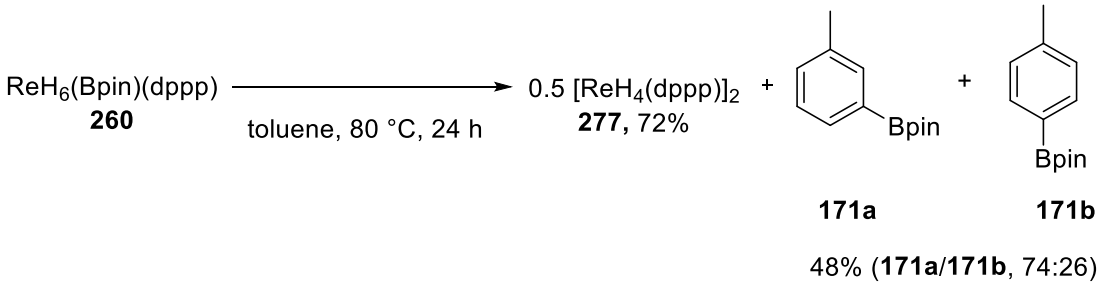

A solution of ReH$_6$(Bpin)(dppp) **260** (100 mg, 0.137 mmol) in toluene (2 mL) was heated at 80 °C for 24 h with stirring. The stirring was stopped and after 48 h large red crystals suitable for X-ray diffraction were formed. The crystals were collected by filtration, washed with toluene (1 mL) and dried under vacuum to give **277** (72%, 59.5 mg). Calculated for $C_{33}H_{44}BO_2P_2Re$ (Mr = 1206.28 g mol^{-1}): C, 53.81; H, 5.02; %. Found: C, 53.78; H, 5.01 %. ^{1}H NMR (500 MHz, Pyridine-d$_5$) δ 7.95 (tt, J = 7.5, 2.3 Hz, 16H, Ar-*H*), 7.24 – 7.20 (m, 24H, Ar-*H*), 2.62 – 2.51 (m, 8H, P-C*H*$_2$-CH$_2$), 2.08 – 1.87 (m, 4H, CH$_2$-C*H*$_2$-CH$_2$), −5.90 (quin., J = 9.5 Hz, 8H, Re-*H*). ^{31}P NMR (202 MHz, Pyridine-d$_5$) δ 19.68. ^{13}C{^{1}H} NMR (126 MHz, Pyridine-d$_5$) δ 145.0 (d, J = 45.7 Hz, Ar), 133.6 – 132.8 (m, Ar), 129.3 (Ar), 128.7 – 128.2 (m, Ar), 35.5 (d, J = 34.0 Hz, P-*C*H$_2$-CH$_2$), 24.1 (s (br), CH$_2$-*C*H$_2$-CH$_2$).

A mixture of *meta* and *para* isomers of (4,4,5,5-tetramethyl-1,3,2-dioxaborolan-2-yl)toluene were formed as by-products in this reaction. The ratio of *meta*/*para* isomers was determined by ^{1}H NMR to be 74:26 and the yield was determined by integration against mesitylene (10 µL) as an internal standard to be 48%. Spectral data were in good agreement with those previously reported.[15]

Procedure B:

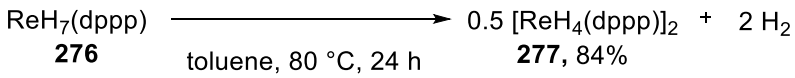

A solution of ReH_7(dppp) **276** (50 mg, 0.082 mmol) in toluene (1 mL) was heated at 80 °C for 24 h with stirring. The stirring was stopped and after 48 h large red crystals were formed. The crystals were collected by filtration, washed with toluene (1 mL) and dried under vacuum to give **277** (84%, 82.6 mg).

6.3 Mechanistic Investigation

Addition of DABCO to solution of 172

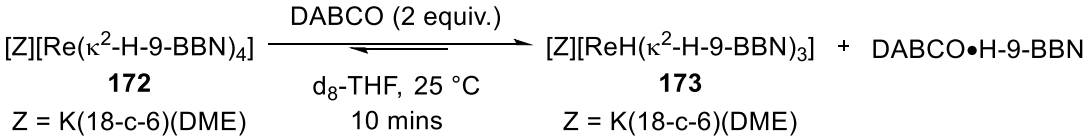

Solid DABCO (4.26 mg, 0.038 mmol) was added to a solution of **172** (20 mg, 0.019 mmol) in THF-d_8 in a Youngs' tap NMR tube. The mixture was analysed by NMR spectroscopy and compared with the NMR spectra prior to DABCO addition. Within 10 minutes, **172** was consumed and the single hydride species, **173**, was observed as well as 1 equivalent of DABCO-BBN adduct. ^{1}H NMR (500 MHz, THF-d_8) δ 3.64 (s, 24H), 3.43 (s, 4H), 3.27 (s, 6H), δ 1.98 – 1.34 (m, 45H, overlapping with DABCO·BBN adduct), -9.80 (s, 7H). ^{11}B NMR (160 MHz, THF-d_8): δ_B 52.7, 2.4 (d, J = 98.2 Hz, DABCO·BBN).

Addition of 9-BBN dimer to solution of 172

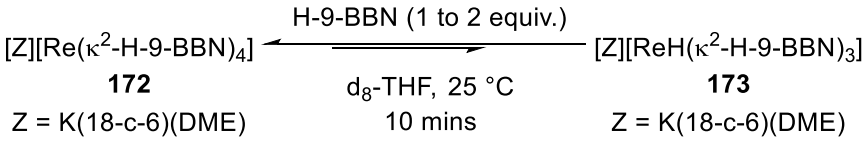

Solid 9-BBN dimer (4.6 mg, 0.019 mmol) dimer was added incrementally in two equal portions to a solution of **172** (20 mg, 0.019 mmol) in THF-d_8 in a Youngs' tap NMR tube. The reaction was analysed by NMR spectroscopy between additions and compared with the NMR spectra prior to DABCO addition. After the first addition of 0.5 equivalents of 9-BBN dimer, **172** was almost fully consumed and a single hydride species, **172**, was observed as well as free 9-BBN dimer. After the second addition of 9-BBN dimer the ratio of **172**/**173** was 98:2 based on the integration of the hydride signals in the ^{1}H NMR spectrum. ^{1}H NMR (500 MHz, THF-d_8) δ 3.63 (s, 24H), 3.43 (s, 4H), 3.27 (s, 6H), 2.13 – 1.21 (m, 60H, overlap

with free 9-BBN), -9.02 (s, 8H). ^{11}B NMR (160 MHz, THF-d_8) δ_B 57.64 (**173**), 29.29 (**172**), 27.98 (BBN dimer), 13.84 (d, *J* = 105.0 Hz, BBN monomer).

C–H borylation of toluene using 165^{DME}

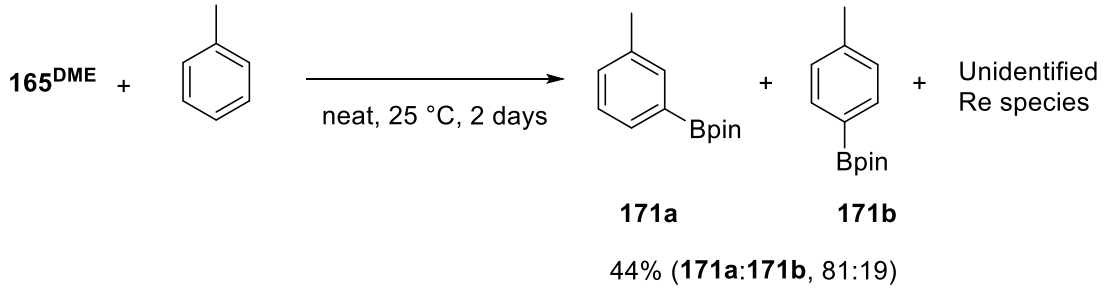

A solution of **165^{DME}** (100 mg, 0.103 mmol) in toluene (1 mL) was stirred at room temperature for 3 days, during which a dark brown precipitate formed. The solvents was evaporated under vacuum and to the residue was added C_6D_6 with trimethoxybenzene (15.7 mg, 0.093 mmol) as an internal standard. NMR analysis of the crude reaction mixture showed that the mono-borylated product was formed as mixture of *meta* and *para* regioisomers **171** (41 % NMR yield, 80:20 (**171a** /**171b**)).

Pyridine hydroboration catalysed by 165^{DME}

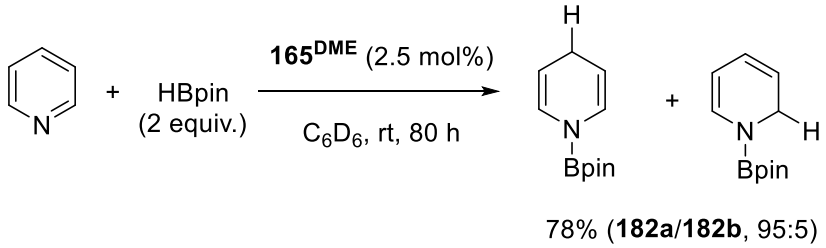

165^{DME} (4.84 mg, 0.005 mmol), pyridine (16.1 μL, 0.20 mmol) and mesitylene (10 μL, 0.053 mmol) as internal standard were combined in C_6D_6 (0.4 mL) in an oven-dried NMR tube sealed with a neoprene rubber stopper. The ratio between pyridine and mesitylene was measured by ^{1}H NMR spectroscopy. HBpin (58 μL, 0.40 mmol) was added and reaction was monitored by ^{1}H NMR spectroscopy for 80 hours at room temperature. NMR analysis of the crude reaction mixture showed that a mixture of the 1,4 and 1,2 products was formed (78% NMR yield, 95:5 (**182a**/**182b**).

'Bench-top' pyridine hydroboration (in air, using 'wet' solvents and reagents)

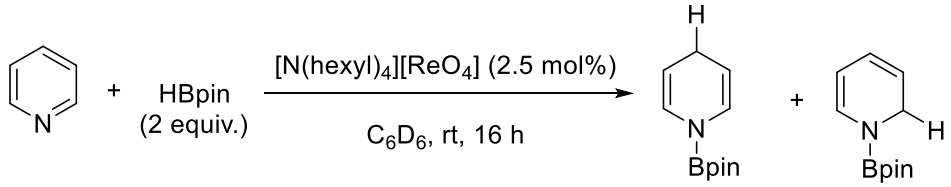

>95% (**182a**/**182b**, 95:5)

$[N(hexyl)_4][ReO_4]$ (3.0 mg, 0.005 mmol), pyridine (16.1 μL, 0.20 mmol) and mesitylene (10 μL, 0.053 mmol) as internal standard were mixed in C_6D_6 (0.4 mL) in an oven-dried NMR tube sealed with a neoprene rubber stopper. The ratio between the N-heterocycle and mesitylene was measured by ^1H NMR spectroscopy. HBpin (87 μL, 0.60 mmol) was added and reaction was monitored by ^1H NMR spectroscopy for 16 hours at room temperature. NMR analysis of the crude reaction mixture showed that a mixture of the 1,4 and 1,2 products was formed (>95% NMR yield, 98:2 (1,4/1,2).

Time-course of addition of dppp to 165^{DME} to form 258

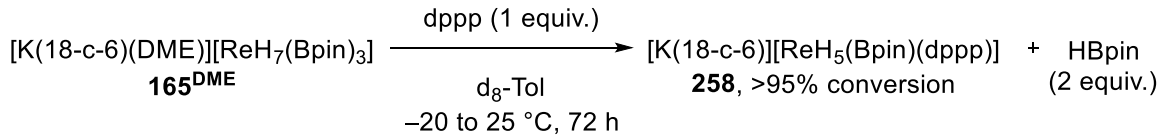

To a solution of $[K(DME)(18\text{-c-}6)][ReH_7(Bpin)_3]$ **165^{DME}** (20 mg, 0.021 mmol) in d_8-toluene (0.5 mL) was added a solution of dppp (8.66 mg, 0.021 mmol) at −20 °C. The reaction was allowed to warm to room temperature slowly over 0.5 h with stirring and was then transferred to a teflon-tapped NMR tube. The progress of the reaction was monitored by ^1H and ^{31}P NMR spectroscopy over the course of 72 h.

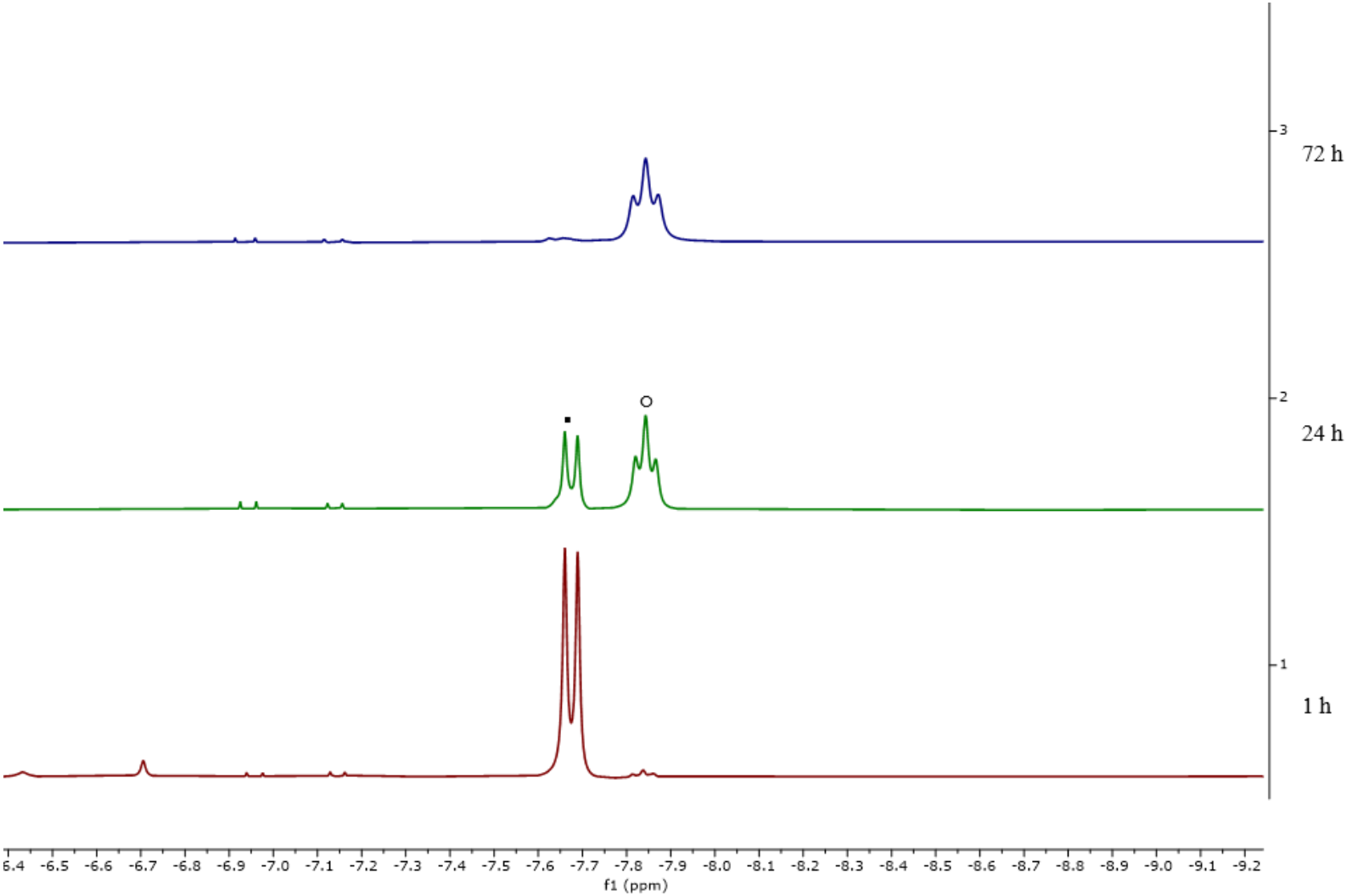

Figure 28. The mixture was analysed by ^{1}H NMR spectroscopy in the hydride region over the course of 16 hours. ▪ monodentate, ○ bidentate.

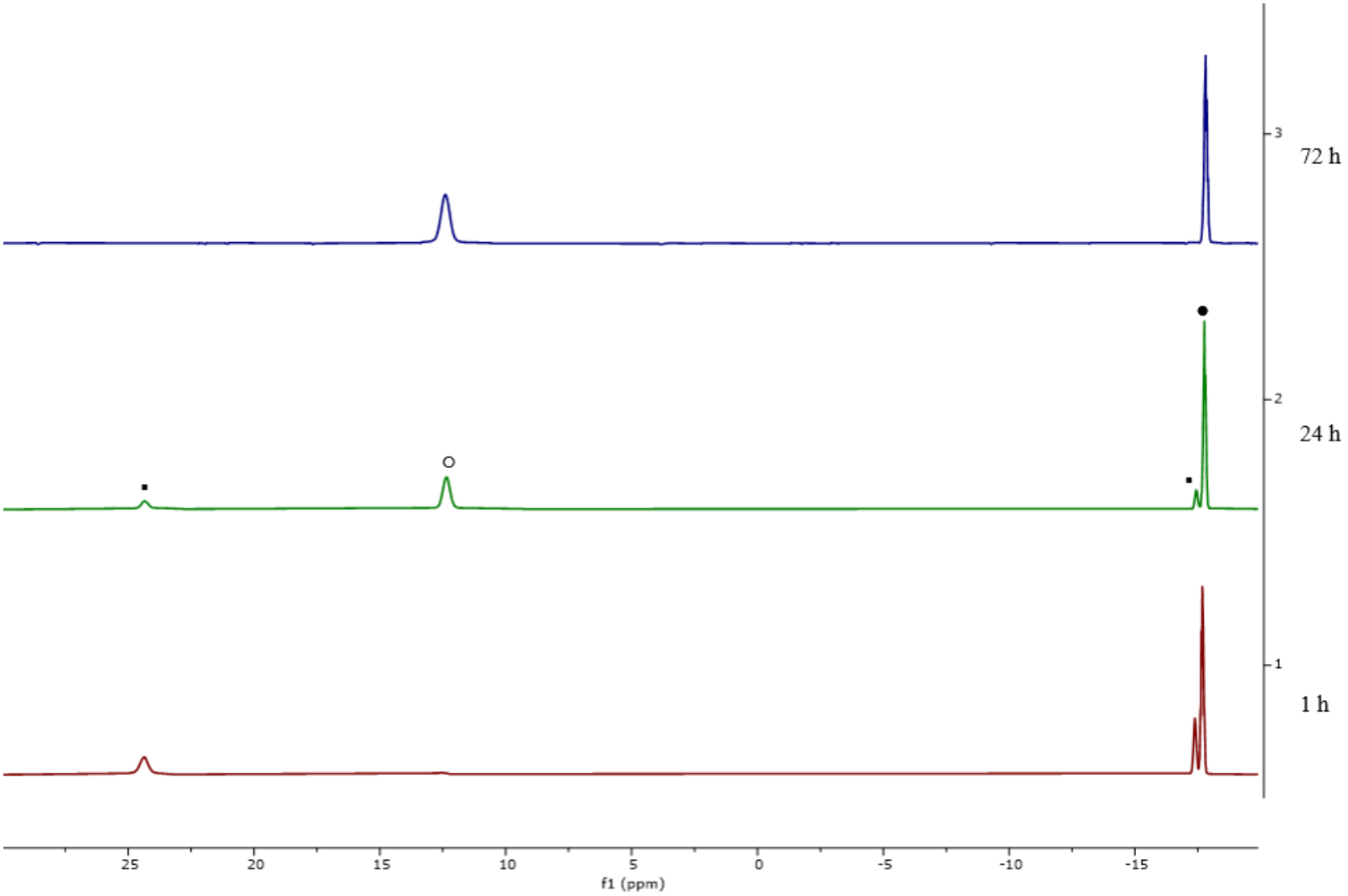

Figure 29. The mixture was analysed by ^{31}P NMR spectroscopy over the course of 16 hours. ▪ monodentate, ○ bidentate, ● dppp.

Time-course C–H borylation of 2-methylfuran (261)

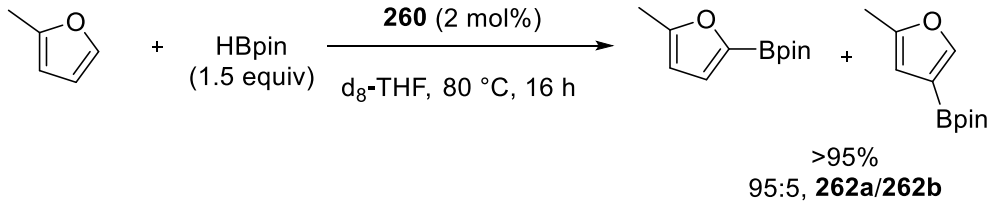

In a Teflon-tapped NMR tube, a solution of $ReH_6(Bpin)(dppp)$ **260** (2.93 mg, 0.004 mmol) and HBpin (44 µL, 0.3 mmol) in d_8-THF (0.5 mL) was added 2-methylfuran (0.20 mmol). The reaction was heated at 80 ºC for 16h and monitored by NMR spectroscopy over the course of the reaction.

Time-course C–H borylation of 3-hexylthiophene (266) to investigate H_2 inhibition

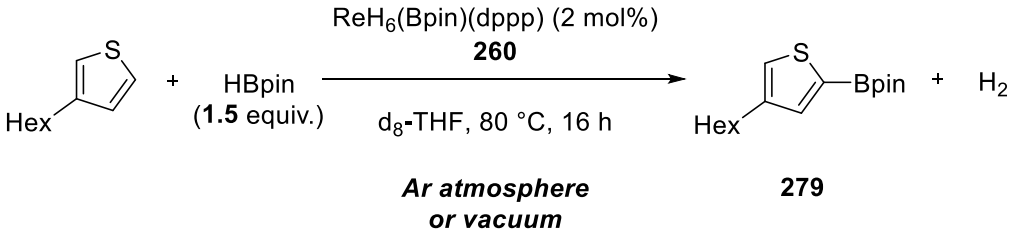

Standard Conditions:

In a Teflon-tapped NMR tube, a solution of $ReH_6(Bpin)(dppp)$ **260** (2.93 mg, 0.004 mmol), mesitylene (10 µL) and HBpin (44 µL, 0.3 mmol) in d_8-THF (0.5 mL) was added 3-hexylthiophene (0.20 mmol). The reaction was heated at 80 ºC for 16h and monitored by *in situ* ^{1}H NMR spectroscopy every 20 mins over the course of the reaction. Final yield 36%.

Vacuum Conditions:

In a Teflon-tapped NMR tube, a solution of $ReH_6(Bpin)(dppp)$ **260** (2.93 mg, 0.004 mmol), mesitylene (10 µL) and HBpin (44 µL, 0.3 mmol) in d_8-THF (0.5 mL) was added 3-hexylthiophene (0.20 mmol). The reaction was freeze-pump-thaw degassed three times and the headspace was evacuated. The reaction was heated at 80 ºC for 16h and monitored by *in situ* ^{1}H NMR spectroscopy every 20 mins over the course of the reaction. Final yield 44%.

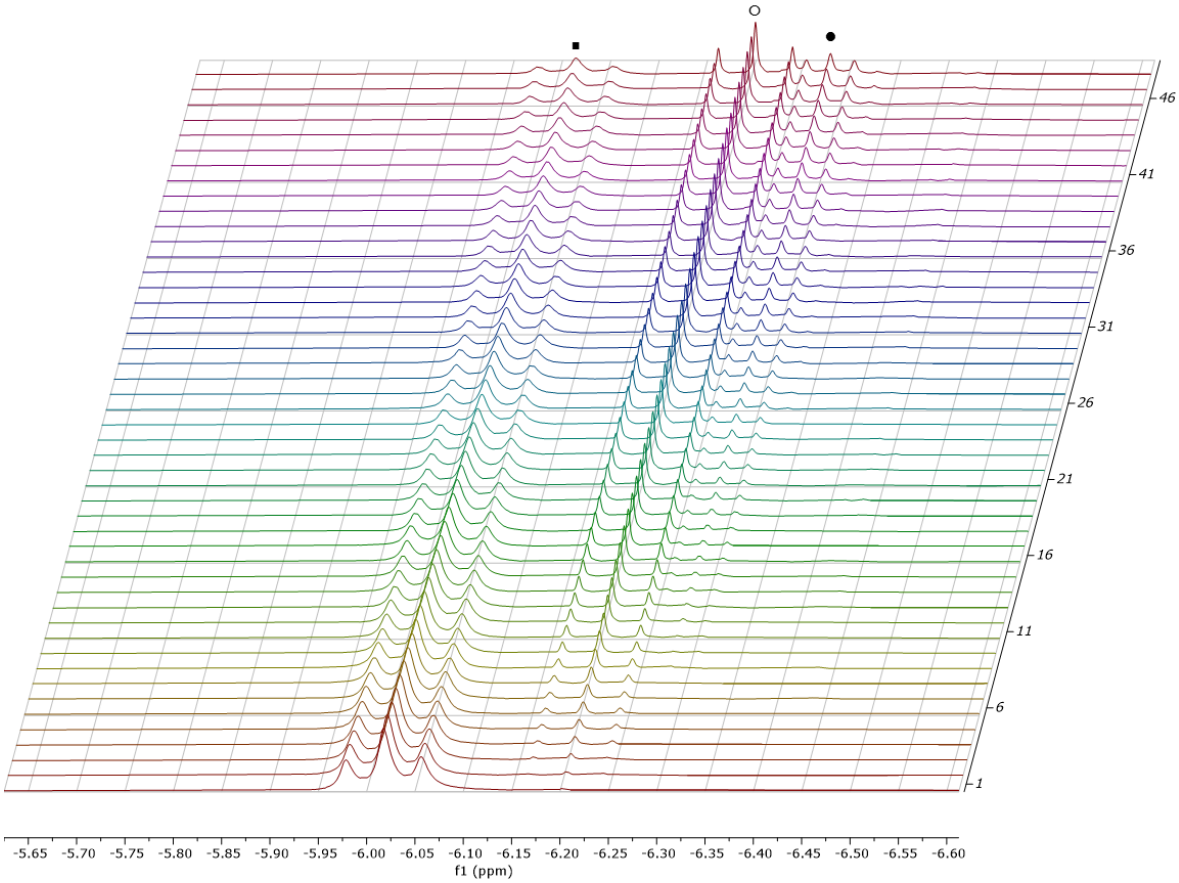

Figure 30. ^{1}H NMR reaction monitoring in the hydride region over the course of 16 hours in d_8-THF under standard conditions. ▪ $ReH_6(Bpin)(dppp)$ **260**, ○ $ReH_7(dppp)$ **276**, ● $Re_2H_8(dppp)_2$ **277**.

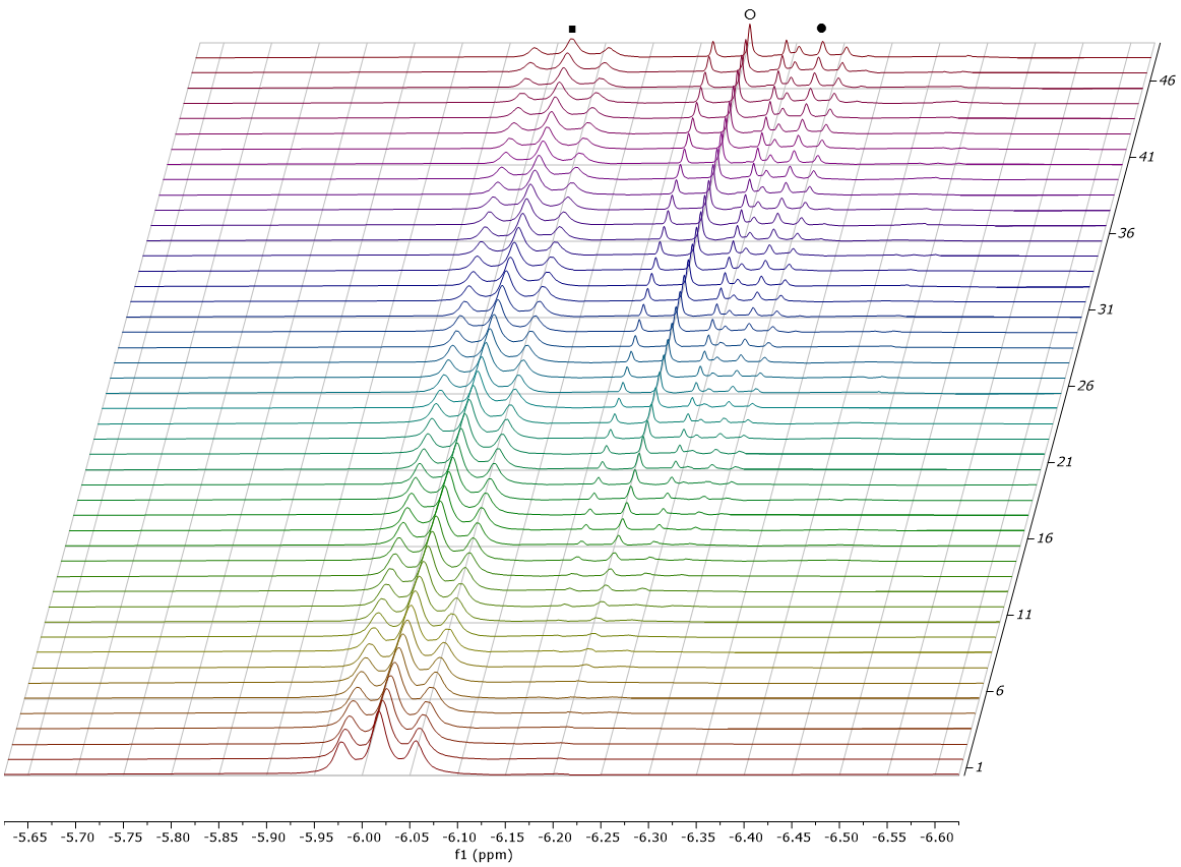

Figure 31. ^{1}H NMR reaction monitoring in the hydride region over the course of 16 hours in d_8-THF under vacuum conditions. ▪ $ReH_6(Bpin)(dppp)$ **260**, ○ $ReH_7(dppp)$ **276**, ● $Re_2H_8(dppp)_2$ **277**.

Reaction of $ReH_6(Bpin)(dppp)$ (260) with an excess of HBpin

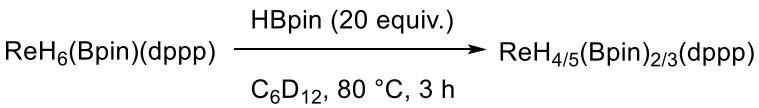

260 **278**

In a Teflon-tapped NMR tube, $ReH_6(Bpin)(dppp)$ **260** (20 mg, 0.027 mmol) and HBpin (79.2 µL, 0.54 mmol) in d_{12}-cyclohexane (0.5 mL) were heated at 80 ºC. The reaction was monitored by NMR spectroscopy over the course of the reaction. N.B. **260** is poorly soluble in d_{12}-cyclohexane at ambient temperature.

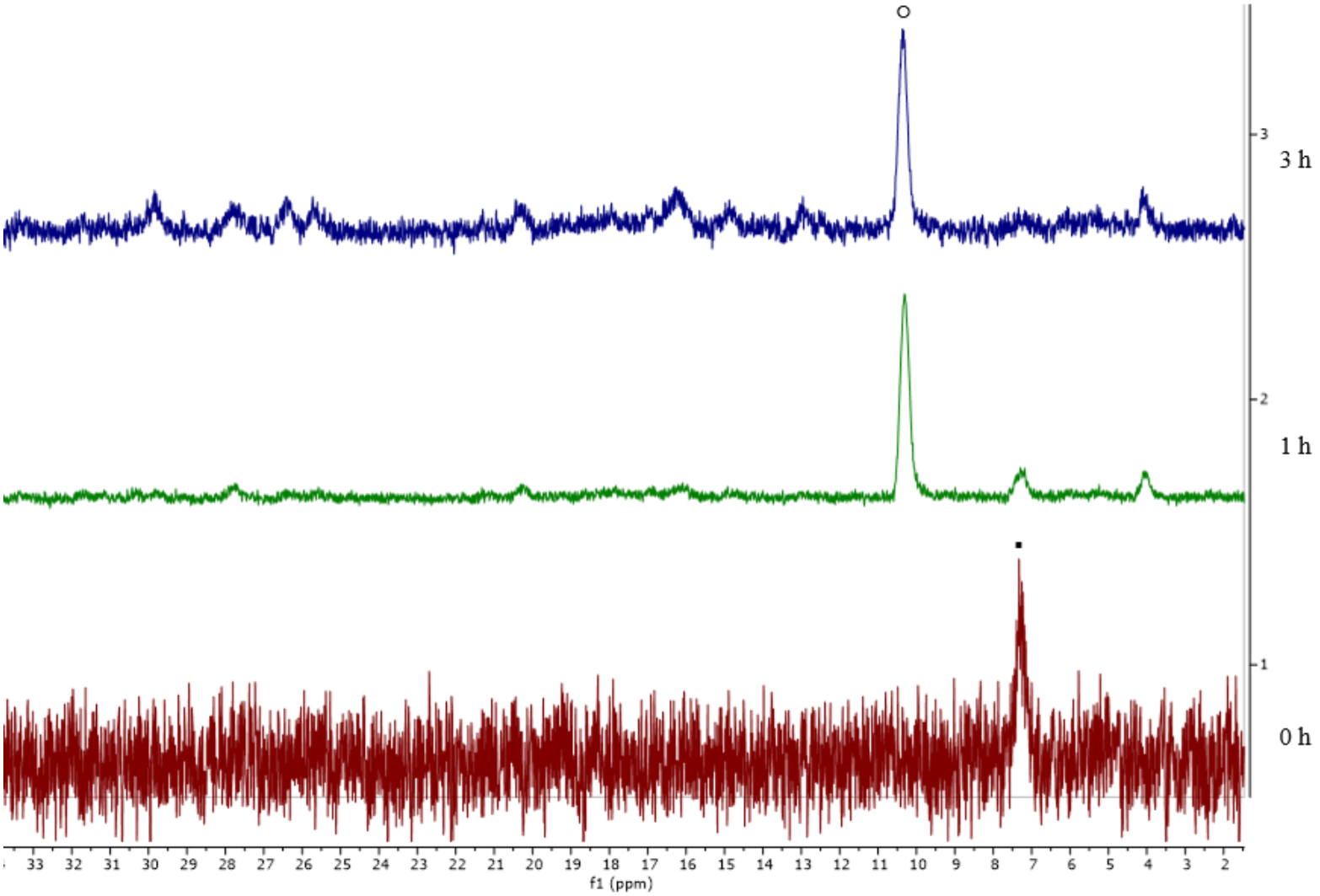

Figure 32. Reaction analysed by ^{31}P NMR spectroscopy over the course of 3 hours. ▪ $ReH_6(Bpin)(dppp)$ **260**, ○ unknown species **278**.

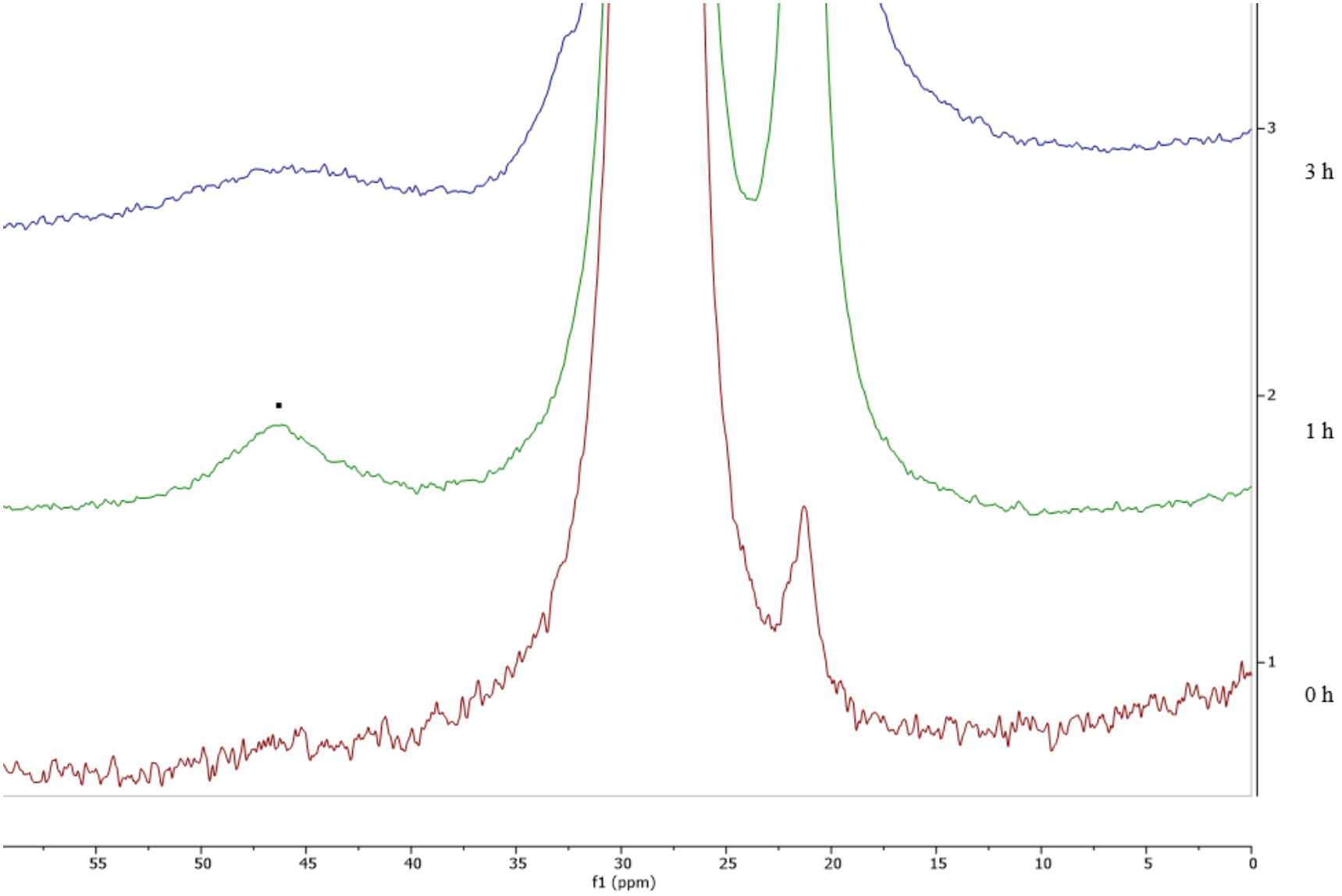

Figure 33. Reaction analysed by ^{11}B NMR spectroscopy over the course of 3 hours. ▪ $ReH_6(Bpin)(dppp)$ **260**.

Catalytic C–H borylation of 3-hexylthiophene with *in situ* formed 278

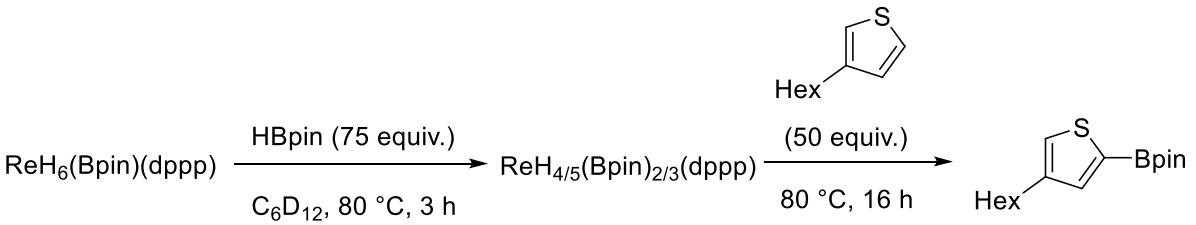

260 **278** 36%, **279**

In a Teflon-tapped NMR tube, a solution of $ReH_6(Bpin)(dppp)$ **260** (2.93 mg, 0.004 mmol) and HBpin (44 µL, 0.3 mmol) in C_6D_{12} was heated at 80 ºC for 2h. A ^1H NMR spectrum was recorded at room 25 ºC. Mesitylene (10 µL) and 3-hexylthiophene (0.20 mmol) were added to the reaction mixture. The reaction was heated at 80 ºC for 16h and monitored by *in situ* ^1H NMR spectroscopy every 20 mins over the course of the reaction. Final yield 36%.

Reaction of $ReH_7(dppp)$ (7) with an excess of HBpin

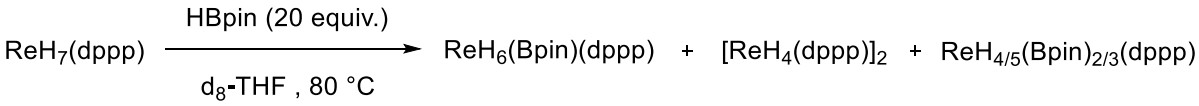

276 **260** **277** **278**

In a Teflon-tapped NMR tube, **276** (16.4 mg, 0.027 mmol) and HBpin (79.2 µL, 0.54 mmol) in d_8-THF (0.5 mL) were heated at 80 ºC. The reaction mixture was analysed by NMR spectroscopy after 16 h.

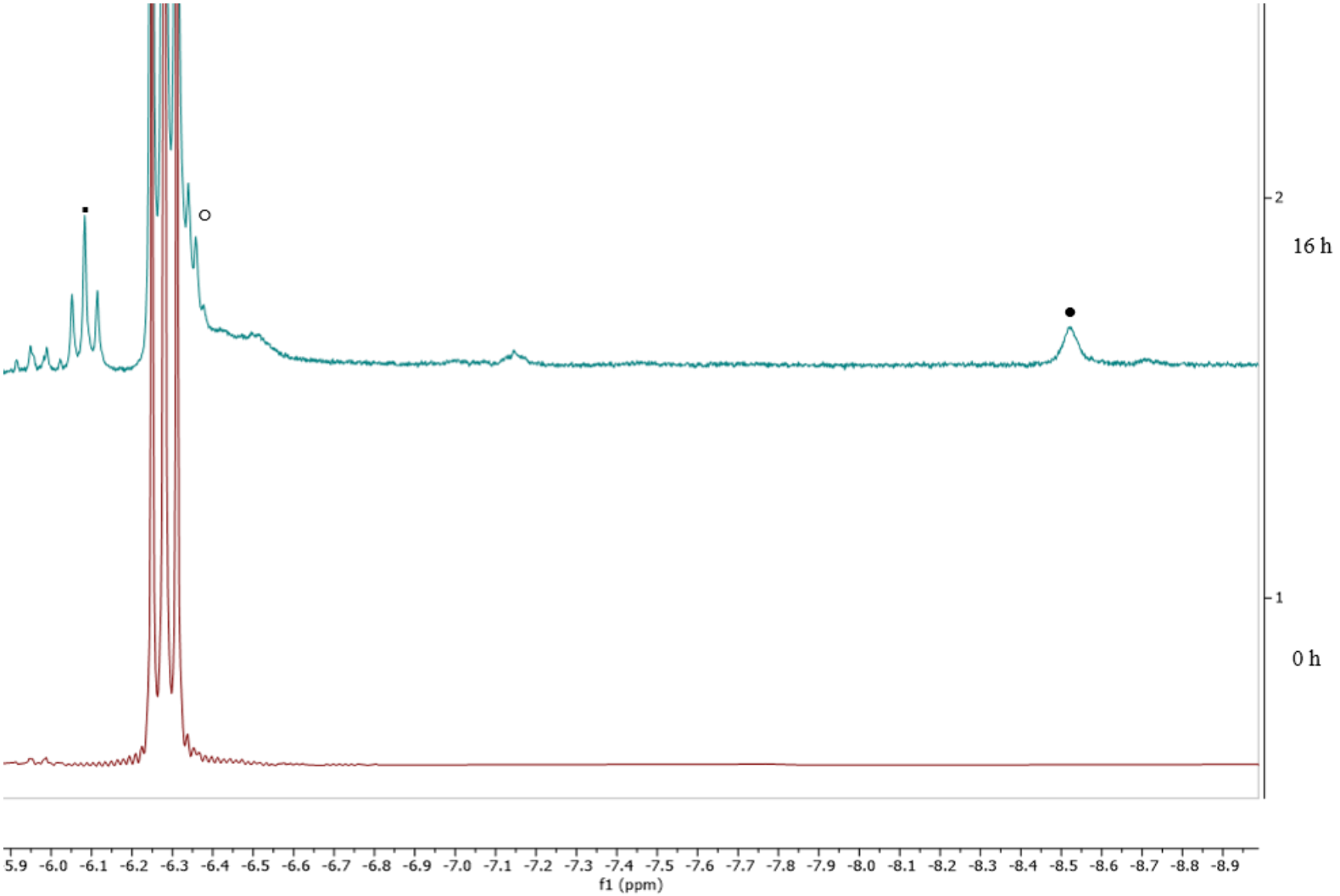

Figure 34. Reaction analysed by ^{1}H NMR spectroscopy over the course of 16 hours. ▪ $ReH_6(Bpin)(dppp)$ **260**, ○ $Re_2H_8(dppp)_2$ **277**, ● $ReH_{4/5}(Bpin)_{2/3}(dppp)$ **278**.

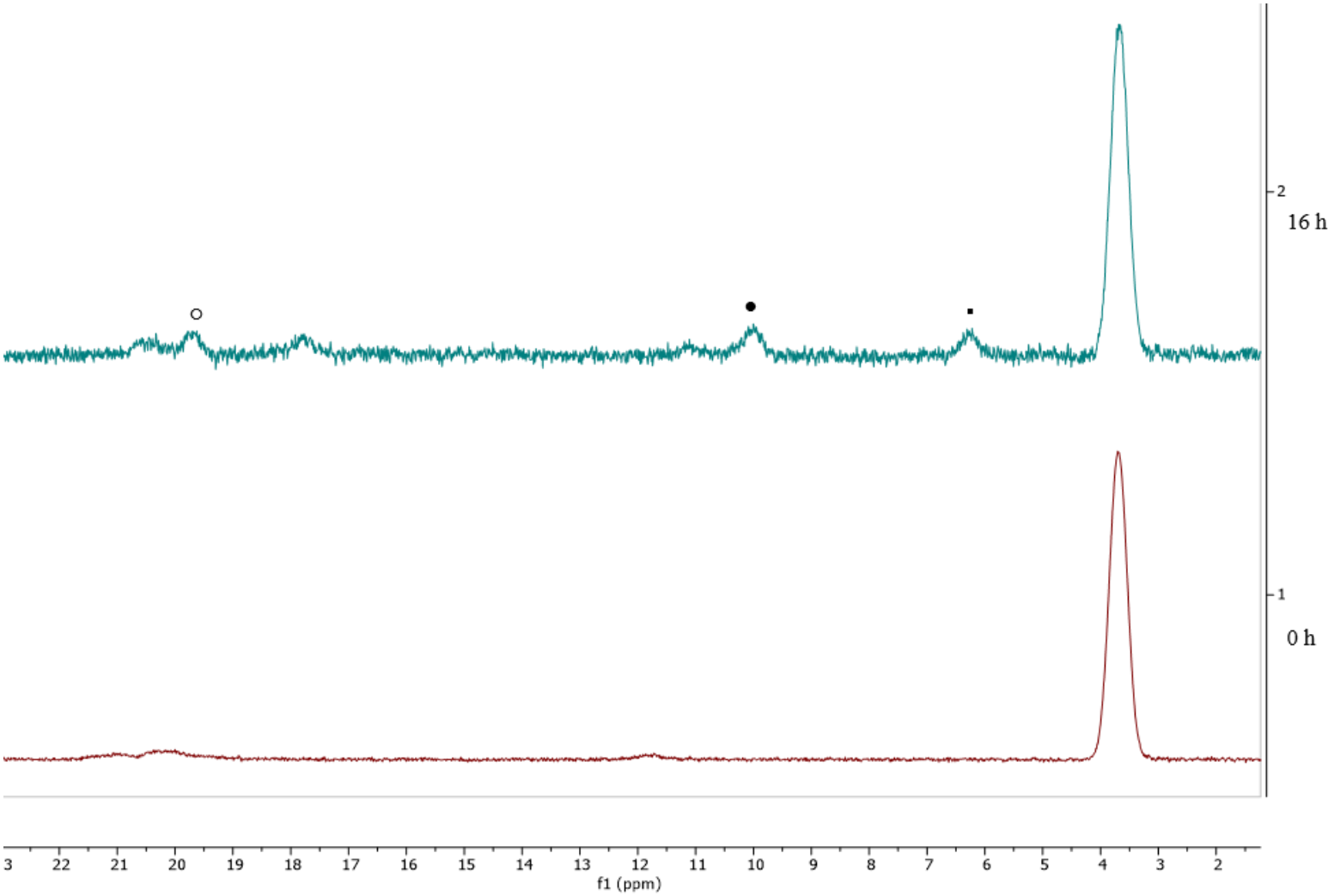

Figure 35. Reaction analysed by ^{31}P NMR spectroscopy over the course of 16 hours. ▪ $ReH_6(Bpin)(dppp)$ **260**, ○ $Re_2H_8(dppp)_2$ **277**, ● $ReH_{4/5}(Bpin)_{2/3}(dppp)$ **278**.

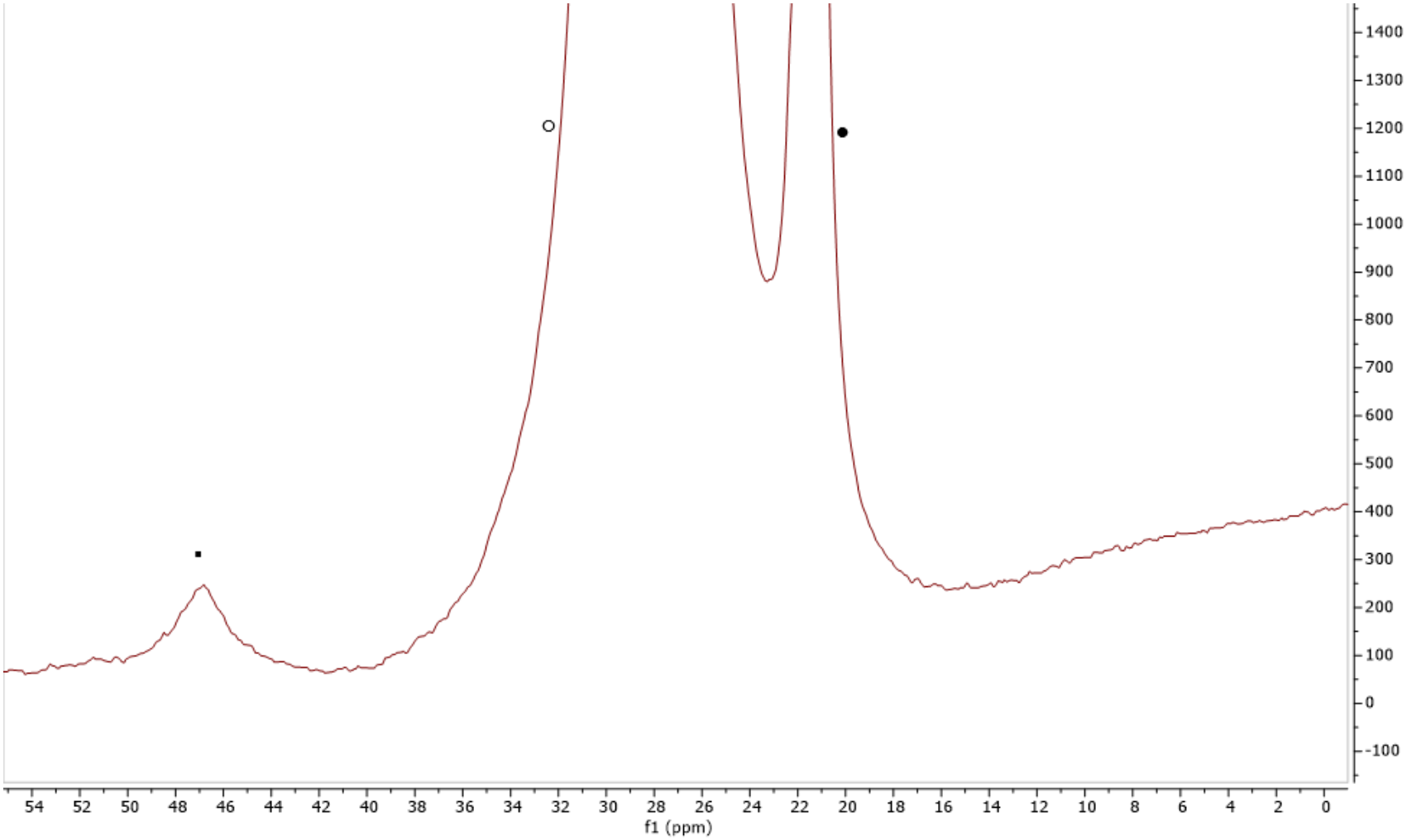

Figure 36. Reaction analysed by ^{11}B NMR spectroscopy after 16 hours. ▪ $ReH_6(Bpin)(dppp)$ **260**, ○ HBpin **21**, ● $O(Bpin)_2$ **278**.

6.4 Procedures for Catalytic Reactions Using Re Catalysts

Perrhenate catalysed hydroboration of *N*-heterocycles

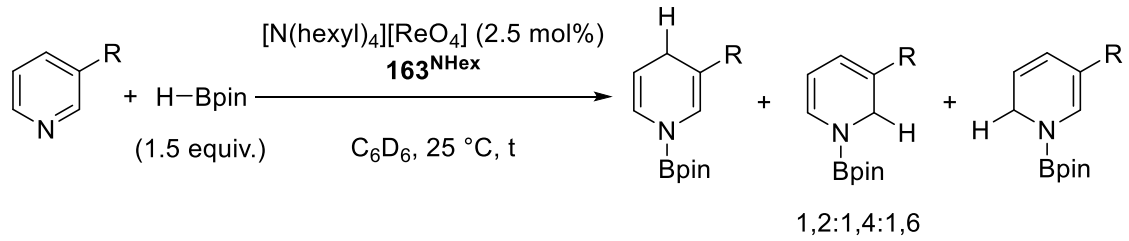

General procedure A:

$[N(hexyl)_4][ReO_4]$ **163^{NHex}** (3.0 mg, 0.005 mmol), the appropriate *N*-heterocycle (0.20 mmol) and mesitylene (10 µL, 0.053 mmol) as internal standard were combined in C_6D_6 (0.4 mL) in an NMR tube sealed with a neoprene rubber stopper. The ratio between the N-heterocycle and mesitylene was measured by ^{1}H NMR spectroscopy. HBpin (58 µL, 0.30 or 0.40 mmol) was added and reaction monitored by ^{1}H NMR spectroscopy to determine the nature and yields of the hydroborated products.

Catalytic C–H borylation of heteroarenes

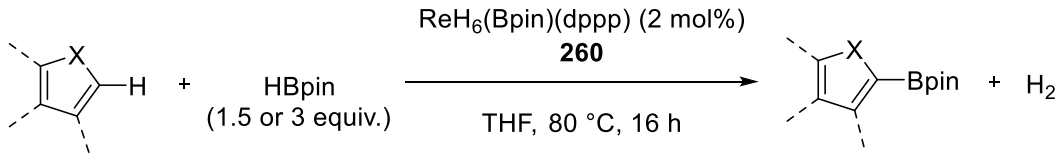

General procedure B:

A solution of **260** (7.33 mg, 0.0125 mmol) and HBpin (110 µL, 0.75 mmol or 220 µL, 1.5 mmol) in THF (2.5 mL) was added the appropriate arene (0.50 mmol) in a 5 mL glass vial sealed with a Teflon-coated lid. The reaction was stirred at 80 ºC for 16 h. The solvent was removed under vacuum and the residue was redissolved in Et_2O and passed through a short silica plug (4 cm height, 1 cm diameter). The filtrate was concentrated to dryness under vacuum and the yield was determined from the ^{1}H NMR spectrum of the crude product using mesitylene (10 µL) as the internal standard. Heteraromatic boronates, particularly furyl boronates, are unstable on silica and so were characterised from the crude mixture and the yield determined by this method.

General procedure C:

A solution of **260** (7.33 mg, 0.0125 mmol) and HBpin (110 µL, 0.75 mmol or 220 µL, 1.5 mmol) in THF (2.5 mL) was added the appropriate arene (0.50 mmol). The reaction was stirred at 80 ºC for 24 to 48 h. The solvent was removed under vacuum and the residue was redissolved in Et_2O and passed through a short silica plug (4 cm height, 1 cm diameter). The filtrate was concentrated to dryness under vacuum and the crude product was purified by column chromatography (petroleum ether/EtOAc) or by recrystallization.

6.5 Catalysis Product Characterisation

Hydroboration of pyridine (**181**):

General procedure A (16 h): NMR yield >95%, 95:5 1,4/1,2.

***N*-(4,4,5,5-tetramethyl-1,3,2-dioxaborolan-2-yl)-1,4-dihydropyridine**

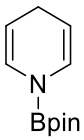

^{1}H NMR (500 MHz, C_6D_6): δ_H 6.52 (dt, *J* = 8.6, 1.7 Hz, 2H), 4.68 – 4.41 (m, 2H), 2.82 (tt, *J* = 3.3, 1.7 Hz, 2H), 0.98 (s, 12H).

^{11}B NMR (160 MHz, C_6D_6): δ_B 23.6.

***N*-(4,4,5,5-tetramethyl-1,3,2-dioxaborolan-2-yl)-1,2-dihydropyridine**

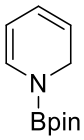

^{1}H NMR (500 MHz, C_6D_6): δ_H 6.79 (dt, *J* = 8.0, 1.9 Hz, 1H), 5.85 – 5.74 (m, 1H), 5.15 – 5.04 (m, 2H), 4.15 (dd, *J* = 4.2, 1.7 Hz, 2H), 1.02 (s, 12H).

^{11}B NMR (160 MHz, C_6D_6): δ_B 23.6.

Spectral data were in good agreement with literature values.[16]

Hydroboration of quinoline (**194**):

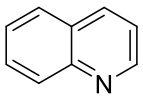

General procedure A (24 h): NMR yield 90%, 80:20 1,4/1,2.

***N*-(4,4,5,5-tetramethyl-1,3,2-dioxaborolan-2-yl)-1,4-dihydroquinoline**

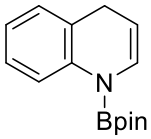

^{1}H NMR (500 MHz, C_6D_6): δ_H 8.11 (dd, *J* = 8.4, 1.2 Hz, 1H), 7.09 (ddd, *J* = 8.8, 7.0, 1.8 Hz, 1H), 6.92 – 6.81 (m, 3H), 4.82 (dt, *J* = 7.8, 3.7 Hz, 1H), 3.32 – 3.30 (m, 2H), 1.00 (s, 12H).
^{11}B NMR (160 MHz, C_6D_6): δ_B 24.6.

***N*-(4,4,5,5-tetramethyl-1,3,2-dioxaborolan-2-yl)-1,2-dihydroquinoline**

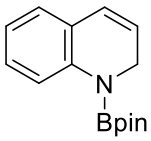

^{1}H NMR (500 MHz, C_6D_6): δ_H 7.77 (d, *J* = 8.2 Hz, 1H), 7.08 (m, 2H), 6.86 (m, 2H), 6.79 (m, 1H), 6.25 (d, *J* = 9.5 Hz, 1H), 5.58 (dt, *J* = 9.6, 4.2 Hz, 1H), 4.14 (dd, *J* = 4.2, 1.8 Hz, 2H), 1.02 (s, 12H).
^{11}B NMR (160 MHz, C_6D_6): δ_B 24.6.

Spectral data were in good agreement with literature values.[17]

Hydroboration of isoquinoline (**196**):

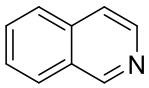

General procedure A (1 h): NMR yield 88%.

1-(4,4,5,5-tetramethyl-1,3,2-dioxaborolan-2-yl)-1,2-dihydroisoquinoline

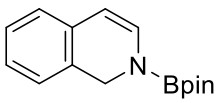

^{1}H NMR (500 MHz, C_6D_6): δ_H 7.02 – 6.97 (m, 1H), 6.89 (dd, *J* = 8.0, 6.8 Hz, 1H), 6.81 (d, *J* = 7.6 Hz, 2H), 6.73 (d, *J* = 7.3 Hz, 1H), 5.62 (d, *J* = 7.5 Hz, 1H), 4.61 (s, 2H), 1.03 (s, 12H).

^{11}B NMR (160 MHz, C_6D_6): δ_B 23.6.

Spectral data were in good agreement with literature values.[18]

Hydroboration of acridine (**197**):

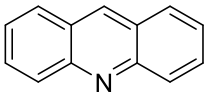

General procedure A (24 h): NMR yield 90%.

1-(4,4,5,5-tetramethyl-1,3,2-dioxaborolan-2-yl)-1,2-dihydroisoquinoline

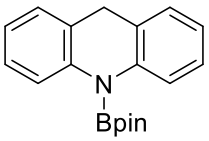

^{1}H NMR (500 MHz, C_6D_6): δ_H 7.81 (d, *J* = 8.4 Hz, 2H), 7.19 – 7.10 (m, 2H), 6.99 – 6.90 (m, 4H), 3.54 (s, 2H), 1.06 (s, 12H).

^{11}B NMR (160 MHz, C_6D_6): δ_B 24.9.

Spectral data were in good agreement with literature values.[18]

Hydroboration of 3-picoline (**198**):

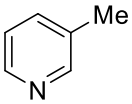

General procedure A (6 h): NMR yield >95%, 96:4 1,4/1,2.

3-methyl-*N*-(4,4,5,5-tetramethyl-1,3,2-dioxaborolan-2-yl)-1,4-dihydropyridine

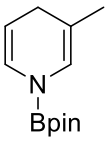

^{1}H NMR (500 MHz, C_6D_6): δ_H 6.59 (dq, *J* = 8.1, 1.6 Hz, 1H), 6.39 (t, *J* = 1.5 Hz, 1H), 4.65 (dt, J = 8.1, 3.3 Hz, 1H), 2.73 (d, *J* = 1.6 Hz, 2H), 1.41 (s, 3H), 1.01 (s, 12H).

^{11}B NMR (160 MHz, C_6D_6): δ_B 23.7.

^{13}C{^{1}H} NMR (126 MHz, C_6D_6): δ_C 127.4, 122.2, 110.4, 102.1, 83.3, 28.4, 24.7, 20.8.

Spectral data were in good agreement with literature values.[16]

3-methyl-*N*-(4,4,5,5-tetramethyl-1,3,2-dioxaborolan-2-yl)-1,2-dihydropyridine

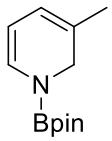

^{1}H NMR (500 MHz, C_6D_6): δ_H 6.62 (d, *J* = 7.8 Hz, 1H), 5.54 – 5.49 (m, 1H), 5.05 (dd, *J* = 7.4, 5.5 Hz, 1H), 4.10 (s, 2H), 1.43 (s, 3H), 1.04 (s, 12H).

^{11}B NMR (160 MHz, C_6D_6): δ_B 23.7.

Spectral data were in good agreement with literature values.[18]

Hydroboration of 3-phenylpyridine (**199**):

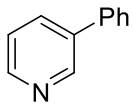

General procedure A (12 h): NMR yield >95%, 95:3:2 1,4/1,2/1,6.

3-Phenyl-1-(4,4,5,5-tetramethyl-1,3,2-dioxaborolan-2-yl)-1,4-dihydropyridine

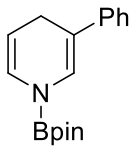

^{1}H NMR (500 MHz, C_6D_6): δ_H 7.28 – 7.23 (m, 2H), 7.19 (d, *J* = 1.2 Hz, 1H), 7.14 – 7.08 (m, 2H), 7.06 – 7.00 (m, 1H), 6.62 (dq, *J* = 8.2, 1.6 Hz, 1H), 4.79 (dt, *J* = 8.1, 3.4 Hz, 1H), 3.17 (dt, J = 3.2, 1.4 Hz, 2H), 1.02 (s, 12H).

^{11}B NMR (160 MHz, C_6D_6): δ_B 24.0.

3-Phenyl-1-(4,4,5,5-tetramethyl-1,3,2-dioxaborolan-2-yl)-1,2-dihydropyridine

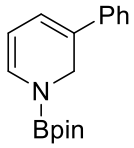

Identified by the characteristic signal, 6.28 (d, *J* = 5.9 Hz, 1H), in the ^{1}H NMR spectrum.

3-Phenyl-1-(4,4,5,5-tetramethyl-1,3,2-dioxaborolan-2-yl)-1,6-dihydropyridine

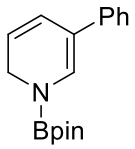

Identified by the characteristic signal, 6.32 (dd, J = 9.7, 1.5 Hz, 1H), in the ^{1}H NMR spectrum.

Spectral data were in good agreement with literature values.[18]

Hydroboration of 3,5-lutidine (**200**):

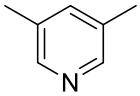

General procedure A (48 h): NMR yield 90%.

1-(4,4,5,5-Tetramethyl-1,3,2-dioxaborolan-2-yl)-3,5-dimethyl-1,4-dihydropyridine

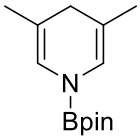

^{1}H NMR (500 MHz, C_6D_6): δ_H 6.45 (s, 2H), 2.59 – 2.52 (s, 2H), 1.48 (s, 6H), 1.04 (s, 12H).
^{11}B NMR (160 MHz, C_6D_6): δ_B 23.95.

Spectral data were in good agreement with literature values.[16]

Hydroboration of 1-methylbenzimidazole (**201**):

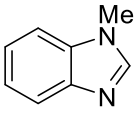

General procedure A (1 h): NMR yield >95%.

1-(4,4,5,5-tetramethyl-1,3,2-dioxaborolan-2-yl)-3-methyl-2,3-dihydro-1H-benzo[d]imidazole

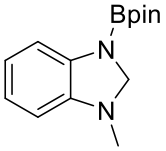

^{1}H NMR (500 MHz, C_6D_6): δ_H 7.48 – 7.41 (m, 1H), 6.85 – 6.73 (m, 2H), 6.30 (dd, *J* = 7.3, 1.3 Hz, 1H), 4.74 (s, 2H), 2.25 (s, 3H), 1.08 (s, 12H).
^{11}B NMR (160 MHz, C_6D_6): δ_B 23.0.

Spectral data were in good agreement with literature values.[18]

Hydroboration of methyl 3-pyridinecarboxylate (**202**):

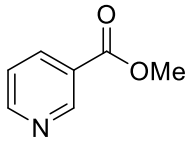

General procedure A (3 h): NMR yield 92%, 11:14:75 1,4/1,2/1,6.

1-(4,4,5,5-tetramethyl-1,3,2-dioxaborolan-2-yl)-1,4-dihydropyridin-3-yl acetate

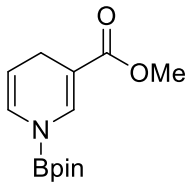

^{1}H NMR (500 MHz, C_6D_6): δ_H 7.78 (s, 1H), 6.31 (d, *J* = 8.0 Hz, 1H), 4.68 (m, 1H), 3.39 (s, 3H), 3.16 (m, 2H), 0.93 ppm (s, 12H).
^{11}B NMR (160 MHz, C_6D_6): δ_B 23.9.

Spectral data were in good agreement with literature values.[19]

1-(4,4,5,5-tetramethyl-1,3,2-dioxaborolan-2-yl)-1,2-dihydropyridin-3-yl acetate

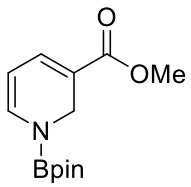

^{1}H NMR (500 MHz, C_6D_6): δ_H 7.09 (dtd, *J* = 6.0, 1.2, 0.8 Hz, 1H), 6.83 (dd, *J* = 7.2, 0.8 Hz, 1H), 4.99 (dd, *J* = 7.2, 6.0 Hz, 1H), 4.59 (d, *J* = 1.2 Hz, 2H), 3.36 (s, 3H), 0.94 (s, 12H).
^{11}B NMR (160 MHz, C_6D_6): δ_B 23.9.

Spectral data were in good agreement with literature values.[18]

1-(4,4,5,5-tetramethyl-1,3,2-dioxaborolan-2-yl)-1,6-dihydropyridin-3-yl acetate

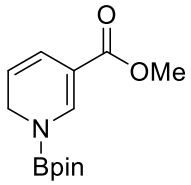

^{1}H NMR (500 MHz, C_6D_6): δ_H 7.97 (t, *J* = 1.2 Hz, 1H), 6.68 (dtd, *J* = 10.0, 2.0, 1.2 Hz, 1H), 4.93 (dtd, *J* = 10.0, 4.0, 1.2 Hz, 1H), 4.01 (dd, *J* = 4.0, 2.0 Hz, 2H), 3.43 (s, 3H), 0.92 (s, 12H).

^{11}B NMR (160 MHz, C_6D_6): δ_B 23.9.

Spectral data were in good agreement with literature values.[18]

Hydroboration of 3-methoxypyridine (**203**):

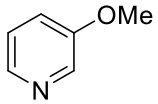

General procedure A (48 h): NMR yield 55%, 37:63 1,4/1,2.

3-Methoxy-1-(4,4,5,5-tetramethyl-1,3,2-dioxaborolan-2-yl)-1,4-dihydropyridine

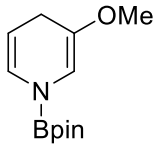

^{1}H NMR (500 MHz, C_6D_6): δ_H 6.57 (dq, I = 8.2, 1.6 Hz, 1H), 6.04 (d, I = 1.1 Hz, 1H), 4.62 (dt, I = 8.0, 3.4 Hz, 1H), 3.18 (s, 3H), 3.07 (dt, I = 3.2, 1.4 Hz, 2H), 1.02 (s, 12H).

^{11}B NMR (160 MHz, C_6D_6): δ_B 24.0.

Spectral data were in good agreement with literature values.[20]

3-Methoxy-1-(4,4,5,5-tetramethyl-1,3,2-dioxaborolan-2-yl)-1,2-dihydropyridine

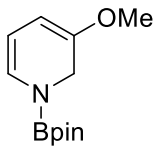

^{1}H NMR (500 MHz, C_6D_6): δ_H 6.48 (d, *J* = 7.2 Hz, 1H), 5.11 (dd, *J* = 7.2, 6.2 Hz, 1H), 4.75 (d, J = 6.1 Hz, 1H), 4.30 (d, *J* = 1.1 Hz, 2H), 3.15 (s, 3H), 1.01 (s, 12H).

^{11}B NMR (160 MHz, C_6D_6): δ_B 24.0.

Spectral data were in good agreement with literature values.[18]

Hydroboration of methyl-3-pyridylketone (**204**):

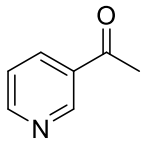

General procedure A (1 h, 1 equiv. HBpin): NMR yield 83%.

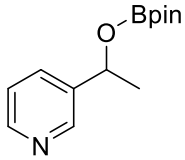

^{1}H NMR (400 MHz, C_6D_6): δ_H 8.71 (d, *J* = 2.3 Hz, 1H), 8.44 (dd, *J* = 4.7, 1.7 Hz, 1H), 7.42 (dt, *J* = 7.9, 2.1 Hz, 1H), 6.74 (ddd, *J* = 7.9, 4.8, 0.9 Hz, 1H), 5.25 (q, *J* = 6.5 Hz, 1H), 1.30 (d, *J* = 6.5 Hz, 3H), 1.00 (s, 6H), 0.97 (s, 6H).

^{13}C{^{1}H} NMR (101 MHz, C_6D_6): δ_C 149.2, 148.2, 132.6, 127.4, 123.3, 82.7, 70.8, 25.1, 24.6, 24.5.

^{11}B NMR (128 MHz, C_6D_6): δ_B 22.5.

C–H borylation of 2-methylfuran (**261**):

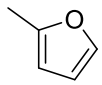

General procedure B (1.5 equiv. HBpin): NMR yield 90%, 95:5 5-B/4-B.

4,4,5,5-Tetramethyl-2-(5-methyl-2-furyl)-1,3,2-dioxaborolane

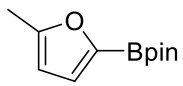

^{1}H NMR (500 MHz, $CDCl_3$) δ 6.99 (d, J = 3.2 Hz, 1H), 6.03 (dd, J = 3.3, 1.0 Hz, 1H), 2.35 (s, 3H), 1.34 (s, 12H).

^{11}B NMR (160 MHz, $CDCl_3$) δ 27.1

4,4,5,5-Tetramethyl-2-(5-methyl-3-furyl)-1,3,2-dioxaborolane

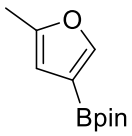

^{1}H NMR (500 MHz, $CDCl_3$) δ 7.22 (s, 1H), 6.15 (d, J = 1.1 Hz, 1H), 2.28 (d, J = 1.0 Hz, 3H), 1.30 (s, 12H).

^{11}B NMR (160 MHz, $CDCl_3$) δ 29.7

Spectral data were in good agreement with literature values.[21]

C–H borylation of 2,3-dimethylfuran (**263**):

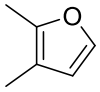

General procedure B (1.5 equiv. HBpin): NMR yield 87%, 95:5 5-B/4-B.

2-(4,5-Dimethyl-2-furyl)-4,4,5,5-tetramethyl-1,3,2-dioxaborolane

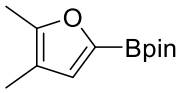

^{1}H NMR (500 MHz, $CDCl_3$) δ 6.87 (s, 1H), 2.25 (s, 3H), 1.94 (s, 3H), 1.32 (s, 12H).

^{11}B NMR (160 MHz, $CDCl_3$) δ 27.1.

3-(4,5-Dimethyl-2-furyl)-4,4,5,5-tetramethyl-1,3,2-dioxaborolane

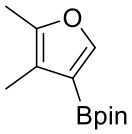

^{1}H NMR (500 MHz, $CDCl_3$) δ 7.57 (s, 1H), 2.19 (d, *J* = 0.9 Hz, 3H), 2.04 (d, *J* = 1.0 Hz, 3H), 1.33 (s, 12H).

^{11}B NMR (160 MHz, $CDCl_3$) δ 29.7.

Spectral data were in good agreement with literature values.[21]

C–H borylation of furan (**264**):

General procedure B (3 equiv. HBpin): NMR yield 87%, 78:22 2,5-B/2,4-B.

2,2'-(2,5-Furandiyl)bis(4,4,5,5-tetramethyl-1,3,2-dioxaborolane)

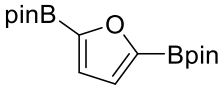

^{1}H NMR (500 MHz, $CDCl_3$) δ 7.06 (s, 1H), 1.32 (s, 12H).

^{11}B NMR (160 MHz, $CDCl_3$) δ 27.3.

2,2'-(2,4-Furandiyl)bis(4,4,5,5-tetramethyl-1,3,2-dioxaborolane)

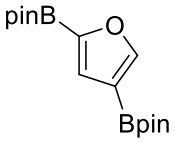

^{1}H NMR (500 MHz, $CDCl_3$) δ 7.96 (s, 1H), 7.28 (s, 1H), 1.32 (s, 12H).

^{11}B NMR (160 MHz, $CDCl_3$) δ 27.3.

Spectral data were in good agreement with literature values.[21-22]

C–H borylation of thiophene (**265**):

General procedure C (3 equiv. HBpin): NMR Yield 60% 72:28 2-B/2,5-B. Column chromatography (SiO_2) hexane/EtOAc (10% to 20%). 2-B isolated yield 39 mg (37%) 2,5-B isolated yield 15 mg (9%).

4,4,5,5-Tetramethyl-2-(2-thienyl)-1,3,2-dioxaborolane

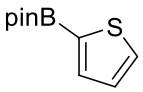

^{1}H NMR (500 MHz, $CDCl_3$) δ 7.68 (dd, J = 3.5, 1.0 Hz, 1H), 7.66 (dd, J = 4.7, 1.0 Hz, 1H), 7.22 (dd, J = 4.7, 3.4 Hz, 1H), 1.38 (s, 12H).

^{11}B NMR (160 MHz, $CDCl_3$) δ 29.0.

2,2'-(2,5-Thienediyl)bis(4,4,5,5-tetramethyl-1,3,2-dioxaborolane)

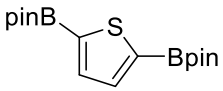

^{1}H NMR (500 MHz, $CDCl_3$) δ 7.66 (s, 2H), 1.34 (s, 12H).

^{11}B NMR (160 MHz, $CDCl_3$) δ 29.1.

Spectral data were in good agreement with literature values.[23]

C–H borylation of 3-hexylthiophene (**266**):

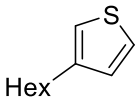

General procedure C (1.5 equiv. HBpin): NMR Yield 55% 5-B exclusively. Column chromatography (SiO_2) hexane/EtOAc (0% to 10%). Isolated yield 66 mg, 43%.

2-(4-Hexyl-2-thienyl)-4,4,5,5-tetramethyl-1,3,2-dioxaborolane

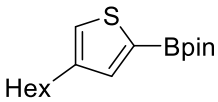

^{1}H NMR (500 MHz, $CDCl_3$) δ 7.48 (d, J = 1.1 Hz, 1H), 7.21 (s, 1H), 2.62 (t, J = 7.7 Hz, 2H), 1.65 – 1.53 (m, 3H), 1.34 (s, 13H), 1.31 – 1.24 (m, 8H), 0.99 – 0.80 (m, 4H).
^{11}B NMR (160 MHz, $CDCl_3$) δ 29.0.

Spectral data were in good agreement with literature values.[24]

C–H borylation of 4,4,5,5-tetramethyl-2-(thiophen-2-yl)-1,3,2-dioxaborolane (**267**):

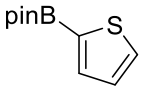

General procedure C (1.5 equiv. HBpin): NMR Yield >95% 5-B exclusively. Recrystallization $CHCl_3$/hexane. Isolated yield 143 mg, 83%.

2,2'-(2,5-Thienediyl)bis(4,4,5,5-tetramethyl-1,3,2-dioxaborolane)

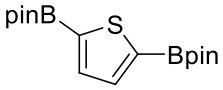

^{1}H NMR (500 MHz, $CDCl_3$) δ 7.66 (s, 2H), 1.34 (s, 12H).
^{11}B NMR (160 MHz, $CDCl_3$) δ 29.1.

Spectral data were in good agreement with literature values.[22]

C–H borylation of 2-phenylthiophene (**268**):

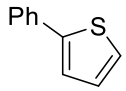

General procedure C (1.5 equiv. HBpin): NMR yield 51% 5-B exclusively. Column chromatography (SiO_2) hexane/EtOAc (10% to 20%). Isolated yield 60.1 mg, 42%.

4,4,5,5-Tetramethyl-2-(5-phenyl-2-thienyl)-1,3,2-dioxaborolane:

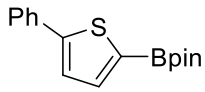

^{1}H NMR (400 MHz, $CDCl_3$) δ 7.69 – 7.64 (m, 2H), 7.63 (d, J = 3.6 Hz, 1H), 7.43 – 7.36 (m, 3H), 7.34 – 7.28 (m, 1H), 1.38 (s, 12H).
^{11}B NMR (160 MHz, $CDCl_3$) δ 29.0.

Spectral data were in good agreement with literature values.[23]

C–H borylation of EDOT (**269**):

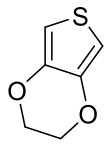

General procedure C (3 equiv. HBpin): NMR yield 45% 82:18 2-B/2,5-B. Column chromatography (SiO_2) hexane/EtOAc (10% to 20%). Isolated yield 52.3 mg, 39% (2-B).

5-(4,4,5,5-Tetramethyl-1,3,2-dioxaborolan-2-yl)-2,3-dihydrothieno[3,4-b][1,4]dioxine

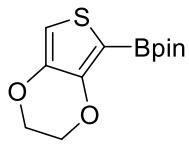

^{1}H NMR (500 MHz, $CDCl_3$) δ 6.62 (s, 1H), 4.36 – 4.25 (m, 2H), 4.19 – 4.12 (m, 2H), 1.33 (s, 12H).
^{11}B NMR (160 MHz, $CDCl_3$) δ 28.3.

2,5-bis(4,4,5,5-tetramethyl-1,3,2-dioxaborolan-2-yl)-3,4-ethylenedioxythiophene

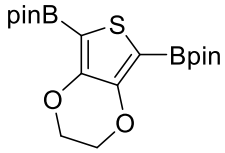

^{1}H NMR (500 MHz, $CDCl_3$) δ 4.26 (s, 4H), 1.32 (s, 24H).

^{11}B NMR (160 MHz, $CDCl_3$) δ 28.3.

Spectral data were in good agreement with literature values.[25-26]

C–H borylation of bithiophene (**270**):

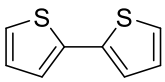

General procedure C (3.0 equiv. HBpin): NMR yield 54% 87:13 2-B/2,2'-B. Column chromatography (SiO_2) hexane/EtOAc (10% to 20%). Isolated yield 52.3 mg, 44% (2-B).

2-(2,2'-Bithiophen-5-yl)-4,4,5,5-tetramethyl-1,3,2-dioxaborolane

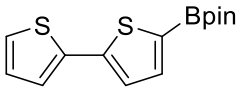

^{1}H NMR (400 MHz, $CDCl_3$) δ 7.55 (d, J = 3.6 Hz, 1H), 7.27 – 7.24 (m, 3H), 7.04 (dd, J = 4.9, 3.8 Hz, 1H), 1.38 (s, 12H).

^{11}B NMR (160 MHz, $CDCl_3$) δ 28.9.

2,2'-(2,2'-Bithiene-5,5'-diyl)bis(4,4,5,5-tetramethyl-1,3,2-dioxaborolane)

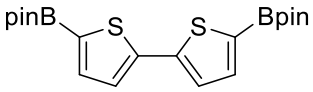

^{1}H NMR (500 MHz, $CDCl_3$) δ 7.52 (d, J = 3.6 Hz, 2H), 7.29 (d, J = 3.6 Hz, 2H), 1.35 (s, 24H).

^{11}B NMR (160 MHz, $CDCl_3$) δ 28.9.

Spectral data were in good agreement with literature values.[23, 27]

C–H borylation of pyrrole (**271**):

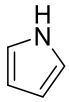

General procedure C (3 equiv. HBpin): NMR yield >95% 2,5-B exclusively. Recrystallization $CHCl_3$/hexane. Isolated yield 115 mg, 72%.

2,5-Bis(4,4,5,5-tetramethyl-1,3,2-dioxaborolan-2-yl)-1H-pyrrole

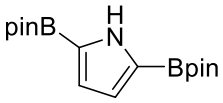

^{1}H NMR (400 MHz, $CDCl_3$) δ 9.30 (s, 1H), 6.86 (d, J = 2.3 Hz, 2H), 1.34 (s, 24H).
^{11}B NMR (128 MHz, $CDCl_3$) δ 28.1.

Spectral data were in good agreement with literature values.[28]

C–H borylation of methyl 2-pyrrolecarboxylate (**272**):

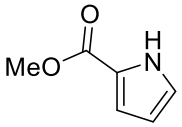

General procedure C (3 equiv. HBpin): NMR yield >95% 2-B exclusively. Column chromatography (SiO_2) hexane/EtOAc (10% to 20%). Isolated yield 116 mg, 92%.

Methyl 5-(4,4,5,5-tetramethyl-1,3,2-dioxaborolan-2-yl)-1H-pyrrole-2-carboxylate

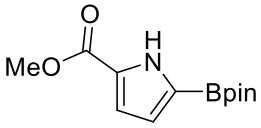

^{1}H NMR (400 MHz, $CDCl_3$) δ 9.50 (s, 1H), 6.90 (dd, J = 3.8, 2.3 Hz, 1H), 6.76 (dd, J = 3.8, 2.5 Hz, 1H), 3.85 (s, 3H), 1.32 (s, 12H).
^{11}B NMR (128 MHz, $CDCl_3$) δ 27.78.

Spectral data were in good agreement with literature values.[29]

C–H borylation of indole (**273**):

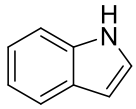

General procedure B (3 equiv., HBpin): NMR yield 89%, 2-B exclusively.

2-(4,4,5,5-Tetramethyl-1,3,2-dioxaborolan-2-yl)-1H-indole

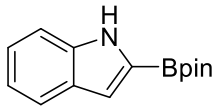

^{1}H NMR (500 MHz, $CDCl_3$) δ 8.68 (s, 1H), 7.80 – 7.58 (m, 1H), 7.44 – 7.33 (m, 1H), 7.28 – 7.19 (m, 1H), 7.15 (s, 1H), 7.11 (ddd, J = 10.4, 5.3, 2.3 Hz, 1H), 1.37 (s, 12H).
^{11}B NMR (160 MHz, $CDCl_3$) δ 28.7.

Spectral data were in good agreement with literature values.[27]

C–H borylation of 5-bromoindole (**274**):

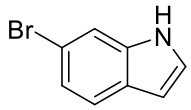

General procedure B (3 equiv., HBpin): NMR yield 24%, 2-B exclusively.

6-bromo-2-(4,4,5,5-tetramethyl-1,3,2-dioxaborolan-2-yl)-1H-indole

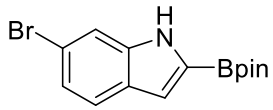

^{1}H NMR (500 MHz, $CDCl_3$) δ 8.64 (s, 1H), 7.55 (s, 1H), 7.24 – 7.21 (m, 2H), 7.11 (dd, J = 2.1, 1.0 Hz, 1H), 1.39 (s, 12H).
^{11}B NMR (160 MHz, $CDCl_3$) δ 28.6.
HRMS-EI (m/z): [M]+ calcd for $C_{14}H_{17}BBrNO_2$, 322.06085; found, 322.05730.

C–H borylation of 5-chloromoindole (**275**):

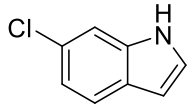

General procedure B (3 equiv., HBpin): NMR yield 42%, 2-B exclusively.

6-Chloro-2-(4,4,5,5-tetramethyl-1,3,2-dioxaborolan-2-yl)-1H-indole

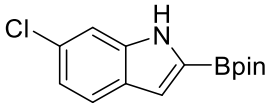

^{1}H NMR (500 MHz, $CDCl_3$) δ 8.74 (s, 1H), 7.58 (d, J = 8.5 Hz, 1H), 7.39 – 7.36 (m, 1H), 7.11 (d, J = 2.7 Hz, 1H), 7.09 (d, J = 1.9 Hz, 1H), 1.39 (s, 12H).

^{11}B NMR (160 MHz, $CDCl_3$) δ 28.5.

HRMS-EI (m/z): [M]+ calcd for $C_{14}H_{17}BClNO_2$, 278.11160; found, 278.11136.

6.6 Procedures for Catalytic Reactions Using Ru/V/Mn Catalysts

Perruthenate catalysed hydroboration of acetophenone and pyridine

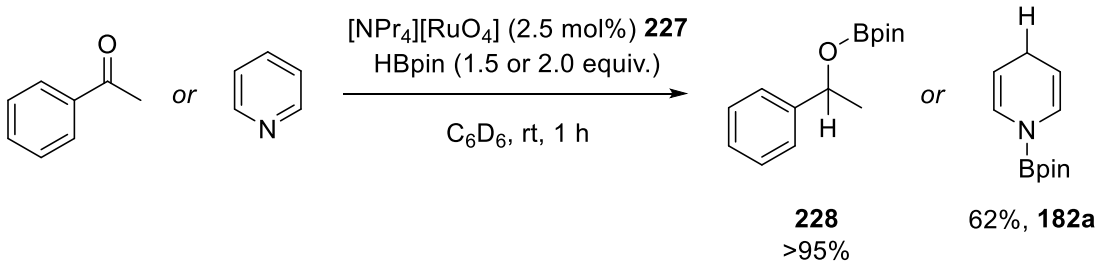

[N(^{i}Pr)$_4$][RuO_4] **277** (1.76 mg, 0.005 mmol), acetophenone (23.4 μL, 0.20 mmol) or pyridine (16.1 μL, 0.2 mmol) and mesitylene (10 μL, 0.053 mmol) as internal standard were combined in C_6D_6 (0.4 mL) in an NMR tube sealed with a neoprene rubber stopper. The ratio between the substrate and mesitylene was measured by ^{1}H NMR spectroscopy. HBpin (44 or 58 μL, 0.30 or 0.40 mmol) was added and reaction monitored by ^{1}H NMR spectroscopy to determine the nature and yields of the hydroborated products.

Permanganate or vanadate catalysed hydroboration/hydrosilylation of 3-methoxyacetophenone

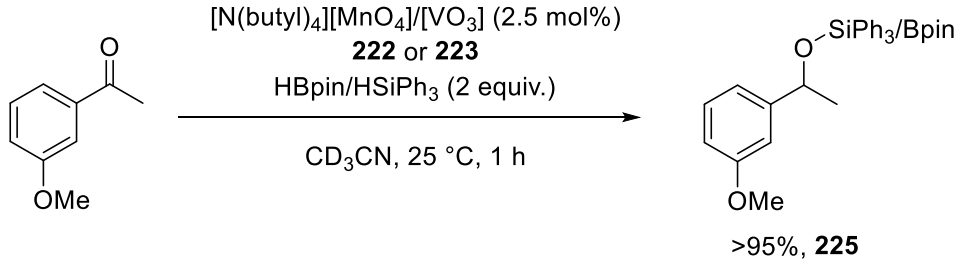

[N(butyl)$_4$][MnO_4] **222** (1.81 mg, 0.005 mmol) or [N(butyl)$_4$][VO_3] **223** (1.71 mg, 0.005 mmol), acetophenone (23.4 μL, 0.20 mmol) and mesitylene (10 μL, 0.053 mmol) as internal standard were combined in CD_3CN (0.4 mL) in an NMR tube sealed with a neoprene rubber stopper. The ratio between the substrate and mesitylene was measured by ^{1}H NMR

spectroscopy. HBpin (58 μL, 0.40 mmol) or $HSiPh_3$ (104 mg, 0.40 mmol) was added and reaction monitored by ^1H NMR spectroscopy to determine the nature and yields of the hydroborated products.

6.7 Attempted Syntheses

Deoxygenation of [PPN][ReO_4] with HBpin

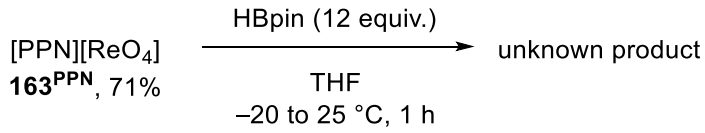

HBpin (43.5 μL, 0.30 mmol) was added to a suspension of [PPN][ReO_4] (20 mg, 0.025 mmol) in THF (0.5 mL) at −20 °C with stirring. The reaction was allowed to warm to room temperature over 1 h and was transferred to an NMR tube and sealed with a neoprene rubber stopper. The reaction mixture was analysed by $^1H/^{31}P/^{11}B$ NMR spectroscopy. The major product/s could not be isolated in high purity due to residual $O(Bpin)_2$.

Cation exchange between [PPN][Cl] with $\mathbf{165^{DME}}$

[PPN][Cl] (43.5 μL, 0.30 mmol) was added to a suspension of [K(DME)(18-c-6)][$ReH_7(Bpin)_3$] $\mathbf{165^{DME}}$ (20 mg, 0.021 mmol) in THF (0.5 mL) at room temperature with stirring. The reaction was stirred for 1 h and was transferred to a Teflon-tapped NMR tube. The reaction mixture was analysed by $^1H/^{31}P/^{11}B$ NMR spectroscopy. A colourless precipitate formed and the NMR spectra exhibited no shift in any resonances. The product was formulated as [PPN][$ReH_7(Bpin)_3$] $\mathbf{165^{PPN}}$ but it was not possible to isolated it in high purity.

Screen of hydroboranes for the deoxygenation of perrhenate

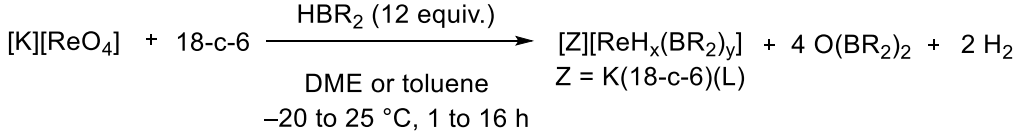

To a suspension of [K][ReO_4] **277** (20 mg, 0.069 mmol) in DME or toluene (1 mL) at −20 °C was added the appropriate borane (0.828 mmol) with stirring. The reaction was slowly allowed to warm to room temperature over 1 to 16 h with stirring. The reaction was transferred to an NMR tube and sealed with a neoprene rubber stopper. The reaction mixture was analysed by $^1H/^{31}P/^{11}B$ NMR spectroscopy to determine the nature of the rhenium hydride species in solution.

Screen of phosphine ligands for coordination to *in situ* formed ruthenium hydride

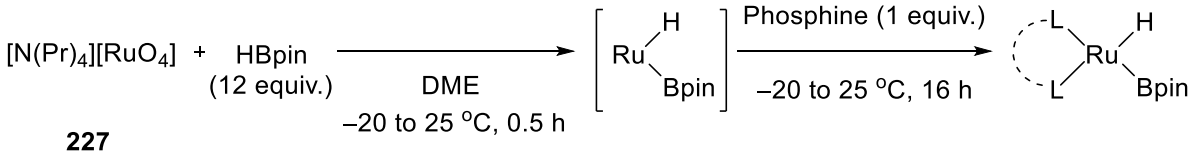

227

HBpin (99 μL, 0.68 mmol) was added to a suspension of [N(^{i}Pr)$_4$][RuO$_4$] **277** (20 mg, 0.057 mmol) in DME (1 mL) at −20 °C with stirring. The reaction was slowly allowed to warm to room temperature over 0.5 h. The reaction was cooled to −20 °C and the appropriate phosphine (0.057 mmol) was added with stirring. The reaction was allowed to warm slowly to room temperature and was stirred for 16 h. The reaction was transferred to an NMR tube and sealed with a neoprene rubber stopper. The reaction mixture was analysed by ^{1}H/^{31}P/^{11}B NMR spectroscopy to determine the nature of the ruthenium hydride species in solution.

Screen of phosphine or N-donor ligands for coordination to 165^{DME}

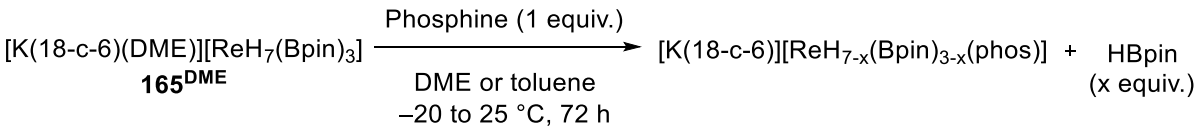

To a solution of [K(DME)(18-c-6)][ReH$_7$(Bpin)$_3$] **165^{DME}** (20 mg, 0.021 mmol) in DME or toluene (0.5 mL) at −20 °C was added the appropriate phosphine or N-donor ligand (0.021 mmol) with stirring. The reaction was slowly allowed to warm to room temperature over 0.5 h. The reaction was allowed to warm slowly to room temperature and was stirred for 16 h. The reaction was transferred to an NMR tube and sealed with a neoprene rubber stopper. The reaction mixture was analysed by ^{1}H/^{31}P/^{11}B NMR spectroscopy to determine the nature of the rhenium hydride species in solution.

6.8 X-ray Crystallography Details

6.8.1 Crystallographic Data

Complex	**[K(18-c-6)][ReH_4(Bpin)(η^2-HBpin)(κ^2-H_2Bpin)] 165^{DME}**	**[N(Hex)$_4$][Bpin(OBpin)$_2$] 168**	**[N(Bu)$_4$][ReH_8(Bpin)$_2$] 167^{H2}**	**[K(DME)(18-c-6)][Re(κ_2-H_2BBN)$_4$] 172**
Chemical formula	$C_{34}H_{77}B_3O_{14}KRe$	$C_{46}H_{88}B_3NO_8$	$C_{28}H_{60}B_2NO_4$ Re	$C_{48}H_{98}B_4KO_8Re$
Mr	967.68	679.11	681.58	1071.83
Temperature (K)	100	120	120	220
Crystal system, space group	Monoclinic, C 1 2/c 1	Monoclinic, P 1 21/n 1	Monoclinic, P 1 21/n 1	Triclinic, P -1
a, b, c (Å)	14.7681(15), 23.105(2), 13.7109(14)	14.704(3), 23.323(3), 14.9430(13)	13.2026(6), 18.1676(9), 15.3939(6)	11.2627(2), 15.9727(3), 16.0123(2)
α, β, γ (°)	90, 91.809(3), 90	90, 110.006(16), 90	90, 106.048(5), 90	96.714(1), 91.290(1), 102.351(2)
V (Å^3)	4676.1(8)	4815.4(13)	3548.5(3)	2791.22(8)
Z	4	4	4	2
ρ_{calc} g/cm^3	1.375	0.937	1.276	1.275
μ (mm^{-1})	2.741	0.065	3.452	2.296
No. of measured and independent reflections	9312, 9312	22934, 9090	68503, 6477	73081, 15734
Parameters/restraints	243/0	503/0	341/34	613/1
Rint	n/a – twinned data	0.2025	0.1227	0.0333
R[$F^2 > 2\sigma(F^2)$], wR(F^2), S	0.0560, 0.1316, 1.155	0.1406, 0.3585, 1.042	0.0541, 0.1127, 1.027	0.0227, 0.0461, 1.039
Δρmax, Δρmin (e Å^{-3})	1.93, -2.50	0.701, -0.435	1.113, -0.856	0.74, -0.70
CCDC Code	1979242	N/A	N/A	1979241

Table 5. Summary of X-ray crystallography data for compounds **165**, **168**, **167^{H2}** and **172**.

Complex	***cis*-(DPEphos)$_2$RuH$_2$ 234**	**[K(18-c-6)][ReH$_5$(Bpin)(dppp)] 258**	**ReH$_6$(Bpin)(dppp) 260**	**Re$_2$H$_8$(dppp)$_2$ 277**
Chemical formula	$C_{72}H_{58}O_2P_4Ru$	$C_{45}H_{67}BKO_8P_2Re$	$C_{40}H_{52}BO_2P_2Re$	$C_{54}H_{60}P_4Re_2$
Mr	1180.13	1034.03	823.76	1205.30
Temperature (K)	120	120	120	120
Crystal system, space group	Monoclinic, C 1 2/c 1	Monoclinic, P 1 21/n 1	Orthorhombic, P b c a	Triclinic, P -1
a, b, c (Å)	21.5695(2), 13.18390(10),41.4942 (4)	12.9998(2), 29.3027(4), 14.5738(2)	11.5282(3), 24.9634(8), 26.1194(9)	9.38140(10), 12.2395(2), 21.7629(3)
α, β, γ (°)	90 96.9640(10) 90	90, 102.8880(10), 90	90, 90, 90	85.9370(10), 85.1180(10), 71.918(2)
V (Å^3)	11712.66(18)	5411.73(14)	7516.7(4)	2364.26(6)
Z	8	4	8	2
ρ_{calc} g/cm^3	1.338	1.269	1.456	1.693
μ (mm^{-1})	3.561	2.2424	3.351	5.287
No. of measured and independent reflections	50298, 12065	112966, 9895	81541, 9931	121195, 17093
Parameters/restraints	720/0	548/0	444/0	638/25
Rint	0.0644	0.0356	0.0687	0.0741
R[F^2 > 2σ(F^2)], wR(F^2), S	0.0491, 0.1339, 1.029	0.0286, 0.0356, 1.151	0.0381, 0.0541, 1.095	0.0421, 0.0720, 1.176
Δρmax, Δρmin (e Å^{-3})	1.261, -1.520	1.113, -0.601	0.981, -0.901	2.188, -1.261
CCDC Code	N/A	2060777	2060776	2060778

Table 6. Summary of X-ray crystallography data for compounds **234**, **258**, **260** and **277**.

6.8.2 Special Refinement Details

[K(DME)(18-c-6)][$ReH_7(Bpin)_3$] **165^{DME}**:

Refined as a 2-component twin. The twin law is

Transforms h1.1(1)->h1.2(2)
-0.42198 -0.57921 -0.04709
1.41915 -0.42195 0.04692
0.00113 0.00043 1.00004

The matrix corresponds to a rotation of 114.9 degrees about [001], so that the crystal is more properly described as a two-domain aggregate. Indexing was carried out with CELL_NOW.

The diffraction images were integrated for both domains using two orientation matrices. The structure was solved and initially refined with the model of the anion consisting of [$Re(BPin)_3$], that is without any hydrogens attached to the metal. All other H-atoms were placed on C in ideal positions, and all non-H atoms were modelled with anisotropic displacement parameters. The Re1 and B2 reside on a crystallographic .2. axis. The cation also has crystallographic two-fold symmetry. The refinement statistics were:
wR2 = 0.133622, GooF = S = 1.17321, Restrained GooF = 1.17321 for all data R1 = 0.056801 for 9034 Fo > 4sig(Fo) and 0.060189 for all 9318 data 242 parameters refined using 0 restraints. The adps were reasonably well-behaved, and when fitted to a TLS librational model (SHELXTL-XP) the residuals were 0.1184 and 0.1142 for the ligand based B1 and B2, respectively. The geometry about Re1 was:

Re1 B1 2.194(10)
Re1 B2 2.173(14)
B2 Re1 B1 118.6(2)
B2 Re1 B1' 118.6(2)
B1 Re1 B1' 122.9(5)
where B1' is the symmetry equivalent of B1 [-x+1, y, -z+1/2].

The final difference map contained several peaks within 1.15 Ang of Re1 with heights between 1.95 to 0.57 e/Ang**3; this is a common effect of residual absorption errors in heavy atom crystal structures. Several other peaks with heights between 1.50 and 0.80 e/Ang**3 were located at between 1.65 and 1.78 Ang from Re1, which are reasonable

distances to hydride ligands. Three of these were assigned as H1-3 and could be refined provided the Re-H was restrained to 1.7 Ang. Other H-atoms could not be convincingly located.

Possible positions for the remaining H-atoms were calculated by DFT (see below). The optimised DFT model of the anion is given below in SHELX format with positions as fractional coordinates based on a metrically cubic unit cell with a = 15 Ang, space group P1.

```
TITL Converted
CELL 0.71073 15 15 15 90 90 90
ZERR 1 0 0 0 0 0 0
LATT -1
SFAC C H B O Re
UNIT 18 43 3 6 1
FVAR 1.00
Re1    5  0.468174  0.044662  0.235850  1.000000 0.05000
H1     2  0.524037  0.129235  0.168335  1.000000 0.06000
H2     2  0.456985 -0.058927  0.275916  1.000000 0.06000
H3     2  0.434675  0.151287  0.277438  1.000000 0.06000
H4     2  0.550133  0.051501  0.317875  1.000000 0.06000
H5     2  0.409193  0.033252  0.329360  1.000000 0.06000
H6     2  0.464340  0.433687  0.345160  1.000000 0.06000
H7     2  0.416840  0.324554  0.342262  1.000000 0.06000
H8     2  0.519235  0.342849  0.398444  1.000000 0.06000
H9     2  0.601327  0.467758  0.242182  1.000000 0.06000
H10    2  0.653086  0.391535  0.316663  1.000000 0.06000
H11    2  0.662597  0.375100  0.199597  1.000000 0.06000
H12    2  0.560360  0.416551  0.074065  1.000000 0.06000
H13    2  0.585504  0.300452  0.083373  1.000000 0.06000
H14    2  0.488496  0.335510  0.025536  1.000000 0.06000
H15    2  0.432060  0.481988  0.172989  1.000000 0.06000
H16    2  0.365211  0.411590  0.104959  1.000000 0.06000
H17    2  0.355810  0.405661  0.222864  1.000000 0.06000
B18    3  0.489155  0.197809  0.217909  1.000000 0.05000
C19    1  0.533247  0.340235  0.255544  1.000000 0.05000
C20    1  0.479596  0.362189  0.340019  1.000000 0.05000
C21    1  0.617577  0.397060  0.252824  1.000000 0.05000
C22    1  0.475087  0.343290  0.168272  1.000000 0.05000
C23    1  0.531446  0.349810  0.083055  1.000000 0.05000
C24    1  0.402850  0.414938  0.167691  1.000000 0.05000
O25    4  0.558183  0.247357  0.259751  1.000000 0.05000
O26    4  0.433034  0.256663  0.169123  1.000000 0.05000
H27    2  0.382888  0.062060  0.157016  1.000000 0.06000
H28    2  0.179809 -0.199400  0.306774  1.000000 0.06000
H29    2  0.292038 -0.159680  0.310686  1.000000 0.06000
H30    2  0.207218 -0.100994  0.367870  1.000000 0.06000
H31    2  0.064155 -0.110743  0.208888  1.000000 0.06000
H32    2  0.088672 -0.024107  0.286099  1.000000 0.06000
```

H33	2	0.097920	-0.004947	0.166603	1.000000	0.06000
H34	2	0.170027	-0.244414	0.132778	1.000000	0.06000
H35	2	0.267963	-0.242642	0.065995	1.000000	0.06000
H36	2	0.277507	-0.252965	0.183289	1.000000	0.06000
H37	2	0.135463	-0.098540	0.040151	1.000000	0.06000
H38	2	0.206325	-0.003527	0.056923	1.000000	0.06000
H39	2	0.245134	-0.096331	-0.004677	1.000000	0.06000
B40	3	0.344768	-0.017444	0.198220	1.000000	0.05000
C41	1	0.206132	-0.079444	0.225734	1.000000	0.05000
C42	1	0.244525	-0.119475	0.136796	1.000000	0.05000
C43	1	0.221851	-0.139372	0.307231	1.000000	0.05000
C44	1	0.107665	-0.053078	0.221177	1.000000	0.05000
C45	1	0.239465	-0.220877	0.129824	1.000000	0.05000
C46	1	0.204368	-0.076668	0.052795	1.000000	0.05000
O47	4	0.258529	-0.000153	0.236714	1.000000	0.05000
O48	4	0.336290	-0.092834	0.142032	1.000000	0.05000
H49	2	0.789766	-0.143290	0.116631	1.000000	0.06000
H50	2	0.671863	-0.126348	0.117762	1.000000	0.06000
H51	2	0.742301	-0.044287	0.070604	1.000000	0.06000
H52	2	0.888319	-0.047744	0.226235	1.000000	0.06000
H53	2	0.842058	0.043353	0.163174	1.000000	0.06000
H54	2	0.832995	0.042933	0.283137	1.000000	0.06000
H55	2	0.811176	-0.211443	0.283299	1.000000	0.06000
H56	2	0.715662	-0.237150	0.348605	1.000000	0.06000
H57	2	0.706367	-0.232687	0.230900	1.000000	0.06000
H58	2	0.820805	-0.075882	0.394597	1.000000	0.06000
H59	2	0.733118	0.005493	0.391943	1.000000	0.06000
H60	2	0.714155	-0.100625	0.439838	1.000000	0.06000
B61	3	0.597000	-0.011430	0.254041	1.000000	0.05000
C62	1	0.742413	-0.044162	0.214282	1.000000	0.05000
C63	1	0.714743	-0.103236	0.296260	1.000000	0.05000
C64	1	0.736739	-0.093311	0.124723	1.000000	0.05000
C65	1	0.833458	0.001071	0.222799	1.000000	0.05000
C66	1	0.738627	-0.201826	0.288724	1.000000	0.05000
C67	1	0.748648	-0.065822	0.385519	1.000000	0.05000
O68	4	0.676509	0.024807	0.215466	1.000000	0.05000
O69	4	0.619528	-0.093702	0.294844	1.000000	0.05000
H70	2	0.497863	-0.028292	0.155297	1.000000	0.06000

In this list the H-atoms attached to Re1 are H1-H5, H27 and H70. The geometry (in Angstrom and degrees) about Re1 is

Re1-B18 2.334 (a borohydride)
Re1-B40 2.148 (a borane)
Re1-B61 2.125 (a boryl)
B18-Re1-B40 120.85
B18-Re1-B61 106.37
B40-Re1-B61 130.22
The Re1-H distances span 1.667 to 1.827 Ang.

The anion deviates substantially from C2 symmetry. If it were present in this crystal structure with the same geometry, disorder would be expected to be substantial and obvious in a Fourier map, but this is not observed. Nevertheless the positions of H4-H6 were inferred from the DFT result using the positions of Re1 and H1-3 to define the orientation of the DFT model. Thereafter H1-7 were allowed to ride on Re1 with Uiso(H) = 1.5Ueq(Re1). Only H2 has full occupancy, the others are disordered by the two-fold axis and have half-occupancy. The final refinement statistics are:

REM mo_jl19002_0m_4 in C2/c
REM wR2 = 0.131599, GooF = S = 1.15474, Restrained GooF = 1.15474 for all data
REM R1 = 0.055955 for 9034 Fo > 4sig(Fo) and 0.059356 for all 9318 data
REM 243 parameters refined using 0 restraints

These figures represent only a tiny improvement over those obtained without any hydrides placed at all (see above, e.g. R1 = 0.056801). The identity of the anion in this structure is thus not established with much certainty by the crystal structure. Although the presence of some hydride density was evident in a difference map, it is also necessary to assign the oxidation-state of Re (+7) on the basis of the colour of the crystal (colourless) and the interpretation of the proton NMR spectrum in terms of seven fluxional hydride ligands.

In addition to the disagreement between the crystal and DFT structures, in the B-Re-B angles, there are also differences in the Re-B bond distances. Overall, the experimental distances and angles are similar to the average values of the DFT model [distances, expt: 2.194(10) and 2.173(14) Ang, DFT average: 2.202 Ang, angles, expt 120 deg, DFT 119.1 deg]. It is possible that the anion is completely disordered, such that all three ligands and the hydrides are scrambled about the metal, and that the geometrical parameters seen crystallographically are averages. A rather complex refinement model was constructed in which each site was occupied by one Bpin ligand with a Re-B distance of 2.334 Ang, and other with a Re-B distance equal to 2.1365 Ang (the average of the the shorter Re-B distances in the DFT model). The hydrides were again placed using the DFT model. The refinement statistics were:

REM mo_jl19002_0m_4 in C2/c
REM wR2 = 0.130242, GooF = S = 1.16066, Restrained GooF = 1.14558 for all data
REM R1 = 0.055962 for 9034 Fo > 4sig(Fo) and 0.059352 for all 9318 data
REM 282 parameters refined using 310 restraints

These are essentially identical to the model described above, but with a larger number of parameters.

[K(DME)(18-c-6)][Re(κ_2-H_2BBN)$_4$] **172**:

A molecule of DME coordinated to K1 (C63, O7, C64, C65, C65A, O8, O8A, C67) was positionally disordered over two positions. As a result, C65/65A were refined with an occupancy ratio of 0.734:0.266, and O8/8A was refined with an occupancy ratio of 0.720:0.280. The hydrides in the anion were placed in positions based on the difference synthesis and refined with free uiso. Bond lengths between C65, C64, and C65A were restrained to be equal within the standard uncertainty of 0.02 through the use of SADI command. Data collected at 220 K due to suspected phase transition upon cooling.

[N(Hex)$_4$][Bpin(OBpin)$_2$] **168**:

The R-factor is quite high (0.1861) for the refined structure of [N(hexyl)$_4$][BpinO(Bpin)$_2$], and the cause of this appears to be associated with significant disorder in the $[N(hexyl)_4]^+$ that could not be adequately modelled even after imposing restraints.

[N(Bu)$_4$][ReH_8(Bpin)$_2$] **167^{H2}**:

While the R-factor was slightly high (0.0541), likely due to significant disorder in the $[NBu_4]^+$ cation that could not be adequately modelled, it is clear that only two boron ligands are present. Due to the poor quality of these data the hydride positions were not located.

cis-(DPEphos)$_2$$RuH_2$ **234**:

No special refinement details.

[K(18-c-6)][ReH_5(Bpin)(dppp)] **258**:

Attempts to split C31 and C32 into two components did not resolve disorder and resulted in unstable refinement; as such this disorder was not modelled any further. Residual electron density from disordered lattice solvent was removed from the structure using the "solvent mask" feature of Olex2 (98 electrons/unit cell) with the lattice solvent identified as 2 molecules of hexane per unit cell.

ReH_6(Bpin)(dppp) **260**:

No special refinement details

$Re_2H_8(dppp)_2$ **277**:

A phenyl substituent on the DPPP ligand coordinated to Re1 (C(22), C(23), C(24), C(25), C(26), C(27), C(22A), C(23A), C(24A), C(25A), C(26A), C(27A)) was disordered over two positions. As a result, the carbon atoms in the ring were split and refined with an occupancy ratio of 0.540:0.460. The central propyl carbon of the DPPP ligand bound to Re2 (C(41), C(41A)) was disordered over two positions. As a result, C(41) was split and refined with an occupancy ratio of 0.405:0.595. The hydrides were placed in positions based on the difference synthesis and refined with free Uiso. The Re-H distances for terminal hydrides (H1, H2, H5, H6) were restrained to a distance of 1.47 Å within the standard uncertainty of 0.01 through the use of DFIX command. The Re-H distances for bridging hydrides (H3, H4, H7, H8) were restrained to a distance of 1.95 Å within the standard uncertainty of 0.01 through the use of DFIX command. The interatomic distances between bridging hydrides (H3 and H4, H7 and H8) were restrained to a distance of 2.1 Å within the standard uncertainty of 0.01 through the use of DANG command.

6.9 References

1. Sheldrick, G., *Acta Crystallogr., Sect. A* **2015,** *71* (1), 3-8.
2. Sheldrick, G., *Acta Crystallogr., Sect. C* **2015,** *71* (1), 3-8.
3. Dolomanov, O. V.; Bourhis, L. J.; Gildea, R. J.; Howard, J. A. K.; Puschmann, H., *J. Appl. Crystallogr.* **2009,** *42* (2), 339-341.
4. Abiko, A., *Org. Synth.* **2002,** *79*, 103.
5. Hadebe, S. W.; Sithebe, S.; Robinson, R. S., *Tetrahedron* **2011,** *67* (23), 4277-4282.
6. Lang, A.; Nöth, H.; Thomann-Albach, M., *Chemische Berichte* **1997,** *130* (3), 363-370.
7. Brown, H. C.; Yoon, N. M., *Isr. J. Chem.* **1976,** *15* (1-2), 12-16.
8. Morris, D. S.; Weetman, C.; Wennmacher, J. T. C.; Cokoja, M.; Drees, M.; Kühn, F. E.; Love, J. B., *Catal. Sci. Technol.* **2017,** *7* (13), 2838-2845.
9. Schoop, T.; Roesky, H. W.; Noltemeyer, M.; Schmidt, H. G., *Organometallics* **1993,** *12* (2), 571-574.
10. Lickiss, P. D.; Lucas, R., *J. Organomet. Chem* **1996,** *521* (1), 229-234.
11. Day, V. W.; Klemperer, W. G.; Yagasakl, A., *Chem. Lett.* **1990,** *19* (8), 1267-1270.
12. Luo, X. L.; Crabtree, R. H., *J. Am. Chem. Soc.* **1990,** *112* (12), 4813-4821.
13. Pickard, C. J.; Needs, R. J., *J. Condens. Matter Phys.* **2011,** *23* (5), 053201.

14. Clark, S. J.; Segall, M. D.; Pickard, C. J.; Hasnip, P. J.; Probert, M. J.; Refson, K.; Payne, M. C., *Z. Kristallogr. Krist.* **2005,** *220* (5-6), 567-570.

15. Press, L. P.; Kosanovich, A. J.; McCulloch, B. J.; Ozerov, O. V., *J. Am. Chem. Soc.* **2016,** *138* (30), 9487-9497.

16. Arrowsmith, M.; Hill, M. S.; Hadlington, T.; Kociok-Köhn, G.; Weetman, C., *Organometallics* **2011,** *30* (21), 5556-5559.

17. Intemann, J.; Lutz, M.; Harder, S., *Organometallics* **2014,** *33* (20), 5722-5729.

18. Zhang, F.; Song, H.; Zhuang, X.; Tung, C.-H.; Wang, W., *J. Am. Chem. Soc.* **2017,** *139* (49), 17775-17778.

19. Fan, X.; Zheng, J.; Li, Z. H.; Wang, H., *J. Am. Chem. Soc.* **2015,** *137* (15), 4916-4919.

20. Kaithal, A.; Chatterjee, B.; Gunanathan, C., *Org. Lett.* **2016,** *18* (14), 3402-3405.

21. Thomas, L. B. J. H. D. A. P. D. S. P., *Molecules* **2020,** *25* (4), 905.

22. Obligacion, J. V.; Semproni, S. P.; Chirik, P. J., *J. Am. Chem. Soc.* **2014,** *136* (11), 4133-4136.

23. Heinrich, A. C. J.; Thiedemann, B.; Gates, P. J.; Staubitz, A., Dual Selectivity: *Org. Lett.* **2013,** *15* (18), 4666-4669.

24. Tanaka, S.; Tanaka, D.; Tatsuta, G.; Murakami, K.; Tamba, S.; Sugie, A.; Mori, A., *Chem. Eur. J.* **2013,** *19* (5), 1658-1665.

25. Rochette, É.; Desrosiers, V.; Soltani, Y.; Fontaine, F.-G., *J. Am. Chem. Soc.* **2019,** *141* (31), 12305-12311.

26. Jayaraman, A.; Misal Castro, L. C.; Fontaine, F.-G., *Org. Proc. Res. Dev.* **2018,** *22* (11), 1489-1499.

27. Maegawa, Y.; Inagaki, S., *Dalton Trans.* **2015,** *44* (29), 13007-13016.

28. Seechurn, C. C. C. J.; Sivakumar, V.; Satoskar, D.; Colacot, T. J., *Organometallics* **2014,** *33* (13), 3514-3522.

29. Pang, Y.; Ishiyama, T.; Kubota, K.; Ito, H., *Chem. Eur. J.* **2019,** *25* (18), 4654-4659.